

RP

REPORT GDC-BTD68-058
CONTRACT NAS 3-3248, T.O.9

FIXED INSULATION DEVELOPMENT PROGRAM FINAL REPORT

FACILITY FORM 802	(ACCESSION NUMBER) = <u>36272</u> (THRU)
	<u>271</u> (PAGES) (CODE)
	<u>CR-105599</u> (NASA CR OR TMX OR AD NUMBER) (CATEGORY)



GENERAL DYNAMICS
Convair Division

Reproduced by
**NATIONAL TECHNICAL
INFORMATION SERVICE**
U S Department of Commerce
Springfield VA 22151

CP 7-58400

271

REPORT GDC-BTD68-058

**FIXED INSULATION DEVELOPMENT PROGRAM
FINAL REPORT**

May 1969

Prepared Under
Contract NAS3-3248, T.O.9

Prepared by
CONVAIR DIVISION OF GENERAL DYNAMICS
San Diego, California

PRECEDING PAGE BLANK NOT FILMED.

FOREWORD

This report summarizes the results of a Fixed Insulation Development Program performed by the Convair Division of General Dynamics. The program objective was to provide a tested and proven design of an acceptable fixed insulation system to replace the jettisonable insulation presently used to protect the cylindrical section of the Centaur liquid hydrogen tank.

This program was performed by Convair for NASA Lewis Research Center and was authorized by contract NAS3-3248, Task Order Number 9.

PRECEDING PAGE BLANK NOT FILMED.

TABLE OF CONTENTS

Section	Page
1 INTRODUCTION.	1-1
2 MATERIAL EVALUATION	2-1
2.1 Foams	2-1
2.1.1 Foam Survey Results	2-1
2.1.2 Test Evaluation	2-1
2.1.3 Conclusions	2-15
2.2 Adhesives	2-16
2.2.1 Survey Results	2-16
2.2.2 Test Results	2-17
2.3 Films.	2-27
2.3.1 Survey Results	2-28
2.3.2 Test Results	2-28
2.4 Thermal Control Coatings	2-29
2.4.1 Survey Results	2-29
2.4.2 Materials Evaluated	2-29
2.4.3 Results of Thermal Radiation Property Evaluation.	2-34
2.5 Constrictive Wrap	2-37
2.5.1 Materials Evaluated	2-41
2.5.2 Test Specimen Fabrication	2-42
2.5.3 Test Methods.	2-42
2.5.4 Test Results	2-45
2.5.5 Material Recommendations	2-52
2.6 Composite Insulation Systems.	2-53
2.6.1 Compression Tests.	2-53
2.6.2 Apparent Thermal Conductivity.	2-54
2.6.3 Friction Tests	2-54
3 THERMODYNAMIC EVALUATION.	3-1
3.1 Fiberglass Strand Constrictive Wrap System.	3-3
3.1.1 Foam Thickness Evaluation	3-3
3.1.2 Insulation Surface Temperature	3-22
3.1.3 Ice Formation on Insulation Panel Surface.	3-29

TABLE OF CONTENTS (Continued)

Section		Page
3.1.4	Fiberglass Constrictive Wrap Temperature	3-32
3.2	Corrugated Constrictive Wrap System	3-32
3.2.1	Surface Temperature Predictions	3-35
3.2.2	Effect of Corrugations on Solar Absorptance	3-37
3.2.3	Comparison with the Fiberglass Strand Constrictive Wrap System	3-38
3.3	Conclusions	3-38
4	DESIGN	4-1
4.1	Sealed Foam Panels	4-1
4.1.1	Design Requirements	4-1
4.1.2	Design Concept	4-1
4.1.3	Panel Configurations	4-2
4.2	Sealed Foam Panel Protective Covering	4-5
4.2.1	Design Requirements	4-5
4.2.2	Material Chosen	4-5
4.3	Constrictive Wrap	4-6
4.3.1	Design Requirements	4-6
4.3.2	Fiberglass Strand Constrictive Wrap Configuration	4-6
4.3.3	Other Constrictive Wrap Designs	4-16
4.3.4	Corrugated Constrictive Wrap Configuration	4-17
4.3.5	Constrictive Wrap Comparisons	4-17
4.4	Protective Shell	4-22
4.4.1	Design Objectives	4-22
4.4.2	Shell Configuration	4-23
5	FABRICATION	5-1
5.1	T-9 Tank Panels	5-1
5.1.1	Material Systems (Combinations)	5-1
5.1.2	Manufacturing Procedures	5-1
5.1.3	Acceptance Criteria	5-2
5.1.4	Fabrication History	5-3
5.1.5	Acceptance Test Results	5-9

TABLE OF CONTENTS (Continued)

Section	Page
5.2	Installation of T-9 Tank Panels 5-15
5.2.1	Summary of Method of Installation. 5-15
5.2.2	Installation of the Panels on the T-9 Tank 5-17
5.3	Fabrication of Constrictive Wrap 5-23
5.3.1	Original Method of Fabrication. 5-23
5.3.2	Revised Method of Fabrication 5-24
5.3.3	Final Method of Fabrication. 5-25
5.4	Installation of Constrictive Wrap. 5-29
5.5	Panel Repair Procedure 5-29
5.5.1	Test Panel Material Systems 5-32
5.5.2	Types of Damages 5-32
5.5.3	Damage Test Procedures. 5-33
5.5.4	Test Results 5-34
6	WEIGHT SUMMARY 6-1
7	COMPARISON OF PAYLOAD LOSSES. 7-1
7.1	Specific Losses 7-1
7.2	Total Losses 7-1
8	SIMULATED ASCENT TRAJECTORY TESTS 8-1
8.1	Simulated Heating/Vacuum Tests 8-1
8.1.1	Test Objective 8-1
8.1.2	Test Specimen Configuration 8-1
8.1.3	Test Fixture Configuration 8-1
8.1.4	Test Results 8-3
8.1.5	Summary of Test Results. 8-3
8.1.6	Conclusions 8-3
8.2	Simulated Cryogenic/Heat/Vacuum Tests 8-7
8.2.1	Effects of Testing on a Cold Wall 8-9
8.2.2	Test Objective 8-11
8.2.3	Test Specimen Configuration 8-11
8.2.4	Test Fixture Configuration 8-11
8.2.5	Test Procedure 8-11
8.2.6	Test Results 8-15

TABLE OF CONTENTS (Continued)

Section	Page
9	CRYOGENIC GROUND HOLD TEST 9-1
9.1	Test Objectives 9-1
9.2	Test Specimen Configuration 9-1
9.2.1	Sealed Foam Panel Configuration 9-2
9.2.2	Sealed Foam Protective Covering Con- figuration 9-8
9.2.3	Constrictive Wrap Configuration 9-8
9.2.4	Instrumentation Configuration 9-8
9.3	Test Procedure 9-8
9.3.1	Material Evaluation Test 9-8
9.3.2	Repair Technique Tests 9-13
9.4	Summary of Test Results 9-16
9.4.1	Material Evaluation Tests 9-16
9.4.2	Repair Technique Tests 9-19
9.5	Thermodynamic Evaluation of Test Results 9-28
9.5.1	Analysis of Surface Temperature Data 9-28
9.5.2	Observation of Ice and Frost Build-Up 9-31
9.5.3	Effects of Simulated Aerodynamic Heating 9-33
10	CONCLUSIONS AND RECOMMENDATIONS 10-1
10.1	Panel Configuration 10-1
10.1.1	Panel Blistering During Warm-Up after Cryogenic Tanking 10-1
10.1.2	Panel Blistering While Being Subjected to the Ascent Trajectory Environment 10-1
10.2	Constrictive Wrap Configuration 10-2
11	REFERENCES 11-1

TABLE OF CONTENTS (Continued)

Appendix I BIBLIOGRAPHY	Page
I.1 Material Research Documents	I-1
I.2 Thermodynamic Analyses Documents.	I-1
I.3 Test Documents	I-2
I.3.1 Thermal Conductivity Tests	I-2
I.3.2 Coldwall Vacuum/Heat Tests	I-2
I.3.3 Surface Coat Tests	I-3
I.3.4 Constrictive Wrap Strand Friction Testing .	I-3
I.3.5 Jet Engine Test	I-3
I.3.6 T-9 Ground Hold and Repair Technique Tests	I-3
I.3.7 Miscellaneous	I-4
I.3.8 T-9 Tank Insulation Panel Acceptance Tests	I-5
I.4 Miscellaneous Documents	I-5
I.5 Drawings	I-5
I.5.1 Convair Drawings	I-5
I.5.2 Goodyear Aerospace Drawings	I-5

PRECEDING PAGE BLANK NOT FILMED.

LIST OF FIGURES

Figure		Page
2-1	The Effect of Thermal Exposure upon Goodyear's GAC-222 Polyurethane Foam.	2-2
2-2	The Effect of Thermal Exposure upon the Zer-O-Cel Polyurethane Foam.	2-2
2-3	The Effect of Thermal Exposure upon the CPR 21-2A Polyurethane Foam.	2-3
2-4	The Effect of Thermal Exposure upon the CPR 32-2C Polyurethane Foam.	2-3
2-5	The Effect of Thermal Exposure upon the CPR 9002-2 Polyurethane Foam.	2-4
2-6	The Effect of Thermal Exposure Tests on Various Rigid Polyurethane Foams	2-5
2-7	The Effect of Thermal Exposure upon the Stafoam AA602 Polyurethane Foam.	2-7
2-8	The Effect of Thermal Exposure upon Goodyear's GAC-222 Polyurethane Foam (Postcured at 400°F for 24 Hours)	2-8
2-9	The Effect of Thermal Exposure upon the Zer-O-Cel Polyurethane Foam (Postcured at 400°F for 24 Hours)	2-8
2-10	The Effect of Thermal Exposure upon the CPR 21-2A Polyurethane Foam (Postcured at 400°F for 24 Hours)	2-9
2-11	The Effect of Thermal Exposure upon the CPR 32-2C Polyurethane Foam (Postcured at 400°F for 24 Hours)	2-9
2-12	The Effect of Thermal Exposure Tests on Various Rigid Polyurethane Foams after Curing at 400°F.	2-10
2-13	The Effect of Thermal Exposure upon the Stafoam AA605 Polyurethane Foam (Postcured Commerically at 400°F for 24 Hours)	2-11
2-14	The Effect of Thermal Exposure upon the Stafoam AA602 Polyurethane Foam (Postcured at 400°F for 24 Hours)	2-11
2-15	The Effect of Thermal Exposure upon Goodyear's GAC-222 Polyurethane Foam (Postcured at 300°F for 24 Hours)	2-12
2-16	The Effect of Additional Thermal Exposure Tests on Various Rigid Polyurethane Foams after Curing at 400°F	2-13
2-17	Thermogravimetric (TGA) and Differential Thermal Analyses (DTA) of the Zer-O-Cel Polyurethane Foam	2-14
2-18	Time-Temperature Curves for Insulation Panel Testing	2-19
2-19	Specimen Configuration for Applying Constant Load to Outer Film During Heating	2-20

LIST OF FIGURES (Continued)

Figure		Page
2-20	Simulated Insulation Panel for the Third Series of Tests	2-21
2-21	Thermogravimetric Analyses of Kapton, MAM, and Various Adhesives	2-27
2-22	Thermal Radiation Property Test Configuration	2-34
2-23	Typical Tensile Strand and Pull-Out Specimens	2-43
2-24	Typical Four Strand Tensile Pull-Out Specimen	2-44
2-25	Tensile Strand Test — Typical Load Stress Versus Strain	2-47
2-26	Creep Test Specimen	2-48
2-27	Total Linear Thermal Expansion of FF-5255, U.S. Polymeric, Inc., (20-End, S-994 — Phenolic Roving) (Parallel to Reinforcement)	2-51
2-28	Thermal Conductivity Test, Uniform Specimen, Virgin Sample, Specimen A	2-57
2-29	Thermal Conductivity Test, Uniform Specimen, Virgin Sample, Specimen B	2-57
2-30	Thermal Conductivity Test, Subjected to Aerodynamic Heating, Specimen A	2-58
2-31	Thermal Conductivity Test, Uniform Specimen, Second Run, Specimen B	2-58
2-32	Thermal Conductivity Test, Uniform Specimen, Virgin Sample, Specimen C	2-59
2-33	Thermal Conductivity Test, Uniform Specimen, Virgin Sample, Specimen D	2-59
2-34	Thermal Conductivity Test, Joint Specimen, Virgin Sample, Specimen E	2-60
2-35	Thermal Conductivity Test, Uniform Specimen, Virgin Sample, Experimental.	2-61
2-36	Strand Friction Test Apparatus.	2-62
2-37	Total Constrictive Wrap Strand Friction Force Over 45 Degrees — Lubricated.	2-64
2-38	Total Constrictive Wrap Strand Friction Force Over 45 Degrees — Vel Soap Cleaned	2-65
2-39	Total Constrictive Wrap Strand Friction Force Over 45 Degrees — Solvent Cleaned	2-65
2-40	Geometrical Relationship of a Strap in Tension over a Cylindrical Sector	2-66
3-1	Insulation Panel Thermal Model	3-4
3-2	Incident Space Heating Rates for Case 1, Table 3-1	3-5
3-3	Incident Space Heating Rates for Case 2, Table 3-1	3-6
3-4	Incident Space Heating Rates for Case 3, Table 3-1	3-6

LIST OF FIGURES (Continued)

Figure		Page
3-5	Liquid Hydrogen Heat Rate Caused by Aerodynamic and Space Heating (Sidewall Only) 25-Minute Coast Trajectory, Maximum Heating	3-8
3-6	Liquid Hydrogen Heat Rate Caused by Aerodynamic and Space Heating (Sidewall Only) 25-Minute Coast Trajectory, Maximum Heating	3-9
3-7	Liquid Hydrogen Heat Rate Caused by Aerodynamic and Space Heating (Sidewall Only) 70-Minute Coast Trajectory, Maximum Heating	3-10
3-8	Liquid Hydrogen Heat Rate Caused by Aerodynamic and Space Heating (Sidewall Only) 70-Minute Coast Trajectory, Minimum Heating	3-11
3-9	Liquid Hydrogen Heat Rate Caused by Aerodynamic and Space Heating (Sidewall Only) 25-Minute Coast Trajectory, Maximum Heating	3-12
3-10	Liquid Hydrogen Heat Rate Caused by Aerodynamic and Space Heating (Sidewall Only) 25-Minute Coast Trajectory, Maximum Heating	3-13
3-11	Centaur Balanced Thrust Venting System	3-18
3-12	Payload Loss for Fixed Insulation Foam Thicknesses	3-20
3-13	Payload Loss Versus Foam Thickness for a 25-Minute Coast Trajectory, Maximum Heating	3-21
3-14	Payload Loss Versus Foam Thickness for a 70-Minute Coast Trajectory, Maximum Heating	3-21
3-15	Payload Loss Versus Foam Thickness for a 70-Minute Coast Trajectory, Minimum Heating	3-22
3-16	Predicted Surface Temperature of 0.4-Inch Foam Versus Wind Velocity	3-23
3-17	Comparative Maximum Outside Surface Temperature for Constrictive-Wrapped Insulation (Trajectory SP47-3C) (Maximum Heating)(Includes-of-Attack Effects)	3-24
3-18	Comparative Maximum Outside Surface Temperatures for Constrictive-Wrapped Insulation (Trajectory SP-29-3C) (Nominal Heating)(Includes Angle-of-Attack Effects).	3-25
3-19	Surface Temperature Versus Flight Time for a 25-Minute Coast Trajectory; Maximum Heating	3-26
3-20	Surface Temperature Versus Flight Time for a 25-Minute Coast Trajectory, Maximum Heating	3-27
3-21	Temperature Gradient Through Fixed Foam Insulation at Maximum Erosion Cloth Temperature (after Approximately 145 Seconds of Flight)	3-28

LIST OF FIGURES (Continued)

Figure		Page
3-22	Frost Thickness Versus Film Coefficient	3-29
3-23	Payload Change Attributable to Ice on Insulation Surface Prior to Launch.	3-31
3-24	Predicted Temperatures on Hinge Fitting and Constrictive Wrap as a Function of Flight Time	3-33
3-25	Temperature Gradients on Hinge Fitting and Constrictive Wrap at the Time of Maximum Temperature	3-34
3-26	Cross-Section through Corrugated Wrap Insulation System Showing Maximum Ice Buildup	3-35
3-27	Temperature Predictions for the Aluminum Corrugated Wrap System.	3-36
3-28	Apparent Solar Absorptance Versus Solar Absorptance for a Corrugated Surface with L/h as a Parameter	3-37
4-1	Load-Strain Properties of Constrictive Wrap Materials	4-7
4-2	Wrap Pressure Versus Radial Deflection	4-13
4-3	Constrictive Wrap Design Parameters	4-13
4-4	Constrictive Wrap End Fitting Configuration	4-14
4-5	Constrictive Wrap Hinge Fitting (Zero Moment Design).	4-15
4-6	Corrugated Constrictive Wrap Concept	4-19
4-7	Corrugated Constrictive Wrap Details	4-20
5-1	MAM Covering of Foam Butt Joint.	5-5
5-2	Layup Tool after Removing the First System B Panel.	5-6
5-3	Blister in the Center of the Concave Surface of the System B DPT Test Panel	5-10
5-4	Typical Blister Showing Blister Association with Foam Voids	5-11
5-5	Priming An Insulation Panel.	5-16
5-6	Applying Adhesive Beads to an Insulation Panel	5-16
5-7	Applying Adhesive to the T-9 Tank	5-17
5-8	Installation Insulation Panels on the T-9 Tank in a Portable Plastic Clean Room	5-18
5-9	Arrangement of Insulation Panels on the T-9 Tank Material Evaluation Tests	5-19
5-10	Arrangement of Insulation Panels on the T-9 Tank Repair Technique Tests.	5-20
5-11	Patched Area on Concave Side of Panel Number 11	5-21
5-12	Damaged Area of Panel Number 6	5-22
5-13	Fiberglass Strand Curing Tool	5-24
5-14	One Operation Cure Cycle Tool.	5-25

LIST OF FIGURES (Continued)

Figure		Page
5-15	Final Configuration of Strand and Hinge Bond Cure Cycle Tool.	5-26
5-16	Pre-Loading the Fiberglass Strands Prior to Oven Cure .	5-27
5-17	Wrap Assembly Proof Testing	5-28
5-18	Constrictive Wrap Assembly Tool in Place Prior to Clamping the Constrictive Wrap	5-30
5-19	Clamping the Constrictive Wrap	5-30
5-20	Wrap Segments Completely Clamped, Hinge Pin Partially Inserted	5-31
5-21	Constrictive Wrap in Place on the T-9 Test Tank. . . .	5-31
8-1	Test Fixture Configuration for Simulated Vacuum/Heating Tests	8-2
8-2	Heat/Vacuum Tests	8-8
8-3	Prelaunch Steady-State Temperature and Pressure Gradients through Sealed Fixed Foam Insulation Panel . .	8-10
8-4	Insulation Panel Test Fixture Before Installation of Panel Specimen	8-13
8-5	Typical Installation of Specimen Panel for Configurations 1 through 4	8-14
8-6	Specimen Panel A1 Showing First Blister Formation — Back Face of Panel at Ambient Temperature Before Test .	8-16
8-7	Specimen Panel A1 Showing Maximum Blister Formation — Back Face of Panel at Ambient Temperature Before Test .	8-17
8-8	Specimen Panel B1 Showing Maximum Blister Formation — Back Face of Panel at Ambient Temperature Before Test .	8-18
8-9	Specimen Panel A3 Showing Maximum Blister Formation — Back Face of Panel at LH ₂ Temperature for 20 Minutes Before Test	8-19
8-10	Specimen Panel B3 Showing Maximum Blister Formation — Back Face of Panel at LH ₂ Temperature for 20 Minutes Before Test	8-20
8-11	Specimen Panel D2 Showing Maximum Blister Formation — Back Face of Panel at LH ₂ Temperature for 20 Minutes Before Test	8-21
8-12	Specimen Panel A6 Showing Maximum Blister Formation — Back Face of Panel at LH ₂ Temperature for 2 Hours Before Test	8-22
8-13	Specimen Panel C7 Showing Maximum Blister Formation — Back Face of Panel at LH ₂ Temperature for 2 Hours Before Test	8-23

LIST OF FIGURES (Continued)

Figure	Page
8-14 Specimen Panel D5 Showing Maximum Blister Formation -- Back Face of Panel at LH ₂ Temperature for 2 Hours Before Test	8-24
8-15 Specimen Panel E1 after Test	8-28
8-16 Specimen Panel E5 after Test	8-29
8-17 Specimen Panel E6 after Test	8-30
9-1 Sycamore Canyon S-4 Test Tower with the T-9 Test Tank Installed	9-2
9-2 T-9 Test Tank Insulation Panel Configuration for the Material Evaluation Test	9-3
9-3 Arrangement of Insulation Panels on the T-9 Tank for the Material Evaluation Tests	9-4
9-4 T-9 Test Tank Station 218.9 and Station 412.7 Tank Rings Insulation	9-5
9-5 T-9 Test Tank Insulation Panel Configuration for the Repair Technique Test	9-6
9-6 Arrangement of Insulation Panels on the T-9 Tank for the Repair Technique Tests	9-7
9-7 T-9 Test Tank Erosion Cloth Cover Installation	9-9
9-8 T-9 Test Tank Constrictive Wrap Configuration	9-10
9-9 T-9 Test Frost Determination Instrumentation	9-11
9-10 T-9 Test Tank Thermocouple Instrumentation Locations	9-12
9-11 T-9 LH ₂ Tank Pressure Cycles	9-14
9-12 T-9 Test Tank-Fixed Insulation Test Results after Six Tanking Tests	9-17
9-13 T-9 Test Tank after Sixth Tanking -- Quad I	9-20
9-14 T-9 Test Tank after Sixth Tanking -- Quad II	9-21
9-15 T-9 Test Tank after Sixth Tanking -- Quad II and III	9-22
9-16 T-9 Test Tank after Sixth Tanking -- Quad III	9-23
9-17 T-9 Test Tank after Sixth Tanking -- Quad IV	9-24
9-18 T-9 Test Tank-Fixed Insulation Test Results after Tanking Test Numbers 7 through 10	9-25
9-19 Station 412 Area of T-9 Test Tank Under Post-Buckling Load	9-27
9-20 Insulation Skin Temperature (T/C-1, T/C-2, T/C-3)	9-29
9-21 T-9 Test Tank Erosion Cloth Temperature after 60-Minute Hold.	9-30
9-22 T-9 Test Tank Erosion Cloth Temperature Versus Wind Velocity	9-32

LIST OF FIGURES (Continued)

Figure	Page
9-23	T-9 Test Tank Erosion Cloth Temperatures (Predicted and Measured) (From Figure 9-22) 9-33

LIST OF TABLES

Table	Page
2-1	Results of Differential Thermal and Thermogravimetric Analyses on Various Polyurethane Foams 2-14
2-2	Temperature Limitations of Polyurethane Foams. 2-15
2-3	Results of Sealed Foam Panel Testing 2-22
2-4	Additional Results of Sealed Foam Panel Testing. 2-23
2-5	Tensile-Shear Strengths of Adhesives 2-25
2-6	Tensile-Shear Strengths of Narmco 7343 and APCO 1252 2-26
2-7	Peel Strengths of Mylar to Mylar Bonds 2-26
2-8	Company and Government Agency Survey 2-30
2-9	Survey of Thermal Control Coating Materials 2-31
2-10	List of Additional Thermal Control Coating Materials Surveyed 2-32
2-11	List of Materials Evaluated for Thermal Radiation Properties 2-33
2-12	Surface Finish Radiation Property Test Program Results 2-38
2-13	Summary of Pre-Impregnated, 20-End, S-994 (HTS) Glass Filament Roving Strand Tests 2-46
2-14	Strand Pull-Out Shear Test (Pre-Impregnated Glass Fabric). 2-49
2-15	Strand Bond Shear Test, Pre-Impregnated Glass Fabric Plus 1-Ply Adhesive 2-50
2-16	Strand Load/Strain Values for S-994 (HTS), 20-End Roving, Phenolic Impregnated (US Polymeric, Inc. FF5255) 2-52
2-17	Compression Data on Insulation Panels 2-53
2-18	Results of Thermal Conductance Measurements on Sealed Foam Insulation (Goodyear System; MAM Film, PE-207 Adhesive, GAC-222 Foam) 2-55

LIST OF TABLES (Continued)

Table		Page
2-19	Results of Thermal Conductance Measurements on Sealed Foam Insulation (Experimental System; MAM Film, Metlbond 225 Adhesive, CPR 32-2C Foam)	2-60
3-1	Assumed Orbital Parameters	3-2
3-2	Heat Transfer through the Forward Bulkhead and Station 219 Ring, and through the intermediate Bulkhead	3-14
3-3	Payload Loss Attributable to Heat Transfer through the Forward Bulkhead and Station 219 Ring	3-15
3-4	Payload Loss Attributable to Heat Transfer through the Intermediate Bulkhead for a 25-Minute Coast Mission	3-15
3-5	Payload Loss Attributable to Heat Transfer through the Intermediate Bulkhead for a 70-Minute Coast Mission	3-15
3-6	Payload Loss with Variations in Foam and Skin Thickness and Surface Emittance.	3-17
4-1	Insulation Panel Materials	4-3
4-2	Strand Load Conditions	4-11
4-3	Constrictive Wrap Aluminum End Fitting Test Data.	4-15
4-4	Comparative Trade-Off Factors for Many Constrictive Wrap Designs	4-18
4-5	Wire Load Conditions	4-21
4-6	Fiberglass Strand Versus Aluminum Corrugation Constrictive Wrap Comparison.	4-21
5-1	Peel Test Results	5-8
5-2	Individual Acceptance Test Results for System A Panels	5-12
5-3	Individual Acceptance Test Results for System B Panels	5-13
5-4	Individual Acceptance Test Results for System C Panels	5-13
5-5	Individual Acceptance Test Results for Spare Panels	5-14
5-6	Individual Acceptance Test Results for System D Panels	5-14
5-7	Individual Acceptance Test Results for System E Panels	5-15
5-8	Summary of Panel Configurations Tested in Panel Repair Program	5-33
6-1	Fixed Insulation Weight Summary (Fiberglass Strand Constrictive Wrap Configuration)	6-2
6-2	Fixed Insulation Weight Summary (Aluminum Corrugation Constrictive Wrap Configuration)	6-3

LIST OF TABLES (Continued)

Table	Page
7-1 Comparison of Payload Losses (Fiberglass Constrictive Wrap Configuration)	7-2
7-2 Comparison of Payload Losses (Aluminum Corrugation Constrictive Wrap Configuration)	7-3
8-1 Results of Testing Sealed Foam Panels with Heat/Vacuum.	8-4
8-2 Results of Testing Dual Sealed/Unsealed Foam Panels with Heat and Vacuum	8-6
8-3 Summary of Heat/Vacuum Testing.	8-7
8-4 Simulated Cryogenic/Vacuum/Heating Test Specimen Configurations	8-12
8-5 Time/Temperature History of Blistering on Test Panels .	8-25
8-6 Analysis of Fixed Insulation Test Panels	8-26
9-1 Evaluation of Material Failures During the T-9 Material Evaluation Test	9-18
9-2 Evaluation of Material Failures During the T-9 Repair Technique Test	9-26

SUMMARY

This report presents the results of an Improved Centaur fixed insulation development program performed for NASA/LeRC by the Convair division of General Dynamics. The objective of the program was to provide a tested fixed insulation system which could be used directly on the Improved Centaur. The technology was based on the results of an earlier investigation performed by NASA/LeRC. That NASA investigation showed that it might be possible to provide an effective insulation system utilizing hermetically sealed foam panels bonded to the Centaur tank. The NASA concept also employed an outer constrictive wrap which was bonded to the panels to maintain a compressive load on the panels.

The Convair program consisted of a material evaluation phase, a thermodynamic evaluation phase, design and fabrication of insulation for a full scale test tank, performance of full scale testing, and performance of other miscellaneous tests required to support the design and analyses. Whereas the NASA concept employed a constrictive wrap which was bonded to the panels, the Convair concept differed in that it employed a removable constrictive wrap so that the constrictive force could be removed when the tank was depressurized. However, the Convair program was terminated prior to its completion when it became obvious that, within the constraints of the contract, a removable constrictive wrap could not be designed which would be rugged enough to withstand handling and flight loads, and yet be light enough so as not to severely degrade payload capability.

As a result of the material evaluation phase of the program, it was recommended that two kinds of foam be investigated, that MAM be used as the sealing laminate, and that three kinds of outer MAM-to-foam adhesives be investigated. These combinations produced five different configurations which were fabricated and tested on the full scale ground hold tanking test. In addition, as a result of optical surface coat property tests, a silicone rubber impregnated fiberglass cloth was recommended for aerodynamic erosion protection. And finally, it was recommended that high strength glass filament roving strands be used for the removable constrictive wrap.

During the thermodynamic evaluation phase of the program it was concluded that the optimum foam thickness to minimize payload loss was 0.6 inches. However, it was found that varying the foam thickness ± 0.2 inches increased the payload loss by only 12 pounds. The thermodynamic analysis also showed that the insulation must have a high emittance to minimize insulation temperatures during aerodynamic heating conditions, and that payload loss is reduced by using the lower conductivity Goodyear 222 foam as opposed to the CPR 32-2C foam. An

analysis of the effects of ice on the surface of the insulation at launch showed that a payload gain of eight pounds is realized with the fiberglass strand constrictive wrap system, due to the ablative function of the ice during boost; and a payload loss of 92 pounds occurs with the corrugated constrictive wrap system, due to ice forming in the corrugations which does not melt or ablate, but is carried into orbit.

The design and fabrication phase included five different combinations of sealed foam panels and a removable constrictive wrap employing glass filament roving strands bonded to aluminum hinge fittings. However, during fabrication two major problems arose. First, the method of manufacture had to be varied in order to obtain a strand-to-aluminum hinge fitting bond which developed the strength of the strand. And second, it was found that the glass strands were extremely sensitive to handling damage in that a significant percentage of glass in the strands could be easily fractured due to undo flexing of the strand. It was determined that special handling fixtures could be devised to limit the degree of strand flexing during handling, but this introduced a measure of "tender-loving-care", and the possibility of a high scrapage rate. Neither of these features are desirable for items of new design. Additionally, it was shown that the sealed panels could be expected to "blister" during ascent. Stretching the glass strands over these blisters could permit portions of the strands to be unsupported and susceptible to aerodynamic flutter. It was felt that a rather extensive wind tunnel program would be required to prove how susceptible the glass strand design would be to flutter, and to test design changes. Studies were performed to develop a more rugged constrictive wrap which would not be susceptible to aerodynamic flutter, but all feasible configurations were extremely heavy and severely degraded payload capability. However, failure to identify a rugged, yet lightweight, removable constrictive wrap led to the decision to terminate the program prior to its completion.

A cryogenic ground hold tanking test was performed to evaluate the adequacy of the alternate materials and to evaluate system performance. The test consisted of tanking and de-tanking a full scale Centaur stub tank six times. Several "blisters" and outer bond line failures occurred due to air cryopumping into the panels during the cryogenically tanked period, but not being able to vent fast enough during de-tanking to preclude a pressure build-up in the panels. After the six tanking cycles, three of the panels were removed and replaced with panels constructed of two different material combinations, all other blistered and/or failed areas were repaired on the remaining panels, and four additional tanking and de-tanking test cycles were performed. It was concluded that panels fabricated with the film-type outer MAM-to-foam adhesive performed the best; however, all material systems tested experienced some material failures. Additionally the 100 percent panel-to-tank bond system performed better than the grid bond system. No problems were encountered in repair of the panels,

and the repaired areas generally performed well during the following four cryogenic tanking test.

Among the miscellaneous tests performed was a series of simulated ascent trajectory tests on six-inch square panels. Two types of tests were run, one simulating ascent vacuum and heating, and another simulating ascent vacuum and heating while the panel was on a cryogenic tank. The former test was intended to determine if problems would be encountered on a relatively inexpensive, although admittedly conservative, test; and the latter test, which more realistically simulated the ascent environment, was performed because blistering problems occurred on the conservative test. These tests showed that whether the panel leaks or not, outgassing of the panel materials due to heat and vacuum occurs to an extent whereby the produced internal pressure in the panel causes the panel to blister. Evidence of this material outgassing at increased temperatures was also shown by thermogravimetric tests.

As required by contract, a complete file of all memos, analyses, reports, etc., which had been issued prior to termination of the program are on file at Convair. A complete listing of these documents, by subject, is given in Appendix I.

1

INTRODUCTION

During 1963, NASA/LeRC conducted an experimental investigation to determine the feasibility of developing a lightweight insulation system for liquid hydrogen tanks of high energy upper stage launch vehicles. These efforts are reported in NASA TN D-2685 (Reference 1-1). The investigation included impact sensitivity tests of the insulation components in the presence of liquid oxygen, aerodynamic tests in which the heating and dynamic pressure conditions were more severe than during a typical launch trajectory, and thermal performance tests of the insulation. The latter tests consisted of (1) thermal conductivity measurements on small insulation samples, (2) heat transfer measurements on insulated subscale tanks filled with liquid hydrogen, and (3) heat transfer measurements on a full scale insulated Centaur tank filled with liquid hydrogen. The insulation system as finally proposed consisted of 0.4-inch thick, two-pound per cubic foot density polyurethane foam panels hermetically sealed within a covering of a foil laminate of Mylar and aluminum. A thin layer of fiberglass cloth over the insulation provided protection from aerodynamic erosion during launch. The insulation was bonded to the tank wall using adhesive in a grid pattern. A constraining force was maintained on the insulation panels by means of a prestressed constrictive wrap of fiberglass roving which was bonded to the insulation panels while under prestress.

The insulating principle is the ability of the gases in the hermetically sealed foam to be cryopumped, thereby providing a vacuum in the foam cells. This gas evacuated system provides an efficient insulation.

This report describes the results of a follow-on program performed by Convair. The objective of the Convair program was to provide a tested and proven design of an acceptable fixed insulation system for the cylindrical section of the Centaur liquid hydrogen tank. Convair was to provide (1) a literature search and material tests to upgrade the materials used previously by taking advantage of state-of-the-art advancements, (2) thermodynamic analyses of the chosen system(s), (3) design of an insulation system for a full scale Centaur test tank, (4) insulation system tests to evaluate the material capability to withstand repeated ground tankings, and (5) measurement of propellant boil-off of an insulated tank during ground hold.

The major configuration difference from the original NASA/LeRC investigation was the development of a constrictive wrap which was removable instead of permanently bonded to the insulation under pre-strain. This requirement was necessary so that the constrictive force could be removed from the tank during the times when the tank was unpressurized.

For convenient reference to all Convair documents published during this program a bibliography is included as Appendix I. It should be noted that many document titles are duplicated in the Reference section, however, all titles are included in Appendix I so as to present one complete list of all published documents according to subject matter.

2

MATERIAL EVALUATION

An extensive materials evaluation program was conducted to update the materials previously selected by NASA/LeRC in their 1963 experimental investigation (Reference 1-1). An additional requirement was to provide material testing to support the design and manufacture of a removable constrictive wrap. The following categories of materials were evaluated: foams, adhesives, films, thermal control coatings, reinforced plastic strands, and composite insulation systems.

2.1 FOAMS

2.1.1 FOAM SURVEY RESULTS. A survey was conducted to select the most promising foams available for evaluation. The survey consisted of a review of the literature and contact of pertinent vendors and agencies to determine the best available products. The requirement for the fixed insulation program was a foam of $\leq 2 \text{ lb/ft}^3$ density capable of taking ascent heating (in the range of 550°F to 700°F) with a minimum of degradation. Reference 2-1 lists the literature, companies, and agencies which were surveyed.

It was found that inorganic foams were not commercially available in the desired density range. The high temperature organic foams such as polyimides, polybenzimidazoles, phenolics, and silicones were also unavailable in low densities. High temperature epoxies were not available in foam sheet stock, and where epoxies were available in liquid form for foam-in-place applications, they were generally low in heat resistance. The only category of foams showing promise in meeting the program's requirements were the more heat-resistant polyurethanes. The following foams were selected for the evaluation phase of the program: the Upjohn Company's CPR 9002-2, CPR 21-2A, and CPR XB 35-89B; National Gypsum's Zer-O-Cel; Expanded Rubber and Plastic Company's Stafoam AA-602; and Goodyear Aircraft Company's GAC-222. The latter was selected as a control since it was the foam used in the original NASA program. The Upjohn Company subsequently changed the designation of their CPR XB 35-89B foam to CPR 32-2C, and the newer designation is used in this report.

2.1.2 TEST EVALUATION. A preliminary test program (Reference 2-2) was established to determine which of the six commercially available polyurethane foams showed the greatest promise for use as insulation panels for the T-9 test tank. In order to accomplish this task, various tests were conducted to determine the relative high temperature characteristics of these polyurethane foams. These tests consisted of weight and dimensional stability tests, weight and dimensional stability tests of postcured foam, and thermogravimetric and differential thermal analysis tests.

2.1.2.1 Weight and Dimensional Stability Tests. The first series of tests was conducted to determine the weight and dimensional stabilities of each foam at seven elevated temperatures. The results obtained from these tests are presented in Figures 2-1 through 2-6.

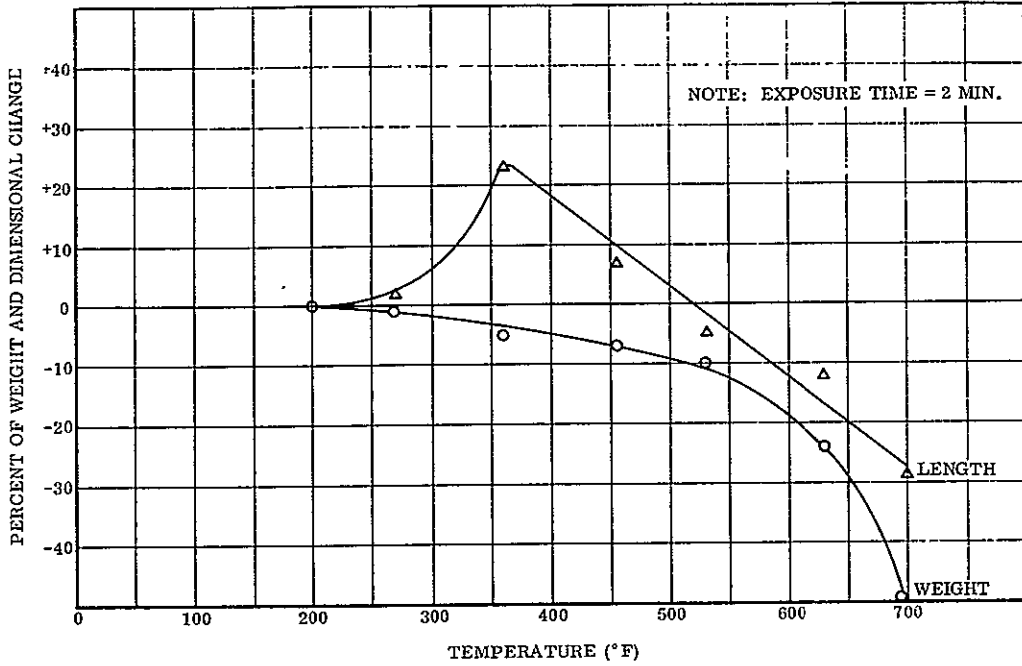


Figure 2-1. The Effect of Thermal Exposure upon Goodyear's GAC-222 Polyurethane Foam

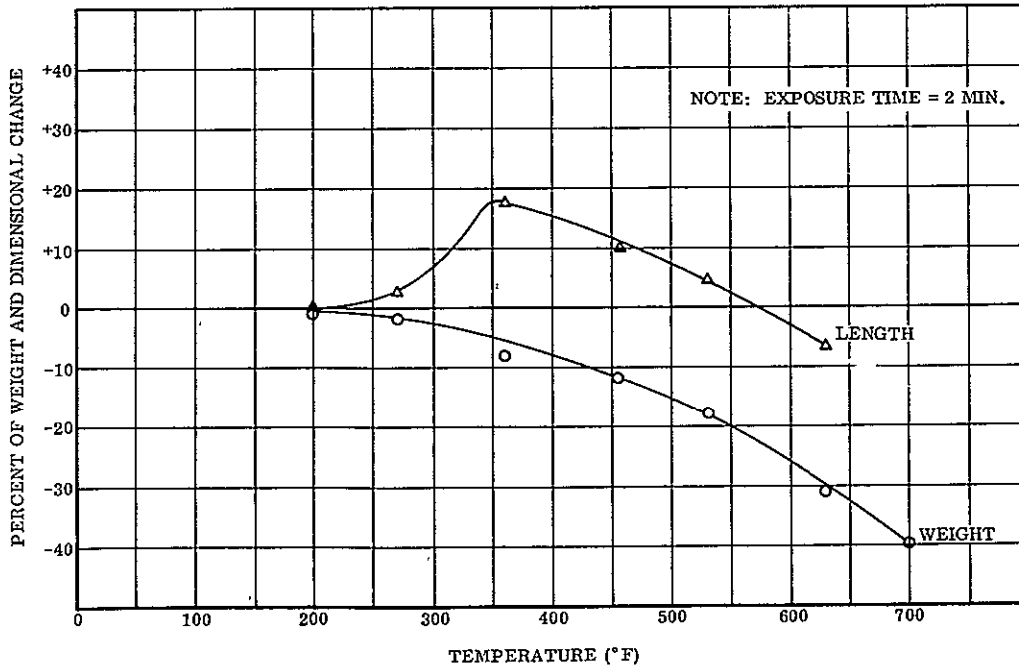


Figure 2-2. The Effect of Thermal Exposure upon the Zer-O-Cel Polyurethane Foam

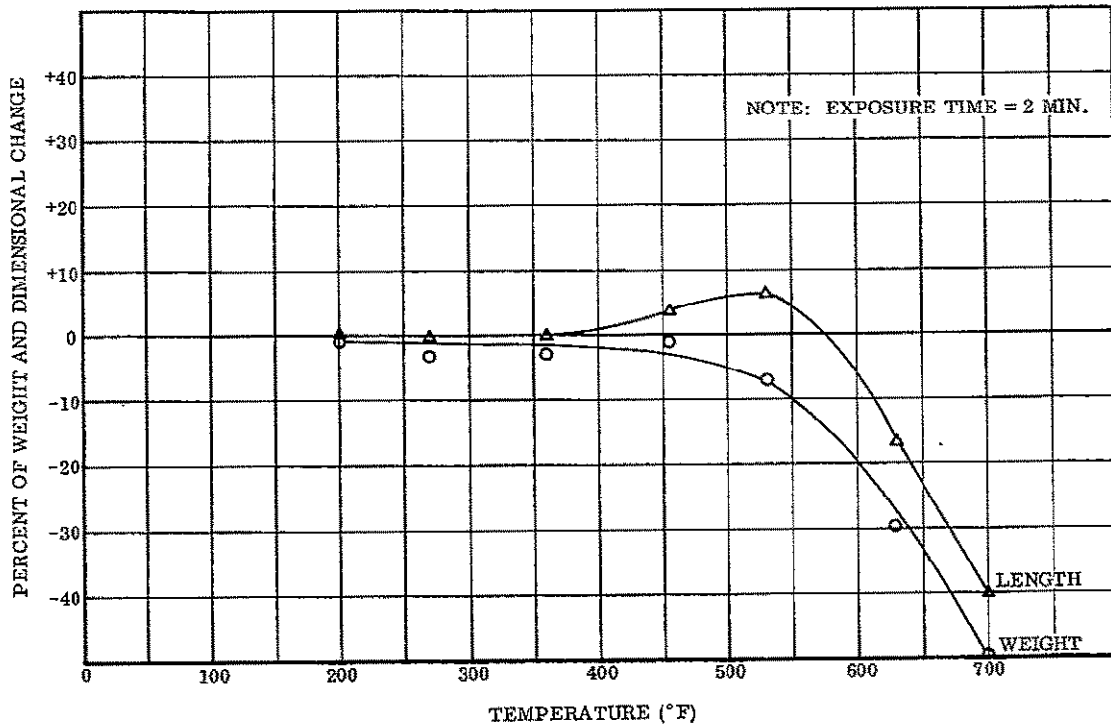


Figure 2-3. The Effect of Thermal Exposure upon the CPR 21-2A Polyurethane Foam

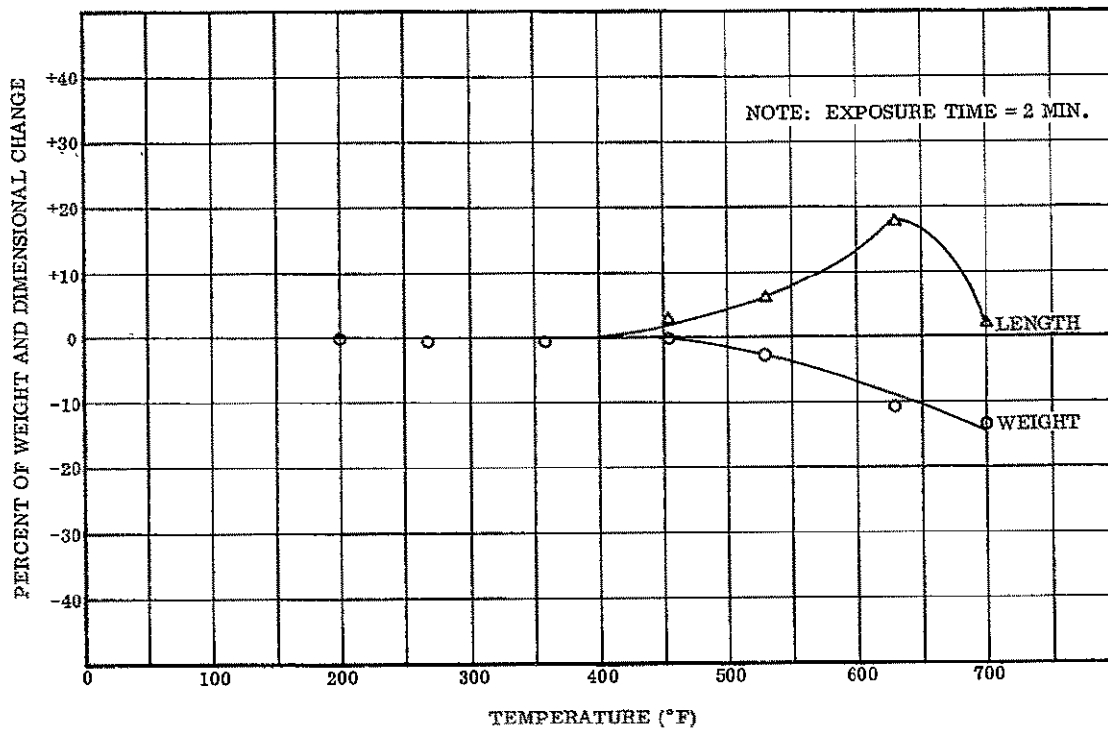


Figure 2-4. The Effect of Thermal Exposure upon the CPR 32-2C Polyurethane Foam

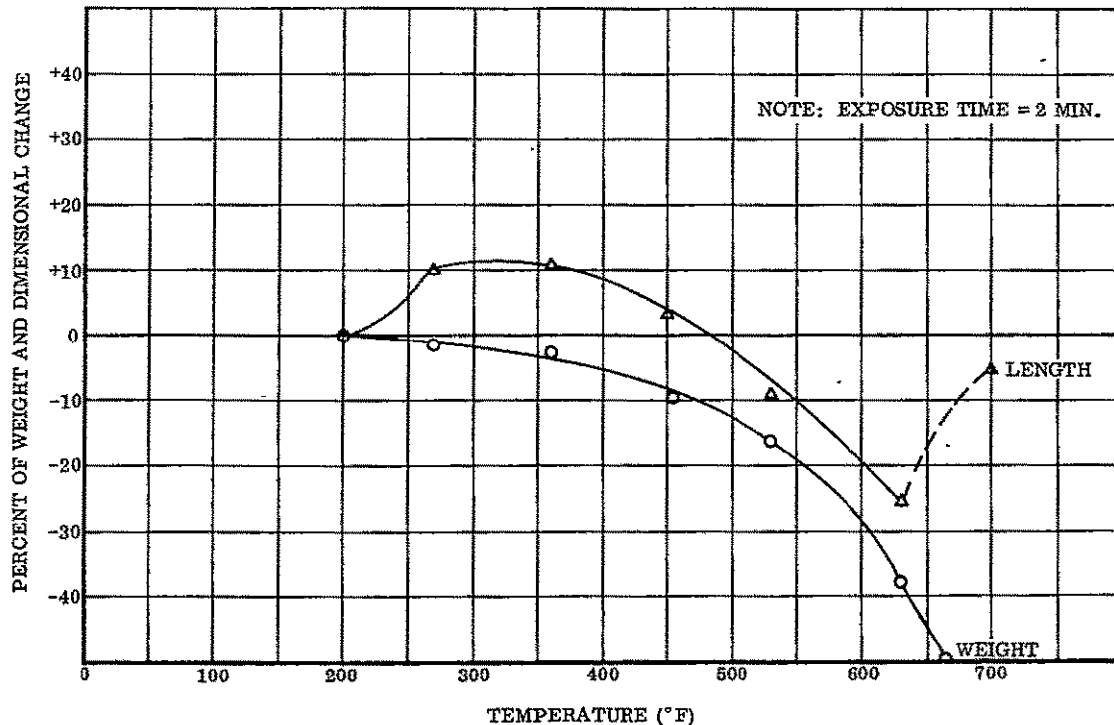


Figure 2-5. The Effect of Thermal Exposure upon the CPR 9002-2 Polyurethane Foam

The procedure used for conducting this series of tests is described below. First, a small panel of each foam was obtained from the respective manufacturers. From each panel two 1-inch by 1-inch by 3/8-inch test specimens were prepared. The specimens were then placed upon an asbestos insulation board, and a thermocouple was attached to the exposed surface of alternate specimens by tension loading. The specimens (a total of ten) were simultaneously placed into a large oven preheated to 200° F. After two minutes, the specimens were removed from the oven, allowed to cool to room temperature, and the percent of change in both the dimensions and weight of each specimen was determined. This test procedure was subsequently repeated at preset oven temperatures of 300, 400, 500, 600, 700, and 800° F. During these two-minute exposure periods, the temperatures of the oven and the surfaces of the specimens were continuously monitored.

In general, between 20 to 30 seconds elapsed before the surface temperature of the specimen reached that of the oven. Although the door of the oven was not open for more than 5 seconds, it was approximately one minute before the oven regained a nominal equilibrium temperature. Even then, the preselected temperature of the oven was never completely recovered. Therefore, the average surface temperature of the specimen during the last minute of exposure was used in plotting the data shown in Figures 2-1 through 2-5. These average temperatures were 200, 270, 345, 425, 525, 595, and 700° F, respectively.

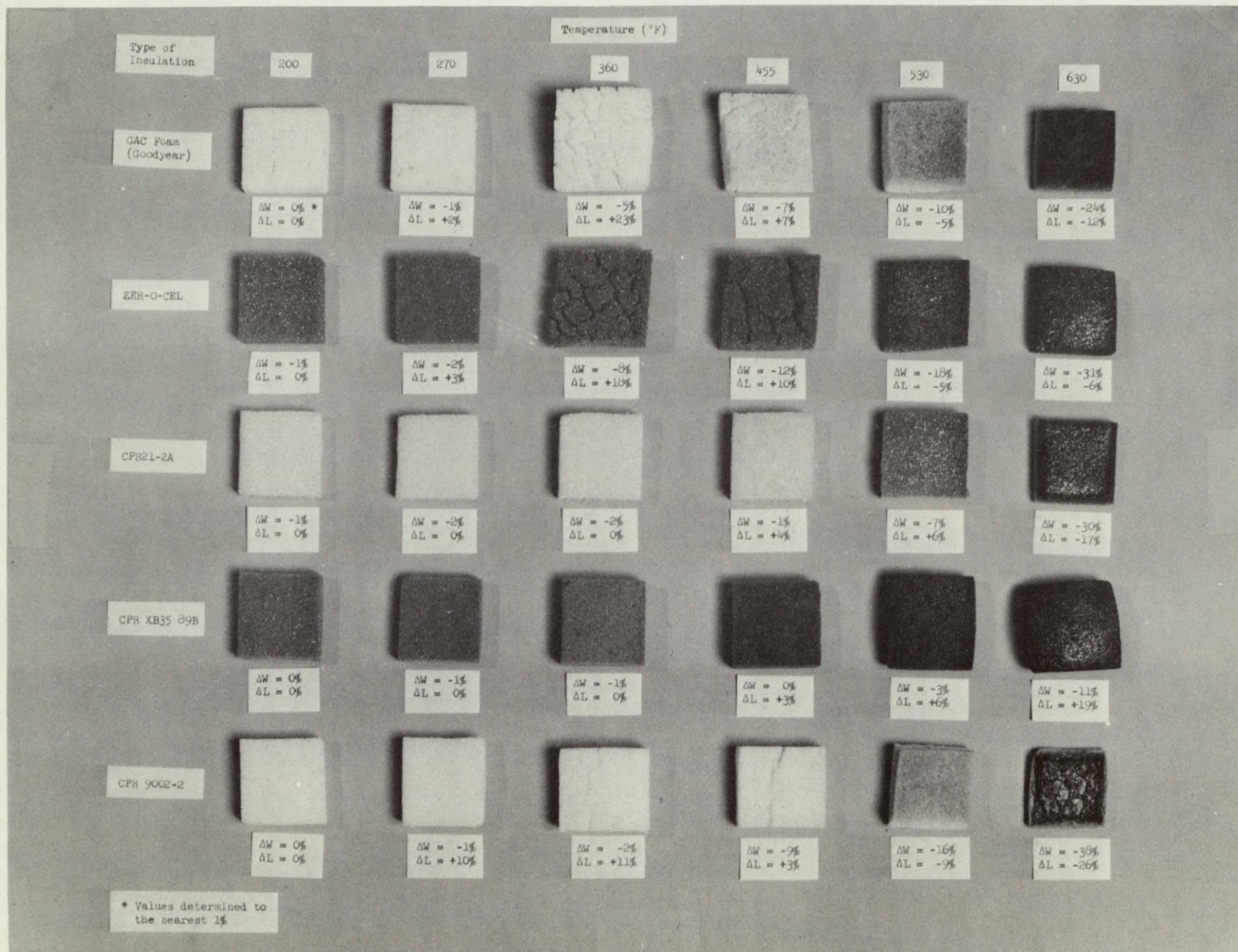


Figure 2-6. The Effect of Thermal Exposure Tests on Various Rigid Polyurethane Foams

Figure 2-6 is a photograph showing representative samples of five types of foam after being exposed to temperatures up to 630° F. The photograph shows the temperature at which severe discoloration and degradation of the foams occur. Also listed is the percentage change of weight and dimension of each foam sample for each test temperature.

Based upon the results of these tests, the CPR 32-2C and CPR 21-2A polyurethane foams were found to be the most stable at all temperatures up to 400° F. At temperatures above 400° F, the CPR 32-2C foam appeared to be the most stable. (See Figure 2-7.)

2.1.2.2 Weight and Dimensional Stability Tests of Postcured Foam. In an attempt to increase the stability characteristics of these foams, a panel of each type was subjected to a postcure treatment of 400° F for 24 hours. The CPR 9002-2 completely distorted and was, therefore, eliminated from further testing.

Again, test specimens were prepared from each panel and subsequently exposed to the thermal test series described in the previous paragraph. The results of the tests showed that the cure treatment reduced the dimensional and weight change characteristics of each foam. (See Figures 2-8 through 2-12.) Three additional panels were received and evaluated later. Stafoam AA602 and AA605 were postcured at 400° F; a Goodyear GAC-222 panel was postcured at 300° F for 24 hours. Results of these tests are presented in Figures 2-13 through 2-16. By comparing Goodyear's 300° F postcured foam with their as-received foam, no appreciable improvement was noted in either dimensional or weight change characteristics.

Figures 2-12 and 2-16 are photographs showing representative samples of seven types of foam after being postcured and then exposed to temperatures up to 700° F. The photographs show the temperature at which discoloration and degradation of the foams occur. Also listed is the percentage change of weight, and length and thickness dimensions of each foam sample for each test temperature.

In order to determine the effect a postcure treatment may have had upon the thermal conductivity of these foams, conductivity measurements were made on a CPR 9002-2 foam in the as-received and the 400° F postcure conditions. The apparent thermal conductivity of the as-received foam was found to increase from 0.15 to 0.22 $\frac{\text{BTU-in.}}{\text{ft}^2\text{-hr.}-^\circ\text{F}}$ in the postcured condition. Both of these measurements were obtained by the "Line-source Method" at room temperature (Reference 2-3).

2.1.2.3 Thermogravimetric and Differential Thermal Analysis Tests. To determine the minimum temperatures at which initial and subsequent weight losses can be expected, a thermogravimetric analysis (TGA) was conducted on each of the as-received foams. A differential thermal analysis (DTA) was also made to determine the temperatures at which any detrimental endothermic or exothermic reactions will occur. These reactions are primarily due to thermal decomposition and oxidative decomposition, respectively. The liberation of volatile constituents is probably responsible for most of the endothermic reaction (thermal decomposition).

Figure 2-17 shows the results of these analyses on the Zer-O-Cel foam and are typical of results obtained for all the other foams. The first or upper curve represents the percent of weight loss occurring at the various temperatures. Point A indicates where the initial weight loss occurred. This weight loss appears to have resulted from the endothermic reaction shown by the two lower DTA curves. The first indication of this endothermic reaction is noted by point B. The temperature at point B is slightly lower than at A, indicating the greater sensitivity of the differential thermal analysis. This greater sensitivity was also noted for the CPR 32-2C specimens. With this foam, a slight endothermic reaction was noted; however, no distinct weight loss was observed. (See Table 2-1.)

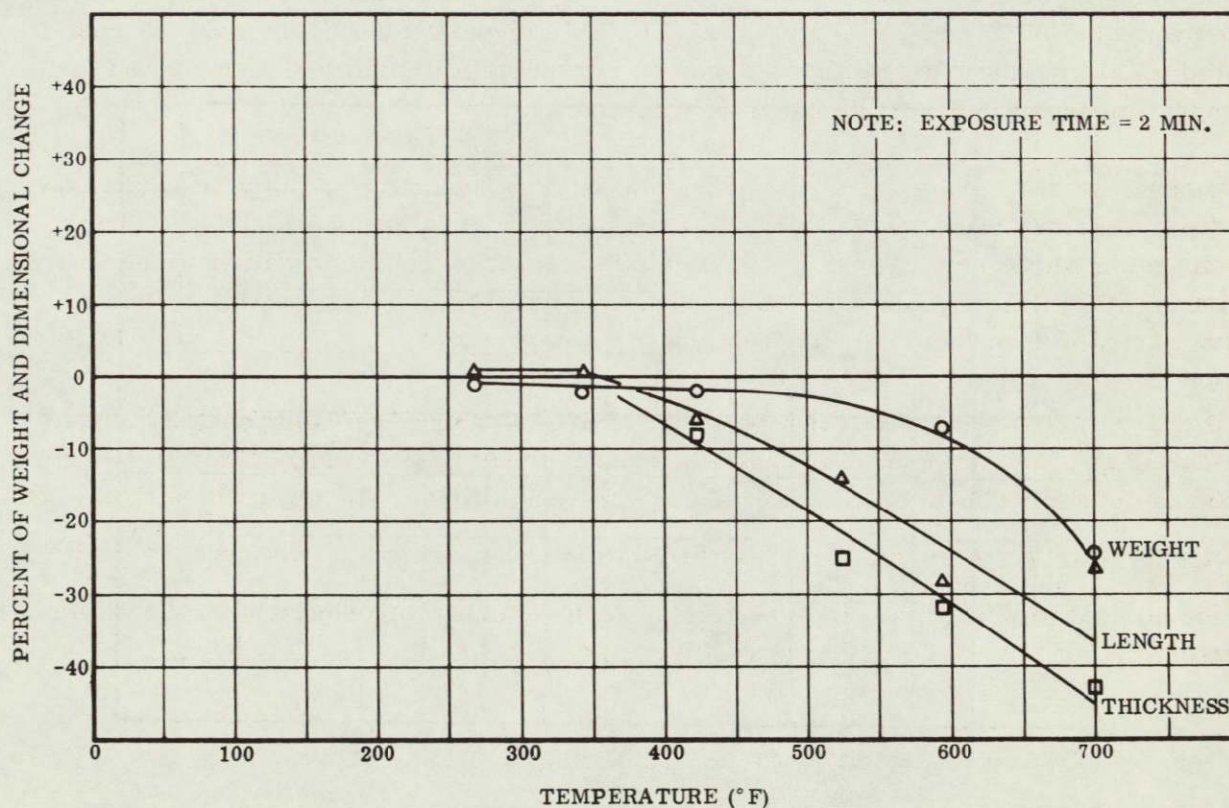


Figure 2-7. The Effect of Thermal Exposure upon the Stafoam AA602 Polyurethane Foam

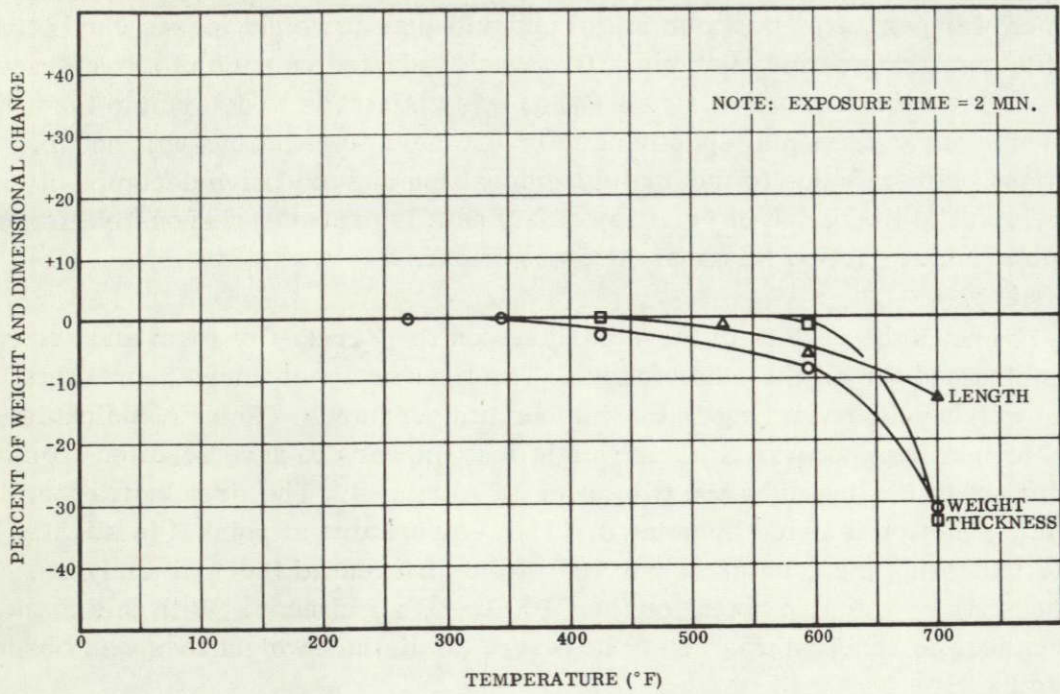


Figure 2-8. The Effect of Thermal Exposure upon Goodyear's GAC-222 Polyurethane Foam (Postcured at 400°F for 24 Hours)

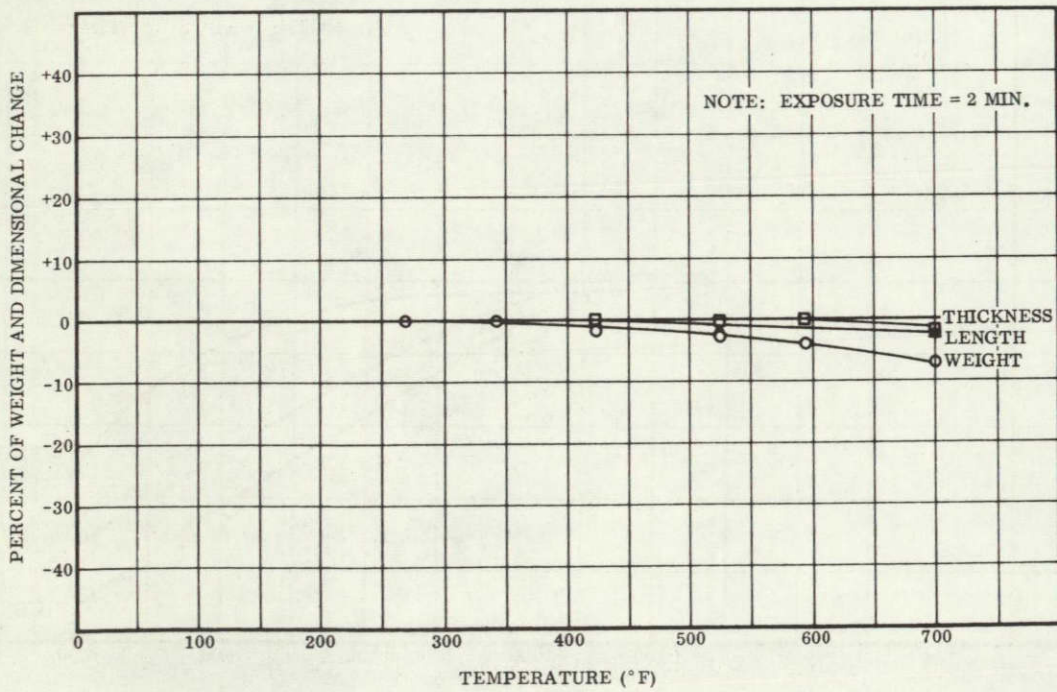


Figure 2-9. The Effect of Thermal Exposure upon the Zer-O-Cel Polyurethane Foam (Postcured at 400°F for 24 Hours)

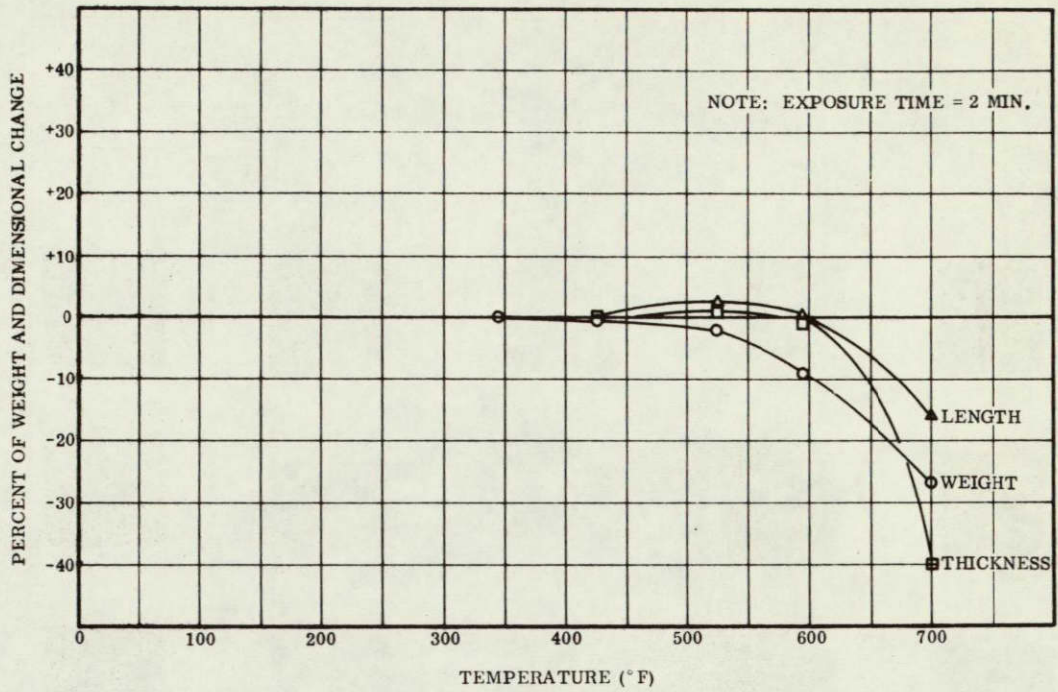


Figure 2-10. The Effect of Thermal Exposure upon the CPR 21-2A Polyurethane Foam (Postcured at 400° F for 24 Hours)

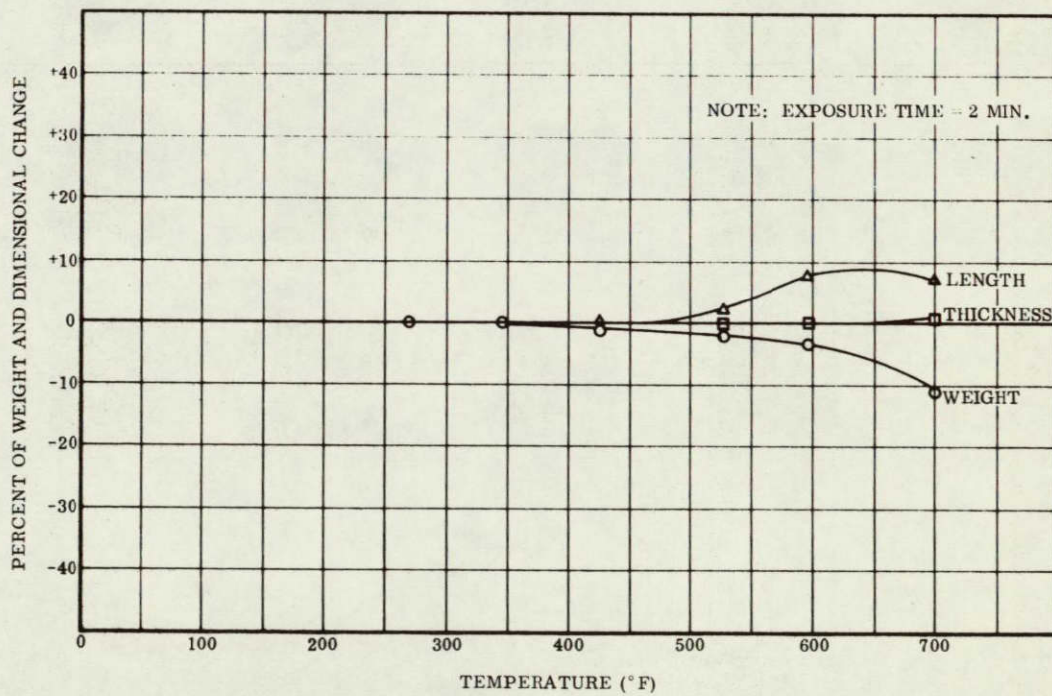


Figure 2-11. The Effect of Thermal Exposure upon the CPR 32-2C Polyurethane Foam (Postcured at 400° F for 24 Hours)

TEMPERATURE (°F)

Type of
Insulation

270

345

425

525

595

700

GAC Foam
(Goodyear)

$\Delta W = 0\%$
 $\Delta L = +2\%$
 $\Delta t = 0\%$

$\Delta W = 0\%$
 $\Delta L = 0\%$
 $\Delta t = 0\%$

$\Delta W = -3\%$
 $\Delta L = 0\%$
 $\Delta t = 0\%$

$\Delta W = -1\%$
 $\Delta L = -1\%$
 $\Delta t = 0\%$

$\Delta W = -0\%$
 $\Delta L = -6\%$
 $\Delta t = -1\%$

$\Delta W = -31\%$
 $\Delta L = -13\%$
 $\Delta t = -33\%$

ZER-O-CEL

$\Delta W = 0\%$
 $\Delta L = 0\%$
 $\Delta t = 0\%$

$\Delta W = 0\%$
 $\Delta L = 0\%$
 $\Delta t = 0\%$

$\Delta W = -2\%$
 $\Delta L = 0\%$
 $\Delta t = 0\%$

$\Delta W = -3\%$
 $\Delta L = -1\%$
 $\Delta t = 0\%$

$\Delta W = -4\%$
 $\Delta L = 0\%$
 $\Delta t = 0\%$

$\Delta W = -7\%$
 $\Delta L = -2\%$
 $\Delta t = -1\%$

CPR21-2A

$\Delta W = 0\%$
 $\Delta L = 0\%$
 $\Delta t = 0\%$

$\Delta W = 0\%$
 $\Delta L = 0\%$
 $\Delta t = 0\%$

$\Delta W = -1\%$
 $\Delta L = 0\%$
 $\Delta t = 0\%$

$\Delta W = -2\%$
 $\Delta L = +3\%$
 $\Delta t = +1\%$

$\Delta W = -0\%$
 $\Delta L = +1\%$
 $\Delta t = 0\%$

$\Delta W = -27\%$
 $\Delta L = -10\%$
 $\Delta t = -40\%$

CPH KB35 09B

$\Delta W = 0\%$
 $\Delta L = 0\%$
 $\Delta t = 0\%$

$\Delta W = 0\%$
 $\Delta L = 0\%$
 $\Delta t = 0\%$

$\Delta W = -1\%$
 $\Delta L = 0\%$
 $\Delta t = 0\%$

$\Delta W = -2\%$
 $\Delta L = +2\%$
 $\Delta t = 0\%$

$\Delta W = -3\%$
 $\Delta L = +2\%$
 $\Delta t = 0\%$

$\Delta W = -11\%$
 $\Delta L = +7\%$
 $\Delta t = +1\%$

Stafom
AA502
($\rho = 3.5 \text{ lb/ft}^3$)

$\Delta W = -1\%$
 $\Delta L = 0\%$
 $\Delta t = 0\%$

$\Delta W = -1\%$
 $\Delta L = +1\%$
 $\Delta t = +3\%$

$\Delta W = -1\%$
 $\Delta L = +4\%$
 $\Delta t = +7\%$

$\Delta W = -2\%$
 $\Delta L = +2\%$
 $\Delta t = +2\%$

$\Delta W = -4\%$
 $\Delta L = 0\%$
 $\Delta t = +1\%$

$\Delta W = -21\%$
 $\Delta L = -10\%$
 $\Delta t = +10\%$

Figure 2-12. The Effect of Thermal Exposure Tests on Various Rigid Polyurethane Foams after Curing at 400°F

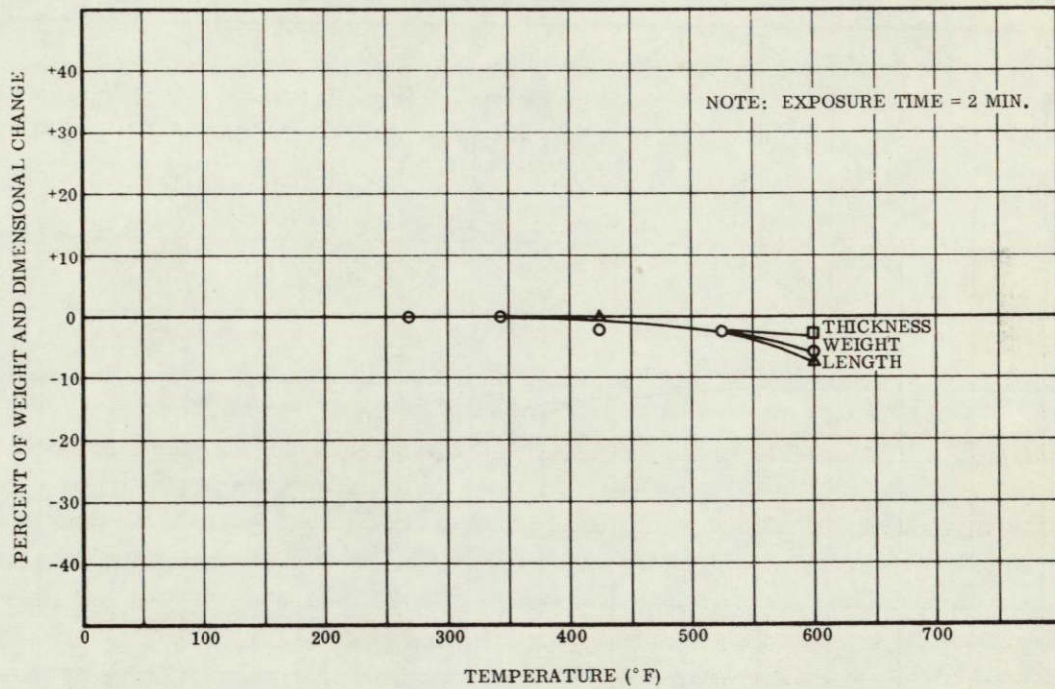


Figure 2-13. The Effect of Thermal Exposure upon the Stafoam AA605 Polyurethane Foam (Postcured Commercially at 400°F for 24 Hours)

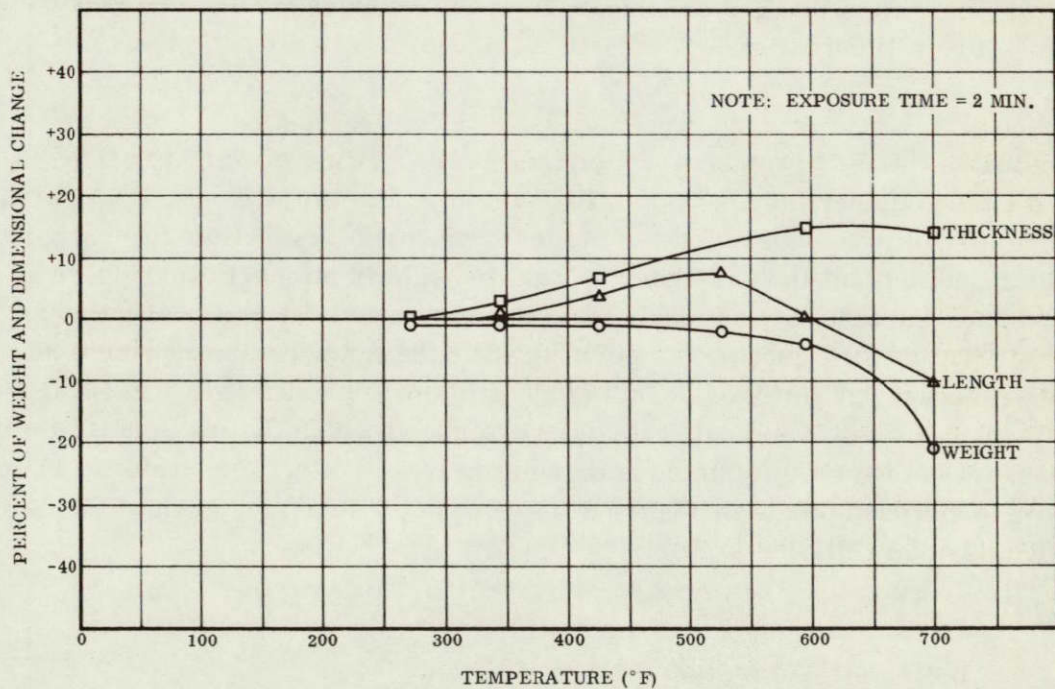


Figure 2-14. The Effect of Thermal Exposure upon the Stafoam AA602 Polyurethane Foam (Postcured at 400°F for 24 Hours)

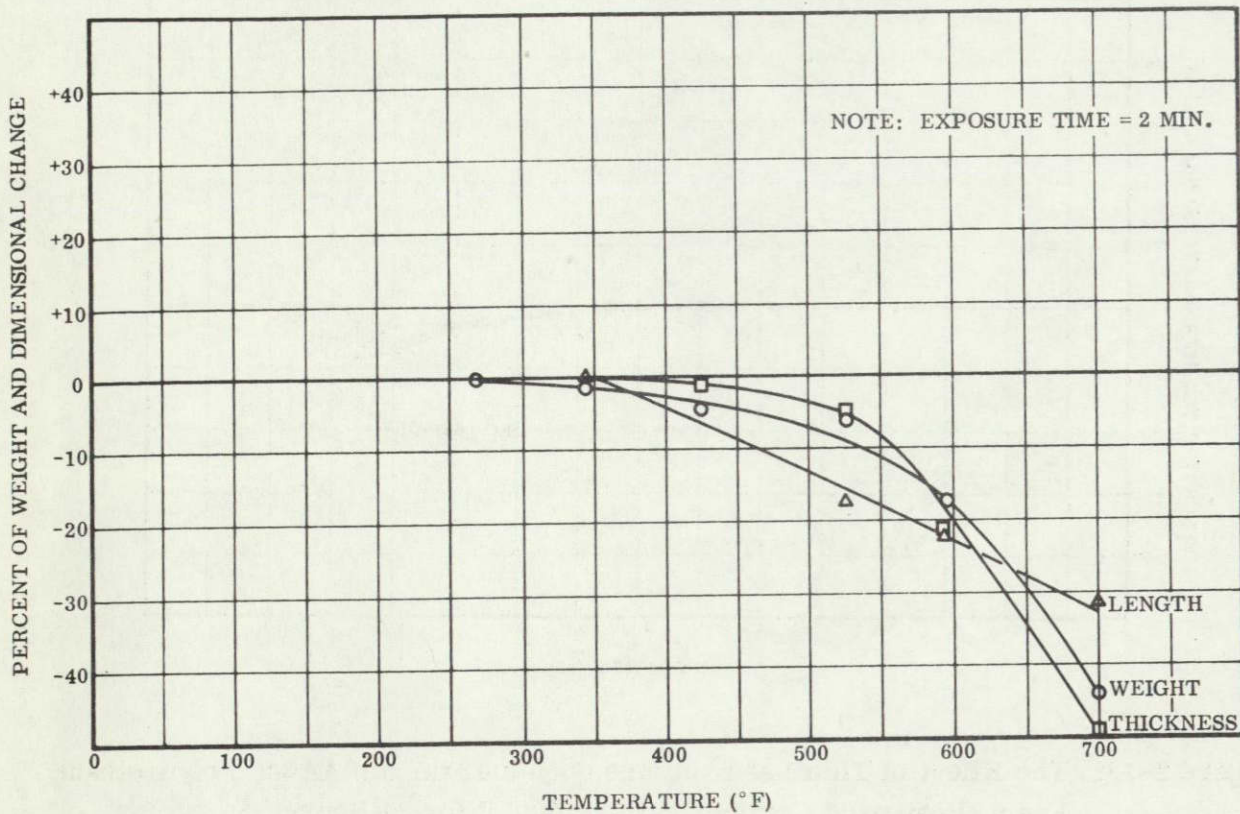


Figure 2-15. The Effect of Thermal Exposure upon Goodyear's GAC-222 Polyurethane Foam (Postcured at 300° F for 24 Hours)

Point C indicates the temperature at which the maximum rate of weight change was observed for the endothermic reaction. By examining the two lower or DTA curves, no exothermic reactions were noted for the foam when run in a helium atmosphere. Therefore, by noting that the endothermic reaction rate in an inert atmosphere is relatively constant and that only an exothermic reaction could cause a positive slope at point D for "DTA-in-air" curve, this point must be the temperature at which the exothermic reaction was initiated. This point is also reflected by the weight loss curve (TGA) by point E. Point F indicates the temperature at which the maximum rate of weight change was observed for this exothermic reaction. The temperatures indicated by the above-mentioned points in Figure 2-17 were determined for each of the as-received foams and are listed in Table 2-1.

TEMPERATURE (°F)

Type of Insulation	270	345	425	525	595	700
Stafoam AA605						
	$\Delta W = 0\%$ $\Delta L = 0\%$ $\Delta t = 0\%$	$\Delta W = 0\%$ $\Delta L = 0\%$ $\Delta t = 0\%$	$\Delta W = -2\%$ $\Delta L = 0\%$ $\Delta t = 0\%$	$\Delta W = -2\%$ $\Delta L = -2\%$ $\Delta t = -2\%$	$\Delta W = -6\%$ $\Delta L = -7\%$ $\Delta t = -3\%$	
Stafoam * AA602 ($\rho = 3.5 \text{ lb/ft}^3$)						
	$\Delta W = -1\%$ $\Delta L = +1\%$ $\Delta t = 0\%$	$\Delta W = -2\%$ $\Delta L = +1\%$ $\Delta t = 0\%$	$\Delta W = -2\%$ $\Delta L = -6\%$ $\Delta t = -3\%$	$\Delta W = -2\%$ $\Delta L = -14\%$ $\Delta t = -25\%$	$\Delta W = -7\%$ $\Delta L = -26\%$ $\Delta t = -32\%$	$\Delta W = -24\%$ $\Delta L = -26\%$ $\Delta t = -43\%$
GAC Foam ** (Goodyear) (300°F cure)						
	$\Delta W = 0\%$ $\Delta L = 0\%$ $\Delta t = 0\%$	$\Delta W = -1\%$ $\Delta L = +1\%$ $\Delta t = +1\%$	$\Delta W = -4\%$ $\Delta L = -4\%$ $\Delta t = -1\%$	$\Delta W = -6\%$ $\Delta L = -17\%$ $\Delta t = -5\%$	$\Delta W = -17\%$ $\Delta L = -22\%$ $\Delta t = -21\%$	$\Delta W = -44\%$ $\Delta L = -31\%$ $\Delta t = -49\%$

* as-received condition
 ** cured at only 300°F for 24 hrs. prior to test

2-13

Figure 2-16. The Effect of Additional Thermal Exposure Tests on Various Rigid Polyurethane Foams after Curing at 400° F

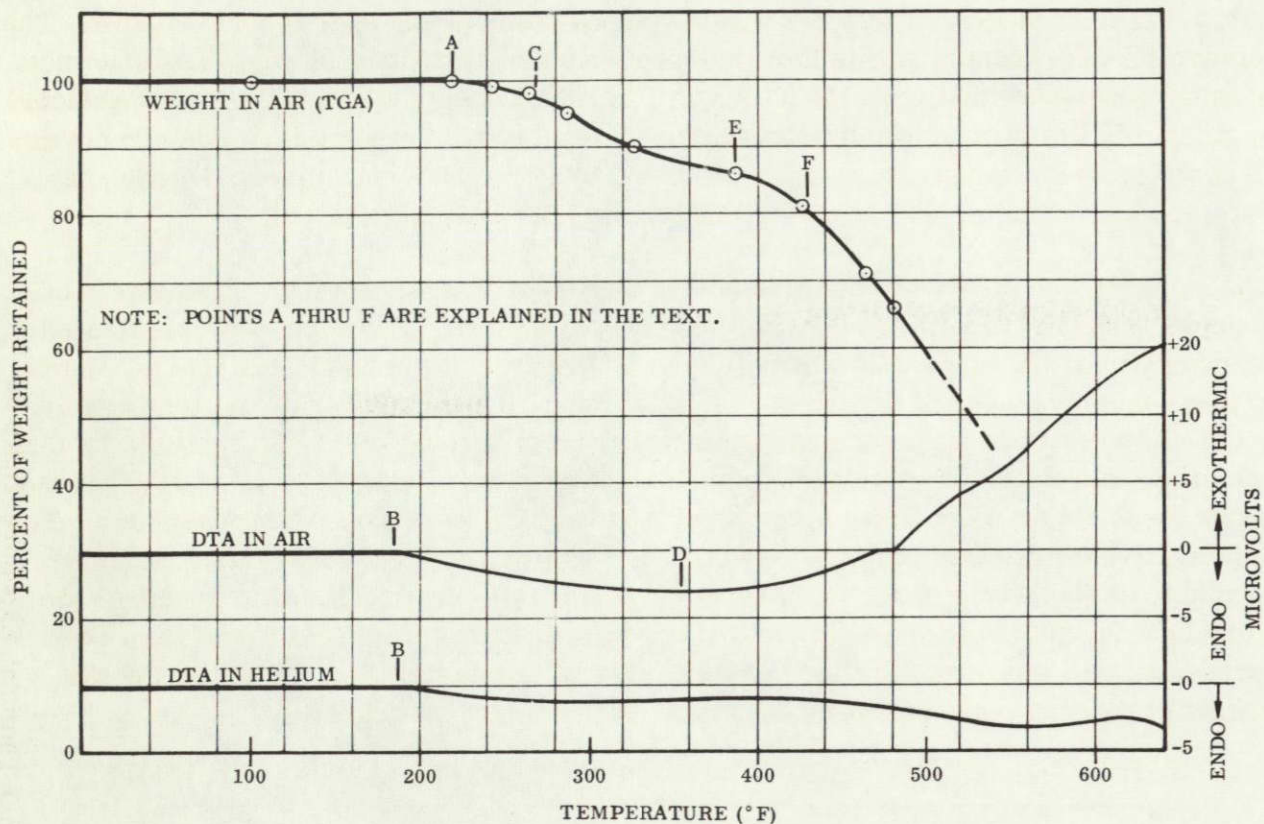


Figure 2-17. Thermogravimetric (TGA) and Differential Thermal Analyses (DTA) of the Zer-O-Cel Polyurethane Foam

TABLE 2-1. RESULTS OF DIFFERENTIAL THERMAL AND THERMOGRAVIMETRIC ANALYSES ON VARIOUS POLYURETHANE FOAMS

Type of Foam	Differential Thermal Analysis (Temp. at which 1st indication of a reaction occurred)		Thermogravimetric Analysis			
			Temp. at Max. Rate of ΔW (°F)		Temp. at Initial ΔW (°F)	
	Point B Endo.	Point D Exo.	Point C Endo.	Point F Exo.	Point A Endo.	Point C Exo.
GAC-222	190	410	250	515	220	445
Zer-O-Cel	185	355	270	430	212	390
CPR 21-2A	190	455	no endo	460	no endo	390
CPR 32-2C	190	380	no endo	470	no endo	425
CPR 9002-2	190	460	260	480	220	410
Stafoam AA602	190	410	(no test)	(no test)	(no test)	(no test)

2.1.3 CONCLUSIONS. Table 2-2 was developed from all the data reported above. The temperatures presented in this table are probably somewhat conservative because most of them were generated from the TGA and DTA tests. Since these tests were conducted at relatively low heating rates (temperature rise rate = 10°F per min.), they do not reflect the optimum temperature capabilities of the foams. During an actual flight, temperature rise rates of 360° to 700° F per minute have been anticipated.

The foam may be allowed to degrade somewhat and still be acceptable. The extent of acceptable degradation would depend upon several factors. However, it would depend primarily upon the method of fabrication and the design of the insulation panels. Each of these factors requires evaluation. For example, if the maximum foam temperature occurs at an altitude where the environmental pressure level is considerably lower than one atmosphere, the temperature limits listed in Table 2-2 may have to be reduced because these limits were based upon an environmental pressure of one atmosphere. The primary reason for this possible reduction is the absence of the restraining pressure available at one atmosphere. It is expected that if this investigation had been extended to include the 400° F postcured foams, these temperature limitations would have been increased. As discussed earlier, an indication of this fact was observed during the series of thermal exposure tests conducted on the postcured foams.

TABLE 2-2. TEMPERATURE LIMITATIONS OF POLYURETHANE FOAMS

Type of Foam	Safe Allowable Temp. (°F)	Maximum Recommended Use Temp. (°F)	Probable Failure Temp. Range (°F)
GAC-222	190	220	220 to 360
Zer-O-Cel	185	212	212 to 360
CPR 21-2A	200	390	390 to 630
CPR 32-2C	270	425	425 to 630
CPR 9002-2	190	220	220 to 360
Stafoam AA602	190	—	—
Definitions of above temperature limits:			
Safe Allowable Temp. = lowest temperature at which no reaction occurred nor any visual, dimension, or weight changes were observed.			
Max. Recommended Use Temp. = lowest temperature at which the first indication of a weight or dimensional change was observed.			
Probable Failure Temp. Range = temperature range at which failure of insulation panel composite may be attributed to foam.			

Although these tests do not simulate the exact thermal environmental conditions normally encountered during flight, they do provide a means for determining the relative stabilities and temperature limitations of each foam. Since it is desirable to evaluate insulation panels identical to those to be used in flight, an attempt was made to fabricate such panels (at a reduced size) and expose them to the anticipated thermal environment. The details of the fabrication procedures used and the tests conducted on these panels are described in Section 8.

2.2 ADHESIVES

The fixed insulation concept as developed by NASA/LeRC required the use of adhesives in several distinct areas. These adhesives had to have distinctly different capabilities for each area. The sealed foam insulation panels were prepared by bonding laminated films to both surfaces of foam sheet stock and then completely sealing the foam panels with bonded edge channels. The adhesive joint on the tank side of the panel had to be capable of cooling rapidly to the boiling point of liquid hydrogen (-423°F), while the adhesive joint on the external face of the panel had to be capable of taking rapid chilling to approximately -50°F followed by rapid heating to approximately 550°F . A third adhesive bond was used to bond the sealed panels to the Centaur tank, and this joint had to be capable of withstanding the rapid cooldown to -423°F . A fourth adhesive bond was used to attach an erosion resistant material to the outer laminated film. In addition to withstanding rapid heating to approximately 550°F , this latter adhesive had to be compatible with the erosion resistant material, which in the Convair concept was a silicone rubber impregnated glass fabric.

2.2.1 SURVEY RESULTS. A literature survey (Reference 2-4) was conducted at the start of the program to investigate the availability of low temperature curing adhesives capable of withstanding the design requirements for the high and low temperature applications. A number of vendors were also contacted during this survey in an effort to determine the best possible adhesives for the program.

The survey indicated that polyurethanes offered the greatest promise for the cryogenic applications. It was decided to evaluate Whittaker Corporation's Narmco 7343 and Applied Plastics Company's 1252 along with various primers and additives for the cryogenic applications. Very little data was available on low temperature curing adhesives for high temperature applications. It was decided to evaluate:

1. General Electric Company's 585 and RTV-108,
2. Dow Corning's 92-018 and DC-282,
3. Leffingwell Chemical Company's 211,
4. American Cyanamid's BXR-116A,
5. Shell Chemical Corporation's Epon 934 and Epon 956,
6. Applied Plastics Company's 1252/1252V, and
7. Isochem Resin Corporation's 460.

The above seven adhesives are all room-temperature curing systems. Therefore, it was decided to also evaluate Whittaker Corporation's Metlbond 225 and Adhesives Engineering's Aerobond 3021, which cure at temperatures as low as 200°F. Goodyear Aerospace Corporation's Vitel PE-207 (used in the original NASA/LeRC program for bonding laminated films to both sides of foam sheet stock), was carried along as a control in the Convair program. Limiting criteria for the cure temperature was selection of a temperature which would not degrade the thermal properties of the foam or the flexibility of the film.

2.2.2 TEST RESULTS.

2.2.2.1 Foam-To-MAM Internal Bond Adhesive. The adhesive candidates for the foam-to-MAM bond on the internal surface were Narmco 7343, APCO 1252/1252V, and Vitel PE-207, the latter being used in the original NASA/LeRC program. All three systems will give bond strengths far in excess of the shear strengths or tensile strengths of the candidate foam systems. The Vitel PE-207 is a heat sealable polyester adhesive having a maximum of approximately 28 percent solids. For spray application, a 10 percent solids solution is normally used. Both the Narmco 7343 and the Vitel PE-207 are colorless in thin films, whereas, the APCO 1252/1252V is a polyurethane adhesive containing a violet dye which has been used successfully in production for bonding foam panels to the forward bulkhead of the Centaur. The dye allows assurance of uniform adhesive coverage of a specified thickness.

A full-scale sealed foam panel was fabricated using the APCO 1252/1252V adhesive. This panel was then compared to an old panel which had been built approximately four years earlier by Goodyear with the Vitel PE-207 adhesive. Flexing of the old panel revealed large unbonded areas, while flexing of the APCO 1252/1252V bonded panel revealed no unbonded areas. The importance of having a complete bond is to minimize cryopumping.

Because of tight schedules and the fact that the T-9 tank test panels were subcontracted to Goodyear Aircraft Company, the foam-to-MAM bond on the internal surface was designated to be made with Vitel PE-207. The reasoning behind this decision was that (1) Goodyear had used the Vitel PE-207 adhesive in making all the panels for the previous NASA/LeRC program, (2) Goodyear had never handled the APCO 1252/1252V system, and (3) Goodyear had existing processes and specifications for bonding with Vitel PE-207 but would have to go through a costly and time consuming learning program to be able to prepare panels with the polyurethane system.

The Vitel PE-207 was tested to support the writing of a Convair specification (GDC 0-00844). The following results were obtained:

1. Viscosity:

Using a Brookfield Viscometer (Model LVF) the following viscosities were determined:

Base	295 cps
Hardener	2190 cps

2. Resin Solids:

Determined per ASTM-D-1259

Base	29%
Hardener	98.5%

3. Tensile Shear Strength:

The specimens were tested in accordance with ASTM-D-1002, except that the adherends were Mylar.

The Mylar was washed with trichloroethylene, followed with a dry cheesecloth wipe and a distilled water rinse. Each adherend was then coated with approximately 0.001 inch of adhesive and allowed to air dry for two hours. The adherends were then mated, giving an 0.50-inch overlap, and placed in a vacuum bag (25 inches of mercury minimum). The overlap was sealed through the bag at a temperature of $265^{\circ}\text{F} \pm 20^{\circ}\text{F}$. Tensile shear strengths (psi) were:

<u>Room Temperature</u>	<u>-320° F</u>
208	204
224	236
221	239
207	186
2222	1178

Based on the test results, GDC Specification 0-00844 was issued with the following requirements:

<u>Property</u>	<u>Requirement</u>	
	<u>Base</u>	<u>Hardener</u>
Viscosity, centipoises	295 ± 25	2190 ± 200
Resin Solids, percent	28 ± 2	98.5 ± 1
Tensile Shear Strength:		
Room Temperature	160 psi minimum	
-320° F	160 psi minimum	

2.2.2.2 Foam-To-MAM External Bond Adhesive. Three series of tests were conducted to evaluate the candidate high temperature adhesives for use on the foam-to-MAM bond external surface. All testing involved the use of one or the other of the time-temperature curves shown in Figure 2-18.

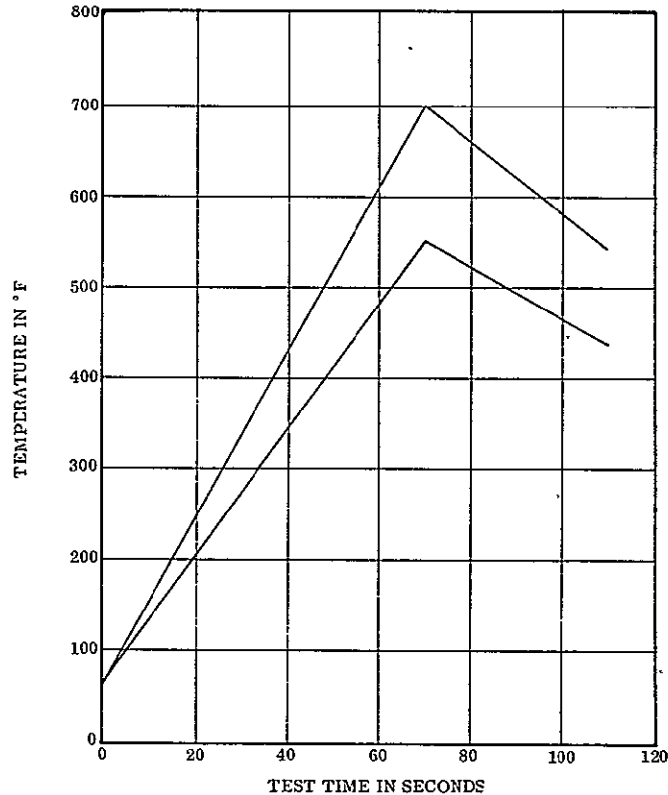


Figure 2-18. Time-Temperature Curves for Insulation Panel Testing

The first series of tests were performed to evaluate the adhesion of DuPont's Kapton polyimide film to foam with various adhesives. A typical 1-inch wide shear specimen was fabricated with foam as one adherend and 2-mil Kapton as the other. In the first two specimens fabricated, one with Vitel PE-207 adhesive and the other with Applied Plastics Company's 1252/1252V, the foam used was CPR's 9002-2 (0.5-inch thick). A thermocouple was inserted in the bondline. The specimen was mounted vertically and a one-pound weight hung from the Kapton film. The specimen was then heated with a quartz lamp bank following the 700° F time-temperature curve on Figure 2-18. In both cases, the foam split open and caused the thermocouple to drop out at a temperature of approximately 500° F. At this point, a switch was made to CPR's 32-2C (0.6-inch thick) foam. Three adhesives were evaluated, i.e., General Electric's 585, Applied Plastics Company's 1252/1252V, and Goodyear's Vitel PE-207.

Two specimens were tested with the APCO 1252/1252V, one after a 24-hour cure and the other after the recommended 72-hour cure. The specimen with the 24-hour cure began to bubble at 600°F and fell apart at 675°F. The specimen with the 72-hour cure as well as the Vitel PE-207 and GE 585 specimens revealed some degradation of the bondline after completion of the 700°F time-temperature curve. However, all three specimens did remain intact.

In the second series of tests, a new specimen configuration (Figure 2-19) was used. Four specimens were fabricated using Vitel PE-207 adhesive, MAM film, and four different foams. Stainless steel film was bonded to the MAM to assure uniform heat distribution. Thermocouples were located at the MAM-foam interface.

The specimen was mounted vertically and a one-pound weight hung from the MAM and stainless steel film. Again the 700°F time-temperature curve of Figure 2-18 was followed. Specimen Number 1, using the GAC foam, failed at the MAM-stainless steel interface upon reaching a temperature of 600°F. Specimen Number 2, using the CPR 21-2A foam, failed at the foam-MAM interface at 625°F. Specimen Number 3, using the CPR 32-2C foam, also failed at the foam-MAM interface at 660°F. Specimen Number 4, using Zer-O-Cel foam failed in the foam at 655°F. In all of the tests, the MAM film remained intact and revealed no apparent degradation.

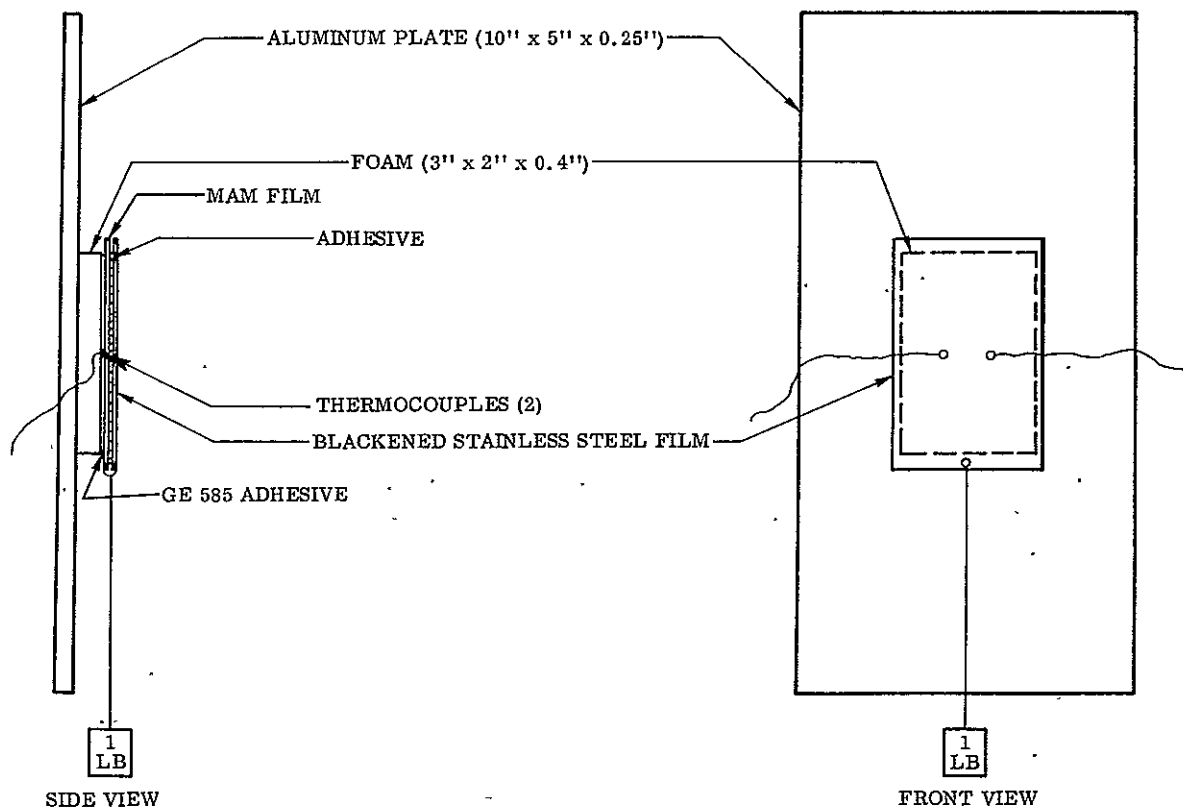


Figure 2-19. Specimen Configuration for Applying Constant Load to Outer Film During Heating

In the third series of tests, small (4 in. by 6 in. by 0.5 in.) sealed insulation panels were used. Although the panels were small, they simulated the full size panels and served as excellent screening devices. When the Vitel PE-207 adhesive was used, the front face was bonded in the same manner as that documented in Reference 1-1. In all other panels, the front face was bonded per the adhesive manufacturer's recommendation. However, the back face and edge channels were fabricated in the same manner on all panels. Two thermocouples were located in the foam-front face bondline. Figure 2-20 shows a typical panel prior to testing.

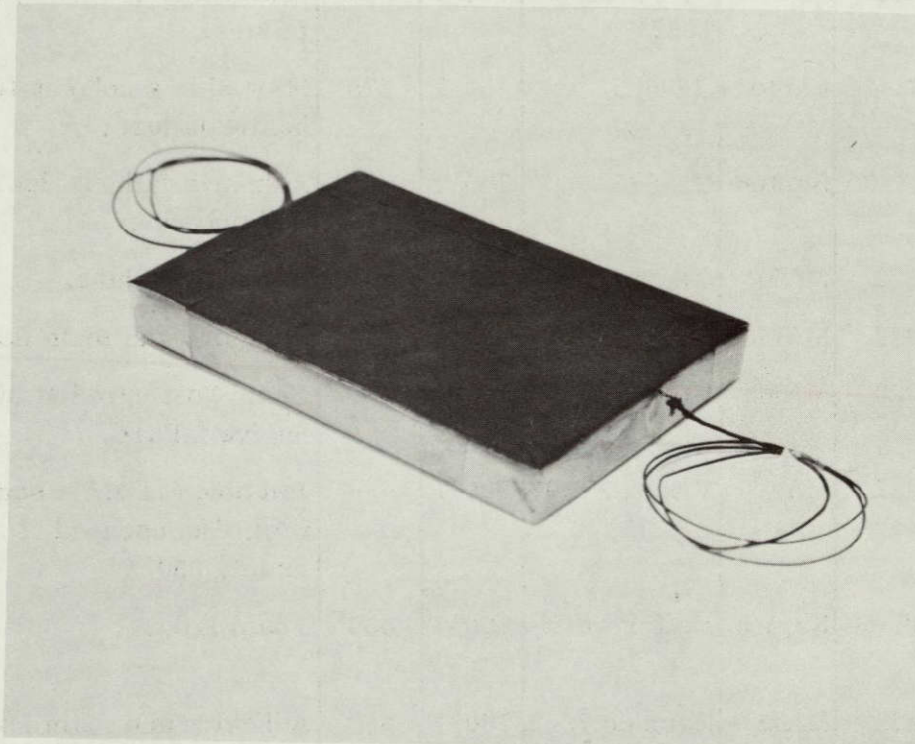


Figure 2-20. Simulated Insulation Panel for the Third Series of Tests

In general, the adhesives used to seal the panels were found to be the weakest link in the system. In all panels, blistering was observed between 200° F and 550° F. The degree and temperature of blistering appeared to be dependent upon the amount of entrapped volatiles. Blistering of this type occurred in panels bonded with Vitel PE-207, APCO 1252/1252V, GE 585, and GE RTV-108. In all cases the adhesive failed and solvent odor was apparent. When Leffingwell 211 epoxy adhesive was used, blistering did not occur until a temperature of 525° F was reached. In this case, failure occurred in the foam. Listed in Table 2-3 are the results of sealed panel testing.

TABLE 2-3. RESULTS OF SEALED FOAM PANEL TESTING

Specimen	Foam	Film	Adhesive	Time-Temp. Curve	Blistering Temp. °F	Remarks
1	GAC-222	MAM	Vitel PE-207	700° F	550	Adhesive failure (suspected leak in film).
2	GAC-222	MAM	APCO 1252/1252V	700° F	350	Seal broke at 700° F, adhesive failure.
3	CPR 32-2C	Kapton	GE 585	550° F	275	Started to smoke at 400° F, adhesive failure.
4	CPR 21-2A	Kapton	GE 585	700° F	—	Adhesive failure, leak in seal, no blistering.
5	GAC-222	MAM	GE 585	550° F	300	Adhesive failure.
6	GAC-222	MAM	GE RTV-108	700° F	300	Adhesive and foam failure.
7	GAC-222	MAM	Vitel PE-207	700° F	450	Foam post cured at 300° F, adhesive failure.
8	GAC-222	MAM	Vitel PE-207	700° F	—	Pin holes in MAM sealed with wax. Gas escaped at approximately 350° F.
9	CPR 32-2C	Kapton	Leffingwell 211	700° F	550	Foam failure.
10	GAC-222	MAM	Narmco 7343	700° F	350	Adhesive and foam failure.
11	CPR 32-2C	Kapton	APCO 1252/1252V	700° F	325	Adhesive failure.
12	CPR 32-2C	MAM	Narmco 7343	700° F	40	Adhesive failure.

Testing indicated that even if a nonvolatile adhesive system is used, such as an epoxy, blistering would occur due to the foam outgassing and rupturing. Additional testing was performed using the nonvolatile, higher temperature curing modified epoxy adhesives. These systems, Metlbond 225 and Aerobond 3021, are supported films having nonwoven nylon as the carrier. The films may be cured under a pressure of 15 psi at temperatures as low as 200° F. Table 2-4 lists the test results obtained with these two systems as well as some additional testing conducted with room temperature curing systems.

TABLE 2-4. ADDITIONAL RESULTS OF SEALED FOAM PANEL TESTING

Specimen No.	Foam	Film	Adhesive	Time-Temp. Curve °F	Blistering Temp. °F	Remarks
13	CPR 32-2C	MAM	BXR-116A	700	425	Adhesive failure, Mylar melted at bondline.
14	CPR 32-2C	MAM	Epon 934	700	460	Adhesive failure, Mylar melted at bondline.
15	CPR 32-2C	MAM	D.C. 92-018	700	300	Adhesive failure.
16	CPR 32-2C 400° F Post Cure	Kapton	Epon 934	700	535	Foam failure.
17	CPR 32-2C	Kapton	ISOCHEM 460	700	500	Foam failure.
18	CPR 32-2C	Kapton	ISOCHEM 460	700	375	Cohesive failure.
19	CPR 32-2C	Kapton	Epon 956	700	500	Foam failure.
20	CPR 32-2C	Kapton	A.E. 3021	700	—	No failure.
21	CPR 32-2C	Kapton	Metlbond 225	700	—	No failure.
22	GAC-222	Kapton	A.E. 3021	700	375	Foam failure.
23	GAC-222	Kapton	Metlbond 225	700	375	Foam failure.
24	CPR 32-2C 400° F Post Cure	Kapton	ISOCHEM 460	700	475	Cohesive failure.

Specimens 13 and 14 both showed combined adhesive failure and Mylar melting at the bondline. Previous tests showed that the MAM would support a load in tensile shear at temperatures up to 660° F. The failure in Specimens 13 and 14 at temperatures of 425° and 460° F, respectively, indicate either poor repeatability or very low strength in peel on the adhesive-Mylar and Mylar-aluminum interfaces.

Based on the above test data, it was decided to evaluate three different adhesives for the foam-to-MAM external bond on the T-9 tank test. The selected systems were Metlbond 225, Epon 956, and Vitel PE-207. The latter was selected as a control, since it was used in the earlier NASA/LeRC program. The T-9 test only evaluated the cryogenic cycling of the sealed insulation systems and therefore did not subject the external

bonds to conditions expected in flight. Additional testing was conducted on sealed foam panels simulating temperature and pressure conditions and this testing is described in Section 8.

2.2.2.3 Panel-To-Tank Bond Adhesive. Candidates for the panel-to-tank bond were the Narmco 7343 and APCO 1252 adhesives with various primers and additives. Tensile shear specimens were fabricated of 0.020-inch EFH301 stainless steel. All specimens were prepared for bonding with a trichloroethylene wash and dry cheesecloth wipe. T-peel testing was accomplished using 0.007-inch thick Mylar as the adherend. Face tension testing was completed using steel blocks bonded together with a thin film (0.002 inch) of Mylar in the adhesive joint.

Two primers and one additive were selected for evaluation. The selected primers (both polyesters) were DuPont's 46950 and Goodyear's Vitel PE-207. The one additive selected was General Electric's Silane A-187.

Initially, several different combinations of adhesives, primers, and additives were evaluated in tensile shear. The results of this testing are listed in Table 2-5. From these results two systems were chosen for further testing; Narmco 7343/Vitel PE-207 primer, and APCO 1252/Vitel PE-207 primer. Additional tensile-shear testing (Table 2-6) as well as peel and face tension testing (Table 2-7) was accomplished. When Narmco 7343 was tested in face tension with and without primer, the results were 1680 psi and 460 psi, respectively. The primed and unprimed values for APCO 1252 were 1412 psi and 505 psi, respectively.

The results of additional tensile-shear testing illustrate the fact that the Narmco 7343 and the APCO 1252 have the same average strengths. However, there is a large scatter band in the Narmco 7343 results. The same inconsistency is also apparent when comparing the results of peel testing from Table 2-7.

After comparing the results of testing, it becomes apparent that the APCO 1252 is the more consistent of the two adhesives. The one drawback to using APCO 1252 is that the adhesive contains solvents, and these solvents could not permeate a Mylar-aluminum-Mylar (MAM) laminated film. The Narmco 7343 is a 100 percent solids system and, in conjunction with the Vitel PE-207 as a primer, was the system recommended for bonding the sealed foam panels to the Centaur test tank. The problem of inconsistency in the adhesive is surmountable by close quality control in manufacture and close surveillance in receiving inspection. Controls on aging, storage environment, and processing must be implemented. Even the lowest tensile-shear strength values obtained with the Narmco 7343 are much greater than the shear strength of the foam insulation.

TABLE 2-5. TENSILE-SHEAR STRENGTHS OF ADHESIVES

Specimen		Primer	Tensile Shear Strength (psi)	
			Room Temperature	-320° F
Narmco 7343	1	None	616	710
	2	None	650	868
	3	None	586	<u>1124</u>
	Avg.		617	901
Narmco 7343	1	Vitel PE-207	1160	2840
	2	Vitel PE-207	936	2000
	3	Vitel PE-207	954	<u>2660</u>
	Avg.		1017	2500
Narmco 7343	1	Narmco 7343/MEK,50/50	606	622
	2	Narmco 7343/MEK,50/50	620	884
	3	Narmco 7343/MEK,50/50	554	<u>686</u>
	Avg.		593	791
Narmco 7343	1	DuPont 46950	720	850
	2	DuPont 46950	696	610
	3	DuPont 46950	620	<u>722</u>
	Avg.		679	727
Narmco 7343 plus 1% Al87	1	None	540	896
	2	None	584	1016
	3	None	566	<u>858</u>
	Avg.		563	923
APCO 1252	1	None	920	—
	2	None	1025	
	3	None	1035	
	Avg.		993	
APCO 1252	1	Vitel PE-207	710	2000
	2	Vitel PE-207	626	1814
	3	Vitel PE-207	720	<u>1910</u>
	Avg.		685	1908
APCO 1252	1	APCO 1252/Ethyl	1336	1390
	2	Actate,50/50	1310	1440
	3		986	<u>1232</u>
	Avg.		1211	1354

TABLE 2-6. TENSILE-SHEAR STRENGTHS OF NARMCO 7343 AND APCO 1252

Specimen	Primer	Tensile Shear Strengths (psi)		Specimen	Primer	Tensile Shear Strengths (psi)	
		Room Temp.	-320° F			Room Temp.	-320° F
Narmco 7343-1	Vitel	1160	2840	APCO 1252-1	Vitel	710	2000
↑ -2	PE-207	936	2000	↑ -2	PE-207	626	1814
-3	↑	954	2660	↓ -3	↑	720	1910
-4		960	1460	↓ -4		970	1962
-5		1376	1510	↓ -5		790	1810
-6		940	1234	APCO 1252-6	Vitel	1024	1940
-7		834	1096	↓	PE-207		
-8		710	1468				
-9		702	1220				
-10		644	1704				
↓ -11	Vitel	656	2060				
Narmco 7343-12	PE-207	660	1650				
	Avg.	878	1742				
					Avg.	807	1906

TABLE 2-7. PEEL STRENGTHS OF MYLAR TO MYLAR BONDS .

Specimen	Primer	Peel Strength (lb/in.)	Specimen	Primer	Peel Strength (lb/in.)
Narmco 7343-1	None	1.80	APCO 1252-1	None	0.50
↑ -2	None	1.80	↑ -2	None	0.40
↓ -3	None	1.50	↓ -3	None	0.80
Narmco 7343-4	None	1.80	↓ -4	None	0.60
		Avg. 1.72	APCO 1252-5	None	0.40
					Avg. 0.54
Narmco 7343-1	None	2.50	APCO 1252-1	Vitel	2.50
plus -2	None	1.75	↑	PE-207	
1% A187 -3	None	2.25	↓ -2	Vitel	2.50
		Avg. 2.17		PE-207	
Narmco 7343-1	Vitel	1.10	APCO 1252-3	Vitel	2.00
↑ -2	PE-207		↓	PE-207	
-2	Vitel	0.50			
	PE-207				
↓					
Narmco 7343-3	Vitel	0.08			
	PE-207				
		Avg. 0.80			Avg. 2.33

2.2.2.4 Erosion Cloth-To-Panel Bond Adhesive. The bond of the erosion cloth to the external MAM surface required a material which could withstand rapid heating to approximately 550°F and be compatible with both silicone rubber and Mylar. Of the various silicone adhesives evaluated, the GE 585 appeared most feasible from a production standpoint. It is pressure sensitive and requires a relatively thin bondline compared to many of the other silicones. The GE 585 was selected for use in producing panels for the T-9 test tank.

Figure 2-21 shows the thermogravimetric analyses of various films and adhesives considered in the fixed insulation program. It can be seen that the Vitel PE-207 outgasses very markedly at temperatures as low as 200°F. It also can be seen that at 550°F all the candidate adhesives show significant outgassing. This outgassing is one of the contributing factors causing adhesive breakdown and blistering in sealed foam panel tests.

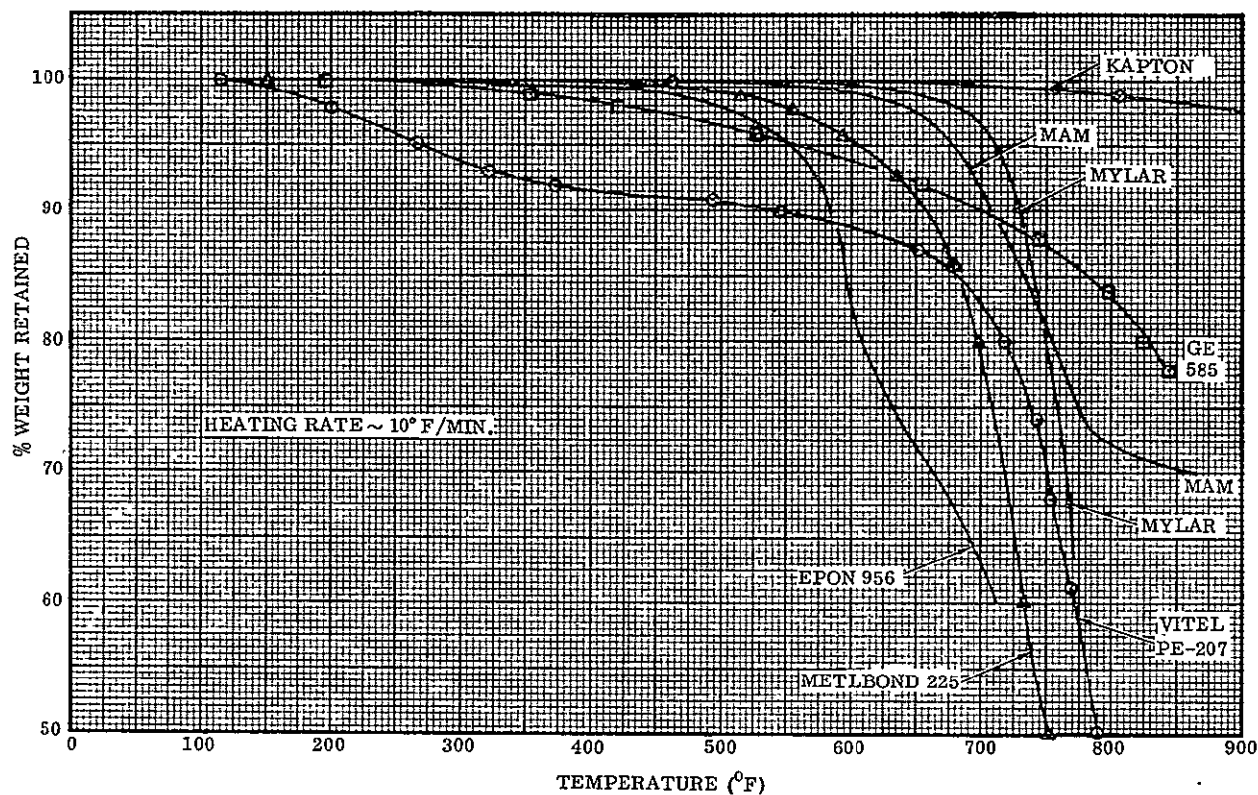


Figure 2-21. Thermogravimetric Analyses of Kapton, MAM, and Various Adhesives

2.3 FILMS

In the sealed foam insulation concept the foam is sealed within a film envelope. The film is required to be as nonpermeable as possible. The original NASA/LeRC program utilized MAM (Mylar-aluminum-Mylar) laminated film.

2.3.1 SURVEY RESULTS. A survey of available films was made and in addition to MAM several other combinations of Mylar and aluminum (MAAM, MAMA, AMA, etc.) as well as a combination of Kapton and aluminum (KAK) were the prime candidates for films having capability of withstanding the ground and flight environments.

It had been previously shown by Goodyear Aerospace Corporation (Reference 2-5) that lamination of a metallic film to an organic film resulted in a composite having a permeability much lower than the original organic film. The organic film provides protection for the metallic film, increases toughness, and modifies the radiative properties. Other organic films such as Tedlar, Aclar, and Teflon were originally considered but were discarded as candidates either because of manufacturing problems or because of potentially poor thermal resistance. MAM and KAK were chosen as the prime candidates for Convair's program. Other combinations of Mylar and aluminum were discarded because of weight considerations. Metallized films had also been considered initially but were discarded early because of (1) poor permeability when compared to laminated films and (2) poor resistance to environmental conditions.

A survey of available sources for the films revealed that MAM was available from Schjeldahl Corporation, Dobeckmun Metal Laminates, Alumiseal Company, Standard Packaging, Riegel Paper Corporation and possibly Arvey Corporation. Kapton composite films were available from Schjeldahl, Riegel, and Arvey Corporations. Most laminated films are available in 60 inch widths, but the laminated Kapton film was available in 37 inch width from Riegel and 23 inch width from Schjeldahl. Most of the commercial Kapton laminate work had been done with copper. The heat resistance of the KAK laminate was suspect since the adhesives generally used were high temperature polyesters. Some work had been done on Kapton-aluminum composites with polyimide adhesives but this was generally experimental.

2.3.2 TEST RESULTS. At the initiation of the Convair program it appeared that the external temperature of the fixed panels could reach 700° F. Later analysis using the candidate material selections indicated a peak temperature of approximately 550° F. Early testing was performed by heating bonded joints rapidly to both 550° F and 700° F. Testing was on composite systems and is reported in Section 2.2.

Mylar is reported (Reference 2-6) to have a melting point of 480° to 510° F when tested with a Fisher-Johns melting point apparatus. This is more of a softening point than a true melting point. Testing showed that MAM at temperatures greater than 550° F could still withstand the expected environmental exposure. MAM was selected for the film for the T-9 test program because of availability, cost, reduced temperature requirements, previous program history, etc. Late in the program, some sealed panels tested under combined heat and vacuum did show local Mylar-to-aluminum failures (see Section 8). However, foam and adhesive failures were the most prevalent causes for panel blistering.

Thermogravimetric analysis was conducted on MAM, Mylar, and Kapton (Figure 2-21). The amount of outgassing at 550°F is less than 1 percent for each of the films. Therefore, in sealed foam panels the contribution of gaseous products by the films at 550°F is negligible compared to those coming from the foams and adhesives.

2.4 THERMAL CONTROL COATINGS

The outer wrap of the Centaur fixed insulation system was needed to provide (1) thermal protection for the overall system from ascent heating during launch and (2) thermal control of the outer surface from solar heating following the initial launch phase. These thermal protection and control requirements clearly indicate that a thermally stable thermal control coating be used with a high temperature resistant substrate and possibly a high temperature insulator as a cover over the low density insulation system. The outer surface will be heated during the launch phase to a peak temperature of about 550°F (depending on the heat capacity and thermal conductivity of the surface coating and substrate materials) with a relatively short peak heating period of one to three minutes. Therefore, the thermal control coating and substrate materials must not be degraded at these elevated temperatures.

2.4.1 SURVEY RESULTS. A survey was conducted to determine the best available thermal control coatings. This survey included the published literature and contact of aerospace companies, government agencies, and coating suppliers. A summary of pertinent information acquired from the survey is given in Tables 2-8, 2-9, and 2-10. The coatings listed in Table 2-9 were under investigation by Lockheed Missiles and Space Company under an Air Force contract, and information on thermal stability, solar absorptance (α) and infrared emittance (ϵ) was not available at the time of the survey.

2.4.2 MATERIALS EVALUATED. Based on the survey, the following coatings were originally recommended for thermal radiation property evaluation:

1. Acrylic tripolymer -- TiO₂ No. PDL-1-2959
2. No. 202-A10 white velvet, 3M's acrylic lacquer
3. No. 302-A10 white velvet, 3M's acrylic enamel
4. M49WC8 flat white acrylic lacquer, Sherwin-Williams
5. Fuller's gloss white silicone No. 517-W-1, TiO₂ pigment in silicone modified alkyd vehicle
6. ITRI S-13 coating (silicone)
7. LMSC's ZnO₂ · SiO₂ pigment in alkali metal silicate vehicle
8. RTV paint with 32 percent PVC-zinc titanate
9. Z-93 (ZnO with potassium silicate)

TABLE 2-8. COMPANY AND GOVERNMENT AGENCY SURVEY

Name of Company or Agency	Location	Type of Coating	Remarks
McDonnell Douglas Aircraft Company	Huntington Beach, California	Aluminum silicate (TTP-28)	Coating was attempted on STD B tanks; too hard to handle and therefore not used. Another limitation is its high temperature cure: 500° F for 2-1/2 hours.
North American Rockwell	Downey, California	Z-93 (ZnO with potassium silicate)	This coating is used on Apollo Service Module. They indicated that this coating would survive ascent heating with surface temperatures to 900° F. It is also used in Surveyor and the Lunar Landing Module.
Goddard Space Flight Center Spacecraft Tech. Div.	Greenbelt, Maryland	Methyl potassium silicate	They have used this coating on a polyurethane foam. It can survive a temperature of 1800° F. They suggested that a 20 mil coating might be sufficient for surviving ascent heating.
Marshall Space Flight Center	Huntsville, Alabama	Z-93 (as above)	They referred to the work by ITRI on this coating. They could not contribute information that was not already available.
TRW	Redondo Beach, California		They have no experience with low α/ϵ ratio coatings. Their requirements are for black coatings with high α and high ϵ .

TABLE 2-9. SURVEY OF THERMAL CONTROL COATING MATERIALS

Coating	Thickness (mils)	Cure	Weight Loss*	Solar Absorptance (α)	Infrared Emittance (ϵ)
ASD silicone-alkyd- TiO ₂	4.6	1-1/2 hrs. at 250° F	0.4%	0.22	—
Acrylic tripolymer — TiO ₂ No. PDL-1-2959	4.0	1-1/2 hrs. at 250° F	1.0%	0.22	0.84
Cot-A-Lac No. 463- 1-500 Flat White	4.6	1-1/2 hrs. at 250° F	—	0.30	—
No. 101-A10 white velvet (alkyd) 3M Company	4.7	1-1/2 hrs. at 250° F	≈6.0%	0.28	—
No. 202-A10 white velvet (acrylic lacquer)	3.5	1-1/2 hrs. at 250° F	5.6%	0.22	0.90
No. 302-A10 white velvet (acrylic enamel)	4.1	1-1/2 hrs. at 250° F	6.7%	0.23	0.91
PT-401 Flat white un- tinted	6.4	1-1/2 hrs. at 250° F	1.7%	0.32	0.90
M49WC8 Flat white acrylic lacquer	5.0	1-1/2 hrs. at 250° F	—	0.24	—
Fuller gloss white silicone, 517-W-1, TiO ₂ pigment in silicone modified alkyd vehicle	—	465° F, can be cured at lower temp.	—	0.29	0.90
Z-93 coating - ZnO with potassium silicate (PS-7)(ST-500 SnO)	—	air dry	none	≈0.175	≈0.940
ZnO ₂ . SiO ₂ pigment in alkali metal silicate vehicle	—	low temperature	none	—	—
Zinc titanate -RTV paint with 32% PVC	—	—	—	0.14	—

*10⁻⁶ torr and 260° F for 48 hrs.

TABLE 2-10. LIST OF ADDITIONAL THERMAL CONTROL COATING MATERIALS SURVEYED

Coating	Characteristics
1. LMSC Lithafrax Coating	Room temperature cure — consists of a commercial LiAlSiO_4 with a potassium silicate binder.
2. LMSC Ultrox coating	Room temperature cure — consists of a commercial $\text{ZrO}_2 \cdot \text{SiO}_2$ pigment washed in HCl and calcined at 1250°C with a potassium silicate binder.
3. LMSC thermatrol 64-100 silicone coating	The vehicle is Dow Corning Q92009, a polymethyl-vinyl siloxane elastomeric dispersion in hydrocarbon solvents (naphtha and xylene) with a TiO_2 pigment.
4. American Cyanamid S7094-3 coating	Consists of Butvar B-98 polyvinyl butyral/Cymel 300 hexamethoxymethyl-melamine pigmented at 60% by volume with unitone OR-640 TiO_2 , and thinned with diacetone alcohol-cellosolve-xylene (40-40-20).
5. American Cyanamid S7094-4 coating	Consists of the tripolymer methyl methacrylate/ethyl acrylate/methacrylic acid (80/10/10) and Epon 201 at a ratio of 70:30 and pigmented with Unitone OR-640 TiO_2 .
6. Mane TiO_2 — acrylic coating	Consists of TiO_2 /acrylic paint with a solids content of 40%.
7. IITRI S-13 silicone coating	Consists of 240 parts by weight of SP-500 ZnO pigment, 100 parts by weight of GE LTV-602 silicone binder, 0.5 parts by weight of GE SRC-05 catalyst, and 184 parts by weight of toluene.

It was determined later that a number of the above coatings were unavailable. Therefore, the list of recommended coatings for evaluation was modified to include those materials listed in Table 2-11. Sherwin-Williams' M49WC8 flat white acrylic paint was not included because previous test data was already available. Andrew Brown's white epoxy paint No. A-423 and Finch Company's white polyurethane paint No. 643-2 were added because they have previously been used by Convair in the Atlas and Centaur programs. A series of films was included for evaluation should white coatings not

survive the ascent heating. Three types of a white silicone rubber impregnated fiberglass cloth were also included for evaluation.

TABLE 2-11. LIST OF MATERIALS EVALUATED FOR THERMAL RADIATION PROPERTIES

Material	Measurement	Ambient Temp.	Elevated Temp.	Remarks
1. Mylar-Aluminum-Mylar Laminate	Both Sides	Yes	Yes	
2. Mylar-Aluminum-Aluminum-Mylar Laminate	Either Side	Yes	No	
3. Aluminized Kapton	Kapton Side	Yes	Yes	
4. White Tedlar Film (Polyvinylfluoride)	N/A	Yes	No	Previous Convair test experience shows shrinkage and browning at approx. 300° F.
5. Acrylic Tripolymer-TiO ₂ No. POL-1-2959	N/A	Yes	Yes	
6. 3M Co. No. 202-A10 White Velvet Acrylic Lacquer (Air Dry)	N/A	Yes	Yes	
7. Same as above except Bake Dry	N/A	Yes	Yes	
8. Full Gloss White Silicone No. 517-W-1	N/A	Yes	Yes	
9. Z-93 (ZnO with Potassium Silicate)	N/A	Yes	Yes	
10. Andrew Brown White Epoxy Paint No. A-423	N/A	Yes	Yes	
11. Finch Co. White Polyurethane Paint No. 643-2	N/A	Yes	Yes	
12. Silicone Rubber Impregnated Fiberglass Cloth No. CHR 2007	Rubberized Side	Yes	Yes	
13. Silicone Rubber Impregnated Fiberglass Cloth No. CHR 1005	Rubberized Side	Yes	Yes	
14. Silicone Rubber Impregnated Fiberglass Cloth No. CHR 3016	Either Side	Yes	Yes	

2.4.3 RESULTS OF THERMAL RADIATION PROPERTY EVALUATION. Thermal radiation property testing, including radiation property degradation due to simulated aerodynamic heating during boost, of the prospective surface finishes listed in Table 2-11 was completed and documented in Reference 2-7.

2.4.3.1 Test Specimen Preparation. Thirteen prospective surface finish materials were evaluated during the radiation property test program, including six paint coatings and seven film-type coatings. Specimens were applied to 15/16-inch diameter discs and mounted in the fixture shown in Figure 2-22.

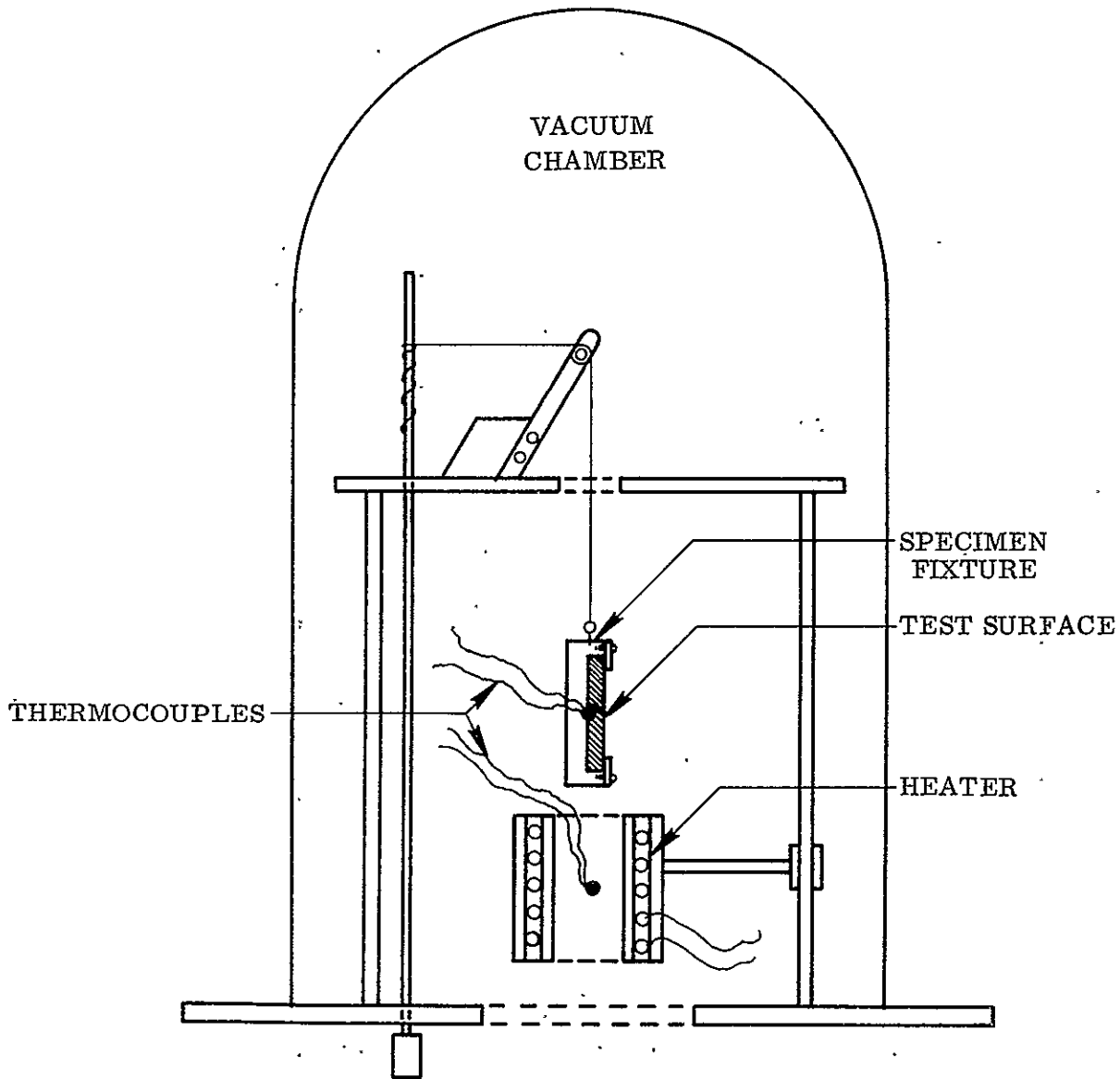


Figure 2-22. Thermal Radiation Property Test Configuration

The following paragraphs give a brief description of the preparation of each set of paint samples.

3M Co. No. 202-A10 White Velvet Acrylic Lacquer

Procedure:

1. A thin coat (approximately 0.5 mil) of Magna Phos-pho-neal primer was sprayed on the aluminum discs.
2. The primer coat was air dried for one hour.
3. A coating of the 202-A10 was sprayed on the primed surface (thickness about 1.3 mils).
4. The paint coating was air dried for three minutes.
5. Steps 3 and 4 were repeated until a total of three coatings had been applied (total thickness about 4 mils).
6. The final coating was air dried for at least one hour before use.

3M Co. No. 202-A10 White Velvet Acrylic Lacquer

Procedure: The previous procedures were repeated except in step 6 the final coatings were heat cured for one hour at 175° F.

Fuller Paint Co. No. 517W-1 High Gloss White Silicone

Procedure:

1. A thin (about 2 mils) coating of the 517-W-1 was sprayed on the unprimed surface of the aluminum discs.
2. The coating was air dried for one hour.
3. A second thin (again about 2 mils) coating of the 517-W-1 was sprayed over the first coating.
4. The second coating was air dried for one hour.
5. The final coating was baked for one hour at 480° F. Final thickness was about 4 mils.

Andrew Brown No. A-423 White Epoxy Paint

Procedure: The coatings were applied according to Convair application Spec. No. 0-75149-3 for the primer and Spec. No. 0-75149-4 for the A-423 paint as follows:

1. The epoxy primer was mixed one part base component to one part catalyst and allowed to set one hour before use.
2. A thin coating (0.5 mil) of the primer was sprayed on the discs and allowed to air dry for four hours.

3. The A-423 white epoxy enamel was mixed one part base component to one part T252 Converter and allowed to set one hour before use.
4. A thin coating (about 1.3 mils) of the epoxy paint was sprayed over the primed surface and allowed to air dry for a few minutes.
5. A thin cross coat of the epoxy paint was sprayed over the first coating and allowed to air dry a minimum of four hours.
6. A third coat of the epoxy paint was sprayed on and again allowed to air dry for a minimum of four hours. The final thickness was about four mils.

Zinc Oxide, Potassium Silicate Coating

Procedure: The zinc oxide (Convair Material Spec. 0-00742-1) and potassium silicate (Convair Material Spec. 0-00741-1) were applied according to Convair application Spec. 0-00139 as follows:

1. Fifty grams of zinc oxide, 25 cc's of potassium silicate and 50 cc's distilled water were mixed in a DeBale Mill for several minutes.
2. A coating was sprayed on the unprimed surface of the aluminum discs and allowed to air dry for three to four minutes (thickness about 1 mil).
3. A second, third, and fourth coating was sprayed over the first, allowing each successive coating to dry for three to four minutes (final thickness about 4 mils).
4. The final coating was air dried for at least four hours before use.

Finch Co. No. 643-2 White Polyurethane Paint

Procedure:

1. Three parts by volume of Finch Co. primer base No. 463-121-A were mixed to 1 part by volume of catalyst.
2. A 0.5 mil thick primer coating was sprayed on the aluminum discs and allowed to air dry for several minutes.
3. Three coats of the 643-2 paint (1.3 mils each coating) were sprayed on, allowing each coat to air dry three or four minutes before applying the next (final thickness 4 mils).
4. The final coatings were air dried for two hours before use.

2.4.3.2 Test Procedure: The radiative properties (α and ϵ) of each finish type (three samples per finish type) were first measured at room temperature.

Each of the samples was then installed in a vacuum chamber as shown in Figure 2-22, the pressure was reduced to approximately 10^{-5} Torr and maintained while the heater temperature was raised to approximately 1050° F. Following a 10-minute stabilization period, the specimen holder was lowered into the heater and the heater power was

increased to heat the specimens to one of three appropriate temperatures (400, 550, or 700°F) in about 70 seconds to simulate the condition expected during flight. When the required time/temperature cycle had been completed the specimen was raised out of the heater, and the chamber immediately back-filled to 5 psia of helium. In approximately 20 minutes, when the specimen had cooled below 120°F, the chamber was opened and the specimen was replaced. Solar absorptance and emittance was again measured at room temperature and compared with the previously determined values.

2.4.3.3 Test Results. The results of the measured solar absorptivity and emittance of the samples tested before and after simulated aerodynamic heating are presented in Table 2-12. The results indicate that external film-type finishes are generally unsatisfactory. These materials show marked blistering and darkening accompanied by significant increases in α/ϵ ratio after heating. Two exceptions to this type of degradation are the Connecticut Hard Rubber Company Silicone Coated Fabrics (CHR 3016 and CHR 2007). These samples are listed in Table 2-12 as surface finish Numbers 10 and 13, respectively.

2.4.3.4 Recommended Materials. Five of the materials tested exhibited satisfactory thermal radiation properties. Those materials were: (1) the silicone rubber impregnated glass cloth numbers CHR 3016, and (2) CHR 2007; (3) Andrew Brown white epoxy paint Number A-423; (4) Fuller gloss white silicone paint Number 417-W-1; and (5) Z-93, a zinc oxide-potassium silicate paint.

Since it was desirable to provide a cloth type erosion cover over the MAM, the silicone rubber impregnated glass cloth seemed ideal because it provided both a cloth covering and the desired thermal radiation properties. The CHR 2007 material was recommended since it is half the weight of the CHR 3016.

It was also desirable to provide an acceptable paint type material for the constrictive wrap and for repair areas after the insulation had been installed on the tank. The Fuller gloss white silicone paint Number 517-W-1 was not desirable because of its required high temperature cure. The Z-93 zinc oxide-potassium silicate paint was not desirable for factory fabricated items because, as noted, it is a very soft paint which is easily scratched during handling. Therefore, the Andrew Brown white epoxy paint Number A-423 was recommended for the constrictive wrap, and either the A-423 or the Z-93 was recommended for on-stand repair areas.

2.5 CONSTRUCTIVE WRAP

The use of filament-wound, pretensioned, continuous nylon or glass filaments (bonded to the sealed foam panels while under pre-tension) had been previously investigated by NASA/LeRC (Reference 1-1), but the new requirements for removability and replacement in the field necessitated the development of a new wrap technique.

TABLE 2-12. SURFACE FINISH RADIATION PROPERTY TEST PROGRAM RESULTS

Surface Finish	Before Aerodynamic Heating Cycle		After Aerodynamic Heating						Remarks
	Solar Absorp- tance	Emit- tance @ 80° F	Solar Absorptance			Emittance @ 80° F			
			400° F	550° F	700° F	400° F	550° F	700° F	
1. Mylar-Aluminum- Mylar (MAM) Bright Side	0.211	0.502	0.216	0.214	0.292	0.489	0.477	0.481	All MAM samples exhibited debonded bubbles after heating.
Satin Side	0.215	0.506	0.218	0.297	0.322	0.498	0.476	0.474	
2. Mylar-Aluminum- Aluminum-Mylar (MAAM)	0.211	0.514	—	—	—	—	—	—	Samples delaminated and debonded from spectrometer coupons during heating. Since pre-heating values were similar to MAM, MAAM was dropped from consideration.
3. Aluminized Kapton (Kapton Side)	0.375	0.566	0.376	0.383	0.402	0.561	0.538	0.588	Samples debonded from spectrometer coupons during heating, were rebonded and tested.
4. 3M Co. Velvet White (Cured at 175° F)	0.245	0.891	0.253	0.263	0.275	0.882	0.878	0.876	Sample surfaces blistered during heating cycles. Investigation indicated paint fails structurally at about 200° F.

TABLE 2-12. SURFACE FINISH RADIATION PROPERTY TEST PROGRAM RESULTS (Continued)

Surface Finish	Before Aerodynamic Heating Cycle		After Aerodynamic Heating						Remarks
	Solar Absorp- tance	Emit- tance @ 80° F	Solar Absorptance			Emittance @ 80° F			
			400° F	550° F	700° F	400° F	550° F	700° F	
5. 3M Co. Velvet White (Air Dry)	0.239	0.891	—	—	—	—	—	—	Test program not completed. Expected to be similar to 4 above.
6. Fuller Gloss White Silicone No. 517-W-1	0.319	0.860	0.319	0.341	0.342	0.857	0.872	0.865	
7. Z-93 (Zinc Oxide and Potassium Silicate)	0.196	0.904	0.194	0.209	0.257	0.909	0.903	0.897	A very soft, flat white finish
8. Andrew Brown White Epoxy No. A-423	0.305	0.879	0.318	0.357	0.417	0.877	0.877	0.815	Coating shows evidence of slight melting at 700° F.
9. Finch Co. White Polyurethane Paint No. 643-2	0.251	0.875	—	—	—	—	—	—	Coating delaminated from spectrometer coupons during heating cycles due to apparent primer failure. Not tested after heating.
10. Silicone-Impregnated Glass Cloth - No. CHR 3016 (16 ounce per square yard)	0.253	0.823	0.262	0.301	0.345	0.830	0.770	0.591*	Samples debonded from spectrometer coupons during heating cycle and were re-bonded. Sample marked (*) was damaged during test procedure and should be considered questionable data.

TABLE 2-12. SURFACE FINISH RADIATION PROPERTY TEST PROGRAM RESULTS (Continued)

Surface Finish	Before Aerodynamic Heating Cycle		After Aerodynamic Heating						Remarks
	Solar Absorp- tance	Emit- tance @ 80° F	Solar Absorptance			Emittance @ 80° F			
			400° F	550° F	700° F	400° F	550° F	700° F	
11. Silicone-Impregnated Glass Cloth - No. CHR 1005 over MAM (6 Ounce per square yard)	0.358	0.834	0.403	0.432	0.481	0.716	0.500*	0.621	All samples showed considerable darkening and bubbling after heating cycle. Sample marked (*) similar to above.
12. Silicone-Impregnated Glass Cloth - No. CHR 1005 Over MAM (Weathered) (6 Ounce per square yard)	0.380	0.816	0.456	0.480	0.583	0.620	0.696	0.605	All samples showed considerable darkening and bubbling after heating cycle.
13. Silicone-Impregnated Glass Cloth - No. CHR 2007 (8 ounce per square yard)	0.252	0.868	0.405*	0.302	0.383	0.863*	0.860	0.852	All samples showed very minor darkening. No bubbling evident. Sample marked (*) had thermocouple failure; therefore temperature reached was uncertain.

The developed constrictive wrap consisted of cured resin impregnated glass filament strands (approximately 0.009 inch thick by 0.1 inch wide) spaced one inch apart, and pre-tensioned to maintain a constrictive load on the insulation during pre-launch operations and flight.

2.5.1 MATERIALS EVALUATED. Reinforced phenolic and epoxy tape material systems were evaluated. Property determinations on individual strand and strand/composite specimens were evaluated at room temperature and at elevated temperatures up to 750° F.

2.5.1.1 Strand Material. Continuous S-994 (HTS) glass filament roving strands consisting of 20 ends (204 monofilaments per end) were chosen for evaluation for use in the lightweight constrictive wrap, rather than "E" glass filaments because of their 20 to 30 percent higher tensile strength, approximately 15 percent higher tensile modulus, and approximately 4 percent lower density. Twenty-end roving rather than 12-end or less was chosen because of off-the-shelf material availability.

Samples of S-994 (HTS), 20-end glass filament roving pre-impregnated with an epoxy resin (E-787, U.S. Polymeric, Inc.) and another sample pre-impregnated with a phenolic system (FF-5255, U.S. Polymeric, Inc.) were selected for preliminary tensile property determinations. These tests included:

1. Ultimate tensile breaking load (pounds)
2. Stress/strain relationships (load vs. strain)
3. Tensile Creep
4. Heat resistance up to 750° F.

2.5.1.2 End Tab Material. Two types of glass fabric/resin systems were selected for evaluation as tabs for holding the roving strands uniformly taut during the stretching of the multiple strands over the external insulation. They are production materials that conform to Convair Material Specifications 0-73008-2 (phenolic, pre-impregnated 181 style glass fabric) and 0-73009-2 (epoxy, pre-impregnated 181 style glass fabric). The 181 style glass fabric was selected because its bi-directional strength properties are nearly equal, and there is less chance of the fabric being misoriented during the lay-up of composite test specimens and/or the actual wrap assembly.

As will be shown in Subsection 2.5.4.4, the interlaminar pull-out shear properties between the roving strand and the metal substrate did not develop the strength of the roving strand. Therefore the use of adhesives was considered to improve the pull-out shear properties. One basic phenolic adhesive system and two epoxy adhesive systems were evaluated. They are listed on the following page.

<u>Adhesive</u>	<u>Type</u>	<u>Form</u>	<u>Applicable Convair Specification</u>
Epon 934	Epoxy	Paste	0-00096-52
FM-1000	Nylon-Epoxy	Film	0-00214-4
HT-424	Epoxy-Phenolic	Film	0-73011-2, Class I
422-J	Epoxy-Phenolic	Film	0-73011-2, Class I

2.5.2 TEST SPECIMEN FABRICATION. The various types of test specimens fabricated and tested are illustrated in Figures 2-23 and 2-24. In most cases, there was enough of the test specimen remaining after the initial test to run additional tests.

The initial roving tensile strand specimens were cured under tension in a special fixture, but use of lay-up techniques simulating those planned in the fabrication of prototype assemblies was considered more appropriate. Therefore composite test specimens were fabricated and tested to evaluate primarily the pull-out shear properties at room temperature, 400°F and 600°F. The individual tensile strand and strand/composite test specimens were cured as follows:

Epoxy System

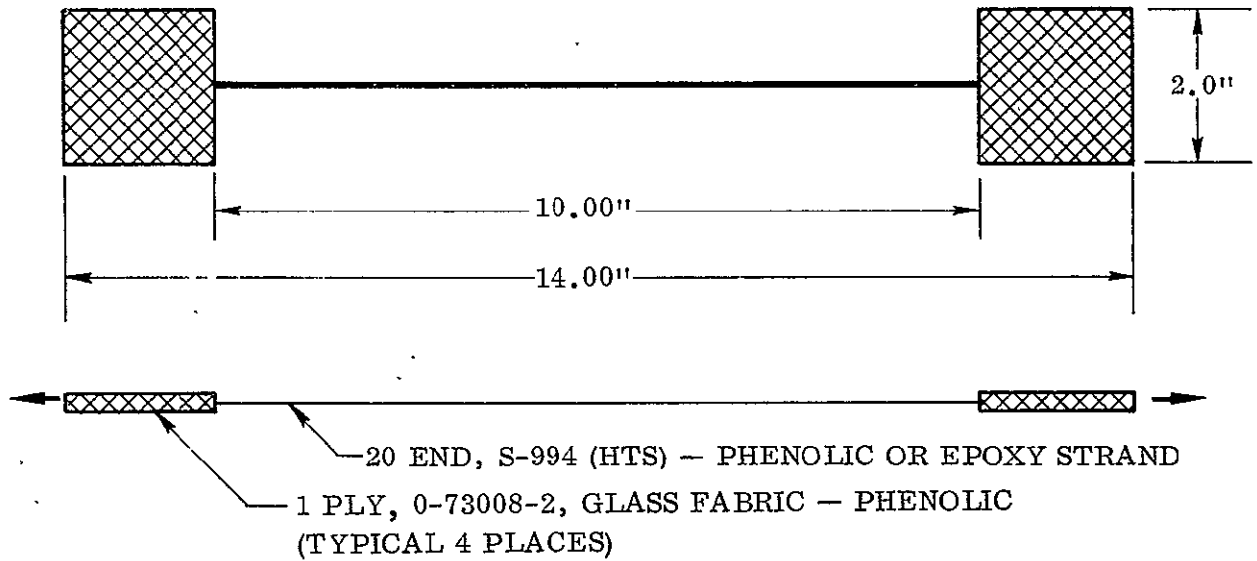
1 hour at 275°F
plus 2 hours at 350°F

Phenolic System*

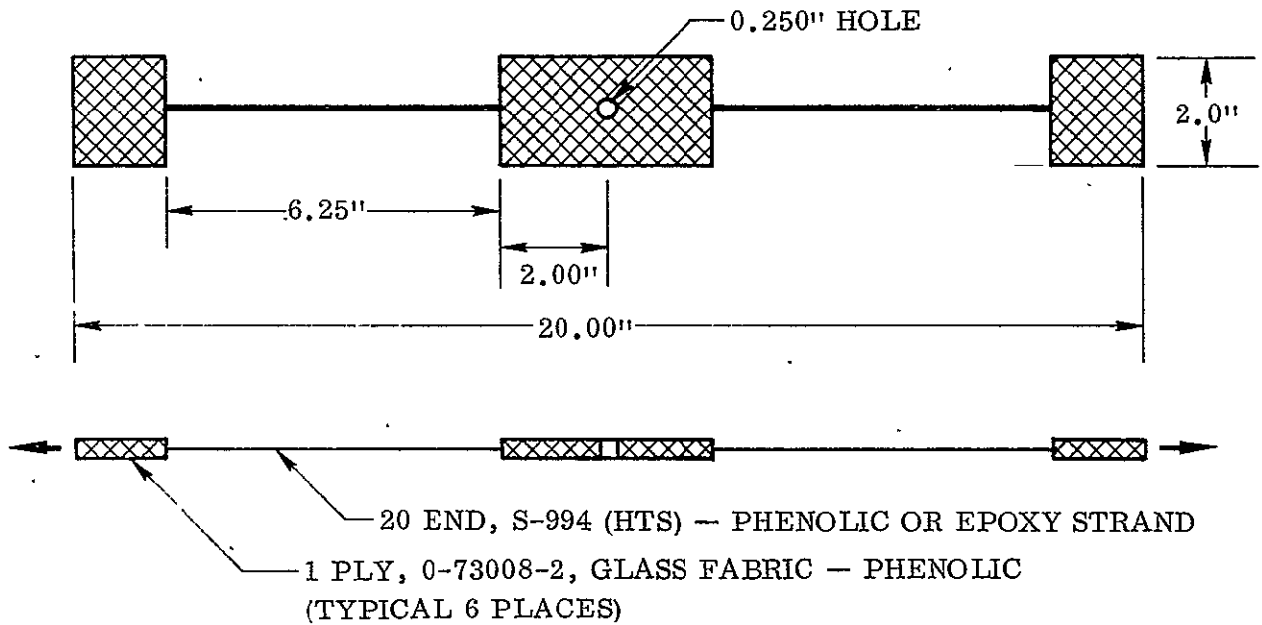
1/2 hour at 150°F
1/2 hour at 250°F
1/2 hour at 300°F
2 hours at 340°F

* The phenolic system used in the roving strand may be cured at 300°F, but the above cure is typical for the glass fabric/phenolic binder in the 0-73008-2 fabric.

2.5.3 TEST METHODS. The general requirements and procedures outlined in ASTM - DW2343-657 "Tentative Method of Testing for Tensile Properties of Glass Fiber Strands, Yarns and Rovings used in Reinforced Plastics" were used for the determination of strand tensile strength properties. Most of the tensile strength and tensile pull-out shear tests were done in an Instron test machine. Several tensile specimens having lengths of 36 inches were tested in a Baldwin machine for high temperature ultimate tensile tests. Individual strand tensile creep tests were done in Arcweld creep testers.



A. TYPICAL TENSILE STRAND SPECIMEN



B. TYPICAL SINGLE STRAND TENSILE PULL-OUT SPECIMEN

Figure 2-23. Typical Tensile Strand and Pull-Out Specimens

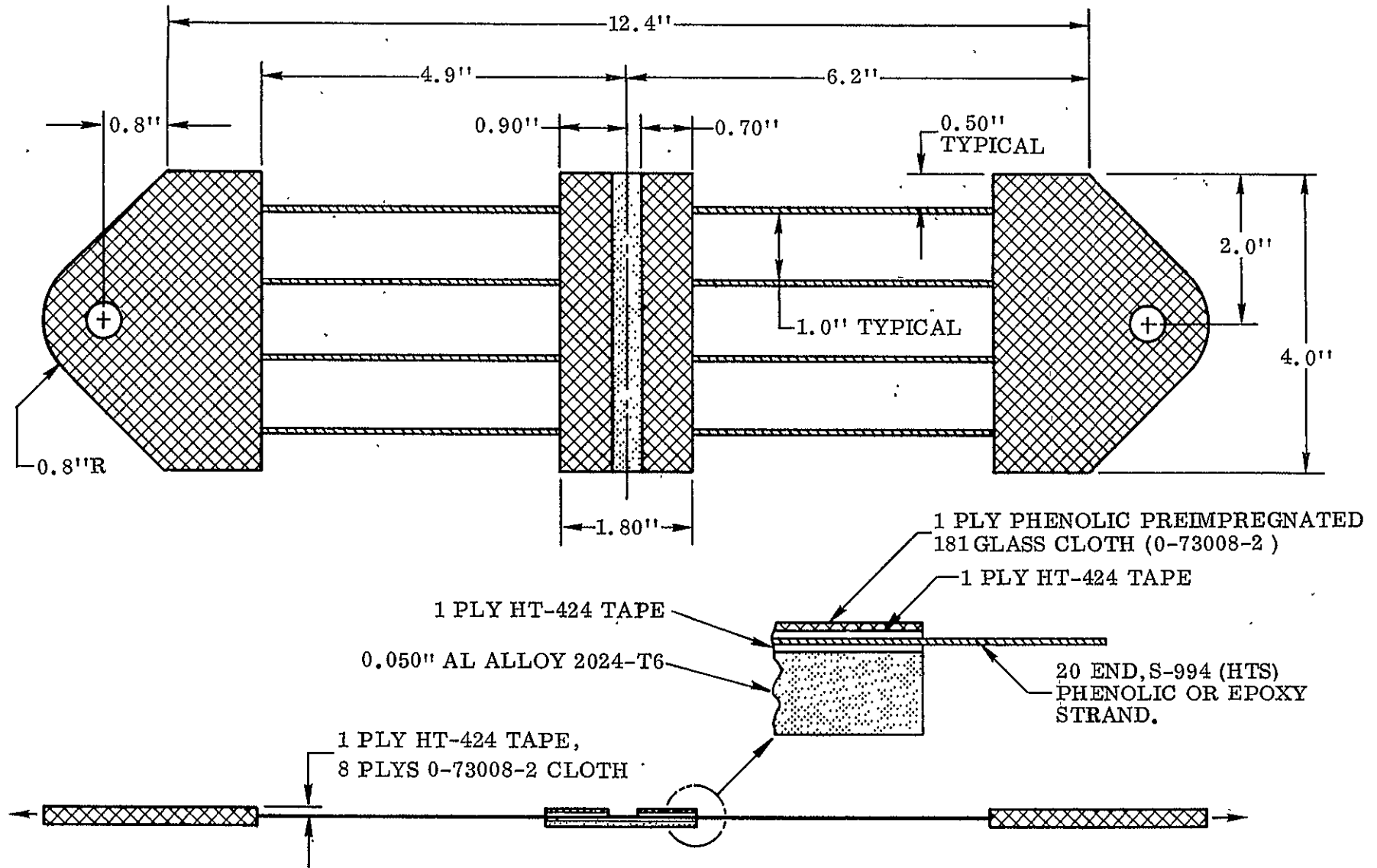


Figure 2-24. Typical Four Strand Tensile Pull-Out Specimen

Several potential problems in testing were (1) proper alignment of the individual roving strands in relation to parallelism to each other, (2) normalcy to end attachment, and (3) stress concentrations at sharp edges. The ultimate tensile strength of the S-994 (HTS) roving strand is high enough so that alignment tolerances were not prohibitive.

A quartz lamp controlled by a variac was used to heat test specimens that were thermocoupled and tested at temperatures of 400°, 600°, and 750°F. Load was applied when the test specimen reached test temperature (one minute, linear heat-up cycle in each case). No significant problems were noted in elevated temperature testing.

2.5.4 TEST RESULTS. The test results for the various strand tensile ultimate and strand tensile pull-out tests are presented in the following paragraphs.

2.5.4.1 Strand Tensile Test. The ultimate tensile strand strength properties of S-994 (HTS), 20-end, pre-impregnated roving with epoxy or phenolic resin binder yielded ultimate load values above 150 pounds. Ultimate tensile strength at elevated temperatures was obtained for phenolic pre-impregnated strands only. A drop off of approximately 18 percent was noted at 750°F for the FF-5255 (S-994/phenolic) 20-end roving strand specimens.

The test results for ultimate tensile strand tests at room temperature (RT) and elevated temperatures are listed in Table 2-13.

The tensile fiber strength values for a single glass roving strand tested at room temperature or at elevated temperatures can be expected to be significantly higher than those for a unidirectional filament-reinforced composite, since the effects of inter-laminar discontinuities are negligible. Unidirectional filament-wound composites using S-glass filament reinforcement will yield a nominal ultimate tensile fiber strength value of 350,000 psi (Source: U.S. Air Force/Owens-Corning) while nominal fiber stress values over 425,000 psi were noted for individual, mono-layer strand specimens tested in this program.

2.5.4.2 Strand Load/Strain Values. Cured resin impregnated strand tensile specimens were loaded to ultimate load in an Instron test machine. A typical load/strain curve for 20-end, S-994 (HTS) phenolic roving is shown in Figure 2-25. The use of bonded tabs was necessary to eliminate slippage of the specimen in the machine jaws.

2.5.4.3 Strand Creep Tests. There was no change in length noted for a cured, 20-end S-glass roving strand specimen loaded to a 50-pound level for approximately eight days. A load value of 50 pounds per strand is less than 1/3 of the average ultimate tensile strength for 20-end S-glass roving, but is in the range of the pre-stress load of the actual design.

TABLE 2-13. SUMMARY OF PRE-IMPREGNATED, 20-END, S-994 (HTS)
GLASS FILAMENT ROVING STRAND TESTS

Test Series	Resin System Type*	Test Temp. °F	Ultimate Tensile Strengths			Remarks
			Load (lb)	Fiber UTS (ksi)	Modulus × 10 ⁶	
I			Avg.	Avg.	Avg.	
I-713	Epoxy	RT	158	386.3	—	All specimens cured in special fixture. No tabs used, and slippage influenced modulus determinations.
I-714	↑	↑	164	401.0	—	
I-715	↑	↑	160(158)	391.2(384.5)	—	
I-716	↑	↑	163.5	399.8	—	
I-717	↓	↑	155	379.0	—	
I-718	Epoxy	↑	147	359.4	—	
II						
I-738	Phenolic		179	437.7	12.4	All specimens were vacuum bag cured with tabs.
I-739	↑		180	440.1	12.0	
I-740	↑		165(169)	403.0(407.5)	11.9(12.0)	
I-741	↑		156	381.0	11.9	
I-742	↑		165.5	404.6	12.0	
III						
I-1064			185	452.3	12.0	Specimens tested to evaluate effect of localized wide band widths.
I-1065		↓	166(182.1)	405.9(446.6)	12.0(12.1)	
I-1066		RT	197	481.7	12.5	
IV						
B-57		750	118	288.5	—	B-57 T.C. lost at 650°F.
B-58		750	110(145)	268.9(344.7)	—	B-58 partial failure at 103 lb. at 750°F; test run at RT.
B-59		750	168	410.8	—	B-59 & B-60 good tests.
B-60		750	168	410.8	—	
B-61		RT	104	254.3	—	B-61 preloaded 8 days with 50 lb.
B-62		↑	187	457.2	—	B-62 for 1.5 days.
V						
I-1131			186	454.8	12.3	All specimens had been pre-loaded for approx. 41 hrs. with 50 lb. wt. prior to test in Series V & VI.
I-1132		↓	207(186)	506.1(455.2)	11.5(12.0)	
I-1140		RT	165.5	404.6	12.1	
VI						
I-1137		750	151	369.2	12.1	
I-1138	↓	750	155(160)	379.0(391.2)	12.4(12.3)	
I-1139	Phenolic	750	174	425.4	12.3	

* Epoxy system was Epon 1031/Epon 828-NMA/BDMA system and phenolic was Ironsides DP-24-2 system. Both systems were used by U.S. Polymeric, Inc., Santa Ana, California to pre-impregnate samples tested.

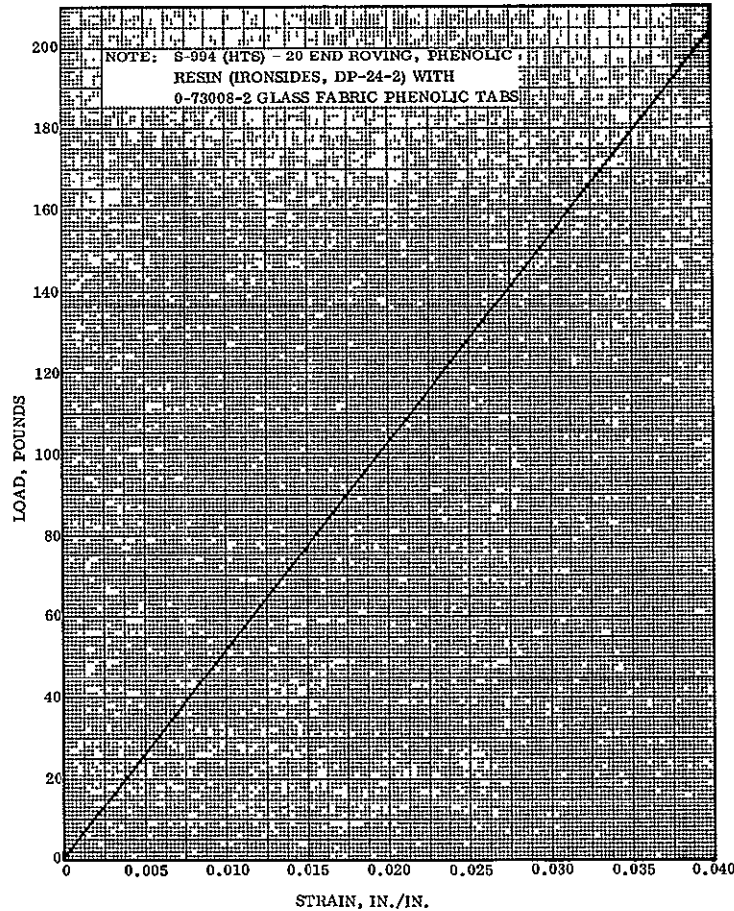
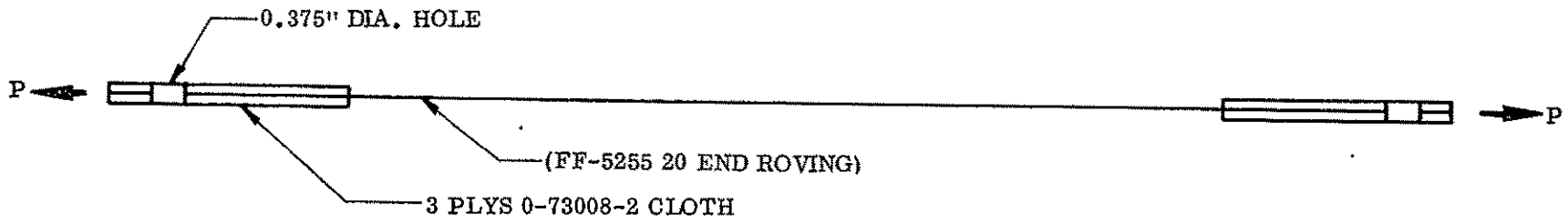
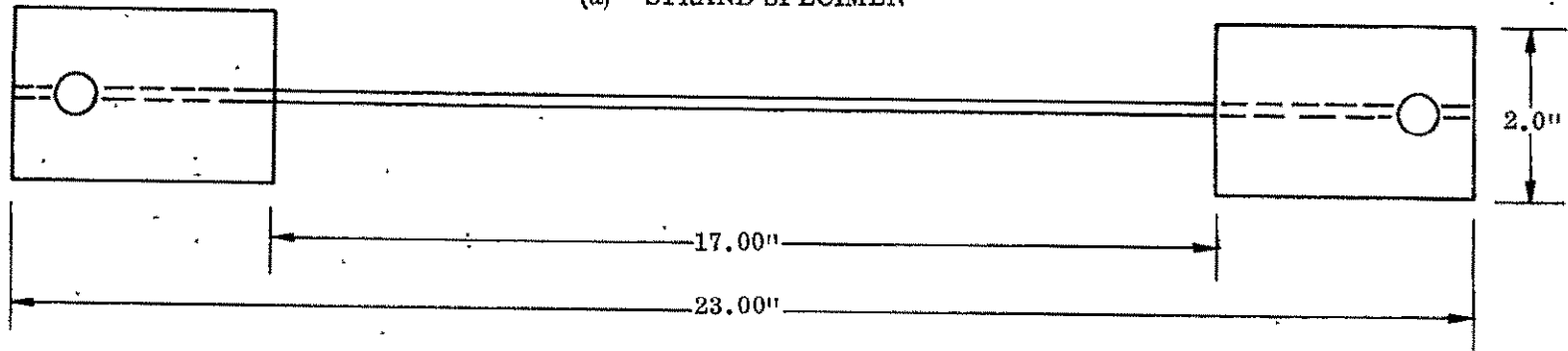


Figure 2-25. Tensile Strand Test — Typical Load Stress Versus Strain

There was no effect on ultimate tensile strength of strand specimens pre-loaded for approximately 40 hours with 50 pounds of weight prior to testing, as shown previously in Table 2-13. No elongation or pull-out was noted in either strand tensile or bond pull-out test specimens (Figure 2-26) that were tested under a constant tensile load of 60 pounds using Arcweld creep-test machines. Tests were in progress for time periods extending up to 51 days, and no visible defects were noted prior to or after testing.

2.5.4.4 Strand Tensile Pull-Out Tests. Strand tensile pull-out tests were run at room temperature, 400° F, and 600° F to evaluate the efficiency of the resin matrix to hold the roving strand between aluminum and/or glass fabric reinforced "tabs." The elevated temperature tests showed that adhesives would be needed in order to get a good bond between the roving strands and the substrates evaluated. This was particularly noted in a single tensile pull-out test (Series I-791, Specimen No. 5, no adhesive used) that had pre-loaded the strand to 60 pounds tensile load prior to start of heating to 600° F (heated in one minute). The pre-load dropped to 57 pounds at 550° F, and the ultimate failure load was 60 pounds at 600° F. Ultimate tensile pull-out test results for specimens using adhesives in test "tabs" indicate that reliable bonds can be expected.

(a) - STRAND SPECIMEN



(b) STRAND PULL-OUT SPECIMEN

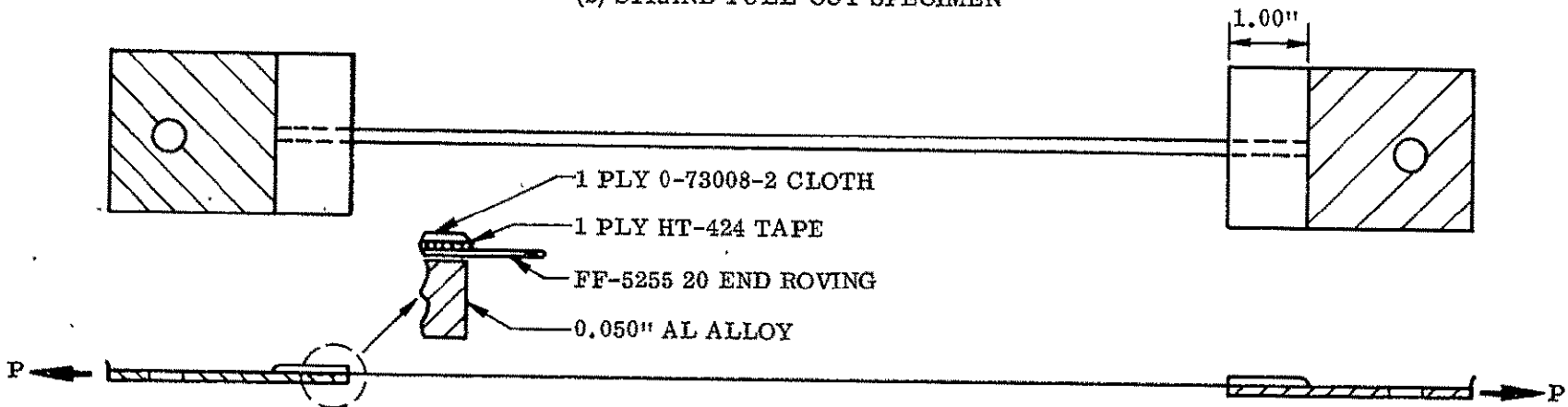


Figure 2-26. Creep Test Specimen

A summary of ultimate tensile pull-out test results is given in Tables 2-14 and 2-15.

TABLE 2-14. STRAND PULL-OUT SHEAR TEST
(PRE-IMPREGNATED GLASS FABRIC)

Test Tab Glass Fabric Pre-Preg	Strand Resin* Reinforcement	Test Length (in.)	Test Temperature (°F)	Ult. Load Average (lb)	Number Of Test Specimens
Phenolic	Phenolic	1.875	RT	102	10
Phenolic	Phenolic	1.875	600	106	4
Epoxy	Epoxy	1.875	RT	132	3
Epoxy	Epoxy	1.0	RT	115	3
Epoxy	Epoxy	1.875	600	60	4

* Epoxy system was EPON 1031/EPON 828-NMA/BDMA and phenolic system was Ironsides DP-24-2 system. Both systems were used by U.S. Polymeric, Inc., Santa Ana, California to impregnate samples tested.

Test Specimen Configuration:

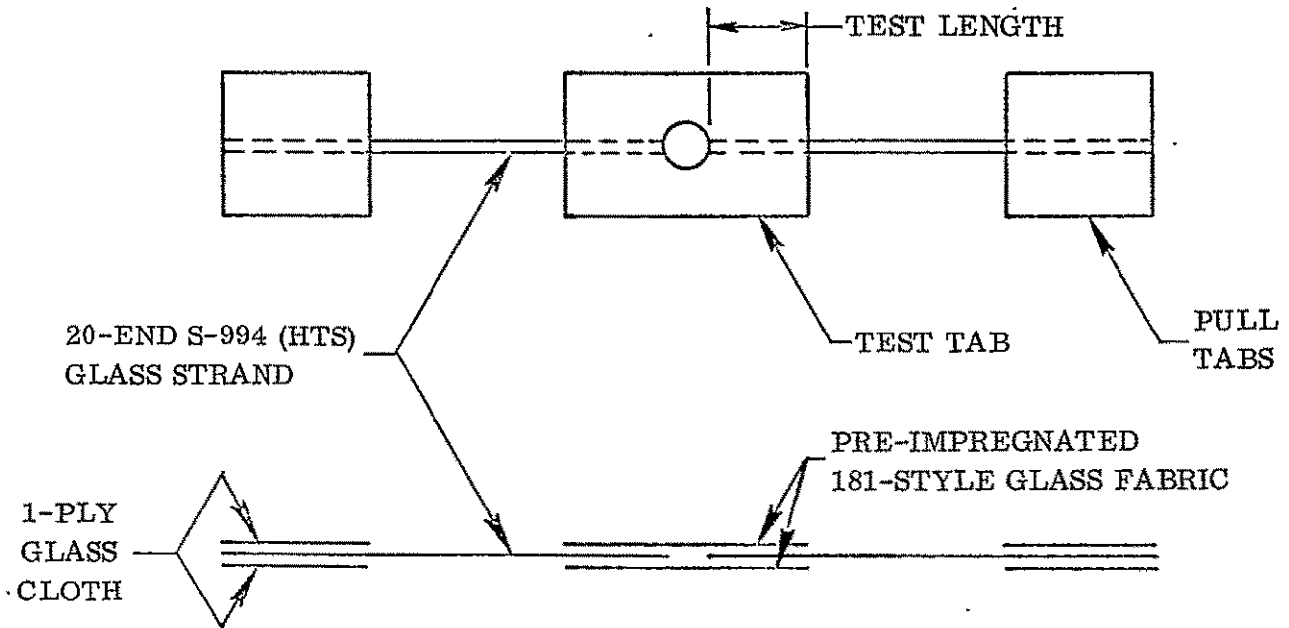


TABLE 2-15. STRAND BOND SHEAR TEST, PRE-IMPREGNATED GLASS FABRIC PLUS 1-PLY ADHESIVE

Test Tab Adhesive	Strand Resin Reinforcement	Test Temperature (°F)	Number Of Strands	Test Length (in.)	Average Ult. Load (lb)	Number Of Test Specimens
Epon 934	Epoxy	RT	1	1 *	148	2
FM-1000 Film	Epoxy	RT	1	1 †	188	2
422 J Film	Phenolic	RT	1	1/2†	177	1
422 J Film	Phenolic	RT	1	3/4†	162	1
422 J Film	Phenolic	RT	1	1 †	175	3
FM-1000 Film	Epoxy	400	4	0.7*	160	1
HT-424 Film	Phenolic	400	4	0.7★	164	6

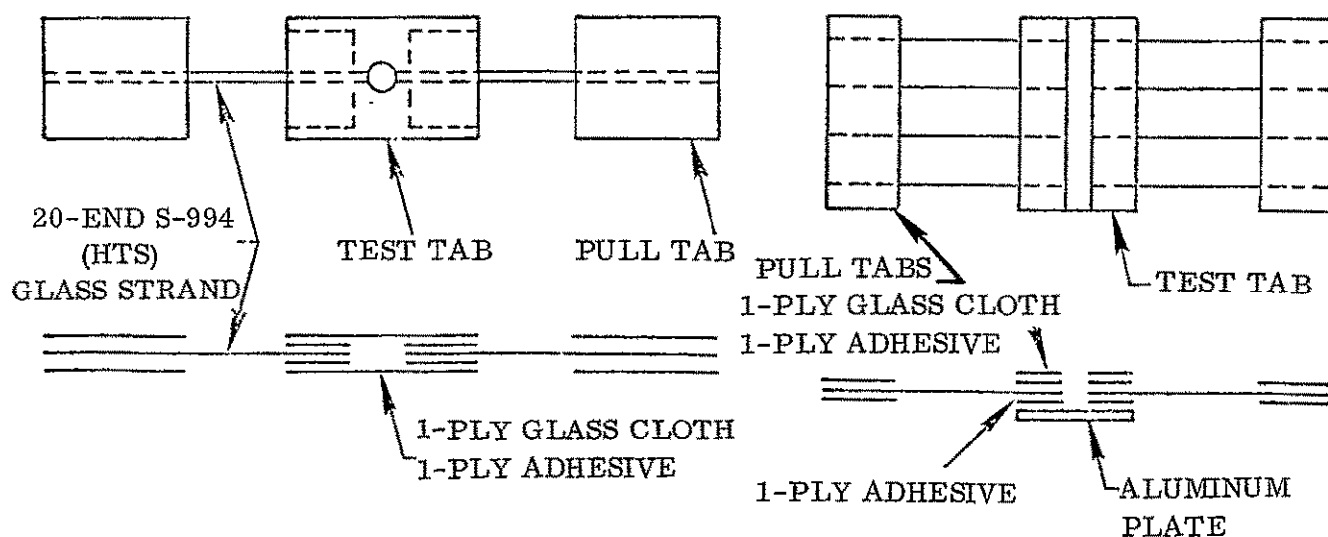
Note:

* Pullout Failure

† Strand Failure

★ Combination Pullout and Strand Failure

Test Specimen Configurations:



2.5.4.5 Thermal Expansion. The thermal expansion characteristics of two specimens of U.S. Polymeric FF-5255 were measured from room temperature to 700° F. The results are plotted in Figure 2-27. Specimens were prepared by laminating 10 pre-impregnated glass strand layers to achieve a thickness of 0.100 inch. The specimens were 1.000 inch long. Measurements were made on a modified Leitz dilatometer in an air atmosphere. Heating rates were manually adjusted to approximately 100° F per hour.

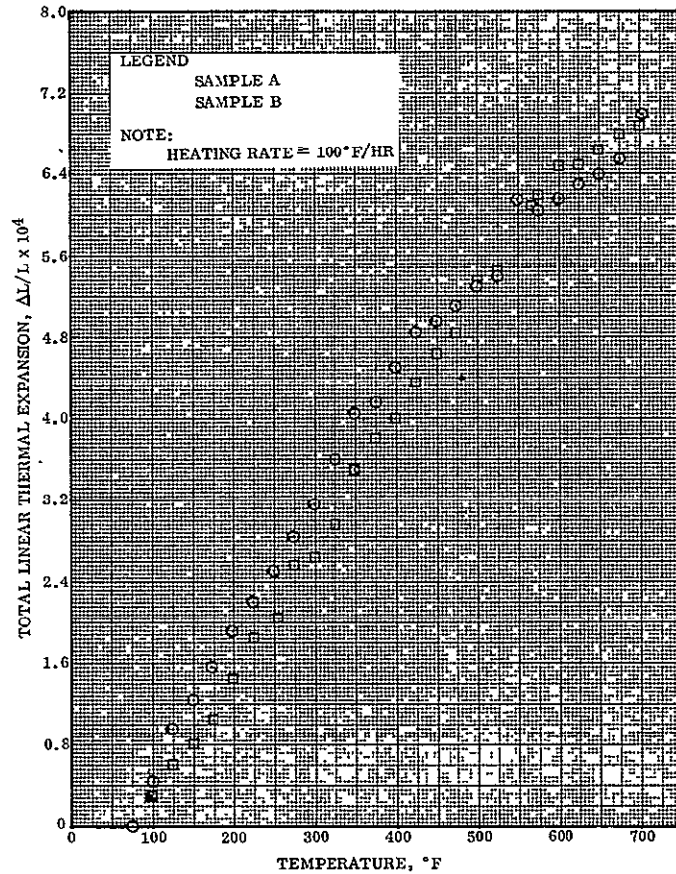


Figure 2-27. Total Linear Thermal Expansion of FF-5255, U.S. Polymeric, Inc., (20-End, S-994 — Phenolic Roving) (Parallel to Reinforcement)

Average coefficients of thermal expansion (α) from room temperature were calculated with the following results:

<u>Temperature</u>	<u>α (average from room temperature)</u>
200° F	1.36×10^{-6} in./in./° F
300	1.29
400	1.32
500	1.25
600	1.20
700	1.10

Indications of a transition were seen between 500 and 600° F.

2.5.4.6 Reproducibility. The stress-strain relationship of the strands was evaluated at several points in the test program (References 2-8, 2-9, and 2-10) using several test techniques to determine the reproducibility of the fabricated strands. Good correlation was obtained between strain gauge and extensometer test data. Table 2-16 shows the data obtained on strands tested in October 1967. These values compare well with Figure 2-25 which was based on specimens built and tested approximately four months earlier.

TABLE 2-16. STRAND LOAD/STRAIN VALUES FOR S-994 (HTS), 20-END ROVING, PHENOLIC IMPREGNATED (US POLYMERIC, INC. FF5255)

Test Series	Load (lb)					
	20	40	60	80	100	120
I-2166	.00397	.0078	.0118	.0157	.0197	.0231
I-2170	.0039	.0078	.0118	.0157	.0196	.0235
I-2168	.0038	.00764	.0115	.0153	.0191	.0229
I-2165	.0039	.0076	.0116	.0153	.0193	.0231
Averages:	.0039	.0077	.0117	.0155	.0194	.02315

2.5.5 MATERIAL RECOMMENDATIONS. As a result of the above testing, it was concluded that commercially available glass filament reinforcements (roving and fabric) pre-impregnated with high temperature resistant phenolic resin systems and epoxy-phenolic type adhesives would meet the design requirements of the proposed constrictive wrap. The following material systems or equivalents were recommended for use in the prototype constrictive wrap assemblies.

1. High Strength Roving Strands

The FF-5255, 20-end roving system (U.S. Polymeric, Inc.) was recommended for the high strength strands.

2. Adhesive System

The HT-424 or 422J high temperature resistant epoxy-phenolic adhesives was recommended to bond the high strength strand to attachment tab substrates.

2.6 COMPOSITE INSULATION SYSTEMS

In contrast to individual materials testing, system support tests were conducted using the sealed panel configuration. These tests included determination of the compressive strength and apparent thermal conductivity of the panel configuration and the friction characteristics of the constrictive strands sliding on the sealed panel configuration.

2.6.1 COMPRESSION TESTS. A series of compression tests were run on the sealed foam panel configuration; however, the edges were not sealed. The systems tested contained MAM faces bonded to the Goodyear foam with the Vitel PE-207 adhesive. The first series of test specimens were cut from a panel prepared by Goodyear for NASA during the initial program in 1963. The second series of specimens were cut from a panel prepared at Convair using foam representative of the foam in the T-9 panels. The MAM used at Convair has a total thickness of 2.5 mils compared to 1.5 mil thick MAM used in the older panel.

All specimens were 1-inch by 1-inch squares and had a thickness of approximately 0.43 inch. The specimens were compressed until a total deflection of 50 percent was obtained. The data is tabulated in Table 2-17. The specimens from the older panel are designated by the letter O, and the specimens from the newer panel are designated by the letter N. The older panel had a higher ultimate strength (at 50 percent deflection), higher yield strength and higher modulus. It was noted that the foam representing the T-9 panels had numerous holes extending well into the foam at an angle to the thickness direction as if the panel had been sliced at an angle. Goodyear thought that the angled holes may have been a result of the particular configuration of the foaming tool at the end from which the test pieces were sliced. The lower properties could be a result of the presence of the aforementioned holes. Aging time and/or batch variation might also account for the difference in properties.

TABLE 2-17. COMPRESSION DATA ON INSULATION PANELS

Specimen	Ult. Comp. Strength at 50% Deflection, psi	Yield Comp. Strength, psi	Comp. Mod., psi
1N	48.0	31.5	893
2N	45.0	31.5	926
3N	45.0	31.2	839
4N	42.5	31.0	798
5N	42.5	30.5	812
	Avg. 44.6	31.1	854
1O	47.0	37.5	1505
2O	47.8	39.5	1522
3O	47.0	39.2	1534
4O	47.5	38.0	1460
5O	47.4	38.0	1491
	Avg. 47.3	38.4	1502

2.6.2 APPARENT THERMAL CONDUCTIVITY. Thermal conductance of specimens of the sealed foam system (MAM film, PE-207 adhesive and GAC-222 foam) was investigated. A low temperature guarded hot plate apparatus (Reference 2-11) was used for all measurements. These conditions and results are tabulated in Table 2-18 and test data are plotted in Figures 2-28 through 2-34.

No significant differences were seen between the joint specimens and the uniform specimens. The simulated aerodynamic heating also produced no significant effects. The differences between the curves obtained for specimen A before and after aerodynamic heating (Reference Figure 2-28 and 2-30) are attributed to effects of high temperature exposure during the first measurement, since the same differences were obtained for Specimen B, (Reference Figures 2-29 and 2-31) which did not see the simulated aerodynamic heating.

Thermal conductance values were also obtained for a second set of sealed foam panels (MAM film, Metlbond 225 adhesive, CPR 32-2C foam). These values are tabulated in Table 2-19 and plotted in Figure 2-35.

Comparison of the data on virgin samples of the two different configurations evaluated shows that the two systems have similar thermal conductance at cryogenic temperatures. At room temperature and temperatures up to 300° F the system containing the Freon blown GAC-222 foam had lower thermal conductance than the system containing the carbon dioxide blown CPR 32-2C foam. Thermal conductance testing of the foam panels requires stabilization times in the orders of hours, and therefore testing at mean temperatures above 300° F would not be feasible. At temperatures higher than 300° F, the Freon blown foams deteriorate quickly while the carbon dioxide blown foams deteriorate quickly at temperatures above 400° F.

2.6.3 FRICTION TESTS. Single-strand frictional forces between samples of the Centaur fixed insulation's silicone rubber impregnated erosion cloth and the constrictive wrap strands were evaluated for a variety of loads and interface conditions. A constrictive force was applied to the fixed insulation foam panels by fixed lengths of circumferential bands of fiberglass-phenolic strands which were pulled around the tank and fastened in 90-degree sections. The tension of these strands had to be sufficient to produce the desired normal force. Additional tension was required to overcome the friction between the strands and the panel surfaces. If the frictional forces were large, the size of the strands would necessarily be significantly larger than that required to apply the desired normal load without failure. These same frictional forces could also cause an uneven loading of the tank. It was desirable to determine the nature and extent of the frictional forces for a variety of assumed situations which could be encountered.

TABLE 2-18. RESULTS OF THERMAL CONDUCTANCE MEASUREMENTS ON SEALED FOAM INSULATION (GOODYEAR SYSTEM; MAM FILM, PE-207 ADHESIVE, GAC-222 FOAM)




Specimen	ΔT (°F)	Mean Temp. (°F)	Thermal Conductivity (BTU-in./hr-ft ² -°F)	Atmosphere
Uniform Specimens (Virgin)				
A	25	56	0.154	GN ₂ at 1 atmosphere.  GN ₂ at 1 atmosphere. Air at 5 microns (cryopumped). Air at 5 microns (cryopumped). GN ₂ at 1 atmosphere.
	12	39	0.149	
	13	-97	0.144	
	39	-81	0.167	
	12	-315	0.064	
	24	-299	0.081	
	15	219	0.250	
	30	227	0.268	
	46	-399	0.006	
	32	-406	0.005	
	31	295	0.316	
	9	304	0.298	
B	45	55	0.155	 GN ₂ at 1 atmosphere. Air at 5 microns (cryopumped). Air at 5 microns (cryopumped). GN ₂ at 1 atmosphere. GN ₂ at 1 atmosphere.
	13	39	0.150	
	14	-98	0.152	
	49	-78	0.169	
	66	-288	0.070	
	18	-312	0.067	
	21	222	0.261	
	40	232	0.258	
	46	-399	0.012	
	68	-387	0.021	
	30	295	0.320	
47	311	0.327		
Uniform Specimens (Virgin) Following Simulated Aerodynamic Heating Exposure on "A"				
A	37	51	0.189	GN ₂ at 1 atmosphere.  GN ₂ at 1 atmosphere. Air at 45 microns. Air at 45 microns. GN ₂ at 1 atmosphere. GN ₂ at 1 atmosphere.
	12	38	0.177	
	14	-98	0.157	
	49	-77	0.169	
	44	-299	0.077	
	13	-315	0.064	
	14	219	0.286	
	31	228	0.300	
	60	242	0.307	
	66	-389	0.028	
	30	-408	0.031	
	7	290	0.379	
33	316	0.376		

TABLE 2-18. RESULTS OF THERMAL CONDUCTANCE MEASUREMENTS ON SEALED FOAM INSULATION (GOODYEAR SYSTEM; MAM FILM, PE-207 ADHESIVE, GAC-222 FOAM) (Continued)

Specimen	ΔT (°F)	Mean Temp. (°F)	Thermal Conductivity (BTU-in./hr-ft ² -°F)	Atmosphere
Uniform Specimens (Virgin) Second Run of "B" Specimens				
B	71	69	0.172	GN ₂ at 1 atmosphere. ↑ ↓ GN ₂ at 1 stmosphere.
	13	39	0.158	
	29	-306	0.071	
	29	296	0.350	
	53	311	0.379	
Comparison of Joint and Uniform Virgin Specimens With High ΔT				
C Uniform	26	-414	0.014	Air at 5 microns - LH ₂ cold face.
	215	-308	0.060	Air at 5 microns - LH ₂ cold face.
	405	-203	0.098	Air at 5 microns - LH ₂ cold face.
	597	-96	0.123	Air at 5 microns - LH ₂ cold face.
D Joint	25	-413	0.013	Air at 12 microns - LH ₂ cold face.
	223	-313	0.052	Air at 12 microns - LH ₂ cold face.
	427	-212	0.097	Air at 12 microns - LH ₂ cold face.
	625	-112	0.120	Air at 12 microns - LH ₂ cold face.
	29	-47	0.170	GN ₂ at 1 atmosphere - Ice water cold face.
	18	< 220	0.255	GN ₂ at 1 atmosphere - Ice water cold face.
E Joint	214	-309	0.059	Air at 10 microns - LH ₂ cold face.
	565	-108	0.131	Air at 10 microns - LH ₂ cold face.
	10	221	0.262	GN ₂ at 1 atmosphere - Boiling water cold face.

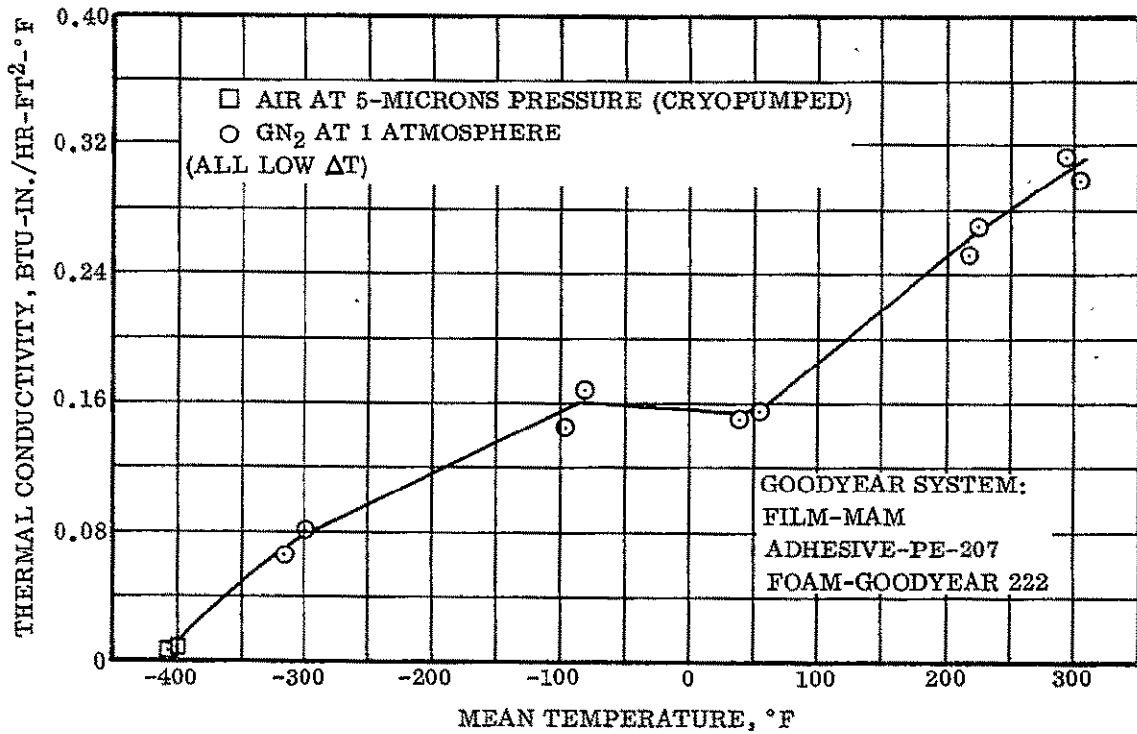


Figure 2-28. Thermal Conductivity Test, Uniform Specimen, Virgin Sample, Specimen A

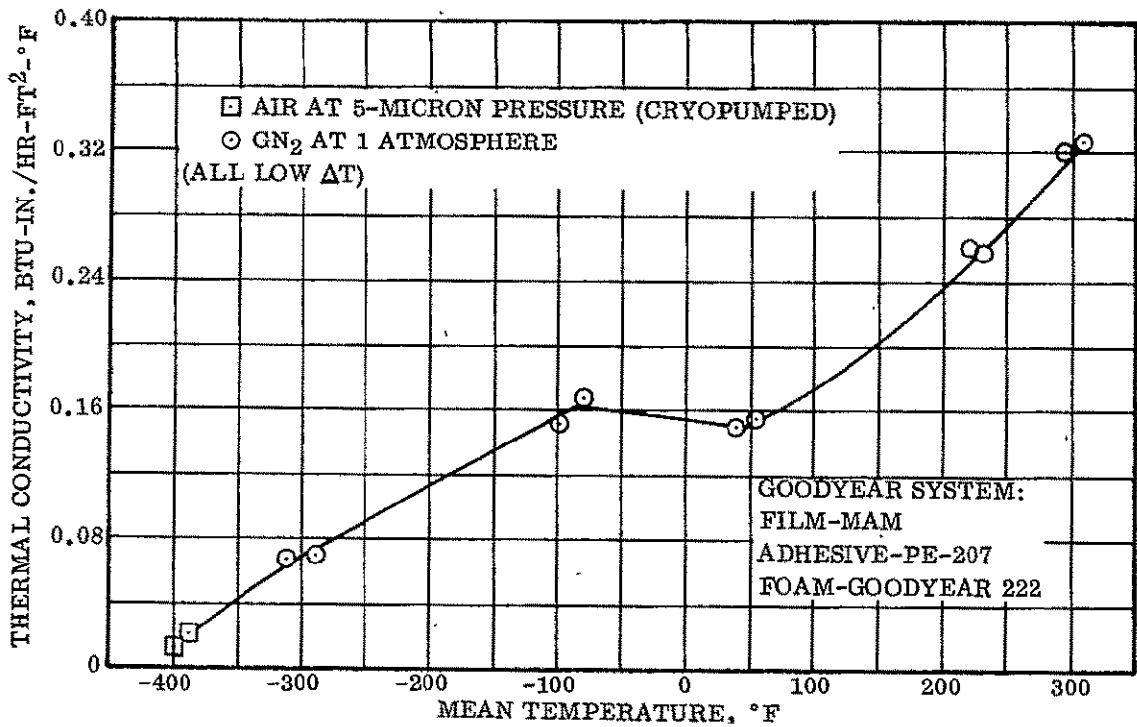


Figure 2-29. Thermal Conductivity Test, Uniform Specimen, Virgin Sample, Specimen B

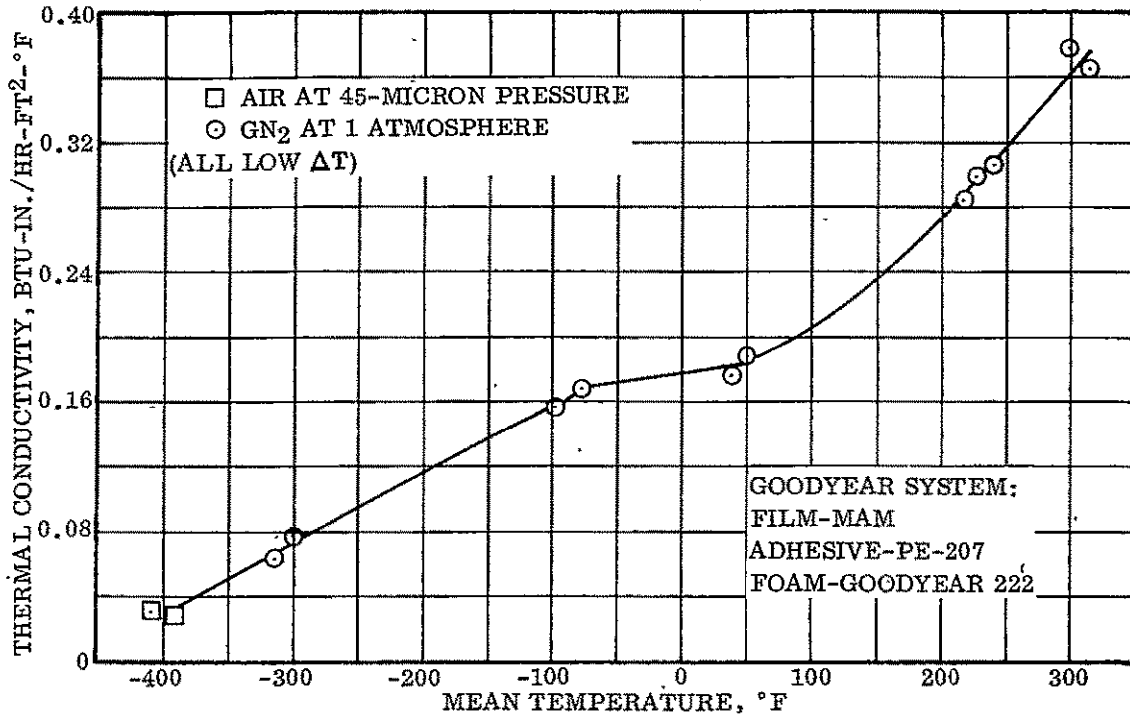


Figure 2-30. Thermal Conductivity Test, Uniform Specimen, Subjected to Aerodynamic Heating, Specimen A

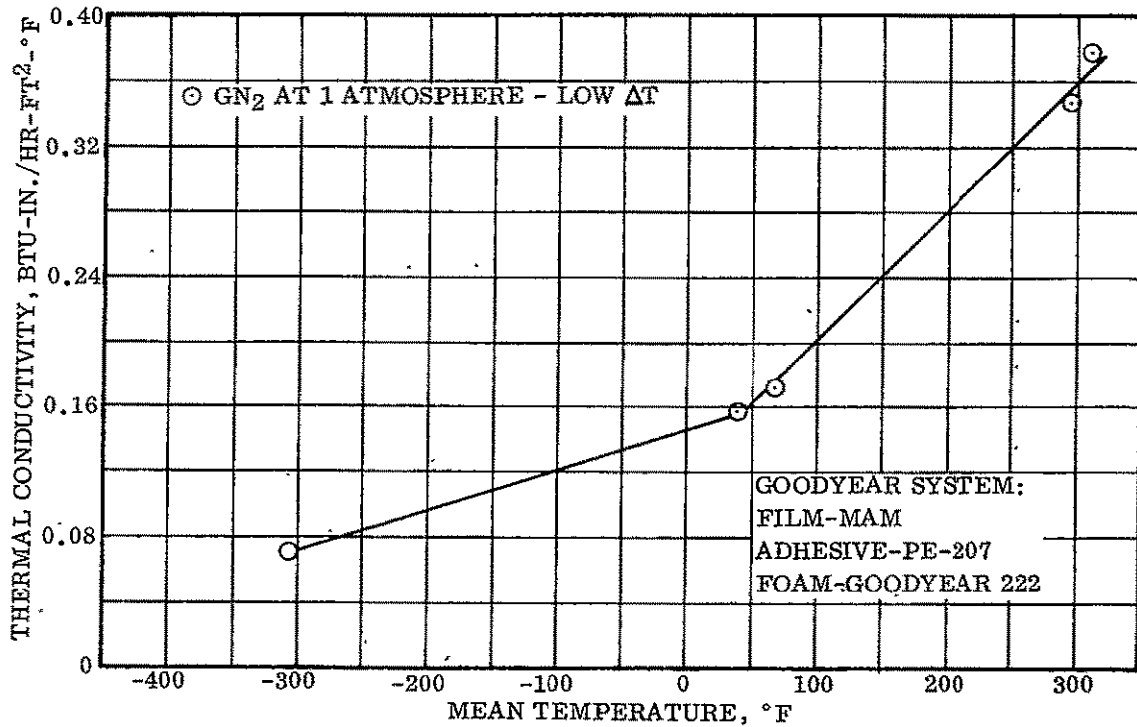


Figure 2-31. Thermal Conductivity Test, Uniform Specimen, Second Run, Specimen B

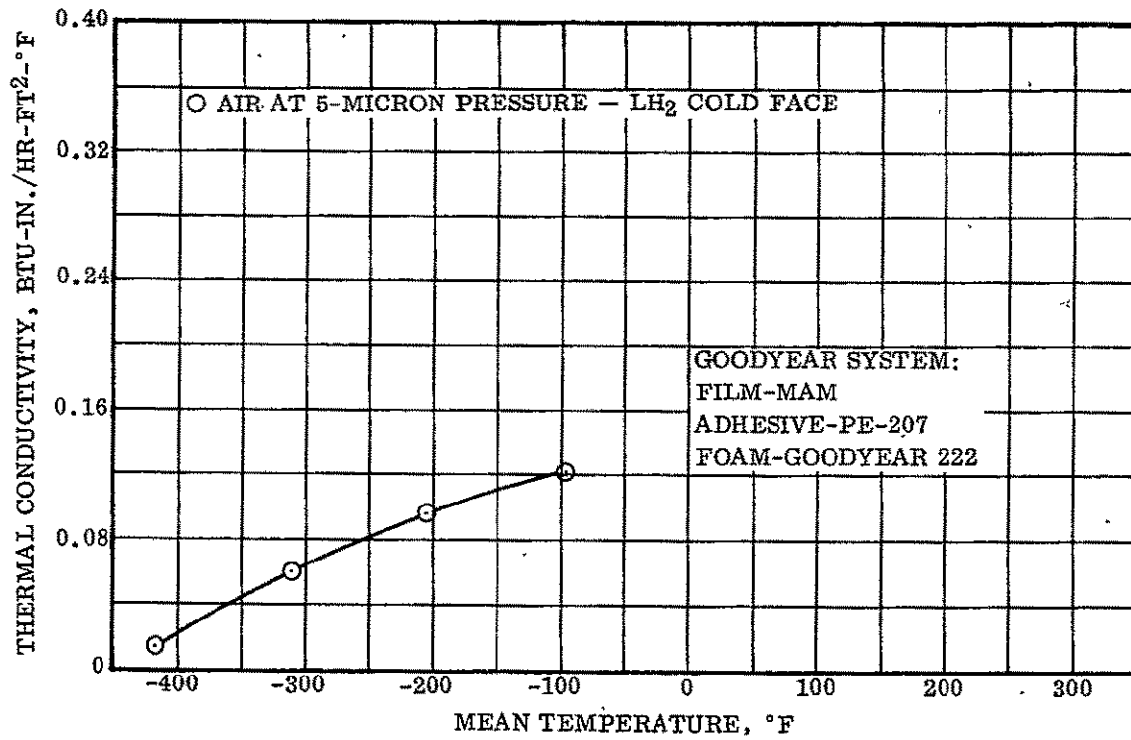


Figure 2-32. Thermal Conductivity Test, Uniform Specimen, Virgin Sample, Specimen C

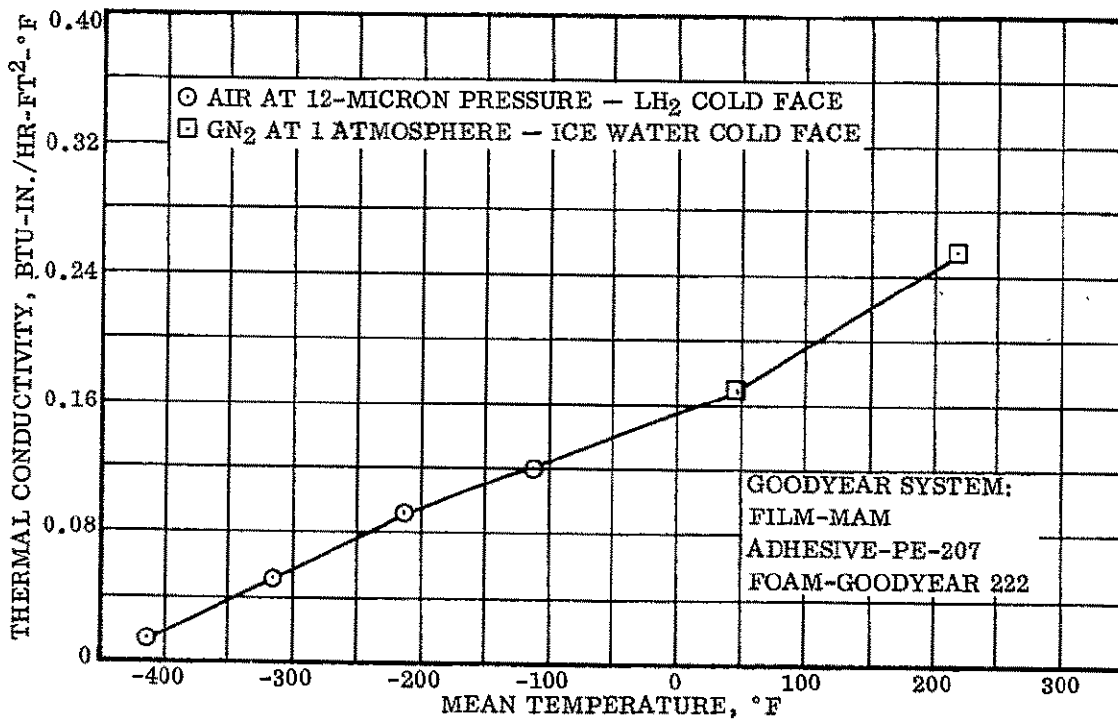


Figure 2-33. Thermal Conductivity Test, Uniform Specimen, Virgin Sample, Specimen D

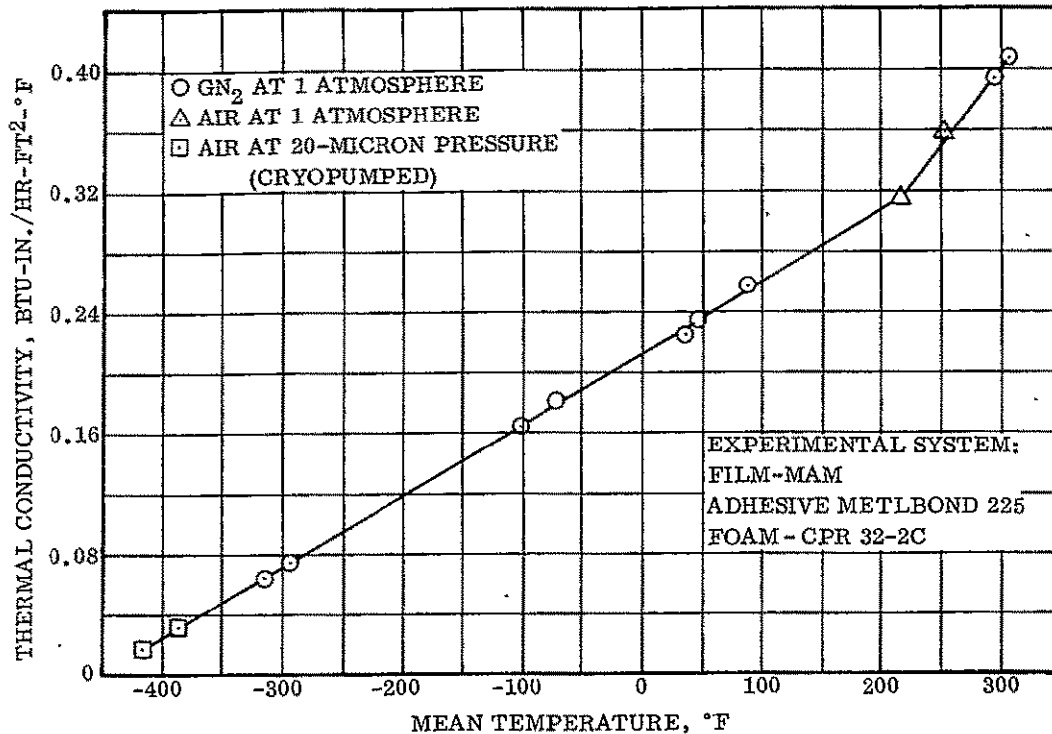


Figure 2-34. Thermal Conductivity Test, Joint Specimen, Virgin Sample, Specimen E

TABLE 2-19. RESULTS OF THERMAL CONDUCTANCE MEASUREMENTS ON SEALED FOAM INSULATION (EXPERIMENTAL SYSTEM; MAM FILM, METLBOND 225 ADHESIVE, CPR 32-2C FOAM)

ΔT (°F)	Mean Temp. (°F)	Thermal Conductivity BTU-in./hr-ft ² -°F	Atmosphere
Uniform Specimen (Virgin)			
30	47	0.235	GN ₂ at 1 atmosphere
8	36	0.226	
107	88	0.258	
12	-101	0.166	
66	-71	0.183	
53	-294	0.075	
16	-313	0.065	GN ₂ at 1 atmosphere
10	217	0.317	Air at 1 atmosphere
81	252	0.360	Air at 1 atmosphere
74	-386	0.031	Air at 20 microns (cryopumped)
15	-416	0.016	Air at 20 microns (cryopumped)
18	295	0.396	GN ₂ at 1 atmosphere
17	307	0.409	GN ₂ at 1 atmosphere

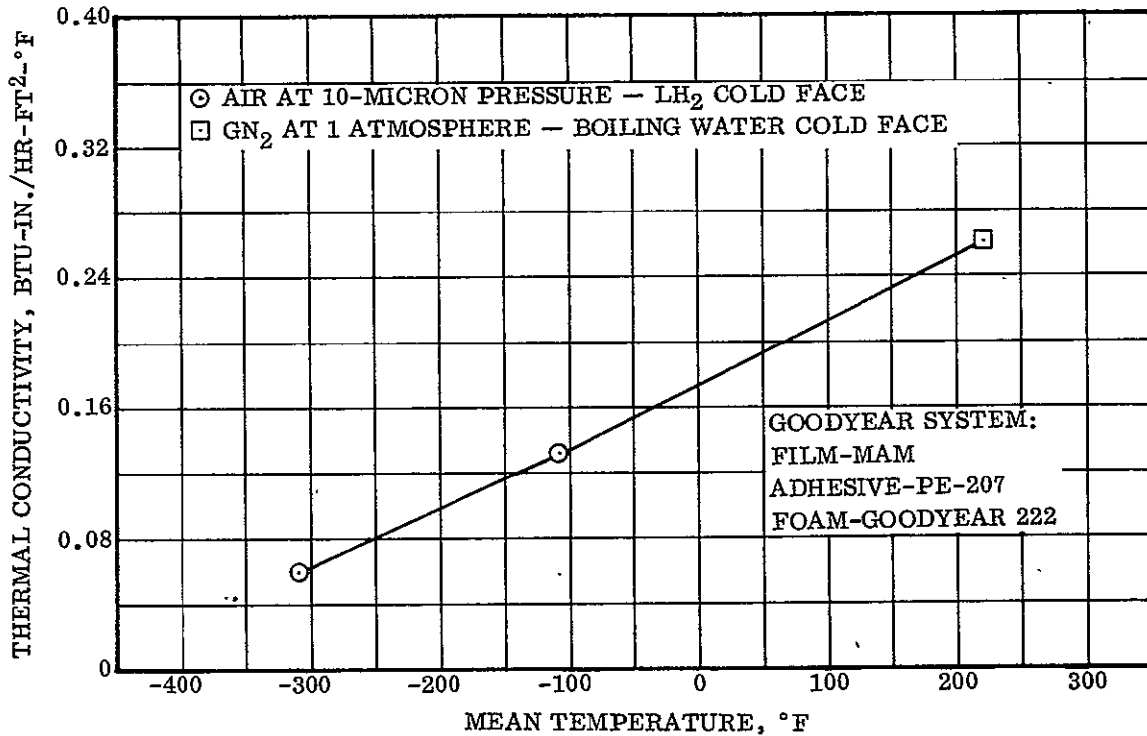


Figure 2-35. Thermal Conductivity Test, Uniform Specimen, Virgin Sample, Experimental

2.6.3.1 Test Materials and Apparatus. Sealed foam test panels were fabricated by Goodyear Corporation from 0.5-inch thick foam and surfaced at Convair with Connecticut Hard Rubber Company Compound 802 silicone rubber. Panels were 2 inches wide and a maximum of 36 inches long. The production configuration constrictive wrap strands, composed of S-994 glass roving and U.S. Polymeric FF-5255 phenolic, were coated with Andrew Brown Company's A-423 white epoxy paint and bonded to glass-phenolic tabs to provide for attachment. The strands were approximately 0.014 inch by 1/8 inch by 74 inches. The as-received condition on both the surfaces was that resulting from normal fabrication including dust, body oil, etc., accumulated in handling. Lubricants tested were obtained from commercial sources.

For test, two sections of foam panel totaling approximately 48.5 inches in length were mounted on a jig support form. This provided an appropriate radius (approximately 62 inches) to approximate the outside radius of the Centaur tank. Double-sided tape and small metal clips, embedded in the underside of the foam, were used to position the panels on the support form and prevent them from sliding. The 48.5-inch total length of panel was equivalent to approximately 45 degrees of the circumference, the angle over which the strands are stretched on the vehicle, assuming that the mid-point of the 90-degree installation arc is fixed.

The jig was placed in a horizontal position, with the fiberglass strand on top of the insulation panels, as shown in Figure 2-36. One end of the strand passed over a pulley to a hook and loading bucket. The other end of the strand was attached to a load cell. The signal from the load cell was recorded on a strip chart recorder. Total error in the load application sensing and recording system was less than ± 0.3 -pound, including allowances for pulley friction in the applied load.

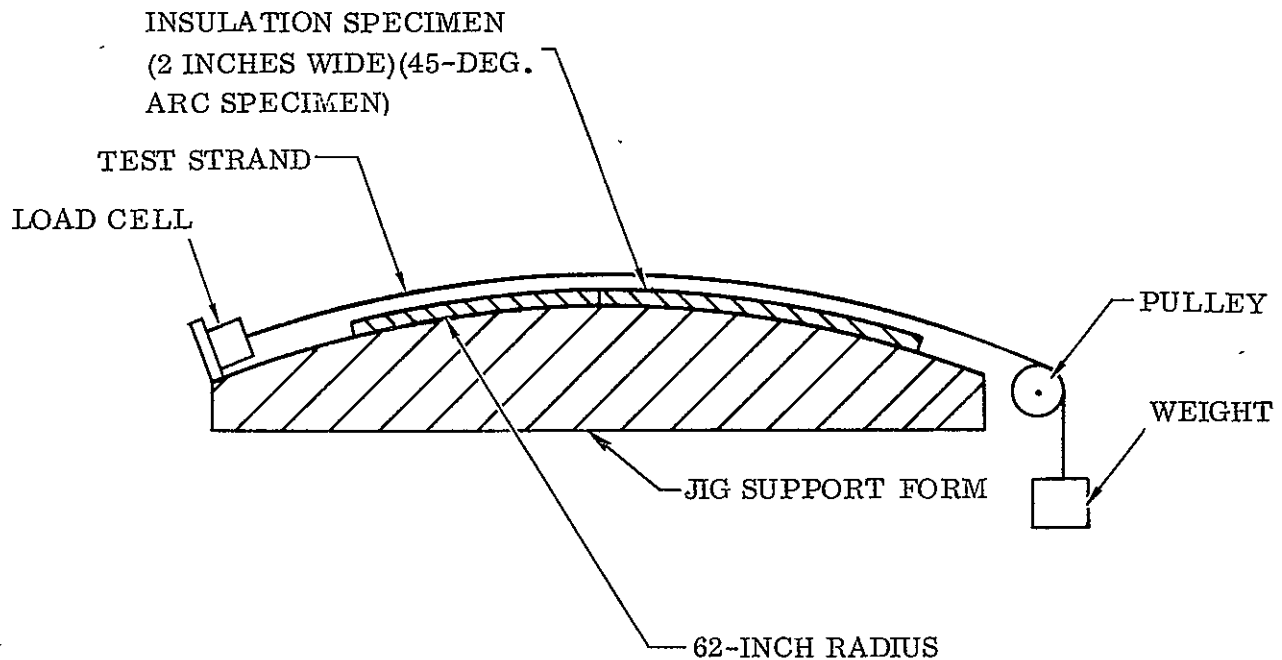


Figure 2-36. Strand Friction Test Apparatus

2.6.3.2 Test Conditions and Procedures. The single-strand frictional forces were measured for the following conditions, cleaning agents, and/or friction reducing agents:

- as-received condition
- Vel soap (dishpan grade)
- mica dust
- talcum powder
- carbowax (20% aqueous solution)
- 10g PEG-400, 40g ethylene glycol, 10g H₂O (organic I)
- Celvacene grease (medium)
- Ucon (50-HB 2000)
- alcohol (commercial grade)
- trichloroethylene (commercial grade)

The lubricants and cleaners used were selected on the basis of their application characteristics and their compatibility with the other materials and installation procedures involved. Virgin samples of each surface were used for each test where a friction-reducing agent was to be tested. These virgin specimens were each cleaned with Vel soap, rinsed with water, and dried before application of the test agent.

Following assembly of the test specimen, the general test procedure consisted of applying a measured load (corrected for pulley friction) at the free end of the strand, recording the load which appeared at the load cell, and calculating the friction force distributed along the interface by subtracting the two loads. Applied loads generally started at 3.5 pounds (effective weight of empty loading system), and were increased in 10 pound increments to a maximum of 63.5 pounds. Calculated friction forces in the simulated 45-degree segment were then plotted against the applied forces for the various conditions.

2.6.3.3 Friction Test Results. Test results are summarized in Figures 2-37, 2-38, and 2-39. For those conditions for which only one test was conducted, a smooth, best fit curve was drawn; where more than one test was conducted under similar conditions, a bounded region is indicated which includes all results.

As Figure 2-37 indicates, nearly all of the lubricants tested lowered the single-strand friction from the as-received condition, with Vel soap, Ucon, and Celvacene being the most effective. Vel soap, however, was considerably more effective in the as-applied, wet condition. Since mica dust is used as a release agent in the manufacture of the silicone rubber surface, the results for the as-received specimens and the mica dust-lubricated specimens fell within the same band.

The band shown for Vel soap includes data obtained over the time span from when a fresh solution had been applied (wet) to 9 days later when the interface was considered "dry", or had at least aged as long as it might in actual use. In addition to the increase in friction as the soap dried, another phenomenon (which was observed in other cases) occurred here, but only during testing of the lubricants. This was the appearance of a significant time for the load seen by the load cell to stabilize following a change in the applied load. In this case, the times involved were in the order of 1 minute; approximately 85 percent of the change in load was seen within 15 seconds. In the other tests involving lubricants, the load cell indicated the full applied load essentially instantaneously, as would be expected. The phenomenon with the dry soap indicated that long-time creep of some nature was occurring in the system, most likely at the friction interface.

This same phenomenon was considerably more apparent when the materials were run dry following the application of cleaning agents, including the Vel soap. For example, the curves in Figure 2-38 show the results of measurements made on materials cleaned with Vel soap (with the exception noted). The upper band represents the range of values obtained in three runs. Times allowed for load distribution stabilization varied from

approximately 15 seconds to 2.5 minutes per point with the resulting friction force values falling toward the top of the band for the shorter times, and the bottom of the band for the longer times. The lower curve shows the actual data points for a single run. Although the test conditions were the same as for the data above, lower friction forces were obtained due to the longer times allowed for stabilization. Values were actually lower than in the as-received condition. Changes in the slope of the curve can be seen as the times changed. The final load (63.5 pounds) was maintained for 120 minutes, although no significant change was seen after 30 minutes; the value obtained was approximately 50 percent of the values in the upper band. A single point obtained by applying the maximum load to an alcohol-cleaned specimen and maintaining it for 10 minutes is also plotted. This fell near the peak of the lower curve.

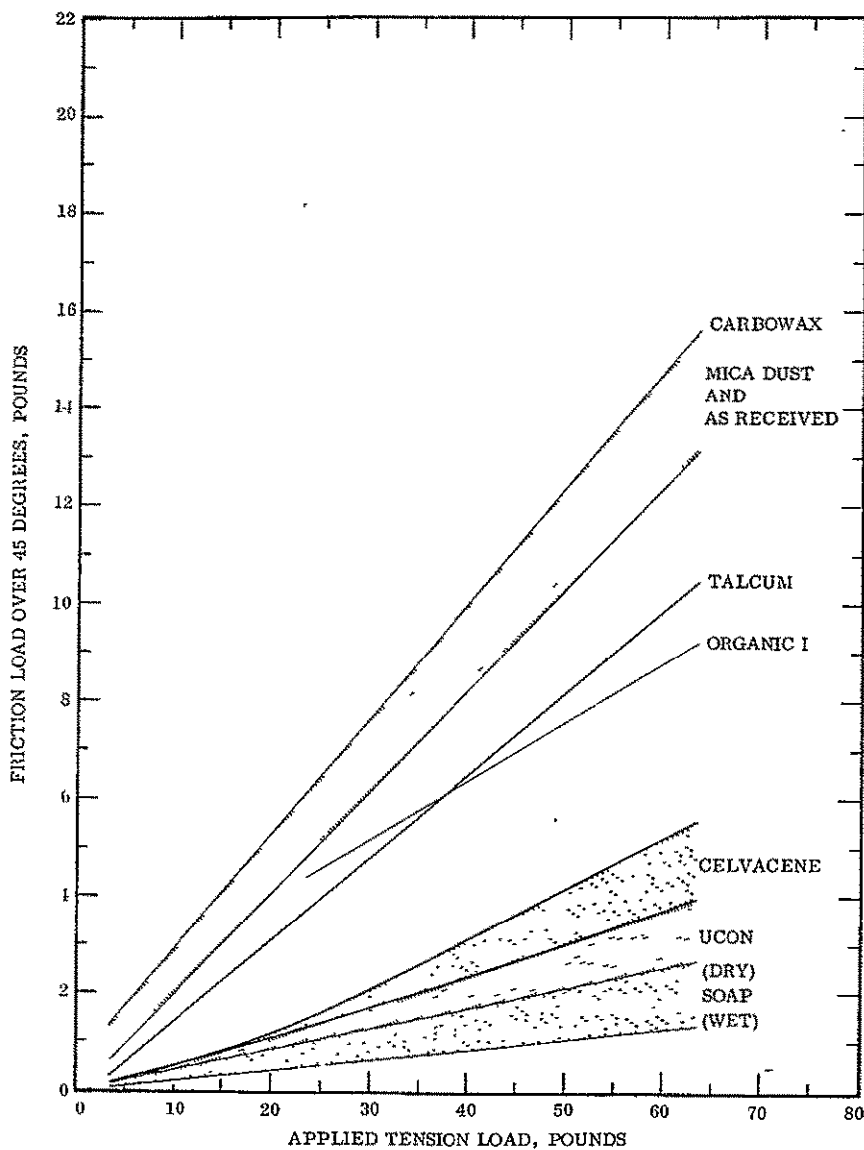


Figure 2-37. Total Constrictive Wrap Strand Friction Force Over 45 Degrees — Lubricated

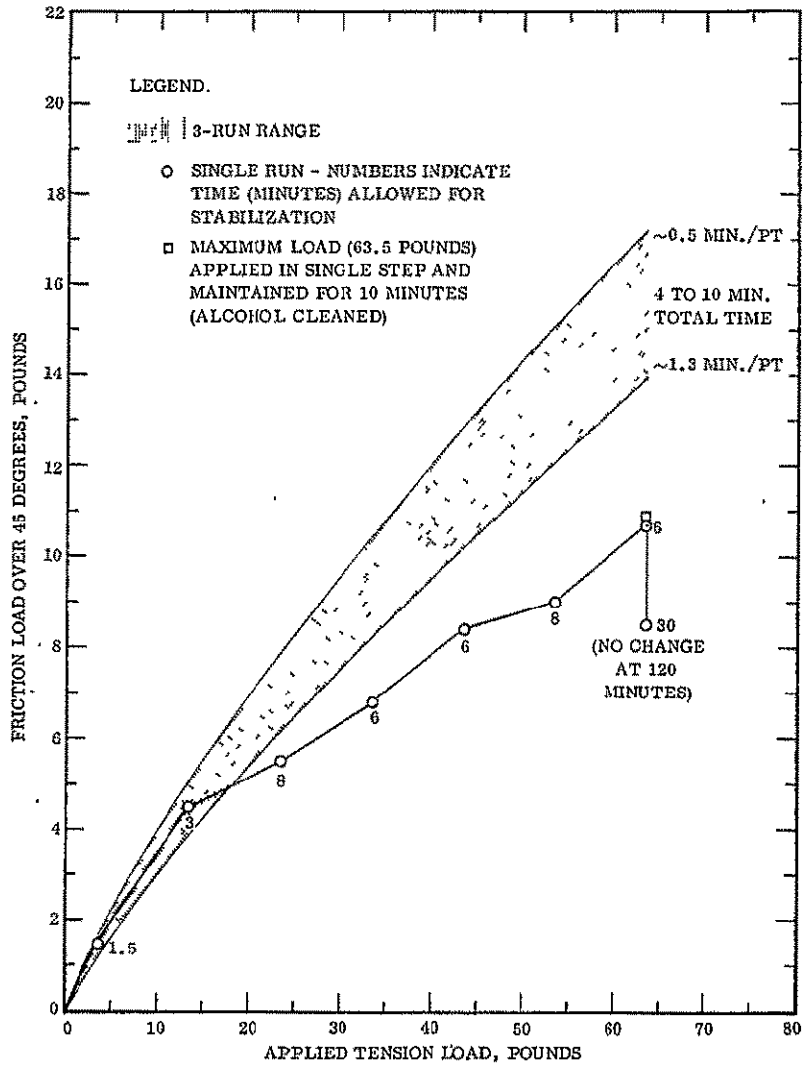


Figure 2-38. Total Constrictive Wrap Strand Friction Force Over 45 Degrees - Vel Soap Cleaned

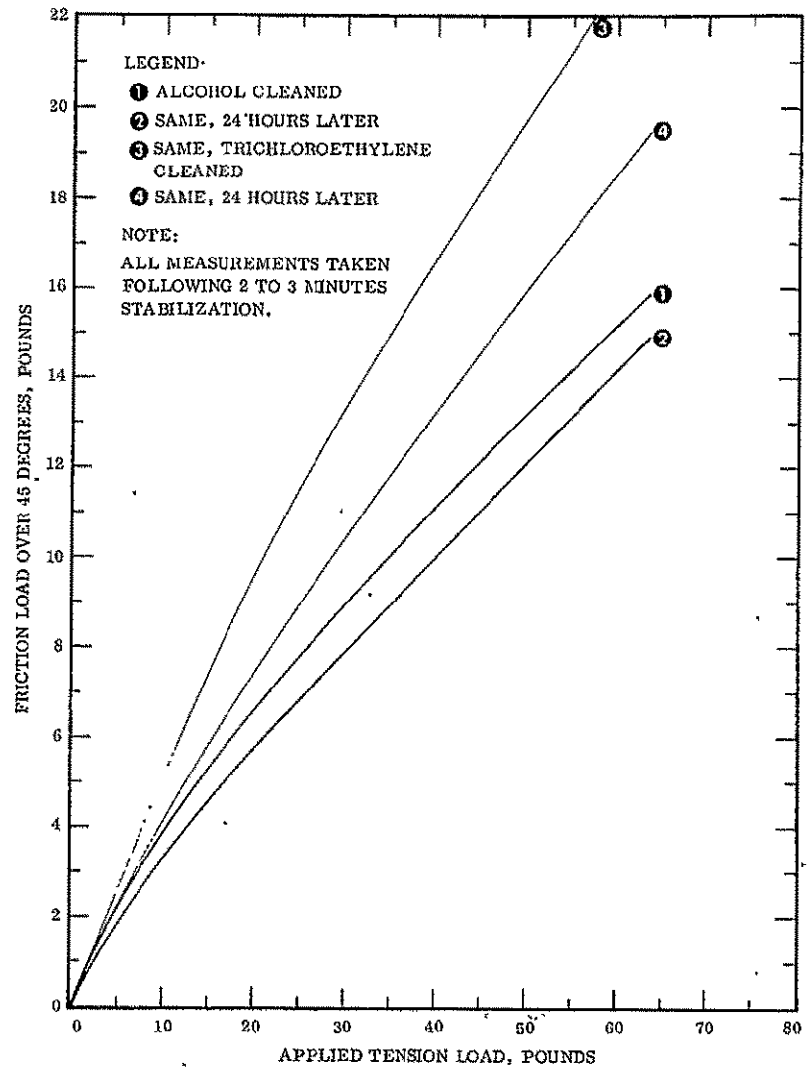


Figure 2-39. Total Constrictive Wrap Strand Friction Force Over 45 Degrees - Solvent Cleaned

The curves in Figure 2-39 show the results of a test series to determine the stabilities of alcohol and trichloroethylene-cleaned surfaces over a 24-hour period. Since both materials introduced large stabilization times, values were obtained by allowing an arbitrary 2 to 3 minutes of stabilization per point. Under these conditions, the alcohol cleaned surface gave results near the as-received condition, which reduced approximately 5 percent after 24 hours; the trichloroethylene cleaned surface values decreased approximately 20 percent in an equal period, but were significantly higher overall. Since the same surfaces were utilized for both tests, it is possible that the decrease seen 24 hours following the trichloroethylene cleaning was, in part, due to continued recovery from the effects of the alcohol. No attempt was made to evaluate the friction forces under these conditions as a function of allowed stabilization times, and it cannot be assumed that solvent cleaning cannot produce less acceptable friction characteristics than those obtained from the as-received condition.

2.6.3.4 Force -- Friction Relationships. In Figure 2-40, a tension strap is shown stretched over a cylindrical sector of angle 2ψ and radius, R . An equating of vertical forces yields:

$$2T \sin \psi = 2 \int_0^\psi N(Rd\theta) (\cos \theta) \quad (2-1)$$

where: T = tension in the strap (assumed uniform)

N = normal force per unit length between the cylinder sector and strap (assumed uniform)

Equation 1 integrates to:

$$2T \sin \psi = 2NR \sin \psi \quad (2-2)$$

$$\text{or } T = NR \quad (2-3)$$

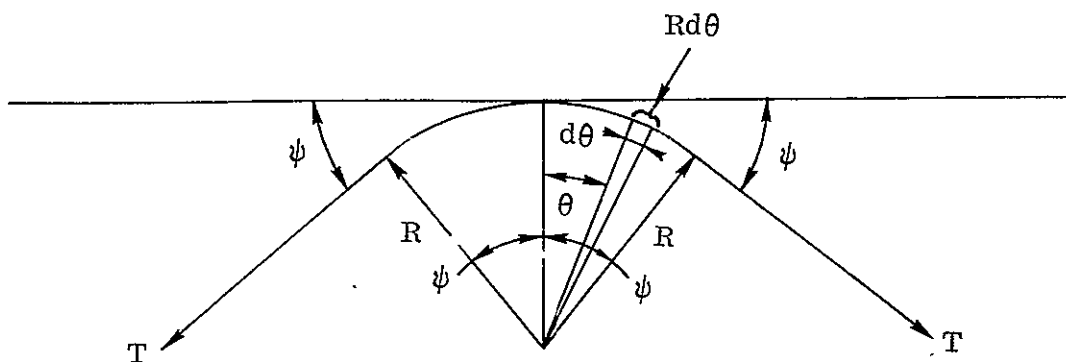


Figure 2-40. Geometrical Relationship of a Strap in Tension over a Cylindrical Sector

Since ψ can be made ever increasingly small without affecting the results of the above equations, one can readily assume that Eq. 2-3 is exactly true for any one point regardless of how T or R may vary between points.

With this relationship established between the tension and the normal forces, the friction factor can now be considered. By definition:

$$F = \mu N \quad (2-4)$$

where:

F = friction force per unit length

μ = coefficient of friction

N = normal force per unit length.

The tension in the strap is reduced by the friction force between the strap and the cylindrical section. The change in the tension over an incremental distance, $Rd\theta$, due to the presence of friction, can be expressed as follows:

$$dT = -\mu NRd\theta \quad (2-5)$$

since: $N = T/R$ (from Equation 2-3),

$$dT = -\mu Td\theta \quad (2-6)$$

Equation 2-6 can be integrated by separation of variables to give:

$$T_{\theta} = T_0 e^{-\mu\theta} \quad (2-7)$$

where: T_0 = tension at point of application

T_{θ} = tension at point θ radians from point of application

Since the friction force over θ radians is equal to $T_0 - T_{\theta}$, then:

$$F_{\theta} = T_0 (1 - e^{-\mu\theta}) \quad (2-8)$$

where:

F_{θ} = total friction force developed over the arc of θ radians.

Since the attachment points on the Centaur tank are spaced every 90 degrees, and are free to stretch the fiberglass strands from both directions, the effective angle over which the strands are stretched is 45 degrees, or 0.785 radians. At this angle, and for reasonable coefficients of friction (less than 0.2), $e^{-\mu\theta}$ is approximately equal to $1 - \mu\theta$, and Eq. 2-8 becomes:

$$F_{0.785} = (0.785)\mu T_o \quad (2-9)$$

The relationships described above can be manipulated to exactly describe the total friction force over any arc, θ , from the experimental data obtained for a 45-degree arc in this investigation. This relationship can be expressed as:

$$F_e = T_o \left[1 - \left(\frac{T_o - F_{45}}{T_o} \right)^{\theta/45} \right] \quad (2-10)$$

where:

F_θ = friction force over θ degrees

T_o = tension load at point of application, pounds

F_{45} = friction force over 45 degrees.

3

THERMODYNAMIC EVALUATION

A thermodynamic evaluation of two fixed insulation systems was performed to (1) optimize foam thickness; (2) determine insulation system temperatures during pre-launch operations, boost phase heating, and coast; (3) determine payload losses attributable to LH₂ boiloff during boost and coast phase heating; and (4) evaluate the effect of ice formation on the insulation panel surface.

The fiberglass strand constrictive wrap system employed sealed foam panels bonded to the LH₂ tank and then covered with a rubber impregnated fiberglass erosion cloth. A constrictive force was provided by stretched fiberglass strands.

The corrugated constrictive wrap system consisted of sealed foam panels bonded to the tank with the constrictive force provided by an aluminum corrugation held to the panels by stretched wires. No erosion cloth was required because the aluminum corrugations provided protection for the sealed panels from aerodynamic erosion.

The results of the thermodynamic evaluation of the two systems are briefly described in this section. For complete details of the analyses, see References 3-1 and 3-2 for the fiberglass strand constrictive wrap system, and Reference 3-3 for the corrugated constrictive wrap system.

The above two systems were evaluated on the following assumptions:

1. All temperature and heating rate calculations were based upon aerodynamic heating rates on a smooth surface, i.e., protuberances were not considered in this analysis.
2. The MAM seal of the foam insulation is 0.0015 inch thick and was assumed to be a part of the erosion cloth for analytical purposes.
3. The SLV-3C/Centaur design trajectory for maximum heating (SP47-3C) was used to predict aerodynamic heating during boost phase (except where noted).
4. There was no carryover of liquid hydrogen during GH₂ venting.
5. The vehicle sidewalls during boost and coast phase heating radiate to the temperature of the Patrick Air Force Base Atmosphere up to an altitude of 82,000 feet and to absolute zero thereafter.

6. The incident space heating rate magnitudes to the cylindrical tank wall for each of the three orbital cases considered were derived with the aid of the Space Vehicle Radiant Energy Program (Reference 3-4). The unit area space heating rates applied to the cylindrical tank were: (1) computed assuming the longitudinal axis of the tank was colinear with the vehicle velocity vector, and (2) averaged around the cylindrical wall surface.
7. The orbital parameters assumed for each of the three orbital cases are shown in Table 3-1.

TABLE 3-1. ASSUMED ORBITAL PARAMETERS

Parameter	Case 1	Case 2	Case 3
	Maximum heating 25-minute coast	Maximum heating 70-minute coast	Minimum heating 25- and 70-minute coast
Time of year of launch	21 December	21 June	21 June
Time of day of launch	0940 EST	0300 EST	1700 EST
Eccentricity	0.0	0.0	0.0
Altitude (n. mi)			
Apogee	90	90	90
Perigee	90	90	90
Right Ascension of the ascending node (degrees)	117.9	198.6	47.9
Orbital inclination to the equator (degrees)	30.55	30.55	30.55
Resulting inclination of the orbital plane to the earth-sun vector (degrees)	35	51	2

8. Only the heat transferred into the liquid hydrogen was considered in this analysis. Heat transfer into the ullage affects tank pressure, but not LH₂ boiloff. The wetted tank area was varied as a function of time to account for the consumption of hydrogen propellant during the first Centaur burn. The wetted sidewall area is 508 ft² between 0-300 seconds, decreases linearly to 179 ft² between 300-585 seconds, and is 179 ft² between 585 seconds and the end of coast.
9. Aerodynamic heating was calculated using Reference 3-5.

3.1 FIBERGLASS STRAND CONSTRICTIVE WRAP SYSTEM

This configuration consisted of sealed foam panels protected from aerodynamic heating by an erosion cloth. Additionally, a compressive load was maintained on the foam insulation and erosion cloth through the use of pre-tensioned fiberglass strands. The detail design and fabrication of this system is more fully explained in Sections 4 and 5, respectively.

3.1.1 FOAM THICKNESS EVALUATION. A parametric study was accomplished to determine the optimum foam thickness consistent with minimizing hydrogen boiloff losses and insulation system weight. This was done by calculating the total LH₂ heat rate during the boost and coast phase of flight. The effect of the heating rate on LH₂ propellant boiloff losses was then calculated to determine the actual payload loss.

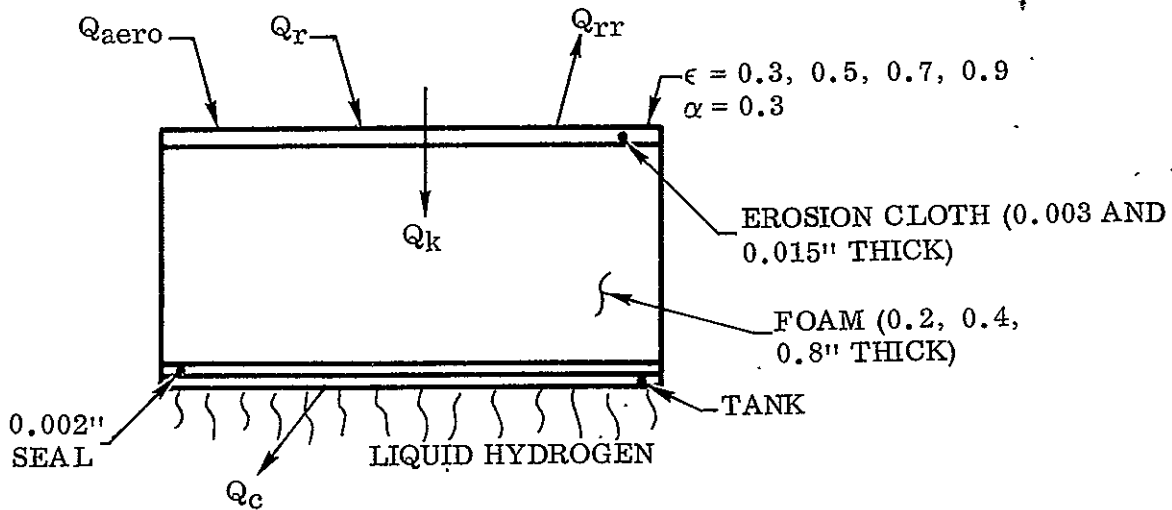
Two types of foam were analyzed: (1) Goodyear 222, a Freon-blown foam having a density of 2.0 lb/ft³, and (2) CPR 32-2C, a CO₂-blown foam having a density of 2.1 lb/ft³ and a higher thermal conductivity than that of the Goodyear 222 foam. The CPR 32-2C foam system was added to this study because of its superior high-temperature properties as described in Subsection 2.1.3.

3.1.1.1 Total LH₂ Heat Rate. The total wetted wall LH₂ tank heat rate during the boost and coast phase of flight is comprised of sidewall heating, and heating from other sources such as through the forward and intermediate bulkheads, and the Station 219 ring area.

3.1.1.1.1 LH₂ Sidewall Heating. Sidewall heating to the settled liquid hydrogen was calculated using the maximum heating design trajectory (SP47-3C) for SLV-3C during the boost phase with three independent coast phase trajectories:

1. Maximum heating for a 25-minute coast (Reference Table 3-1, Case 1),
2. Maximum heating for a 70-minute coast (Reference Table 3-1, Case 2), and
3. Minimum heating for a 70-minute coast (Reference Table 3-1, Case 3).

Heat transfer was calculated for foam thicknesses of 0.2 inch, 0.4 inch, and 0.8 inch. Each foam thickness was analyzed with an erosion cloth thickness of 0.003 inch and 0.015 inch, and each combination of foam and erosion cloth thickness was analyzed with a surface emittance, ϵ , of 0.3, 0.5, 0.7, and 0.9. A low value of solar absorptance, α , is necessary to minimize solar radiation during coast, and a value of 0.3 was assumed. This is a reasonably attainable value for the range of temperature anticipated for this insulation system, (485° F maximum — Reference Subsection 3.1.2). A representation of the thermal model along with assumed material properties is shown in Figure 3-1.



- Q_{aero} = Aerodynamic Heat Flux
- Q_r = Solar, Earth Thermal, and Earth-Reflected Radiation Heat Flux
- Q_{rr} = Re-Radiated Heat Flux
- Q_k = Heat Transferred by Conduction
- Q_c = Heat Transferred by Convection into Liquid Hydrogen

THERMOPHYSICAL PROPERTIES

<u>EROSION CLOTH</u>		<u>FOAMS</u>	
THERMAL CONDUCTIVITY		FREON BLOWN THERMAL CONDUCTIVITY	CO ₂ BLOWN THERMAL CONDUCTIVITY
TEMP (°R)	($\frac{BTU}{HR-FT-°R}$)	TEMP °R	($\frac{BTU}{HR-FT-°R}$)
537	0.0899	40	0.003
605	0.0865	190	0.008
627	0.0938	450	0.014
852	0.103	600	0.015
1032	0.109	1100	0.033*
			*Estimated
	$\rho = 120 \frac{LB}{FT^3}$		$\rho = 2 \frac{LB}{FT^3}$
	$C_p = 0.26 \frac{BTU}{LB-°R}$		$C_p = 0.3 \frac{BTU}{LB-°R} @ 460°R$
			$C_p = 0.5 \frac{BTU}{LB-°R} @ 810°R$

Figure 3-1. Insulation Panel Thermal Model

Sidewall-averaged incident space heating rates for each of the trajectories considered are presented in Figures 3-2 through 3-4. Case 1 (Figure 3-2) was chosen because the 35° orbital inclination relative to the earth-sun vector resulted in maximum LH₂ heating for a relatively short 25-minute coast. Case 2 (Figure 3-3) was chosen on the basis that the increased orbital plane inclination to the earth-sun vector resulting from this orbit provided the maximum incident energy to the tank by maximizing the time in the sun and increasing the sidewall area projected to the sun for a greater portion of the orbit. Case 3 (Figure 3-4) is the resulting near-minimum space heating trajectory which was chosen for its launch directly into the earth's shadow. It should be noted that a minimum heating case for a 25-minute coast is contained within the minimum heating case for a 70-minute coast.

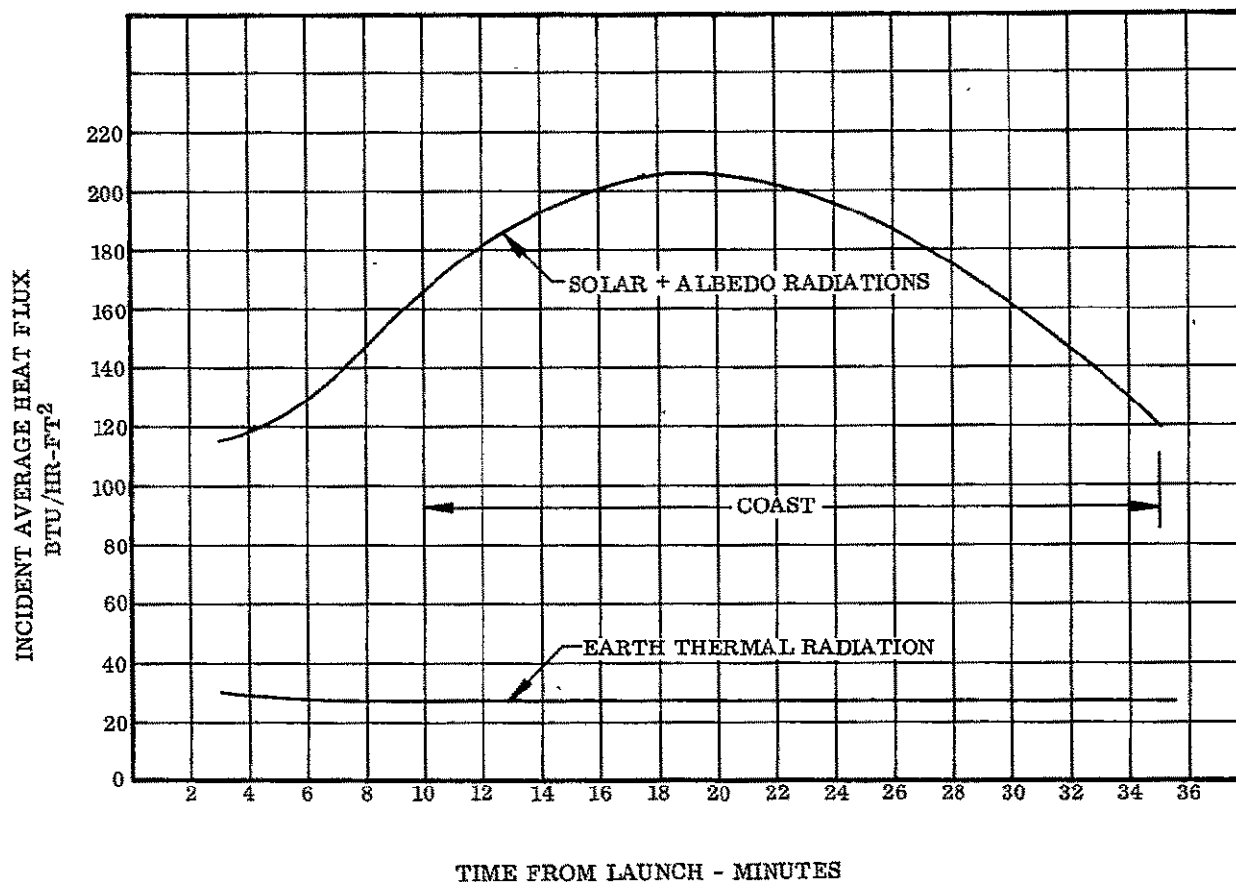


Figure 3-2. Incident Space Heating Rates for Case 1, Table 3-1

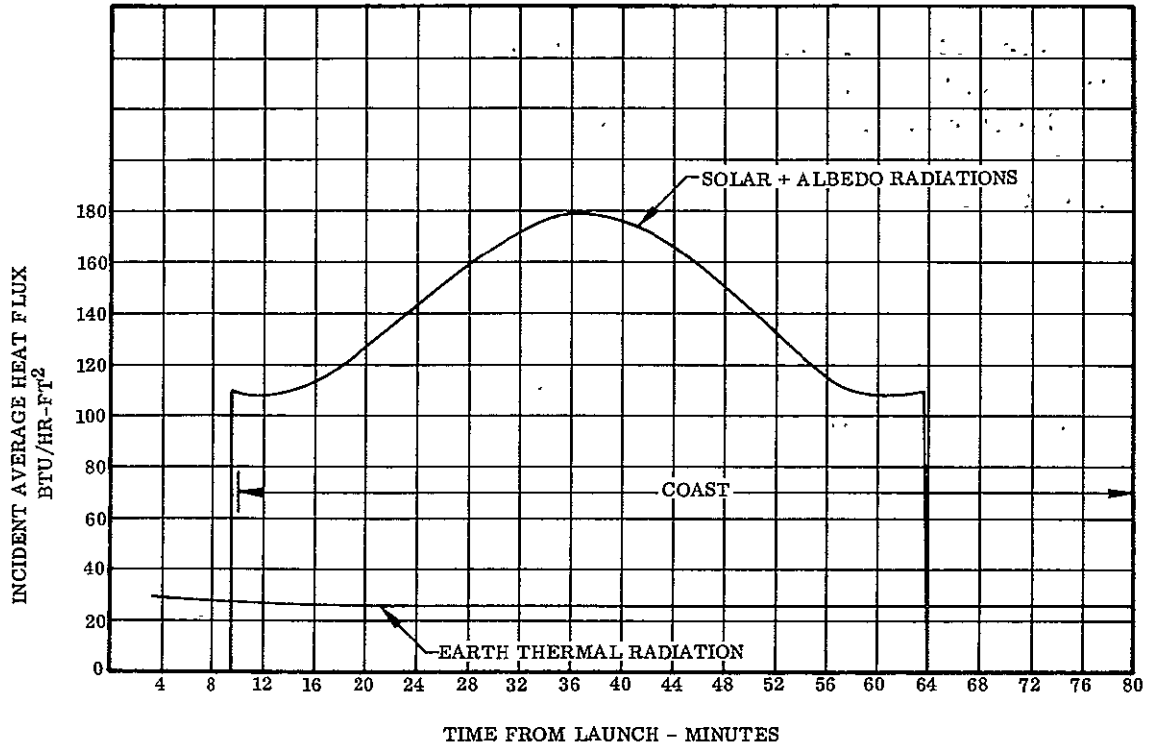


Figure 3-3. Incident Space Heating Rates for Case 2, Table 3-1

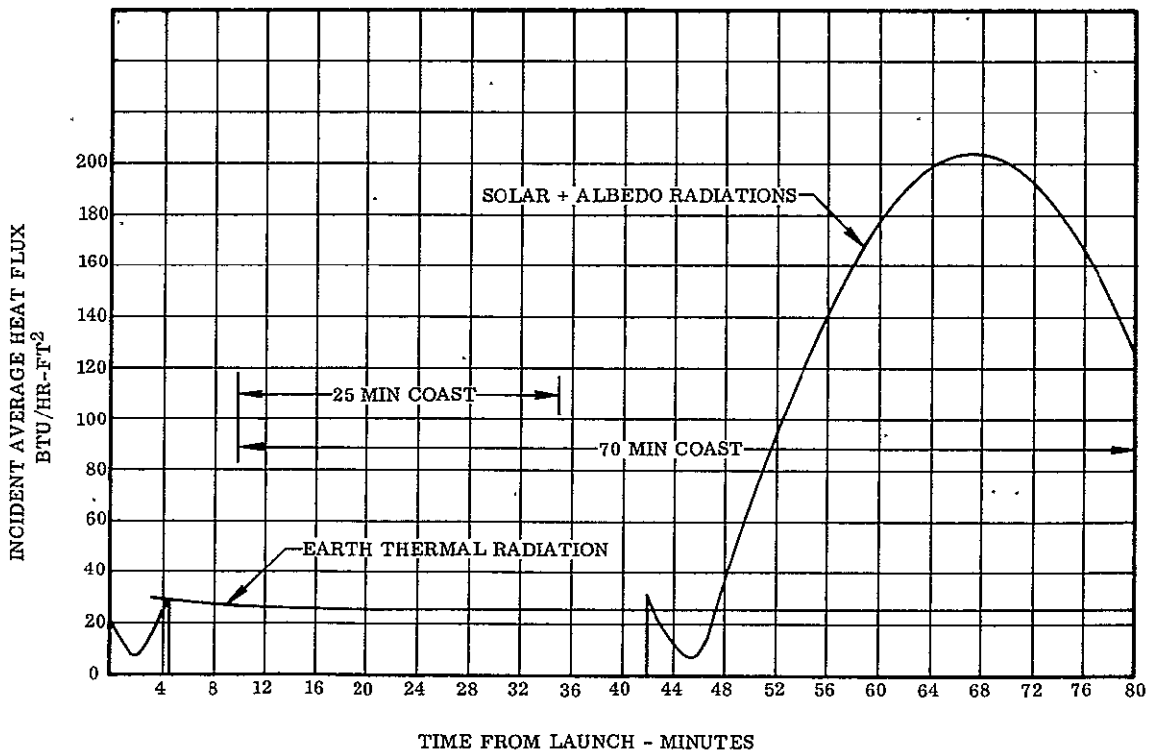


Figure 3-4. Incident Space Heating Rates for Case 3, Table 3-1

The heat flow into the liquid hydrogen was determined for each combination of erosion cloth thickness, foam thickness, surface emittance, and trajectory. Typical results of sidewall heating are shown in Figures 3-5 through 3-10. It is shown in Figure 3-5 that LH₂ heating varied inversely with both foam thickness and erosion cloth thickness during the early phase of aerodynamic heating. The influence of erosion cloth thickness was reversed after the maximum heat rate was attained as the stored heat in the 0.015-inch thick erosion cloth began to transfer into the LH₂. The sidewall heating rate for the current Centaur jettisonable insulation system is also shown in Figure 3-5. Coast phase heating rates are shown in Figure 3-6 for the 25-minute coast maximum heating trajectory, in Figure 3-7 for the 70-minute coast maximum heating trajectory, and in Figure 3-8 for the 70-minute coast minimum heating trajectory. Heat flow rates in Figures 3-5 through 3-8 were based upon a surface emittance of 0.9 and a solar absorptance of 0.3. Figures 3-9 and 3-10 show the sidewall heat rate for a foam thickness of 0.4 inch and surface emittances of 0.3, 0.5, 0.7, and 0.9. LH₂ heating during boost phase varied inversely with the surface emittance (Figure 3-9) because a high surface emittance caused re-radiation of a greater amount of energy than a low surface emittance. LH₂ heating during the coast phase varied directly with the surface emittance (Figure 3-10) because the increase in earth-thermal heating exceeded the increase in re-radiated energy. (The discontinuity in the time scale between Figures 3-9 and 3-10 was employed to accommodate greater accuracy on the vertical scale. This gap in the time scale between the two curves is not significant and in no way affects the conclusions drawn from the two figures.) Final selection of a high or low surface emittance was dependent upon the relative contributions of boost phase and coast phase heating. The longer the duration of coast, the greater the relative contribution of coast phase heating.

3.1.1.1.2 Other Sources of LH₂ Heating. Additional sources of heat transfer into the liquid hydrogen through the forward bulkhead, Station 219 ring, and intermediate bulkhead were based upon values reported in Reference 3-6 for a similar study. The heat flow through the forward bulkhead was based upon a one-half inch foam insulation. Only the heat transferred into the liquid was considered in this analysis. Heat transferred through the Station 219 ring was based upon Reference 3-7, except that the effect of the helium purge was subtracted for this analysis. A fiberglass honeycomb adapter similar to the Surveyor barrel section was assumed for this analysis to determine heat flow through the Station 219 ring. The heat transfer rate across the intermediate bulkhead was assumed constant at 1500 BTU/HR as reported in Reference 3-8.

The total heat into the liquid hydrogen propellant for each thermal model was determined for the boost phase (0 - 155 seconds), sustainer phase (155 - 250 seconds), and Centaur main engine firing plus coast (250 - 2100 seconds for the 25-minute coast and 250 - 4800 seconds for the 70-minute coast) by integrating heat rate (BTU/HR) for each time period.

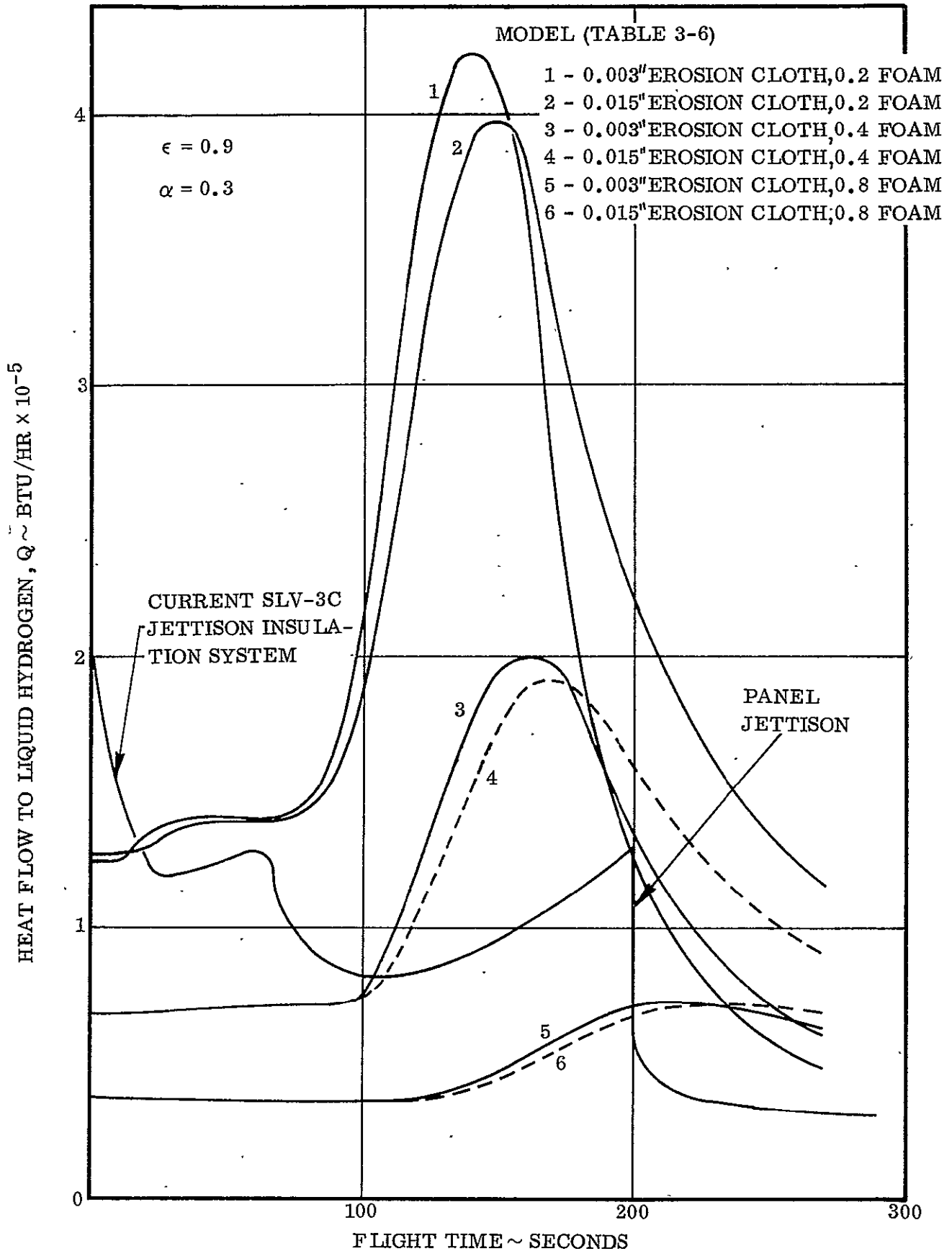


Figure 3-5. Liquid Hydrogen Heat Rate Caused by Aerodynamic and Space Heating (Sidewall Only) 25-Minute Coast Trajectory, Maximum Heating

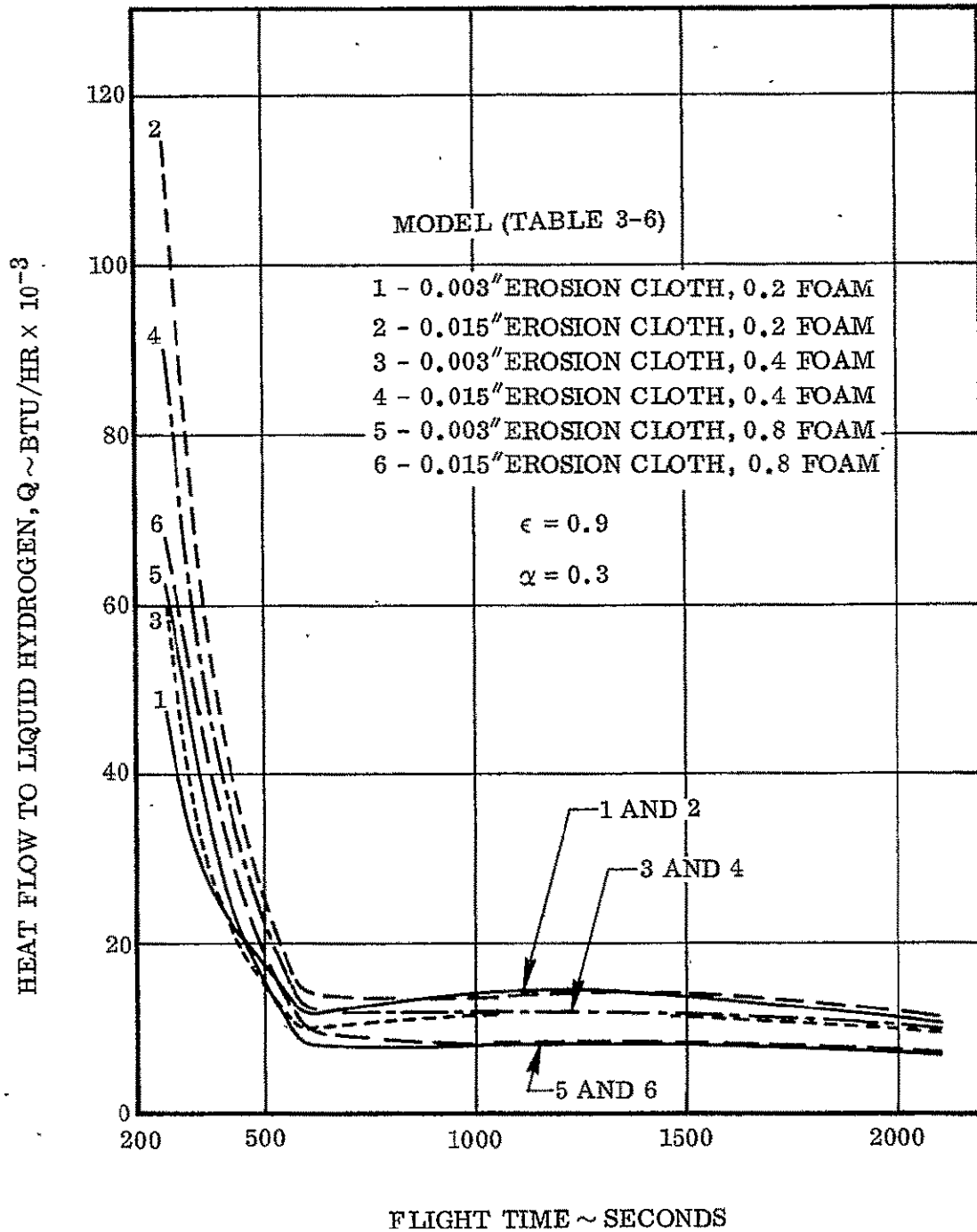


Figure 3-6. Liquid Hydrogen Heat Rate Caused by Aerodynamic and Space Heating (Sidewall Only) 25-Minute Coast Trajectory, Maximum Heating

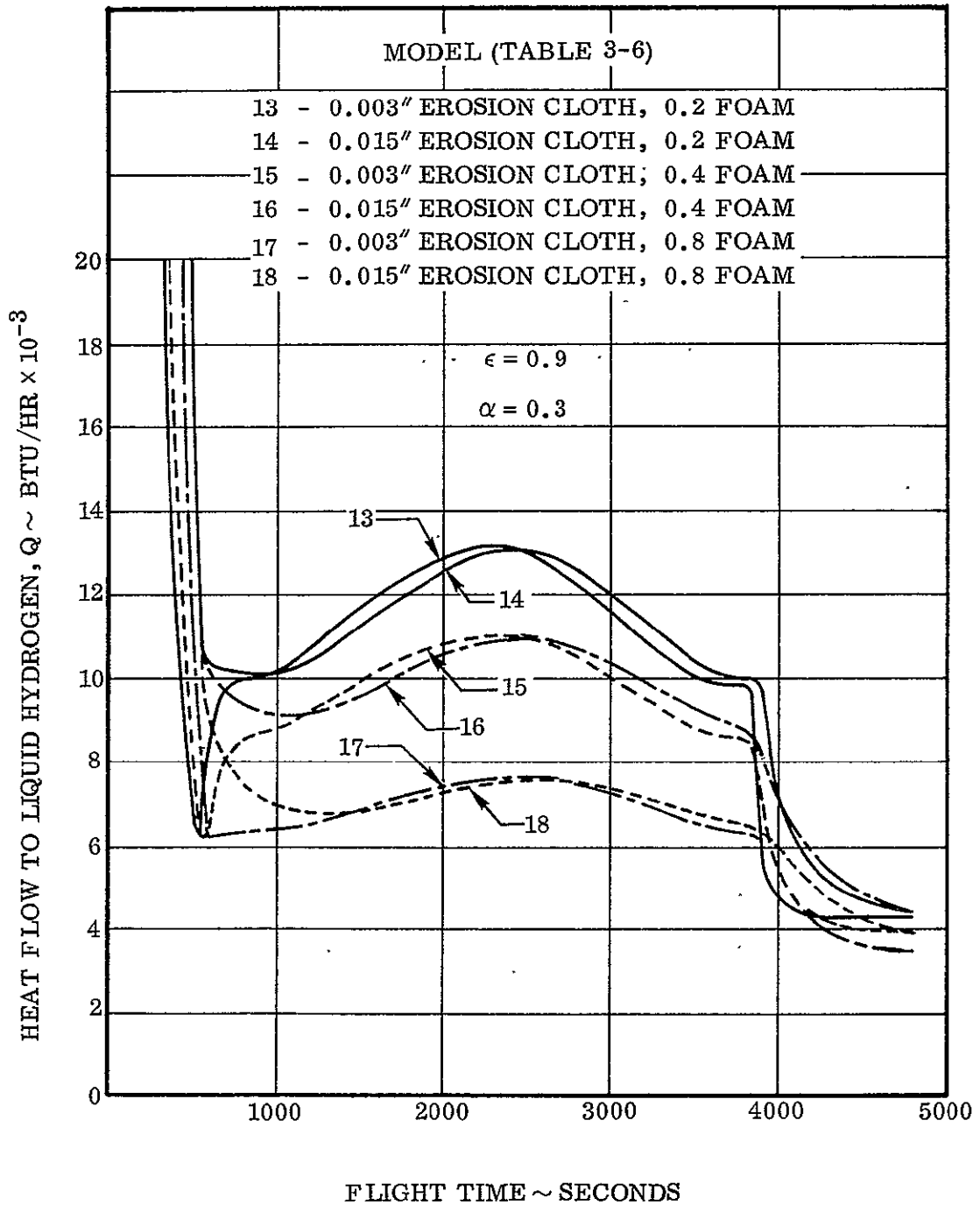


Figure 3-7. Liquid Hydrogen Heat Rate Caused by Aerodynamic and Space Heating (Sidewall Only) 70-Minute Coast Trajectory, Maximum Heating

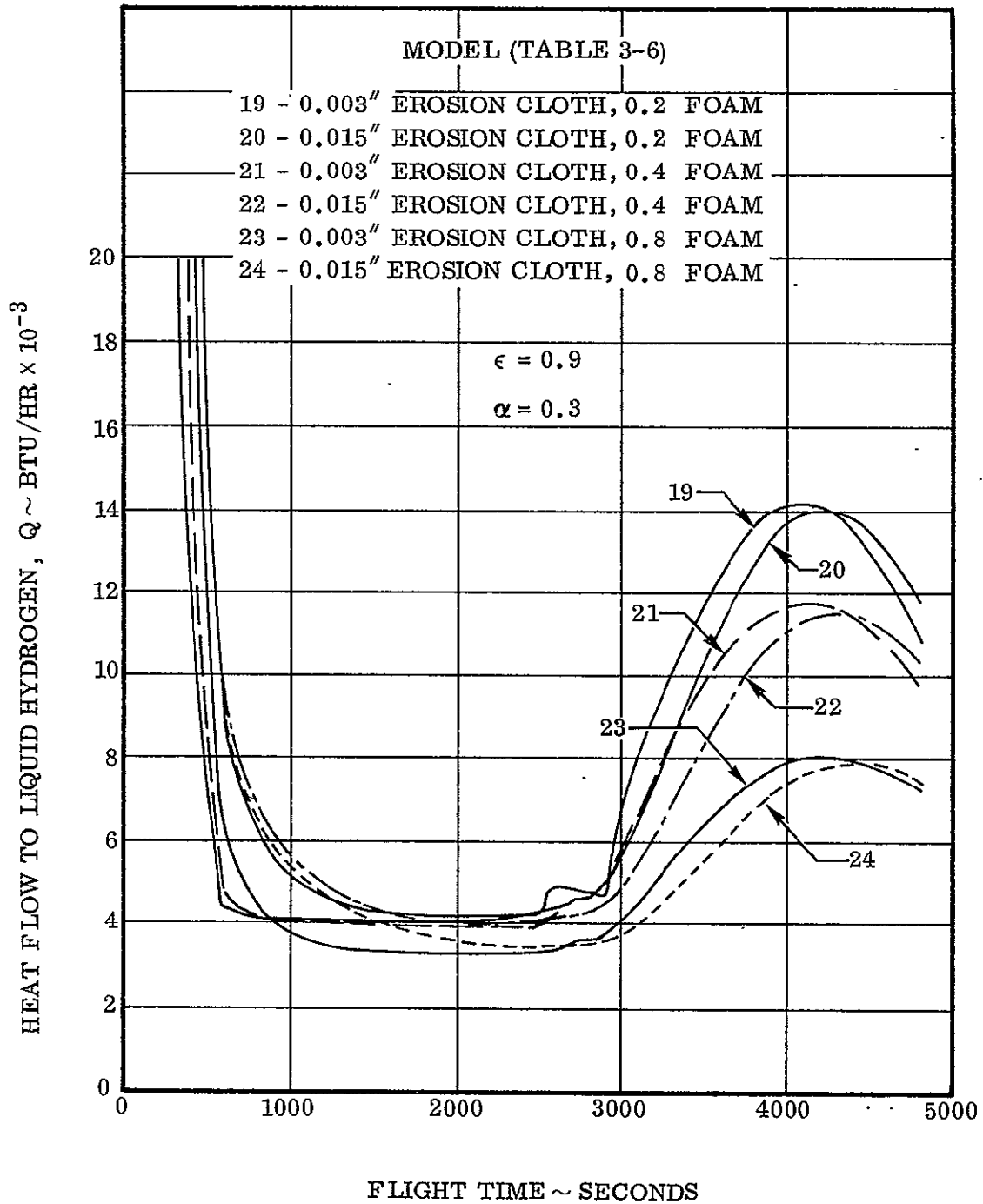


Figure 3-8. Liquid Hydrogen Heat Rate Caused by Aerodynamic and Space Heating (Sidewall Only) 70-Minute Coast Trajectory, Minimum Heating

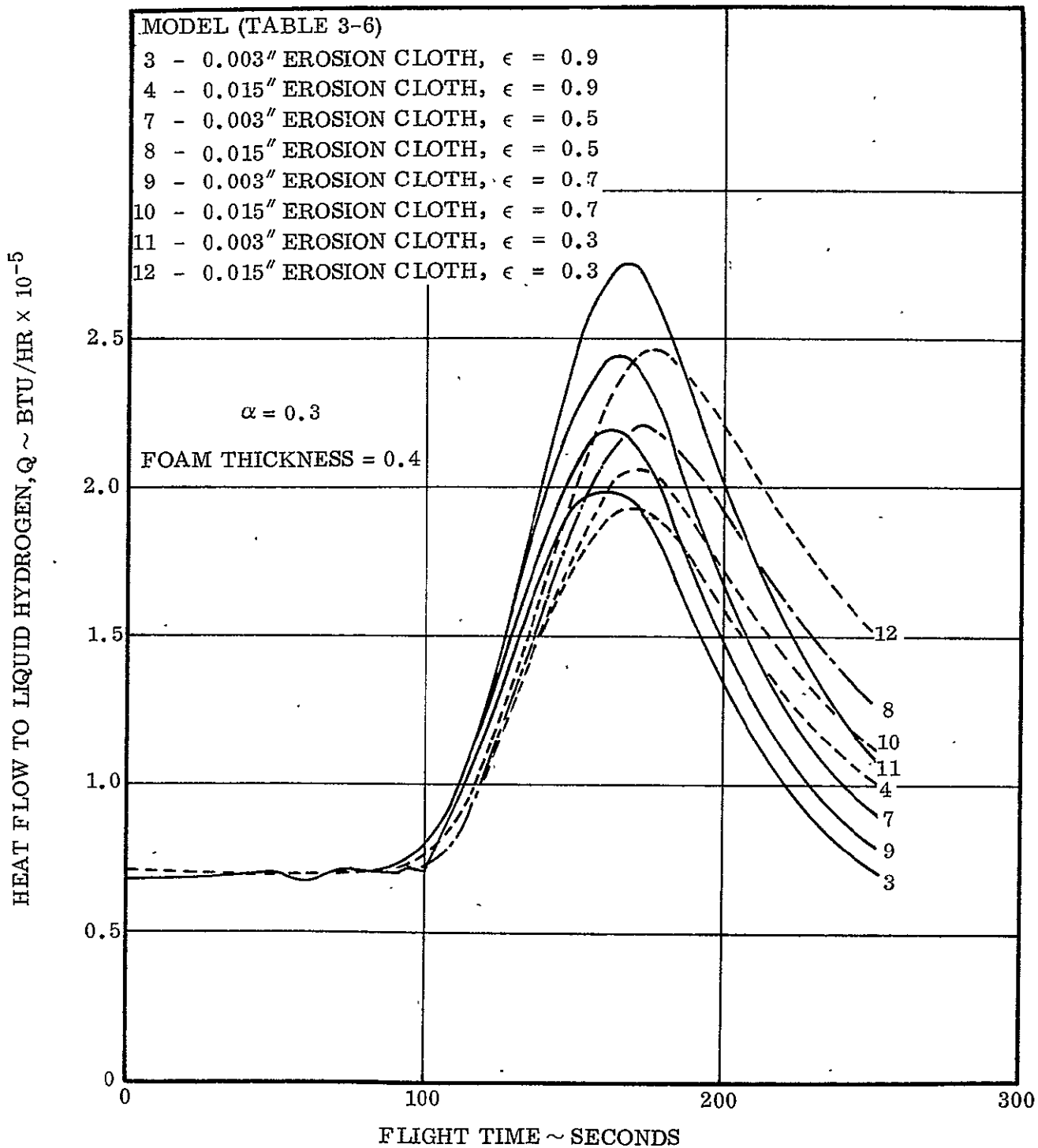


Figure 3-9. Liquid Hydrogen Heat Rate Caused by Aerodynamic and Space Heating (Sidewall Only) 25-Minute Coast Trajectory, Maximum Heating

$\alpha = .3$
 FOAM THICKNESS = .4

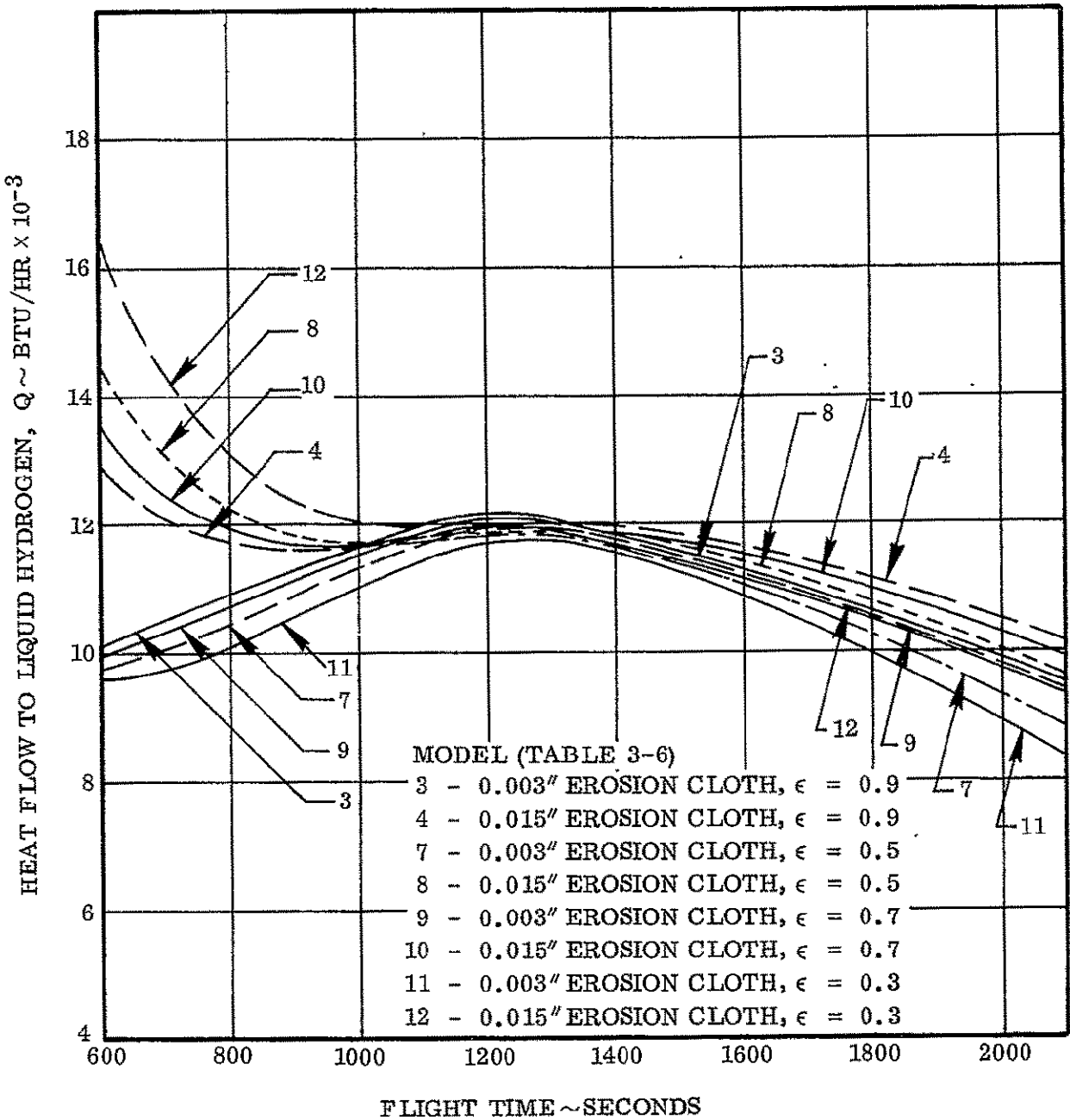


Figure 3-10. Liquid Hydrogen Heat Rate Caused by Aerodynamic and Space Heating (Sidewall Only) 25-Minute Coast Trajectory, Maximum Heating

The total heat transfer through the forward bulkhead and Station 219 ring, and through the intermediate bulkhead for both a 25-minute and 70-minute coast is tabulated in Table 3-2.

TABLE 3-2. HEAT TRANSFER THROUGH THE FORWARD BULKHEAD AND STATION 219 RING, AND THROUGH THE INTERMEDIATE BULKHEAD

Flight Interval (sec)	Heat, Q (BTU)				
	0-155	155-250	250-300*	250-2100	250-4800
Forward Bulkhead	658	231	54	NA	NA
Station 219 Ring	200	120	53	NA	NA
Total	858	351	107		
Intermediate Bulkhead	65	40	NA	771	1895

* Liquid level recedes below Station 219 at about 300 seconds.

It was assumed that all heat transfer to the LH₂ from launch until the end of the parking orbit caused liquid evaporation and venting. This assumption led to a simplified method of analysis. Comparison with a more rigorous analysis indicated that the effect of this assumption upon optimizing foam thickness was negligible and was therefore a justified simplification. The weight of the vented hydrogen was calculated by dividing the heat input to the liquid by the heat of vaporization of hydrogen, L, (188 BTU/LB). The weight of vented propellants was then multiplied by the payload tradeoff factor for each phase of flight, which is summarized below:

1. Boost Phase (0 - 155 seconds)

$$\frac{\partial \text{Payload}}{\partial \text{LH}_2 \text{ vented}} = -0.336$$

2. Sustainer Phase (155 - 250 seconds)

$$\frac{\partial \text{Payload}}{\partial \text{LH}_2 \text{ vented}} = -0.382$$

3. Coast Phase (250 - end of coast)

$$\frac{\partial \text{Payload}}{\partial \text{LH}_2 \text{ vented}} = -0.777$$

Payload trade-off factors were based on a fixed volume tank. Payload loss attributable to heat transfer through the forward bulkhead and Station 219 ring is given in Table 3-3 and payload loss attributable to heat transfer through the intermediate bulkhead for a 25-minute and 70-minute coast is given in Tables 3-4 and 3-5, respectively.

TABLE 3-3. PAYLOAD LOSS ATTRIBUTABLE TO HEAT TRANSFER THROUGH THE FORWARD BULKHEAD AND STATION 219 RING

Flight Interval (sec)	Heat Energy, Q (BTU) (From Table 3-2)	Weight of Vented Hydrogen (lb) $\frac{Q}{L}$	Payload Loss (lb) $\frac{Q}{L} \times \frac{\partial \text{Payload}}{\partial \text{LH}_2 \text{ vented}}$
0-155	858	4.56	1.53
155-250	351	1.87	.71
250-300	107	.57	.44
Total	N/A	N/A	2.68

TABLE 3-4. PAYLOAD LOSS ATTRIBUTABLE TO HEAT TRANSFER THROUGH THE INTERMEDIATE BULKHEAD FOR A 25-MINUTE COAST MISSION

Flight Interval (sec)	Heat Energy, Q (BTU) (From Table 3-2)	Weight of Vented Hydrogen (lb) $\frac{Q}{L}$	Payload Loss (lb) $\frac{Q}{L} \times \frac{\partial \text{Payload}}{\partial \text{LH}_2 \text{ Vented}}$
0-155	65	0.34	0.11
155-250	40	0.21	0.08
250-2100	771	4.10	3.18
Total	N/A	N/A	3.37

TABLE 3-5. PAYLOAD LOSS ATTRIBUTABLE TO HEAT TRANSFER THROUGH THE INTERMEDIATE BULKHEAD FOR A 70-MINUTE COAST MISSION

Flight Interval (sec)	Heat Energy, Q (BTU) (From Table 3-2)	Weight of Vented Hydrogen (lb) $\frac{Q}{L}$	Payload Loss (lb) $\frac{Q}{L} \times \frac{\partial \text{Payload}}{\partial \text{LH}_2 \text{ Vented}}$
0-155	65	0.34	0.11
155-250	40	0.21	0.08
250-4800	1895	10.08	7.83
Total	N/A	N/A	8.02

3.1.1.2 Total Payload Loss. The total payload loss for 24 of the 72 thermal models of Reference 3-1 is listed in Table 3-6. These 24 thermal models include only the fiberglass strand system, and only the Freon-blown Goodyear 222 foam.

The payload loss due to sidewall heating for the three time periods listed is obtained by integrating heat rate curves (Figures 3-5 through 3-10 are examples) of the thermal model being considered with respect to flight time, dividing the resultant total heat transferred (BTU) by the heat of vaporization of hydrogen, L, (188 BTU/LB), and multiplying the resultant weight of vented hydrogen by the appropriate payload trade-off factor from Subsection 3.1.1.1.2.

The 2.7 pounds of payload loss through the forward bulkhead and Station 219 ring is obtained from Table 3-3. The 3.3 and 8.0 pounds of payload loss through the intermediate bulkhead for 25-minute and 70-minute coast flights, respectively, is obtained from Tables 3-4 and 3-5.

Two additional effects of varying heat input to the hydrogen are pressure decay and propellant density effects.

Propellant venting is affected by the primary vent valve regulated pressure decay from the pre-liftoff setting at lockup to the setting at initiation of burp pressurization prior to first main engine start. The pressure decay results from changes in GH₂ vent flow-rate due to changes in tank heating and the change in atmospheric pressure acting upon the venting system. The amount of hydrogen vented during boost phase due to tank pressure decay was calculated by the relationship:

$$\text{Weight GH}_2 \text{ Vented} = \frac{\Delta P C_{SL} C_1 M_L}{L}$$

where

- ΔP = Pressure decay in psi
- C_{SL} = Specific heat of LH₂ in BTU/LB °R
- C_1 = Slope of vapor pressure curve in °R/psi
- M_L = Weight of liquid tanked in lbs
- L = Heat of vaporization in BTU/LB

The ΔP used in the above relationship was obtained from the tank pressure versus flow-rate curves shown in Figure 3-11, which is based upon data from balanced-thrust vent system testing conducted at NASA/LeRC. Vented propellants resulting from a decay in LH₂ tank pressure for the 24 thermal models considered are listed in Table 3-6. The payload trade-off factor for sustainer flight was used to determine payload loss.

TABLE 3-6. PAYLOAD LOSS WITH VARIATIONS IN FOAM AND SKIN THICKNESS AND SURFACE EMITTANCE

Model Description																								
Model	1	2	3	4	5	6	7	8	9	10	11	12	13	14	15	16	17	18	19	20	21	22	23	24
Form Thickness ~ Inches	0.2	0.2	0.4	0.4	0.8	0.8	0.4	0.4	0.4	0.4	0.4	0.4	0.2	0.2	0.4	0.4	0.8	0.8	0.2	0.2	0.4	0.4	0.8	0.8
skin Thickness ~ Inches	0.003	0.015	0.003	0.015	0.003	0.015	0.003	0.015	0.003	0.015	0.003	0.015	0.003	0.015	0.003	0.015	0.003	0.015	0.003	0.015	0.003	0.015	0.003	0.015
Surface Emittance	0.9	0.9	0.9	0.9	0.9	0.9	0.5	0.5	0.7	0.7	0.3	0.3	0.9	0.9	0.9	0.9	0.9	0.9	0.9	0.9	0.9	0.9	0.9	0.9
Coast Trajectory	← 25-minute maximum heating →								← 70-minute maximum heating →								← 70-minute minimum heating →							
Payload Loss ~ Pounds																								
0-155 Seconds	17.0	15.8	7.2	6.9	2.9	2.8	7.7	6.8	7.5	7.0	7.9	7.2	17.0	15.8	7.2	6.9	2.9	2.8	17.0	15.8	7.4	6.9	2.9	2.8
155-250 Seconds	8.4	12.4	7.2	8.0	3.6	3.4	9.1	9.8	8.0	8.9	19.6	11.2	8.1	12.1	7.2	8.2	3.6	3.4	8.2	12.1	7.4	8.3	3.6	3.4
250-END Seconds	33.2	43.6	30.2	36.5	25.4	28.1	31.1	40.6	30.5	38.4	32.3	44.8	53.4	66.1	19.5	69.0	41.7	45.7	43.3	54.7	40.8	48.6	35.5	38.9
Pressure Decay (0-250 Seconds)	7.1	6.4	3.3	2.6	1.0	0.9	2.3	1.8	2.9	2.4	2.2	1.3	8.1	6.2	3.2	2.7	1.0	1.0	8.2	7.1	3.2	2.4	1.0	0.9
Propellants Tanked (Density Effects)	23.8	19.9	-10.8	-11.9	-31.0	-31.0	-3.6	-8.4	-7.8	-9.4	1.1	-3.3	23.8	20.2	-11.1	-11.9	-31.0	-31.0	23.6	19.7	-10.3	-11.9	-31.0	-31.3
Forward Bulkhead and 219 Ring	2.7	2.7	2.7	2.7	2.7	2.7	2.7	2.7	2.7	2.7	2.7	2.7	2.7	2.7	2.7	2.7	2.7	2.7	2.7	2.7	2.7	2.7	2.7	2.7
Intermediate Bulkhead	3.3	3.3	3.3	3.3	3.3	3.3	3.3	3.3	3.3	3.3	3.3	3.3	8.0	8.0	8.0	8.0	8.0	8.0	8.0	8.0	8.0	8.0	8.0	8.0
Insulation Weight	46.0	91.0	63.0	108.0	97.0	142.0	63.0	108.0	83.0	108.0	46.0	91.0	63.0	91.0	63.0	108.0	97.0	142.0	46.0	91.0	63.0	108.0	97.0	142.0
Total Payload Loss ~ Pounds	141.5	195.1	106.1	156.1	104.9	152.2	116.1	168.6	110.1	161.3	123.1	175.2	167.1	222.1	129.7	183.6	125.9	174.6	157.0	211.1	122.2	173.0	119.7	167.1

3-17

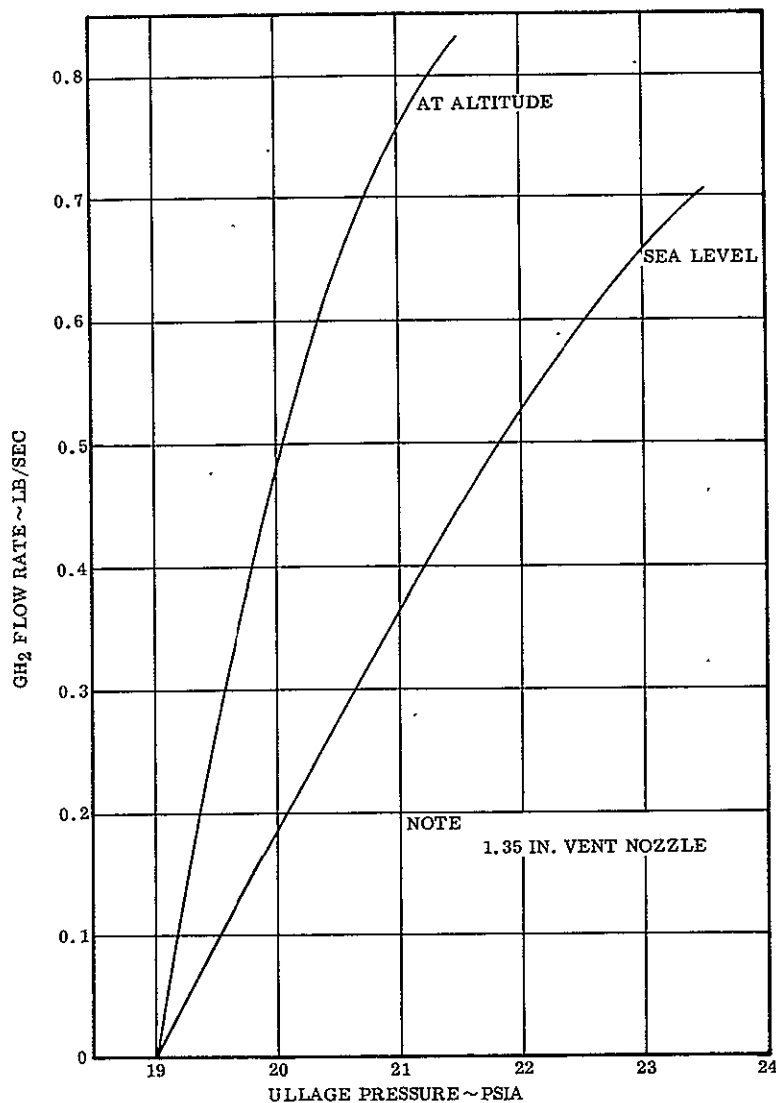


Figure 3-11. Centaur Balanced Thrust Venting System

The density of tanked propellants, and therefore the amount of tanked propellants, is affected by the efficiency of the insulation system. The higher the heat input to the liquid propellant, the more vapor which is entrained and the lower the effective density. Reference 3-9 gives the bubble rise rate for GH₂ bubbles in LH₂ and was used in providing an analytical model for determining the effect of foam thickness upon effective LH₂ density. The model assumes all liquid heating to be added at a point equidistant from the bottom of the tank and the liquid surface. The length of time a bubble remains in the liquid can then be determined by dividing the distance from the point of heat addition to the liquid surface by the bubble rise rate. The amount of GH₂ below

the liquid surface was then determined by multiplying this time by the heating rate and dividing by the heat of vaporization. Therefore, the effective density was obtained from the relationship:

$$\rho_{\text{Effective}} = \frac{(V_{\text{GH}_2})(\rho_{\text{GH}_2}) + (V_{\text{T}} - V_{\text{GH}_2})(\rho_{\text{LH}_2})}{V_{\text{T}}}$$

where

V_{GH_2} = Volume of GH_2 below liquid surface

V_{T} = Total volume

ρ_{GH_2} = Density of GH_2

ρ_{LH_2} = Density of LH_2

The effective density and therefore the weight of LH_2 tanked was calculated based upon the maximum LH_2 heating rate experienced during boost phase for each thermal model. This was done to prevent liquid from being forced through the vent valve by the reduction in effective density as the heating rate increased during boost. The results of the analysis are listed in Table 3-6. The payload loss is increased or decreased based upon the current SLV-3C/Centaur Liquid Hydrogen propellant weight of 5315 pounds. Consideration of propellant density in this analysis constituted a major effect on the optimization of foam thickness and upon the total predicted payload penalty of an insulation system. The payload tradeoff factor for propellants tanked is: _____

$$\frac{\partial \text{Payload}}{\partial \text{LH}_2 \text{ tanked}} = -0.277$$

3.1.1.3 Determination of Optimum Foam Thickness. In order to determine the optimum foam thickness, plots of payload loss due to insulation weight versus foam thickness, and payload loss due to hydrogen boiloff versus foam thickness were prepared, (Figure 3-12). Note that for zero foam thickness, the weight of insulation equals the weight of erosion cloth and adhesive. The increase in panel weight shown by the slope of the curve is attributable to the increase in foam weight. The hydrogen boiloff curves shown in Figure 3-12 are for only one emissivity and one of the three trajectories assumed. Similar hydrogen boiloff curves for the other emissivities and trajectories were plotted during the performance of the rigorous thermal analysis of Reference 3-1.

It should be noted in Figure 3-12 that as foam thickness and insulation weight increase, payload loss increases, whereas the payload loss caused by the boiloff of liquid hydrogen decreases. Therefore, the next step was to graphically add the payload loss for insulation weight and hydrogen boiloff to determine the net payload loss as a function of

foam thickness. The results of this graphical addition are shown in Figures 3-13, 3-14, and 3-15, for the 25-minute coast maximum heating trajectory, the 70-minute coast maximum heating trajectory, and the 70-minute coast minimum heating trajectory, respectively. As noted in the figures, a separate curve is plotted for each value of skin thickness and surface emittance. Most of the values for the curves were obtained from Reference 3-1 since payload losses for only 24 of the 72 thermal models utilized in Reference 3-1 are shown in Table 3-6 for illustrative purposes. Additionally, Figure 3-13 shows one curve which uses the higher conductivity CO₂-blown foam.

The following conclusions can be drawn from an evaluation of Figures 3-13, 3-14, and 3-15:

1. Payload loss will be minimized with a high emittance surface coating,
2. Payload loss will be minimized by using a thin, light weight erosion cloth,
3. Payload loss will be minimized by using a foam thickness of 0.6 inches,
4. Coast trajectory has negligible effect on the shape of the curve,
5. Payload loss is minimized by using a low conductivity foam,
6. The use of a higher conductivity foam does not alter the shape of the curve,
7. The shape of the curve is similar for the three coast trajectories.

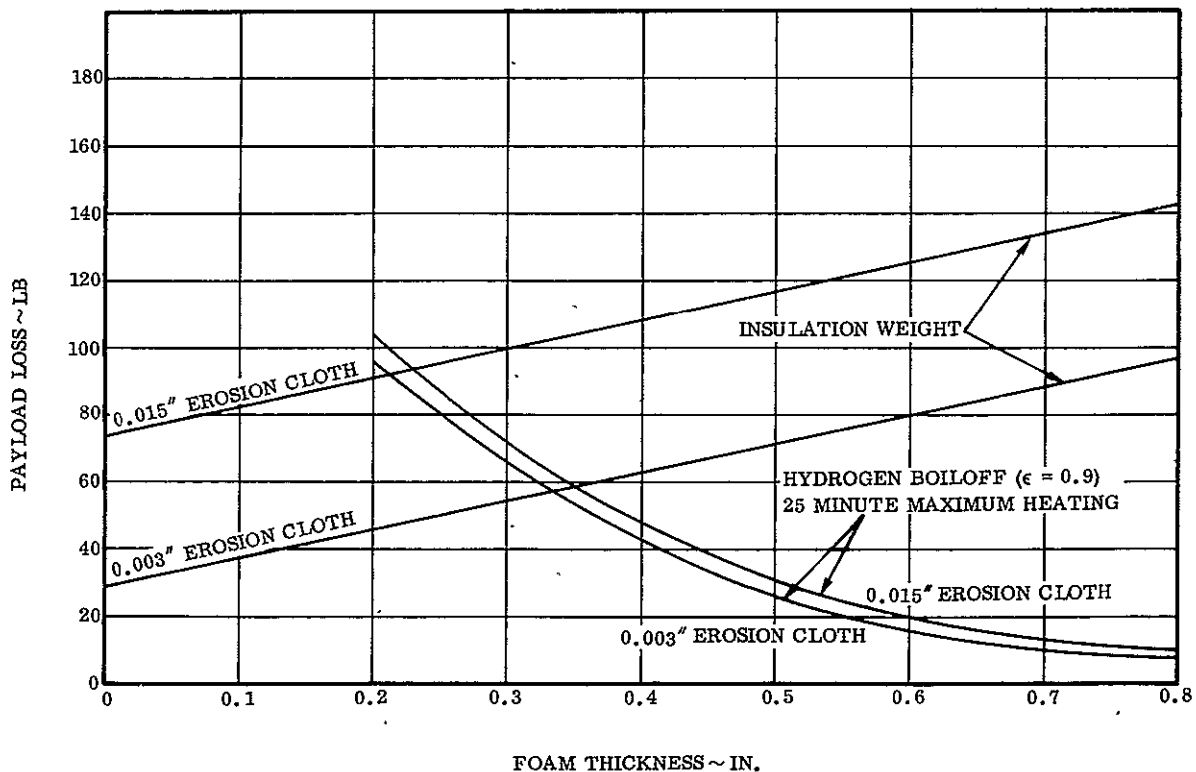


Figure 3-12. Payload Loss for Fixed Insulation Foam Thicknesses

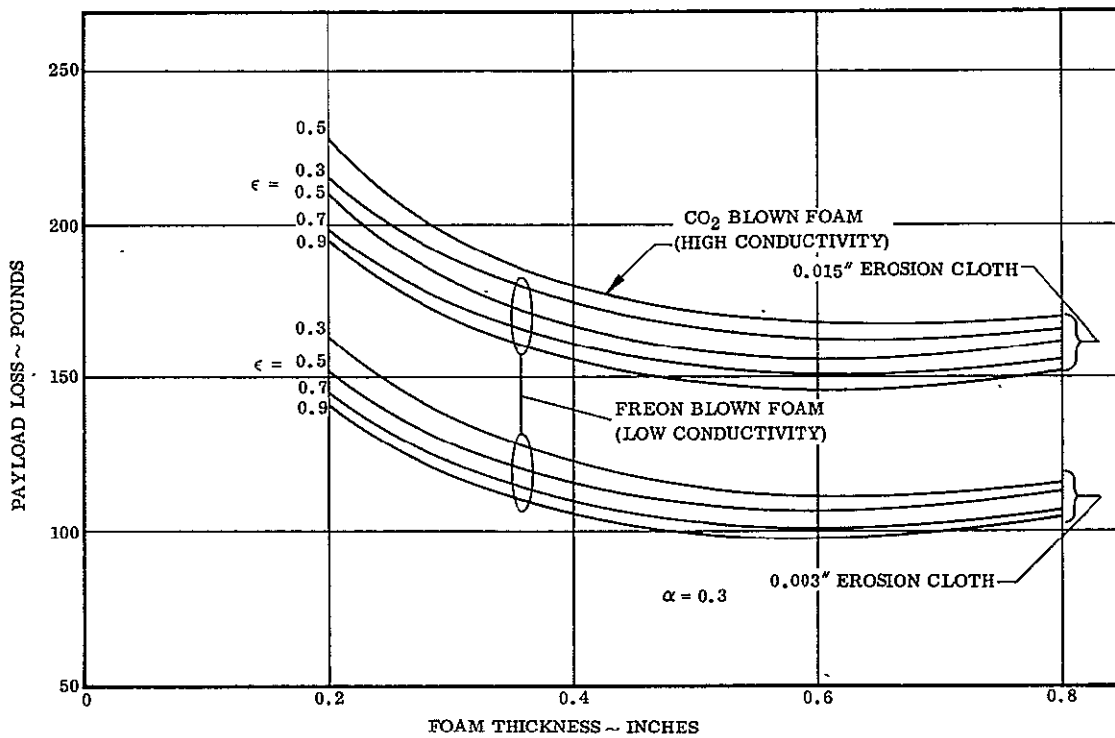


Figure 3-13. Payload Loss Versus Foam Thickness for a 25-Minute Coast Trajectory, Maximum Heating

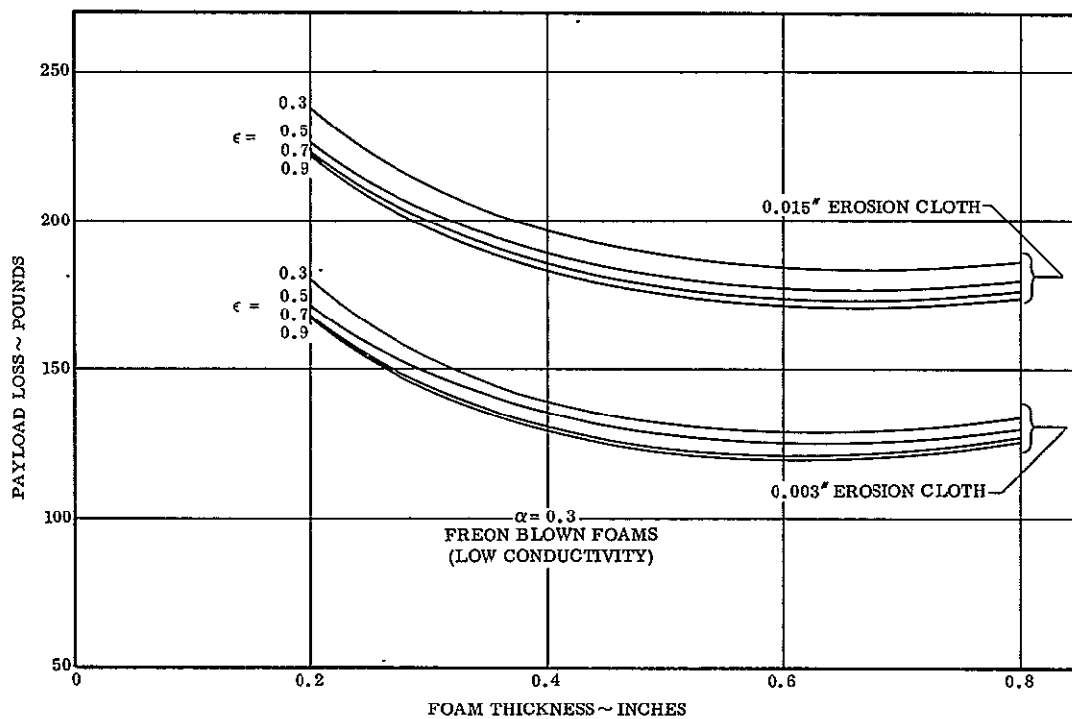


Figure 3-14. Payload Loss Versus Foam Thickness for a 70-Minute Coast Trajectory, Maximum Heating

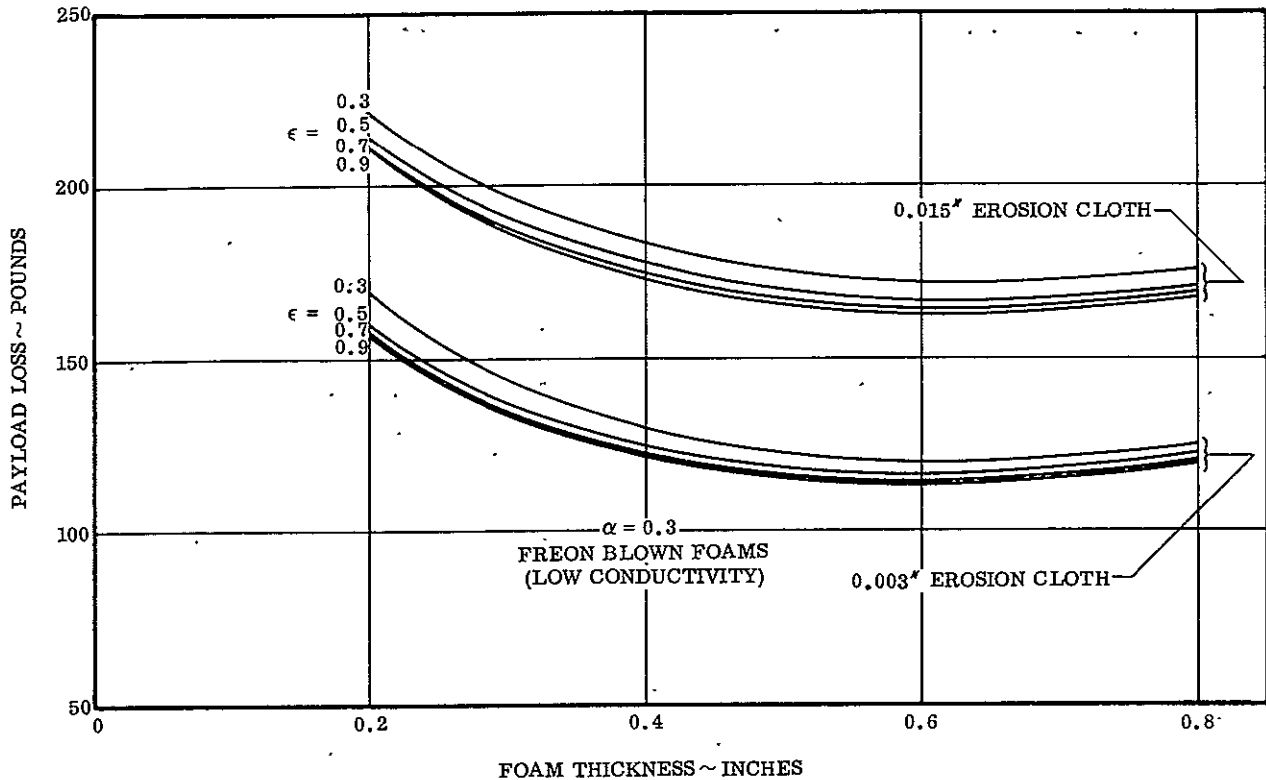


Figure 3-15. Payload Loss Versus Foam Thickness for a 70-Minute Coast Trajectory, Minimum Heating

The payload tradeoff curves are relatively flat and a variation of ± 0.2 inches from the optimum thickness results in an additional payload loss of only about 12 pounds. For this reason, and because of previous experience in the manufacture of 0.4-inch foam panels, it was decided to use 0.4-inch foam panels for the T-9 test tank.

3.1.2 INSULATION SURFACE TEMPERATURE. The foam is sealed in Mylar-aluminum-Mylar laminate (MAM) to prevent outside gases for cryopumping into the foam. The sealed foam panels are then covered by an erosion cloth that serves three purposes: (1) it protects the foam panels from damage during pre-launch operations, (2) it protects the foam panel from aerodynamic erosion, and (3) it has surface optical properties to minimize the temperature of the insulation system during boost phase heating and to minimize LH₂ heating during boost and coast.

3.1.2.1 Prelaunch Insulation Surface Temperature. Prelaunch surface temperatures are dependent upon ambient temperature and wind velocity as shown on Figure 3-16. Only with a combination of high temperature and high wind velocity will the surface temperature exceed 32°F. Therefore, ice will usually form on the insulation panels during pre-launch operations after LH₂ is tanked.

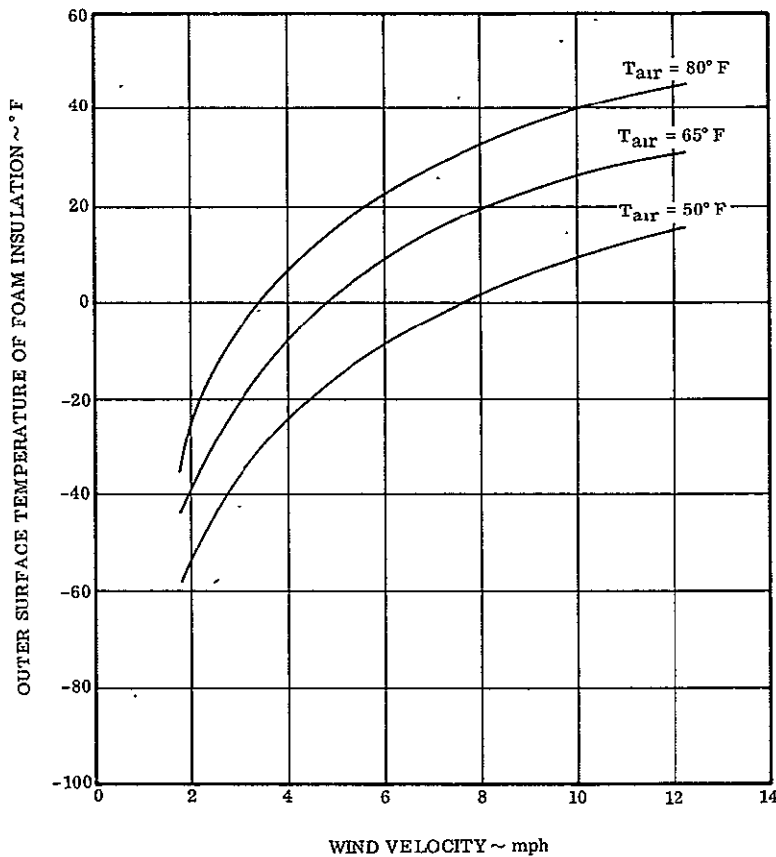


Figure 3-16. Predicted Surface Temperature of 0.4-Inch Foam Versus Wind Velocity

3.1.2.2 Insulation Surface Temperature During Flight. The effect of the erosion cloth is demonstrated in Figure 3-17, which shows maximum boost phase surface temperature as a function of erosion cloth thickness for surfaces having an emittance of 0.1, 0.5, and 0.9. The maximum foam temperature during flight must be limited to prevent damage to the insulation system. This can be accomplished with an erosion cloth having a high emittance.

Surface temperature can also be limited by increasing the thickness of erosion cloth, but this is detrimental in that the payload is thereby diminished. Figure 3-18 shows the same information as Figure 3-17, except the data is plotted for a nominal heating trajectory. It also demonstrates the desirability of having a high outer surface emittance.

The maximum erosion cloth temperature predictions shown in Figures 3-17 and 3-18 are based upon the aerodynamic heating rate that includes the effect of the flight angle-of-attack. Additional curves of temperature versus flight time with a 25-minute coast are shown in Figures 3-19 and 3-20 for an insulation panel of 0.4 inch of foam with surface emittance and erosion cloth thickness as the parameters (angle-of-attack

effects not included). Note that a heavier erosion cloth thickness reduces the maximum temperature, but that the erosion cloth temperature stays hot for a longer period of time, which results in a higher heat flow into the hydrogen during Centaur main engine firing and the early stages of coast, as shown on Figures 3-5 through 3-10. The decrease in payload capability caused by additional hydrogen boiloff is shown in Table 3-6. Thick erosion cloths, therefore, are undesirable from a payload tradeoff standpoint because of the increase in panel weight and because of an increase in hydrogen boiloff.

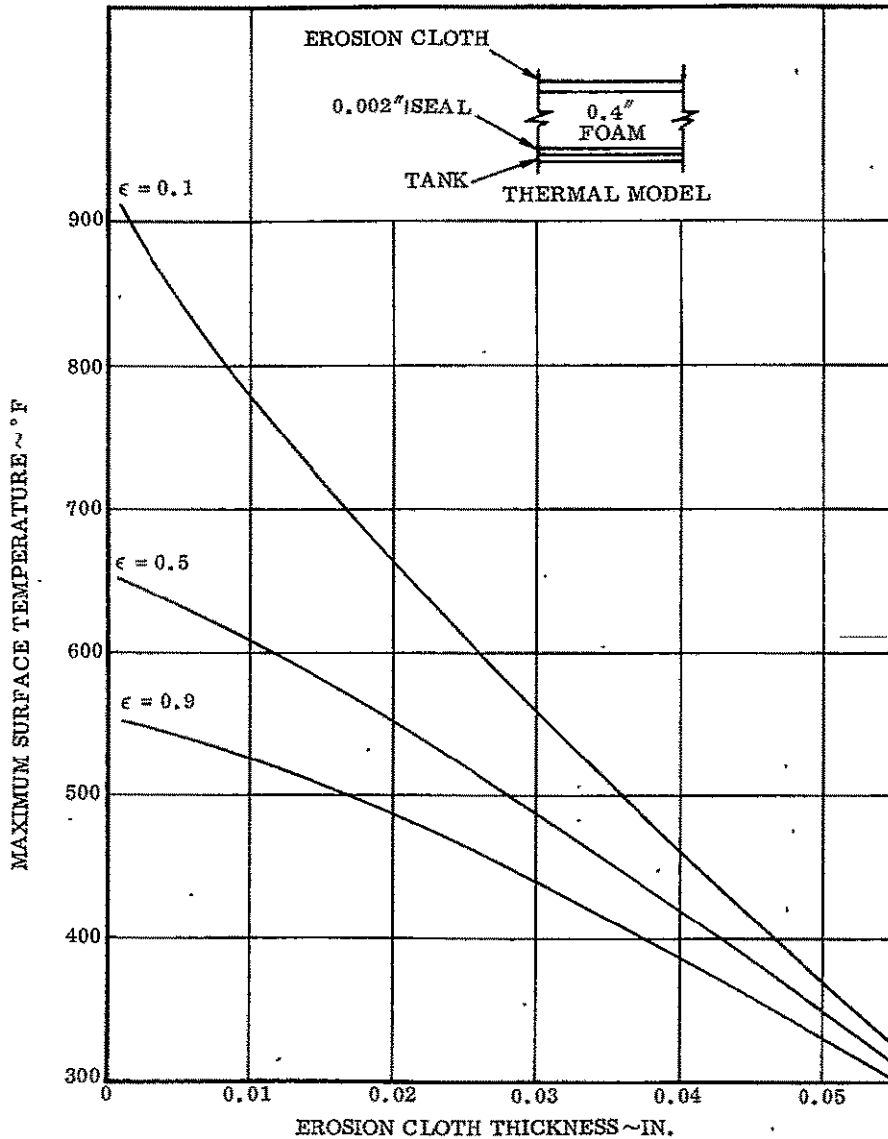


Figure 3-17. Comparative Maximum Outside Surface Temperature for Constrictive - Wrapped Insulation (Trajectory SP47-3C) (Maximum Heating) (Includes Angle-of-Attack Effects)

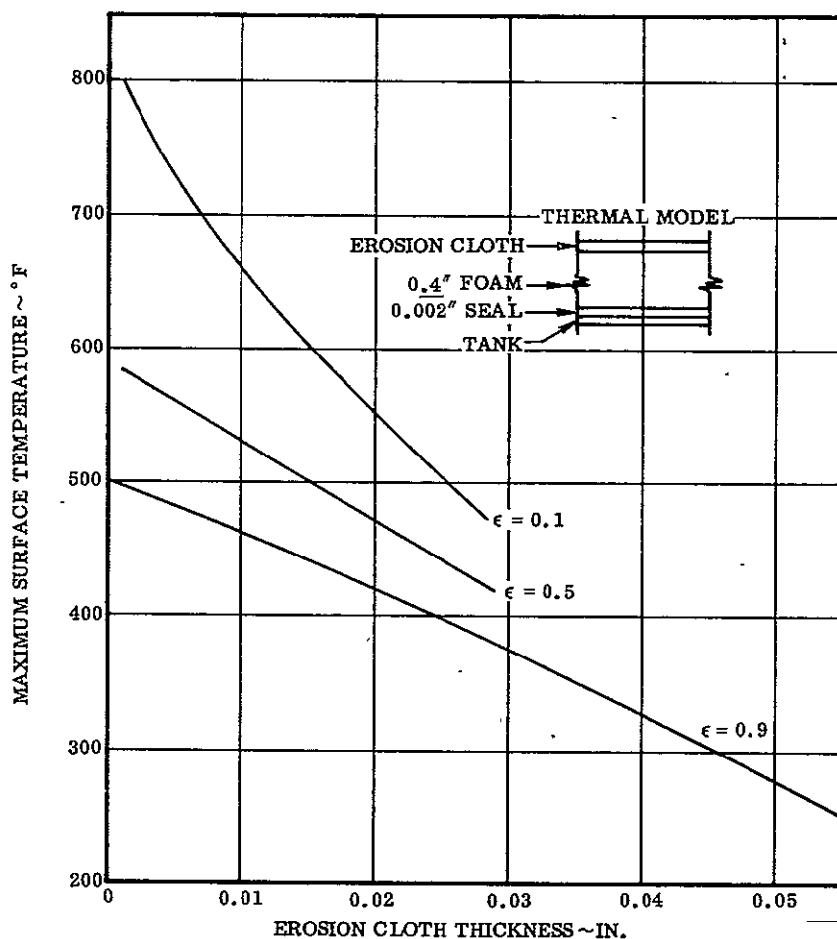


Figure 3-18. Comparative Maximum Outside Surface Temperatures for Constrictive — Wrapped Insulation (Trajectory SP-29-3C) (Nominal Heating) (Includes Angle-of-Attack Effects)

Figure 3-21 shows the temperature gradient through the foam at the time of maximum erosion cloth temperature for foam thicknesses of 0.2, 0.4, and 0.8 inch. There is essentially no temperature gradient through the 0.003-inch erosion cloth and surface temperature of the erosion cloth is shown as foam temperature. There is about a 10° F temperature gradient through the 0.015-inch erosion cloth. This is a very small gradient, and the maximum foam and erosion cloth temperatures can be considered equal.

Silicon-impregnated glass cloth (CHR-2007) was selected for the erosion cloth material because of its excellent radiation properties both before and after exposure to the high temperatures predicted during ascent heating (Subsection 2.4.3.4), and because of its light weight and durability. The total thickness of the CHR-2007 erosion cloth and the adhesive required to attach it to the foam panel is about 0.020 inch. Therefore the maximum predicted erosion cloth flight temperature (Figure 3-17) is 485° F. For the nominal trajectory, the maximum erosion cloth temperature is 420° F (Figure 3-18).

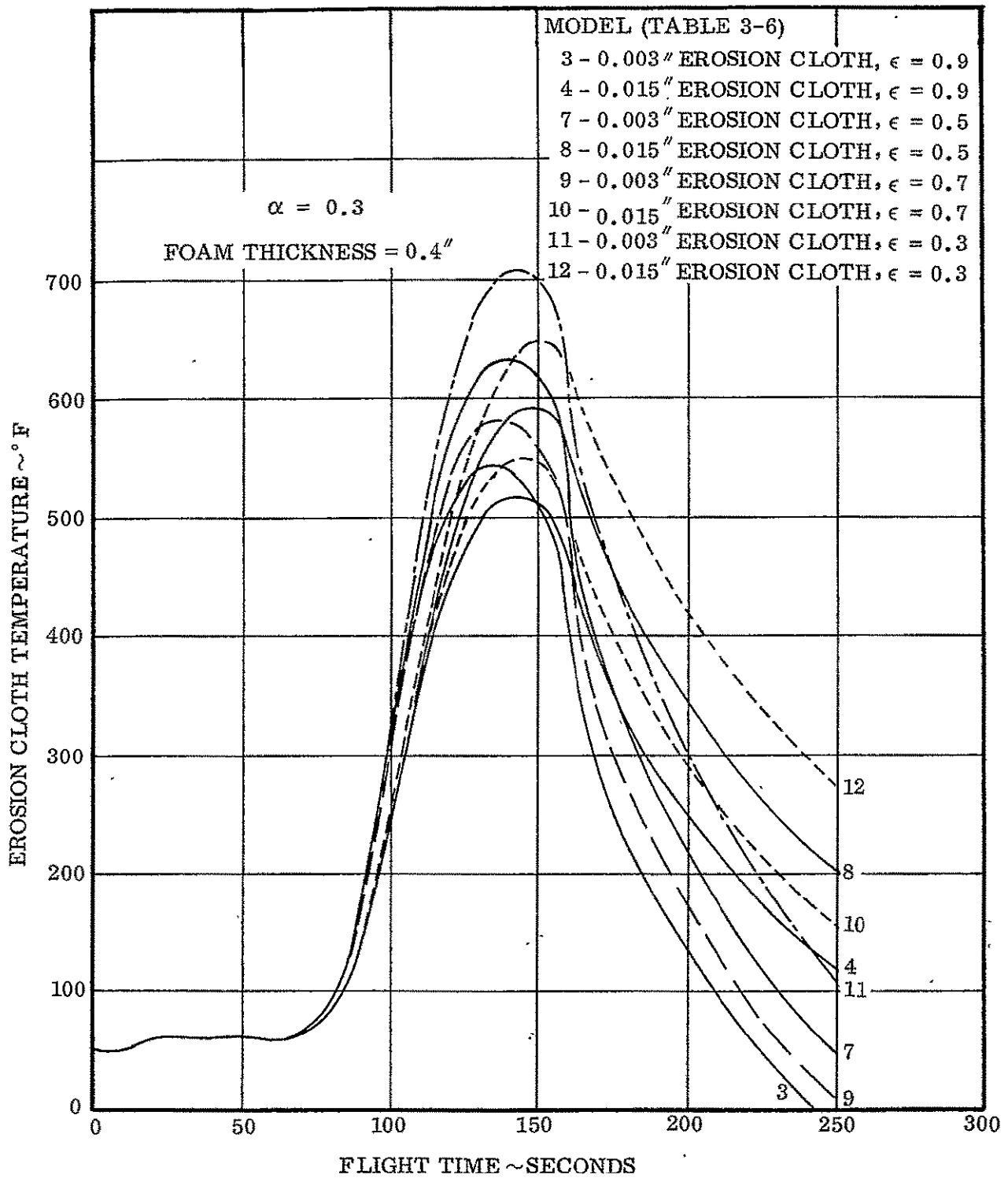


Figure 3-19. Surface Temperature Versus Flight Time for a 25-Minute Coast Trajectory, Maximum Heating

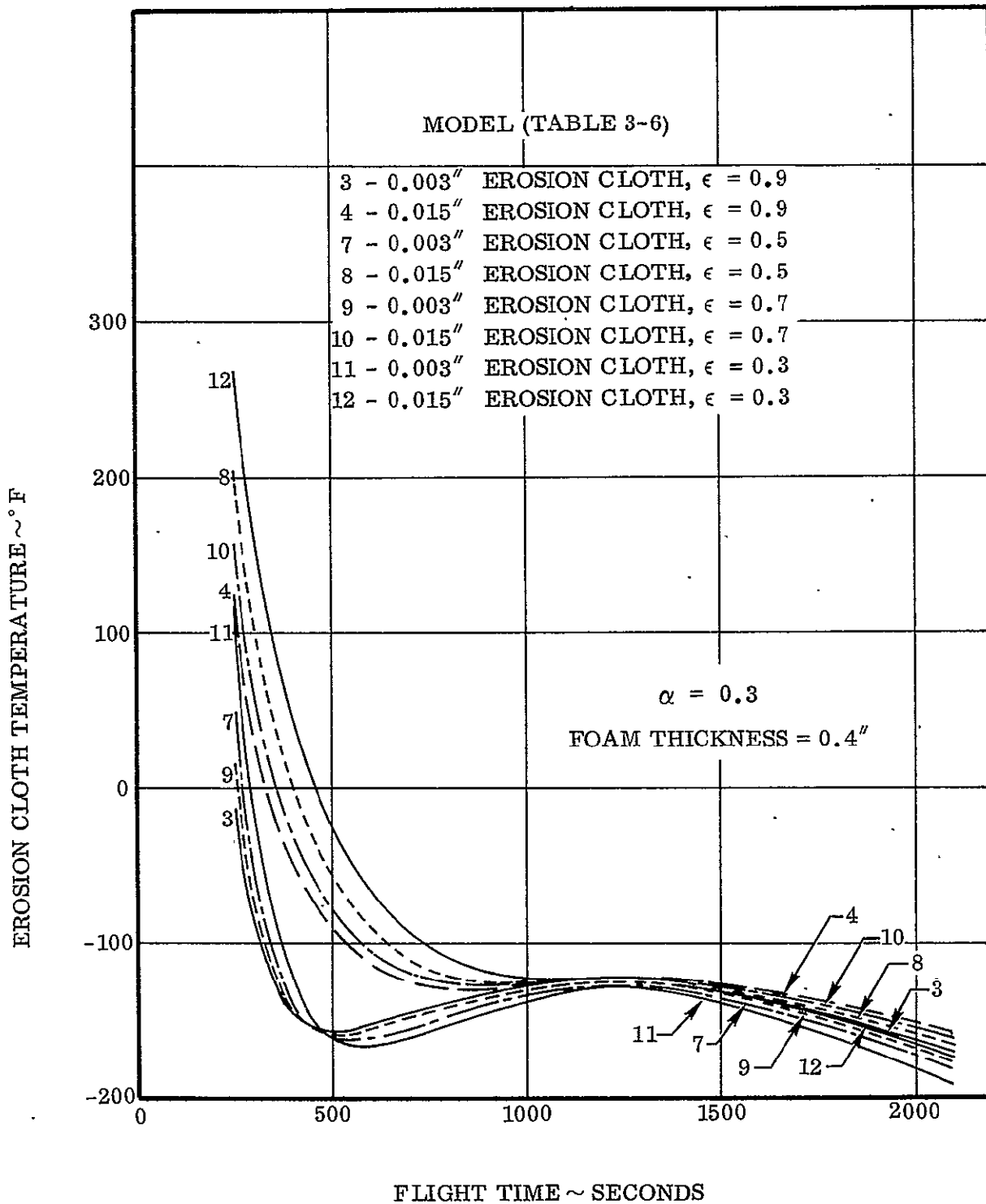


Figure 3-20. Surface Temperature Versus Flight Time for a 25-Minute Coast Trajectory, Maximum Heating

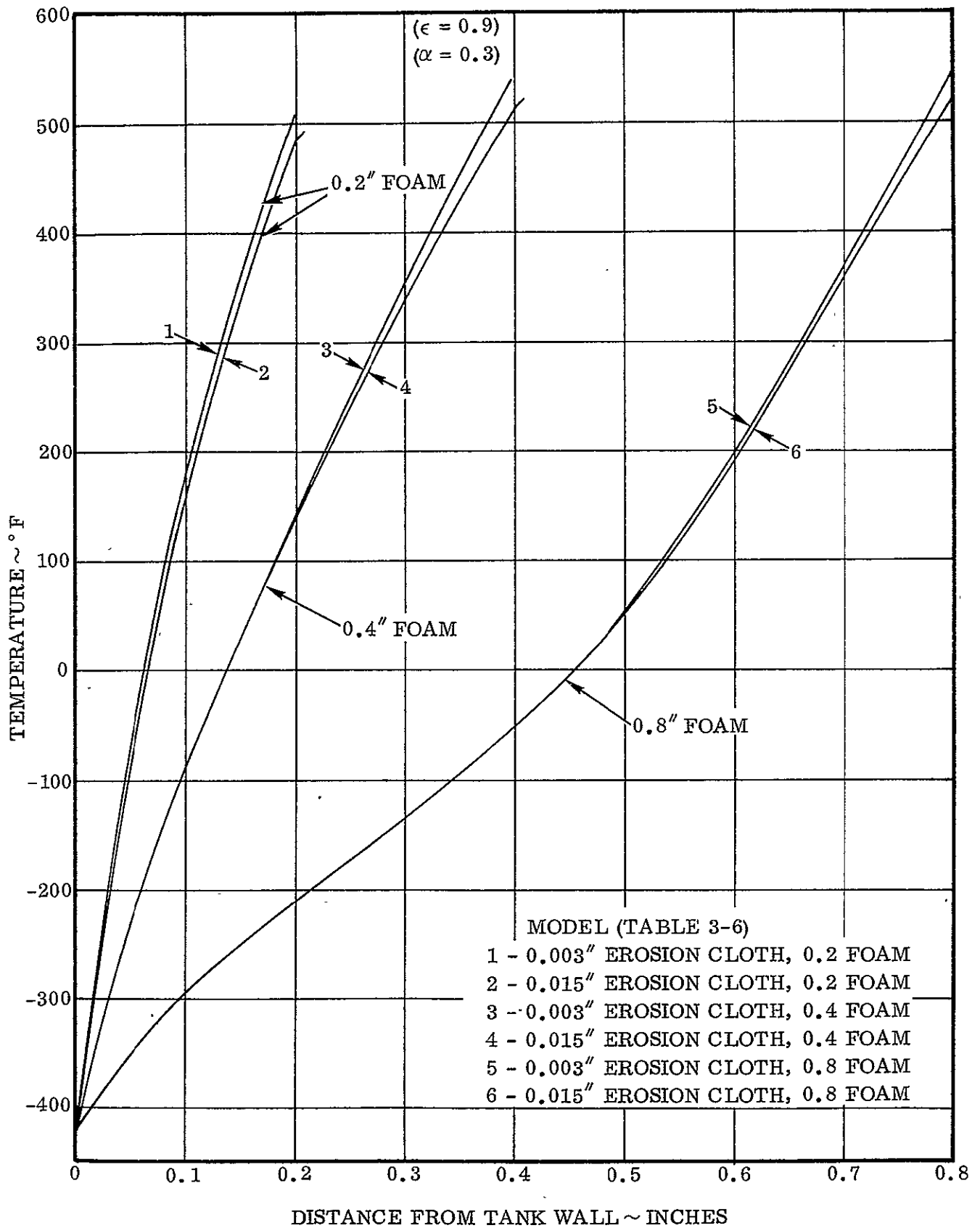


Figure 3-21. Temperature Gradient Through Fixed Foam Insulation at Maximum Erosion Cloth Temperature (After Approximately 145 Seconds of Flight)

3.1.3 ICE FORMATION ON INSULATION PANEL SURFACE. Ice formation is detrimental to the insulation system if it decreases payload capability. Whether or not ice decreases payload capability depends on the quantity of ice that forms on the insulation panel, which in turn depends upon the wind velocity, air temperature, humidity, and panel surface temperature. All of these variables are time dependent.

The quantity of ice that will form on the outer surface of the insulation panels is difficult to predict with certainty. An approximation of ice thickness was made and was based upon published data for ice formation on a surface at a temperature that approximates the insulation panel surface temperature. Reference 3-10 reports test results of frost formation on a cylinder in a crossflow of humid air while the surface temperature of the cylinder was maintained at 20° F. Ice thickness was measured for several different air velocities across the cylinder. Ice thickness for a steady-state condition is plotted in Figure 3-22 as a function of the average film coefficient on the cylinder. Ice thickness increases as the film coefficient and air velocity decrease.

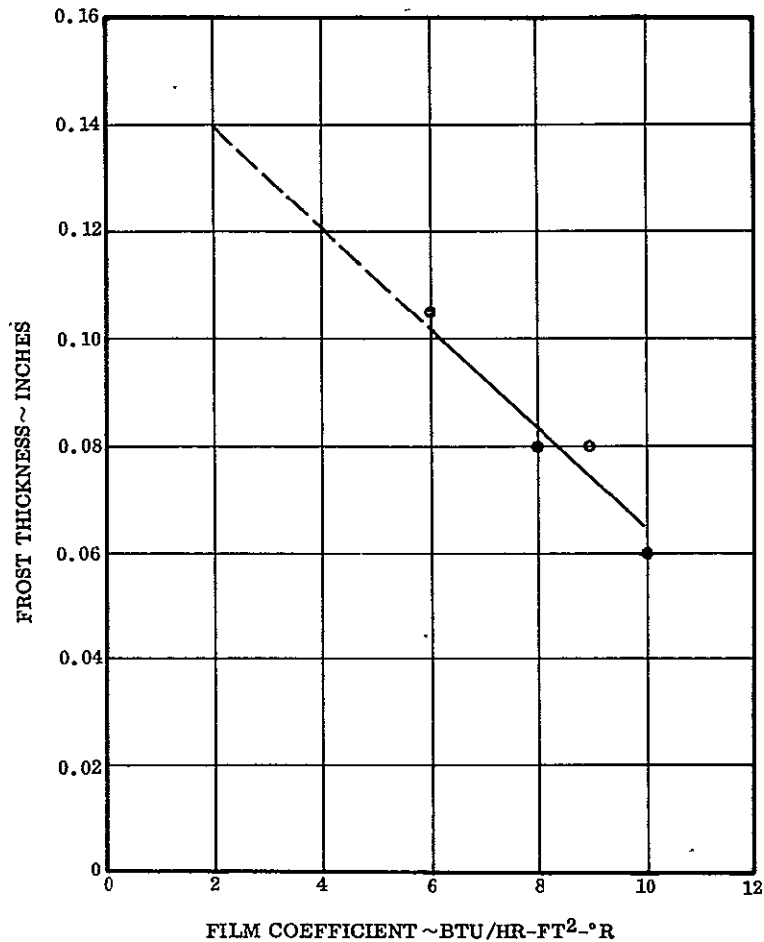


Figure 3-22. Frost Thickness Versus Film Coefficient

The maximum ice buildup on the insulation panels occurs when the wind velocity is at a minimum. Based upon data from previous Centaur launches, minimum wind velocity at Cape Kennedy is about 5 mph. The forced convection film coefficient for a 5 mph wind is about 2 BTU/hr-ft² - °R. Extrapolating the data from Reference 3-10 in Figure 3-22, the maximum predicted ice thickness on the insulation panels for a Centaur launch at Cape Kennedy is about 0.14 inch.

Ice thickness up to about 5/16-inch was measured during the T-9 tests (see Subsection 9.5.2). Average ice thickness over the entire insulation panel surface during the T-9 test was about 0.2 inch. Considering all the uncertainties in the determination of the maximum quantity of ice that can form on the insulation surface, a thickness of 0.3-inch was assumed in order to calculate the effect on payload capability.

Ice density varies between 6 lb/ft³ and 41 lb/ft³ (Reference 3-10). Ice observed on the T-9 tank had a very light, powdery appearance and the density appeared to be closer to 6 lb/ft³ than it was to 41 lb/ft³. Therefore, a value of 16 lb/ft³ was assumed as a likely density for calculating the mass of ice on the vehicle insulation system prior to launch. The weight of ice on the insulation panels prior to launch is 200 pounds for a thickness of 0.3 inch and a density of 16 lb/ft³. An aerodynamic heating analysis, using a minimum heating trajectory for the SLV-3C/Centaur (SP-19-3C), was performed to determine the quantity of ice removed during boost heating as a function of time.

The following tradeoff factors were used to determine payload loss:

<u>Flight Time (Seconds)</u>	<u>$\frac{\partial \omega_{ice}}{\partial \omega_{payload}}$</u>
0-50	155
51-100	50
101-153	17

It was assumed that no ice was shaken off the vehicle by vibrational forces or swept off the vehicle by viscous forces. Ice was removed from the vehicle only by melting caused by aerodynamic heating. The ice performed the same function as an ablation system by decreasing tank heating. The predicted change in payload capability is plotted on Figure 3-23 as a function of ice thickness. Payload capability increased by 8 pounds for an ice thickness of 0.3 inch (for a density of 16 lb/ft³). Payload increased because:

1. Much of the ice melts off during the early moments of flight when the payload tradeoff factors are high, and
2. The ice acts as an ablator to keep the insulation skin temperature low, which reduces LH₂ heating, thereby reducing boiloff losses.

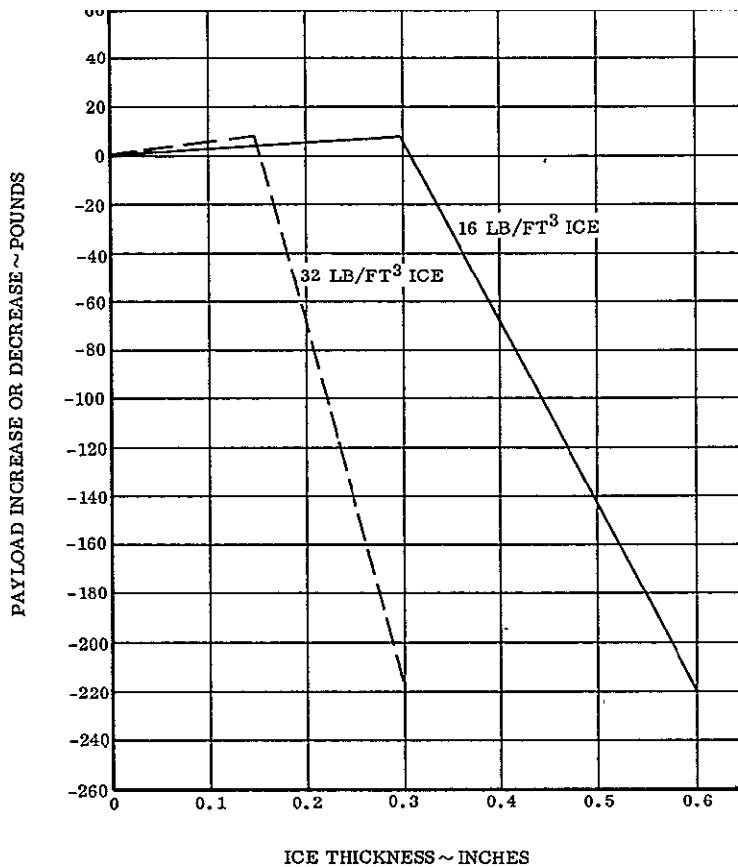


Figure 3-23. Payload Change Attributable to Ice on Insulation Surface Prior to Launch

The maximum quantity of ice that can be melted by aerodynamic heating for a minimum heating trajectory is 0.3 inch (16 lb/ft³ density). Any excess is carried into orbit where the loss in payload is one pound for each pound of ice. It is shown in Figure 3-23 that the payload loss increased significantly when ice thickness exceeded 0.3 inch. Thickness actually represents mass because the curve is based on a density of 16 lb/ft³. For greater ice densities, the curve on Figure 3-23 must be changed accordingly. For example, ice densities of 32 lb/ft³ cause payload losses if the thickness exceeds 0.15 inch. A thickness of 0.3 inch and density of 32 lb/ft³ reduce payload by 220 pounds.

Additional tests would be required to reduce the uncertainties in the calculation of payload losses attributable to ice.

3.1.4 FIBERGLASS CONSTRICTIVE WRAP TEMPERATURE. A compression force is maintained on the insulation panels through the use of a constrictive wrap as described in Sections 4 and 5. The constrictive wrap is loaded in tension and imparts a radial force on the insulation panels. Constrictive wrap and hinge fitting temperatures are shown as a function of flight time on Figure 3-24. Point A is a typical cross-section of constrictive wrap and reaches a maximum temperature of 485°F. In general, the constrictive wrap is in intimate contact with the erosion cloth. Intimate contact is important from a heat transfer standpoint because heat is transferred by conduction from the constrictive wrap through the erosion cloth and foam insulation into the liquid hydrogen. Locally, the constrictive wrap is bridged from the aluminum hinge fitting to the erosion cloth (point B, Figure 3-24) causing a hot spot to form. The temperature at point B is hot because there is aerodynamic heat transfer on both sides of the constrictive wrap and there is no direct conductive heat transfer path to the erosion cloth. Heat transfer between constrictive wrap and erosion cloth occurs only by radiation. The maximum temperature of the constrictive wrap at point B is 705°F as shown on Figure 3-24. The temperature gradient along the constrictive wrap is shown on Figure 3-25. It can be seen that there are sharp temperature discontinuities where the constrictive wrap bridges the gap between the hinge fitting and erosion cloth. It was subsequently proposed to modify this area by filling the gap between the constrictive wrap and erosion cloth with silicone rubber to avoid the temperature discontinuity and to decrease the stress loads in the constrictive wrap where it is attached to the hinge fitting. This same condition will exist, however, any place the constrictive wrap does not directly contact the insulation panels. Depressions in the foam can cause this same condition to appear. Hinge fitting temperature, point C, reaches a maximum of 313°F. The temperature of the adhesive that is used to attach the constrictive wrap to the hinge fitting is approximately the same as the hinge fitting temperature.

3.2 CORRUGATED CONSTRICTIVE WRAP SYSTEM

A corrugated constrictive wrap system was proposed as an alternate design to the fiberglass strand constrictive wrap system.

The corrugated wrap system is shown in Figure 3-26. The corrugations are not purged during ground hold. Holes in the outer surface permit gas within the corrugations to vent during vehicle ascent in order to prevent a burst load on the corrugations. The corrugated wrap has sufficient mass and strength to protect the foam insulation from aerodynamic erosion during boost phase heating and therefore replaces the erosion cloth.

An analysis was accomplished on an 0.020-inch corrugated aluminum constrictive wrap to determine the temperature distribution on the corrugated surface and to determine the effect of the corrugated wrap on payload losses.

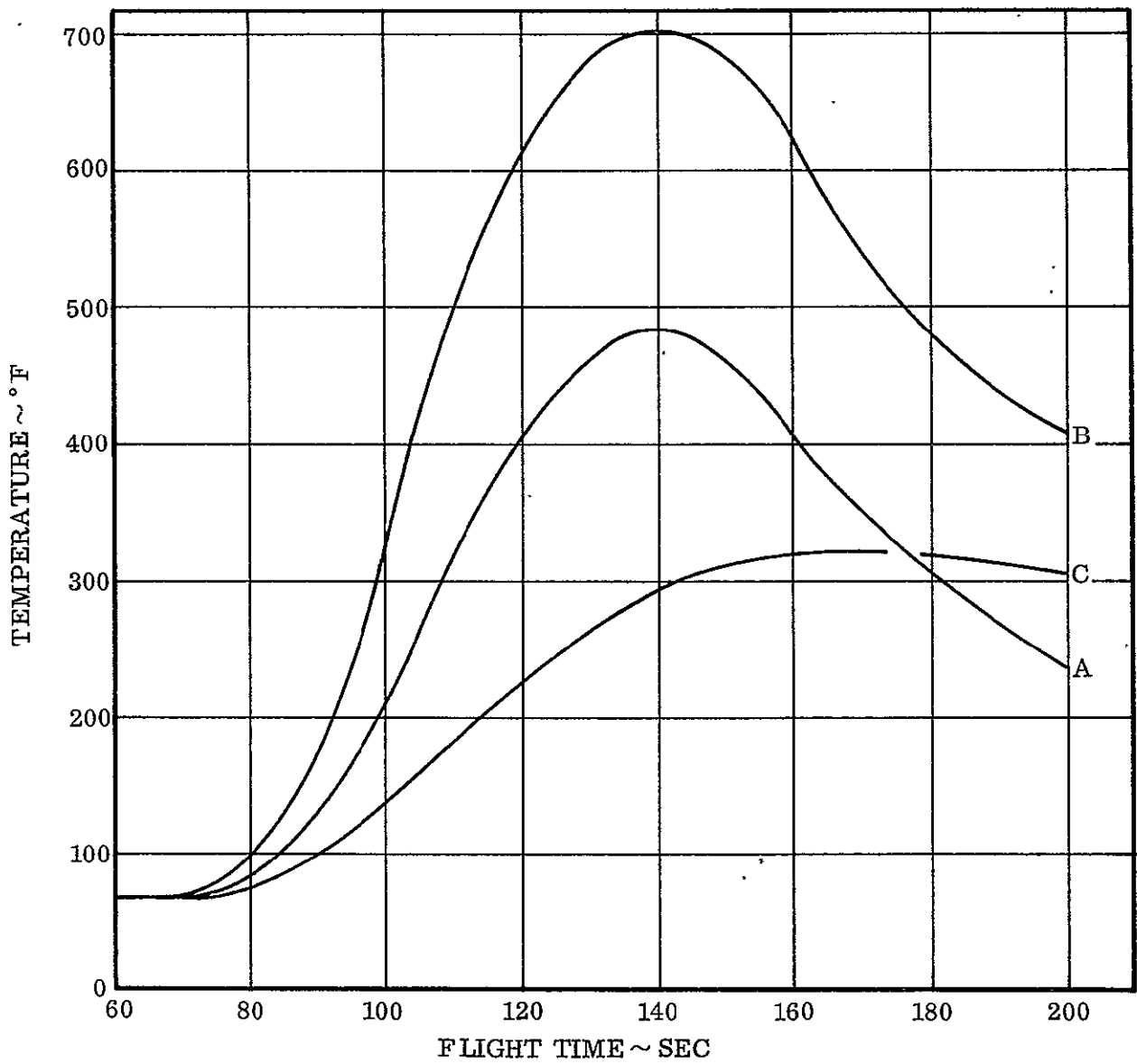
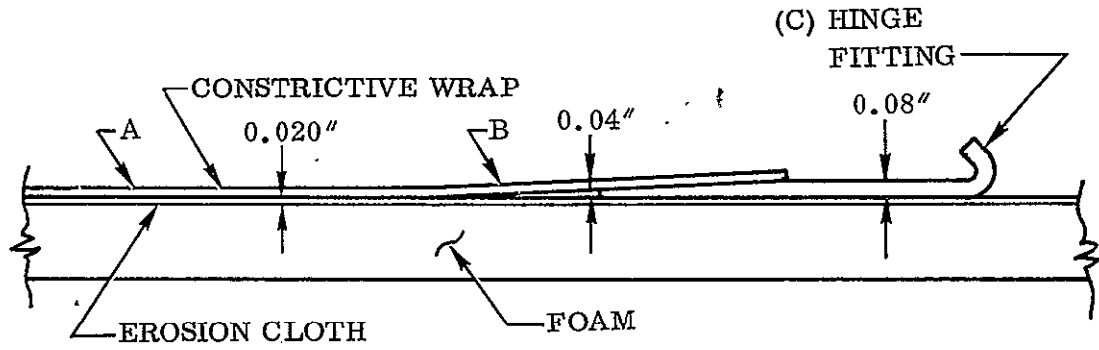


Figure 3-24. Predicted Temperatures on Hinge Fitting and Constrictive Wrap as a Function of Flight Time

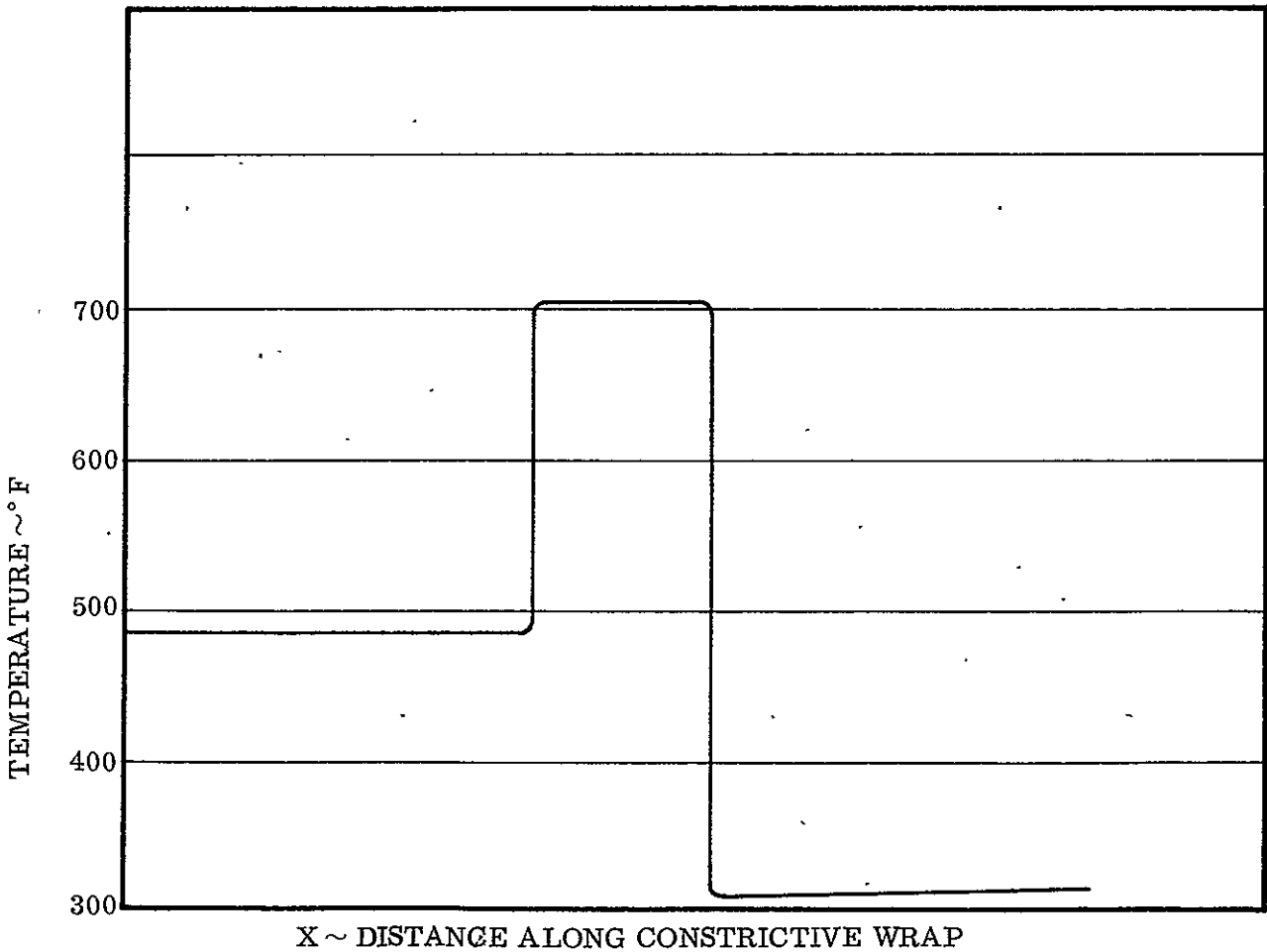
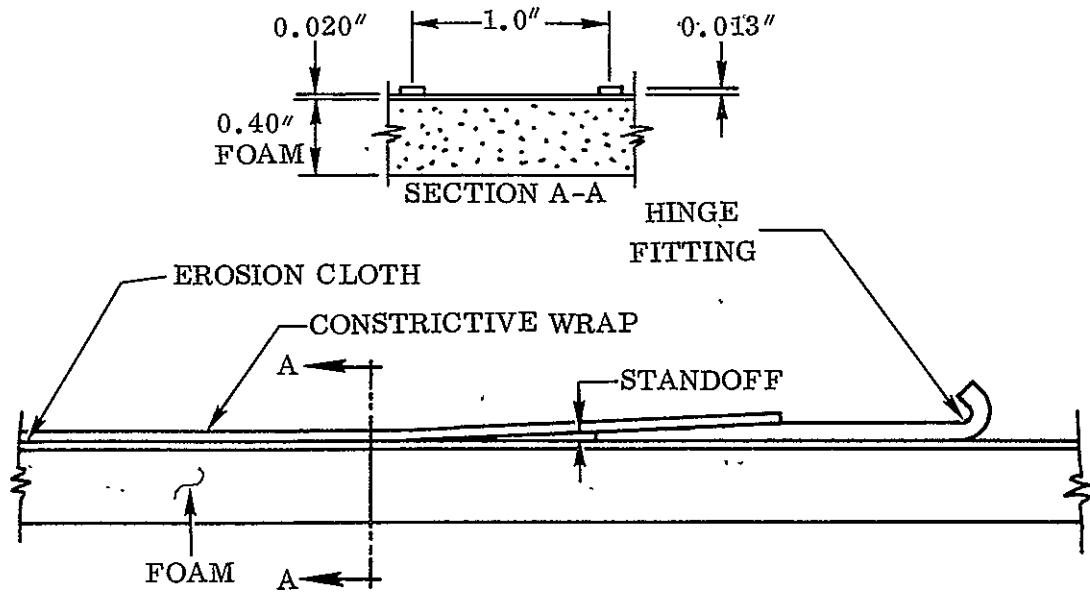
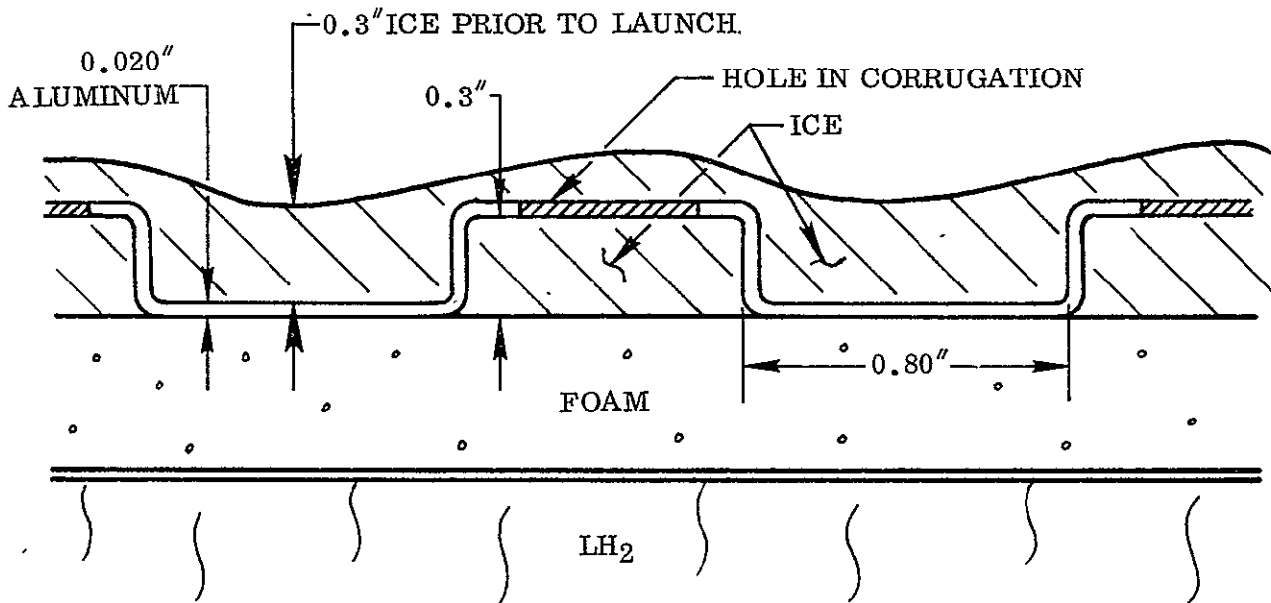


Figure 3-25. Temperature Gradients on Hinge Fitting and Constrictive Wrap at the Time of Maximum Temperature



$$\rho_{\text{ICE}} = 16 \text{ LB/FT}^3$$

Figure 3-26. Cross-Section Through Corrugated Wrap Insulation System Showing Maximum Ice Buildup

3.2.1 SURFACE TEMPERATURE PREDICTIONS. Temperature predictions were made for two areas: (1) on the corrugated aluminum, and (2) on the foam surface underneath the holes in the corrugations. It was assumed that aerodynamic heat flux was uniform over exposed surfaces of the corrugations (heating factor equals one). Re-radiation from all surfaces of the corrugations to the environment was calculated during ascent heating and coast phase heating. Radiation from the concave surfaces of the corrugations considered the local view factors to the environment. The maximum temperature of the corrugations during boost phase heating is shown on Figure 3-27 as a function of flight time. Because of the high thermal conductivity of aluminum, the temperature gradient from the top to the bottom of the corrugation is less than 1°F. Maximum temperature is 516°F in the typical area of the panels where there are no protuberance effects. Where the corrugation is in contact with the foam, the temperature of the MAM seal and foam interface is equal to the temperature of the aluminum and reaches a peak value of 516°F. The MAM is exposed to that portion of the boundary layer that flows into the cavity formed by the holes in the corrugation. For analytical purposes it was assumed that each hole formed an individual cavity that had a base/height ratio of one. Reference 3-11 describes the ratio of heat flux in a cavity to heat flux on a flat plate for various base/height ratios. The heat flux at the bottom of a cavity having a base/height ratio of one is 20 percent of the flat plate heat flux. MAM temperature, where it is adjacent to a hole in the corrugation, is shown on Figure 3-27 and in the

absence of ice reaches a maximum temperature of 255°F. MAM and/or foam temperatures in excess of about 350°F may cause the panel to blister. This temperature will be exceeded only where the corrugation comes in contact with the MAM.

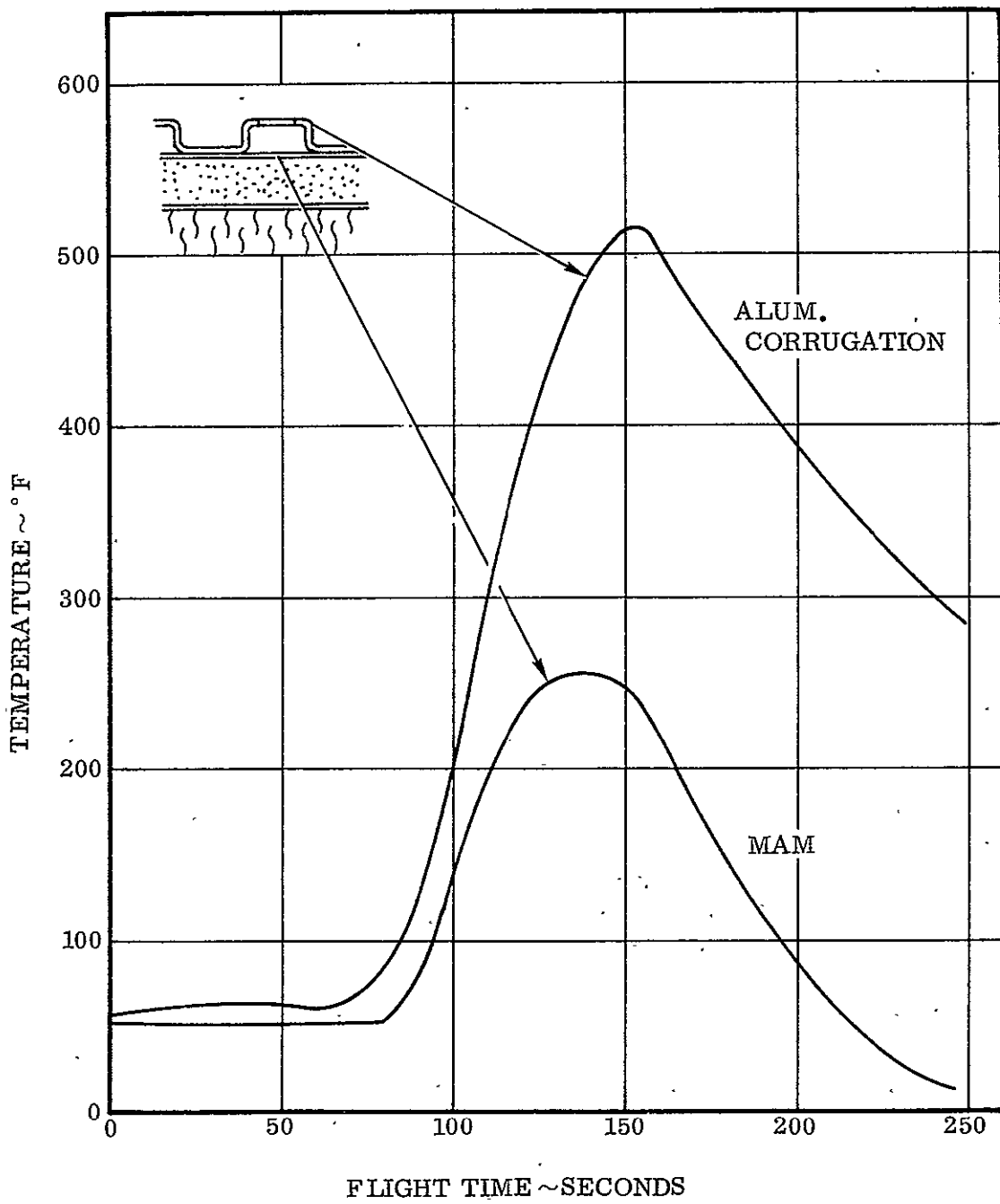


Figure 3-27. Temperature Predictions for the Aluminum Corrugated Wrap System

3.2.2 EFFECT OF CORRUGATIONS ON SOLAR ABSORPTANCE. The corrugations increase the solar absorptance of the insulation surface. This increases the heat input to the liquid hydrogen during coast and decreases payload capability. Reference 3-12 describes the effect of corrugations (surface cavities) on solar absorptance as a function of L/h , where L is the height of the corrugation and h is the width. The increase in solar absorptance (apparent absorptance), is plotted on Figure 3-28 for several ratios of L/h . It was assumed that the solar absorptance was 0.3 on a non-corrugated surface. A corrugated surface painted with a surface coating having an absorptance of 0.3 has a greater apparent absorptance in the cavities (or depressions) in the corrugations because solar energy becomes "trapped." (Solar absorptance at the top of the corrugations is unaffected by the cavities.) For a surface with an L/h ratio of 0.2, the apparent absorptance in the cavities is 0.35, thereby increasing the hydrogen boiloff losses and reducing payload capability.

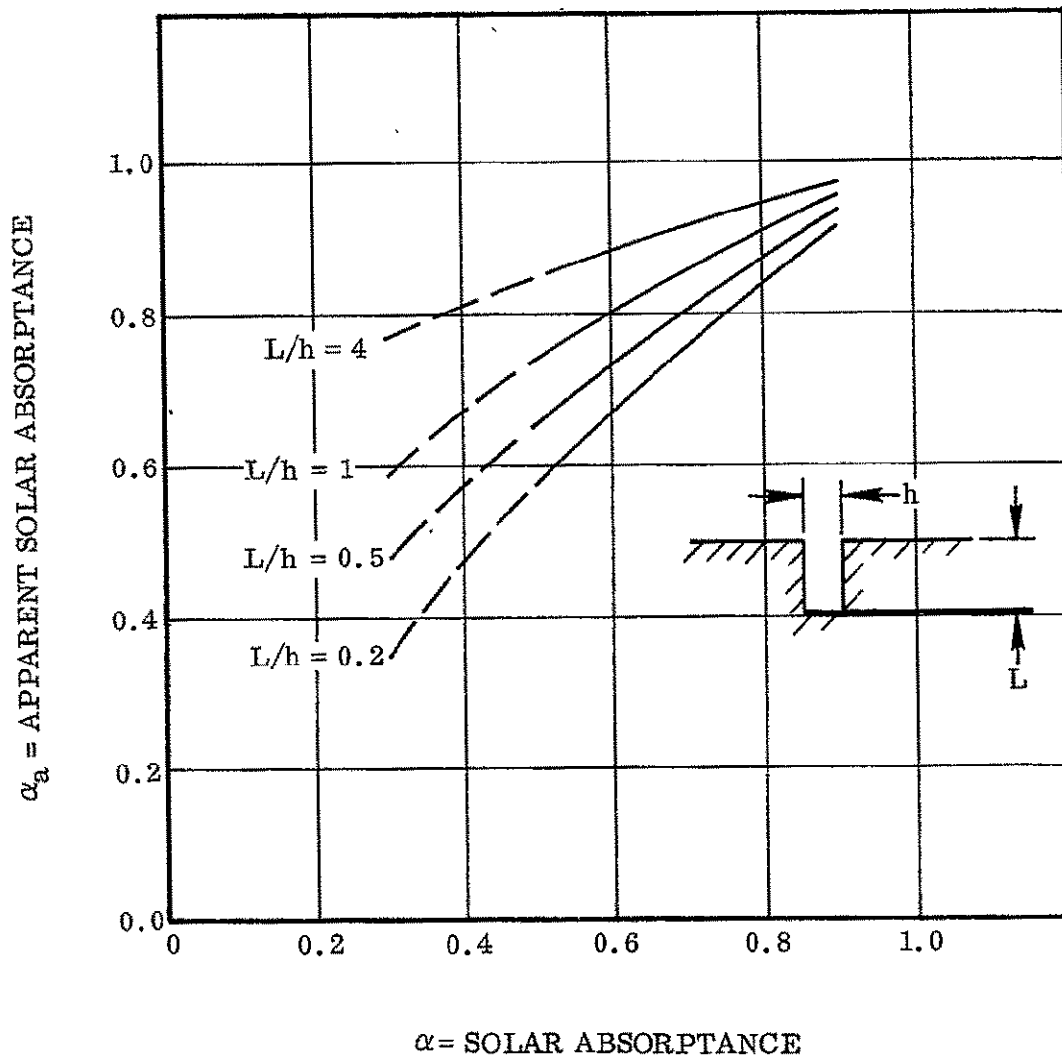


Figure 3-28. Apparent Solar Absorptance Versus Solar Absorptance for a Corrugated Surface with L/h as a Parameter

3.2.3 COMPARISON WITH THE FIBERGLASS STRAND CONSTRICTIVE WRAP SYSTEM. The increase in solar absorptance causes the liquid hydrogen boiloff loss to increase over that of the fiberglass strand system. The corrugated wrap is also heavier than the fiberglass wrap (see Section 6), which also causes more LH₂ to boiloff and vent because of the greater quantity of heat that it absorbs.

Conditions causing ice buildup are described in Subsection 3.1.3. With the fiberglass wrap system, a maximum buildup of 0.3 inch of ice forms on the external surface of the insulation. This ablates during flight, thereby increasing payload capability by 8 pounds. Ice inside the corrugations (Figure 3-26) does not melt, and reduces payload capability by 92 pounds. Payload losses for the fiberglass strand system, corrugated aluminum system, and current jettison system are compared in Section 7.

3.3 CONCLUSIONS

In summary, the following conclusions were drawn from the thermodynamic analyses performed on the sealed foam insulation concept:

1. The optimum foam thickness to minimize payload loss is 0.6 inch. However, varying the foam thickness by ± 0.2 inch decreases payload capability by only about 12 pounds.
2. The exterior of the insulation system must have a high emittance to minimize insulation temperatures during the aerodynamic heating condition and to minimize LH₂ boiloff, and therefore payload loss, during boost and coast.
3. Payload losses are less with the lower conductivity Goodyear 222 foam than with the CPR 32-2C foam.
4. Ice will form on the surface of a 0.4-inch foam insulation. This results in an increase in payload capability of 8 pounds in the fiberglass constrictive wrap system because all the ice melts off and performs an ablative function. The ice on the corrugated aluminum wrap system, however, causes a decrease in payload capability of 92 pounds.

4

DESIGN

The design of the fixed insulation system was based largely on the results of the previous NASA/LeRC experimental investigation (Reference 1-1). That investigation showed that closed-cell polyurethane foam, hermetically sealed in a Mylar-aluminum-Mylar laminate, provided an efficient insulation for cryogenic tanks. The NASA concept also provided a constrictive outer wrap which consisted of prestressed fiberglass roving bonded to the insulation panels while under prestress.

The major design goals of the Convair program were to provide (1) hermetically sealed foam panels using current state-of-the-art materials, (2) a removable constrictive wrap, and (3) a protective ground handling shell which would protect the insulation panels and constrictive wrap from inadvertent handling damage.

4.1 SEALED FOAM PANELS

4.1.1 DESIGN REQUIREMENTS. Eight design requirements were established for the design of the sealed foam panels.

1. Use the cryopumping properties of sealed foam panels for increased insulation efficiency.
2. Use the basic sealed foam system designed and tested by NASA in their previous program.
3. Minimize aerodynamic heating into the tank.
4. Minimize radiant heating into the tank.
5. Minimize ice on the tank at launch.
6. Provide a minimum weight design.
7. Maintain bond to the tank through the prelaunch and flight.

4.1.2 DESIGN CONCEPT. The design concept was to provide hermetically sealed foam insulation panels which would be formed to a 60-inch radius and bonded to the Centaur tank. The width of the panels was based on the availability of the size of MAM sealing laminate, as in the previous NASA/LeRC program. The length of the T-9 test tank was approximately 63 inches, and since the previous NASA/LeRC program had shown that panels as long as 90 inches could be handled, the panels for the T-9 tank were fabricated to the full tank length of 63 inches.

The position of panels on the tank was determined by consideration of tank protuberance locations. It was desirable to locate the three protuberance cutouts (two vacuum bulkhead bosses and the fill drain outlet) well within the area of the panel to avoid difficulties of sealing at or near the edge of a panel.

The design for the vacuum bulkhead boss cutouts consisted of a small sealed panel, approximately 2 by 2-1/2 inches, installed in a sealed cutout in the basic panel. The small panel was attached to the basic panel by large Mylar channels which completely enveloped the small panel. A hole was cut through the small panel to clear the vacuum bulkhead boss with a 1/8-inch radial clearance.

The design for the fuel fill and drain outlet consisted of a radial cutout in the basic panel. The edges of the cutout were framed by a formed Mylar inverted zee edge seal. Upon installation of the basic panel to the tank, un-sealed cut foam pieces were provided to fit between the zee edge seal and the fill and drain outlet duct. The inverted zee design was the same as employed in the previous NASA/LeRC design and was used for the T-9 test tank. However, Convair decided to reverse the slope of the zee for future designs to facilitate installation and repair.

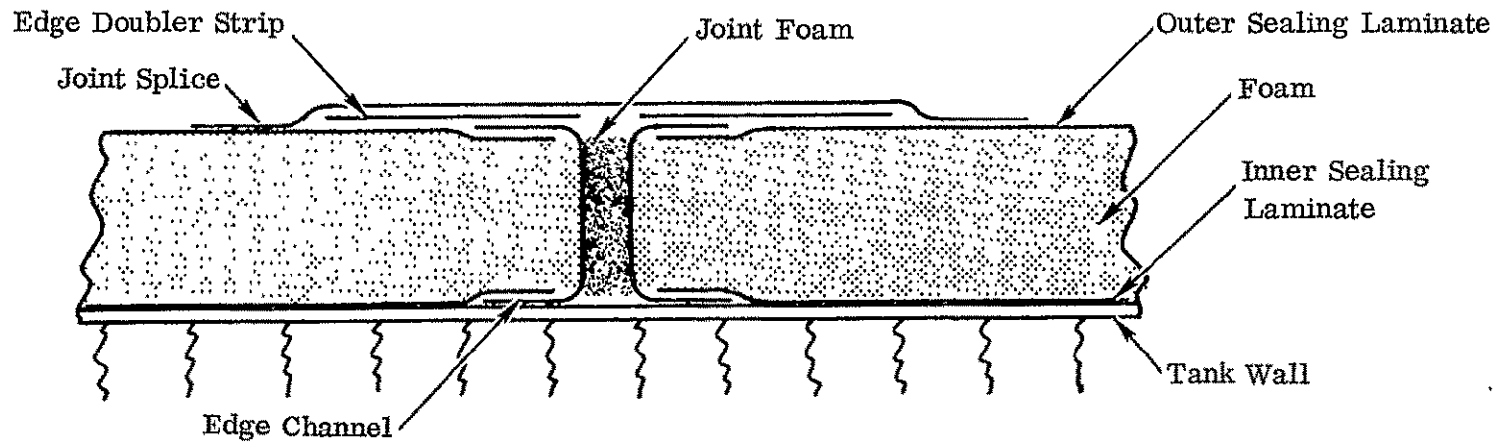
4.1.3 PANEL CONFIGURATIONS. Five sealed foam panel material configurations were designed and tested on the T-9 test tank. The materials selected were the result of vendor surveys and material evaluation tests as described in Section 2. The five configurations are tabulated in Table 4-1. For fabrication history and test results see Sections 5 and 9, respectively. For complete design details see drawings 55-07053 and 55-07224. A brief description of the major material components follows.

4.1.3.1 Foams. From the conclusions of Subsection 2.1.3 and Table 2-2, two foams were chosen for evaluation on the full scale T-9 tank test.

The first foam chosen was the same as had been used in the previous NASA/LeRC program, i.e., Goodyear Aerospace Corporation's GAC-222 polyurethane foam. The foam employed Freon as the blowing agent, and had a density of $2.0^{+0.2}_{-0.3}$ pounds per cubic foot.

The second foam chosen was designated as CPR 32-2C, manufactured by The Upjohn Company, Chemical Plastics Research Division. The foam is also a polyurethane foam, but employs carbon dioxide as the blowing agent, and has a density of 2.1 ± 0.2 pounds per cubic foot. As explained in Section 2, this foam was chosen to be evaluated because it showed slightly better stability at high temperatures.

TABLE 4-1. INSULATION PANEL MATERIALS



Component	System				
	A	B	C	D	E
Outer Sealing Laminate	1.5 Mil MAM	1.5 Mil MAM	1.5 Mil MAM	1.5 Mil MAM	1.5 Mil MAM
Outer Sealing Laminate Adhesive	PE-207	Metlbond 225 0.06 lb per sq. ft.	Epon 956	Metlbond 225 0.045 lb per sq. ft.	Metlbond 225 0.06 lb per sq. ft.
Foam	GAC-222	CPR 32-2C	CPR 32-2C	GAC-222	GAC-222
Foam Thickness	0.4 in.	0.4 in.	0.4 in.	0.4 in.	0.4 in.
Inner Sealing Laminate Adhesive	PE-207	PE-207	PE-207	PE-207	PE-207
Inner Sealing Laminate	1.5 Mil MAM	1.5 Mil MAM	1.5 Mil MAM	1.5 Mil MAM	1.5 Mil MAM
Edge Channels	2 Mil Mylar	2 Mil Mylar	2 Mil Mylar	2 Mil Mylar	2 Mil Mylar
Edge Channel Adhesive	PE-207	PE-207	PE-207	PE-207	PE-207
Edge Doubler Strips	1 Mil Mylar	1 Mil Mylar	1 Mil Mylar	1 Mil Mylar	1 Mil Mylar
Edge Doubler Adhesive	PE-207	PE-207	PE-207	PE-207	PE-207
Edge Dip	PE-207	PE-207	PE-207	PE-207	PE-207
Joint Splice	1.5 Mil MAM	1.5 Mil MAM	1.5 Mil MAM	1.5 Mil MAM	1.5 Mil MAM
Joint Foam	GAC-222	CPR 32-2C	CPR 32-2C	GAC-222	GAC-222
Joint Adhesive	Narmco 7343	Narmco 7343	Narmco 7343	Narmco 7343	Narmco 7343
Panel To Tank Adhesive	Narmco 7343	Narmco 7343	Narmco 7343	Narmco 7343	Narmco 7343

4.1.3.2 Sealing Material. The sealing material used was the same as used in the previous NASA/LeRC tests, i. e., a laminate of aluminum foil (0.0005 in.) with Mylar film (0.0005 in.) on each side of the foil. The aluminum foil, having no measurable permeability, acted as the principal vapor barrier. The tough Mylar films supplied strength to the laminate and prevented damage to the foil during fabrication and installation of the panels on the tank. The laminate was bonded to both surfaces of the foam which added considerable rigidity to the foam slabs and allowed the panels to be formed into moderate contours without heat forming of the foam. The edges of the panel were covered with preformed channels of two-mil Mylar and one-mil Mylar doubler strips and then sealed with a dip in the PE-207 polyester adhesive.

4.1.3.3 Sealing Laminate Adhesives. As described in Subsection 2.2.2.1, the inner sealing laminate was bonded to the foam with Goodyear Aerospace Corporation PE-207. This is a polyester adhesive which was used by NASA/LeRC on their previous program, and exhibited adequate bonding properties at the cold temperature environment experienced by the inner surface of the panel. It is a liquid adhesive cured by the application of a hand iron set at 265°F. As described previously in Subsection 2.2.2.2, three types of adhesives were used to bond the outer sealing laminate to the foam. The System A panels used PE-207, which was used on the previous NASA/LeRC program. However, this adhesive evidenced instability at the high temperatures (up to 550°F) experienced by the outer surface of the panels during flight. Therefore, two other adhesives were chosen from the results of the tests of Section 2.

Systems B, D, and E used Metlbond 225 adhesive. The Metlbond 225 adhesive is a modified epoxy adhesive on a nonwoven synthetic fabric carrier, and is manufactured by the Narmco Materials Division of the Whittaker Corporation. It is cured in an oven at 225°F.

System C used EPON 956 adhesive, a two-part modified epoxy liquid adhesive, manufactured by the Shell Chemical Division of the Shell Oil Company. It is cured at room temperature.

4.1.3.4 Panel-To-Tank Adhesive. As described previously in Subsection 2.2.2.3, the panel-to-tank adhesive chosen was Narmco 7343, a polyurethane adhesive which was used in the previous NASA/LeRC program. PE-207 was used as a primer in conjunction with the Narmco 7343. Two adhesive patterns were used. A grid employing adhesive beads at six-inch intervals was one system used (previously used in the NASA/LeRC program). The other system entailed a 100 percent adhesive bond area.

4.2 SEALED FOAM PANEL PROTECTIVE COVERING

During the previous NASA/LeRC program it was found that the outer MAM laminate would erode away under the combined forces of aerodynamic heating and dynamic loading. After the MAM laminate eroded away, the foam was exposed; and it too was destroyed under the heating and dynamic loading. However, NASA/LeRC proved that the application of a thin layer of fiberglass cloth on the outside of the MAM laminate protected the laminate sufficiently to preclude its erosion. The type of cloth used in the Convair program was slightly different than that used by NASA/LeRC in order to obtain the required optical properties of the outer surface.

4.2.1 DESIGN REQUIREMENTS. Three requirements for the design of the panel protective covering were established.

1. Protect the outer MAM laminate from:
 - a. exceeding its maximum temperature limitations,
 - b. aerodynamic erosion during flight,
 - c. service damage when the ground handling shell is not installed.
2. Provide an optimum thermodynamic surface as follows:
 - a. absorptivity ≤ 0.30
 - b. emissivity ≥ 0.85 .
3. Minimize weight.

4.2.2 MATERIAL CHOSEN. With the fiberglass strand constrictive wrap concept, the outer protective covering also must provide the required surface absorptivity (α) and emissivity (ϵ) characteristics. Fiberglass cloth alone, as was used in the previous NASA/LeRC program, does not meet the α and ϵ requirements. However, as was shown in the thermal control coating test results of Subsection 2.4, a silicone rubber impregnated glass cloth, designated CHR-2007, does meet the α and ϵ requirements for temperatures up to 550° F.

The outer protective coating used for the T-9 test tank was the CHR-1005 because of availability of material. This material is similar to the CHR-2007 except it has a slightly lighter weight fiberglass cloth and less silicone rubber impregnated into the cloth. However, it was proposed to use the CHR-2007 on future designs since it met the α and ϵ requirements.

As described previously in Subsection 2.2.2.4, the adhesive used to bond the rubber impregnated glass cloth to the insulation panels was SR-585, a silicone adhesive manufactured by General Electric Company.

4.3 CONSTRUCTIVE WRAP

The previous NASA/LeRC program identified a need for a constraining force on the outer surface of the sealed foam panels. That design consisted of fiberglass roving wound around the tank using a filament winding apparatus with the fiberglass roving under a constant tension load during winding. Additionally, the roving was bonded to the insulation panels during the winding process while it was subjected to the tension load. Therefore, since the roving was bonded to the insulation panels while subjected to the tension load, it was not removable, and further, it was not possible to remove the constrictive force. The goal of the Convair design was to provide a constrictive wrap which was removable.

4.3.1 DESIGN REQUIREMENTS. Four requirements for the design of a constrictive wrap were established.

1. Provide a constrictive force to:
 - a. hold the insulation panels against the tank during tank shrinkage,
 - b. hold the insulation panels against the tank during maximum airloads in case of panel bond failure,
 - c. prevent flutter of the insulation panel protective cover in case of cover bond failure.
2. The wrap had to be removable to:
 - a. relieve compression forces when the tank is degassed,
 - b. facilitate repair of the insulation panels and constrictive wrap.
3. The wrap had to be compatible with the absorptivity and emissivity requirements of the outer surface of the panel protective covering. These requirements were:
 - a. absorptivity ≤ 0.30 ,
 - b. emissivity ≥ 0.85 .
4. The wrap had to withstand aerodynamic heating with and without bridging over irregularities in the insulation panel surface.

4.3.2 FIBERGLASS STRAND CONSTRUCTIVE WRAP CONFIGURATION. After preliminary investigations of several constrictive wrap configurations, it was agreed by NASA/LeRC and Convair to develop a loaded strand type of design. The following discussions describe the rationale used to evolve the fiberglass strand constrictive wrap configuration.

4.3.2.1 Strand Material. In order to provide loaded strands which would maintain a constrictive force on the insulation over the range of dimensional changes of the circumference of the insulation, it was necessary to investigate the load-strain and stress-strain characteristics of several materials. The dimensional changes of the circumference of the insulation were the result of tank dimensional changes due to internal pressure and temperature, foam deformation under the constrictive force, and tank and foam thickness tolerances.

Figure 4-1 shows the load-strain characteristics of three materials which represent the range of materials studied. Nylon strands were not considered because a large enough load could not be obtained, even at extremely large strain values. Steel wire was not considered because of the relatively large load required to obtain the required strain. The fiberglass S-994 HTS, 20-end roving, provided a satisfactory load/strain relationship, and was chosen for this design.

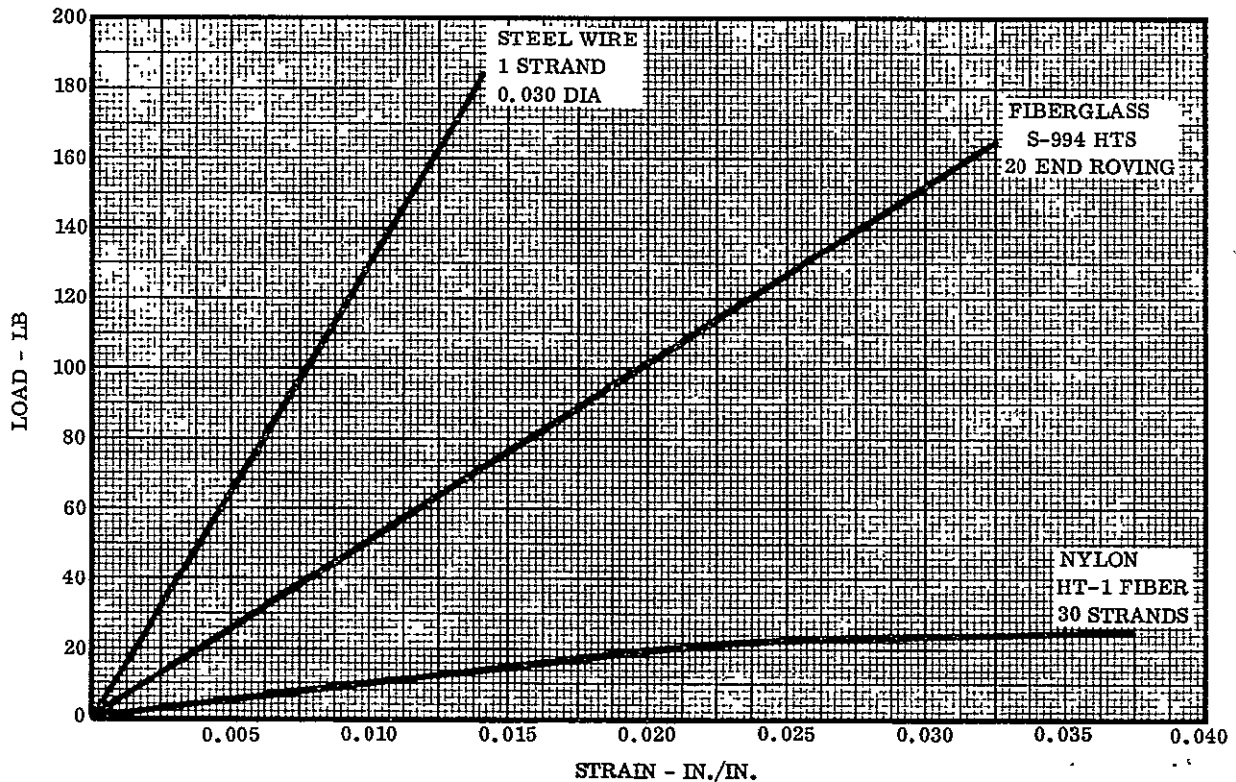


Figure 4-1. Load-Strain Properties of Constrictive Wrap Materials

4.3.2.2 Required Strand Length. It was decided that the strands would be fabricated in quarter segments and would be loaded by fabricating the wrap strands shorter than the physical circumference of the outside surface of the insulation. However, due to the circumferential dimension changes referred to previously, it was necessary to determine the strain requirements at the smallest possible circumference dimension.

Assuming the "as-built" tank conditions at 0 psig and 70°F, the minimum tank circumferential dimension when the wrap would be in place would be when the tank was filled with cryogenics, with an internal pressure of 4.0 psig in the fuel tank. Additionally, it was assumed the radial tolerance on the tank and foam could be ±0.10 inch. For foam deformation under the constrictive wrap load, a bearing load of 5.0 psi was assumed. And finally, it was assumed that the desired minimum crush pressure applied by the constrictive wrap should be 0.5 psi. With these assumptions, the required strand length of each quarter segment was then calculated as follows:

Let

L_S = length of strand per quadrant with strain.

L_W = length of strand per quadrant without strain.

ϵ_N = net strain required for desired crush pressure at the tank conditions specified.

Net Strain Calculations

1. Tank expansion under an internal pressure of 4.0 psig

$$\epsilon = \frac{\Delta L}{L} = \frac{P}{AE} = \frac{4(60)}{0.016(28.7)(10^6)} = +0.000523 \text{ in./in.}$$

$$\begin{aligned} \Delta R &= \frac{2\pi R + 2\pi R\epsilon}{2\pi} - R = R(1+\epsilon) - R \\ &= 60.00(1+0.000523) - 60.00 = +0.031 \text{ inches.} \end{aligned}$$

2. Tank contraction at -423°F

$$\Delta T = 423 + 70 = 493^\circ \text{F}$$

$$\alpha = 0.65 \times 10^{-5} \text{ in./in. per } ^\circ \text{F}$$

$$\epsilon = \frac{\Delta L}{L} = \alpha \Delta T = 0.65 \times 10^{-5} \times 493 = -0.00320 \text{ in./in.}$$

$$\Delta R = R(1+\epsilon) - R = 60.00(1-0.0032) - 60.00 = -0.192 \text{ inches.}$$

3. Foam insulation deformation with 5.0 psi bearing load

FOAM PROPERTIES:

$$\left. \begin{array}{l} f_{cy} = 30 \text{ psi} \\ E = 1500 \text{ psi} \end{array} \right\} \text{ (Reference 4-1)}$$

$$E = \frac{f_{cy}}{\epsilon}; \epsilon = \frac{f_{cy}}{E} = \frac{30}{1500} = 0.020 \text{ in./in.}$$

For $f_c = 5.0$ psi

$$\epsilon = 0.020 \left(\frac{5}{30}\right) = 0.0033 \text{ in./in.}$$

For $t = 0.4$ inch

$$\Delta t = 0.0033 (0.4) = 0.00133 \text{ inch}$$

Radius with No Bearing Load = 60.40 inches

Radius with 5.0 psi Bearing Load = 60.40 - 0.00133 = 60.398 inches

Therefore

$$\Delta R = 60.398 - 60.40 = -0.002$$

$$L_{\text{No Bearing Load}} = 2\pi R = 2\pi (60.40) = 379.505 \text{ inches}$$

$$L_{5.0 \text{ psi Bearing Load}} = 2\pi R = 2\pi (60.398) = 379.493 \text{ inches}$$

$$\epsilon = \frac{\Delta L}{L} = \frac{379.505 - 379.493}{379.505} = -0.000031 \text{ in./in.}$$

4. Tank and foam thickness tolerance

Nominal Radius = 60.40 inches

$$\Delta R = -0.10 \text{ inch}$$

Minimum Radius = 60.40 - 0.10 = 60.30 inches

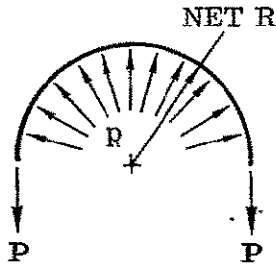
$$\epsilon = \frac{\Delta L}{L} = \frac{2\pi (60.40) - 2\pi (60.30)}{2\pi (60.40)} = -0.001655 \text{ in./in.}$$

5. Wrap crush pressure of 0.50 psi

Net radius change from the above calculations

a. Tank expansion under an internal pressure of 4.0 psig	+0.031 inches
b. Tank contraction at -423° F	-0.192 inches
c. Foam insulation deformation with 5.0 psi bearing load	-0.002 inches
d. Tank and foam thickness tolerance	<u>-0.100 inches</u>
NET ΔR	<u>-0.263 inches</u>

Therefore, net R = 60.40 - 0.26 = 60.14 inches



$$P = pR = 0.5 (60.14) = 30.07 \text{ lb/in.}$$

Assume Strands @ 1 in.; P = 30.07 lb/Strand

From Figure 4-1; $\epsilon = -0.00575 \text{ in./in.}$

Summary of Strains

1. Tank expansion under 4.0 psig	+0.000523 in./in.
2. Tank contraction at -423° F	-0.003200 in./in.
3. Foam insulation deformation with 5.0 psi bearing load	-0.000031 in./in.
4. Tank and foam thickness tolerance (R nominal -0.10)	-0.001655 in./in.
5. Wrap crush pressure of 0.50 psi	-0.005750 in./in.
NET STRAIN, ϵ_N ,	<u><u>-0.010113 in./in.</u></u>

Therefore

$$L_S = \frac{\pi D}{4} = \frac{\pi(120.80)}{4} = 94.876 \text{ inches}$$

Also

$$L_S = L_W + \epsilon_N L_W = L_W (1 + \epsilon_N)$$

$$L_W = \frac{L_S}{1 + \epsilon_N} = \frac{94.876}{1 + 0.010113} = 93.926 \text{ inches}$$

Total strand strain per quadrant

$$L_S - L_W = 94.876 - 93.926 = 0.950 \text{ inch}$$

These calculations show that at the conditions which give the insulation minimum outside circumferential dimension, each wrap quarter segment should be fabricated 93.926 inches long to give a 0.50 psi crush pressure.

4.3.2.3 Strand Loads at Various Conditions. As seen from the strain calculations, the wrap strain at 0.50 psi crush pressure and the minimum insulation outside surface radius ($R_{\text{Nominal}} - 0.10$) is 0.00575 in./in. Adding the strain associated with the radius tolerance of 0.10 inch (which has been shown to be 0.001655 in./in.), gives a strain of 0.00741 in./in., which is the wrap strand strain with a nominal radius. Adding the radius tolerance strain again gives a strain of 0.00907 in./in., which is the wrap strand strain for a nominal radius plus 0.10 inch. From Figure 4-1, the strand load associated with these three strand strains is 30, 38, and 46 pounds. These three conditions are tabulated in Table 4-2. Also tabulated in Table 4-2 are the three radius tolerance conditions for the tank at two other tank environmental conditions, i.e., (1) tank at room temperature and 4.0 psig internal pressure in the fuel tank and (2) tank at -423°F and 25.5 psig internal pressure in the fuel tank. These strains and loads are calculated similarly to the procedure outlined above, and are only tabulated here.

TABLE 4-2. STRAND LOAD CONDITIONS
CENTAUR TANK AT -423°F AND 4.0 PSIG

Tolerance Condition	Strand Strain (in./in.)	Load/Strand (lb)
$R_{\text{Nominal}} - 0.10$	+0.00575	30
R_{Nominal}	+0.00741	38
$R_{\text{Nominal}} + 0.10$	+0.00907	46

CENTAUR TANK AT ROOM TEMPERATURE AND 4.0 PSIG

Tolerance Condition	Strand Strain (in./in.)	Load/Strand (lb)
$R_{\text{Nominal}} - 0.10$	+0.00895	46
R_{Nominal}	+0.01061	54
$R_{\text{Nominal}} + 0.10$	+0.01227	63

CENTAUR TANK AT -423°F AND 25.5 PSIG

Tolerance Condition	Strand Strain (in./in.)	Load/Strand (lb)
$R_{\text{Nominal}} - 0.10$	+0.008351	42
R_{Nominal}	+0.009921	51
$R_{\text{Nominal}} + 0.10$	+0.011591	59

It is interesting to note that for the same radius tolerance condition, the largest strand load associated with the three tank environmental conditions occurs with the tank at room temperature and 4.0 psig in the fuel tank. This is the condition present when the wrap is installed on the tank, indicating that the largest load per strand occurs as the wrap is installed, and not during flight.

4.3.2.4 Strand Load Profile. The installation strand load was applied by exerting a tensile load at each end of the quarter segment strands, thereby "stretching" the strands around the tank. Therefore, the actual strand load at various points would not be constant, as implied by Table 4-2, but would vary due to friction between the strand and the outer panel covering material. If the friction load were very large, the strand would be only lightly loaded in the middle of the segment and heavily loaded at the ends. However, as discussed in Subsection 2.6.3.3, this was not the case. The friction forces varied with the type of lubricant used, if any, but in all cases the friction force at the center of the quarter segment (45° of tank circumference) was 20 to 30 percent of the applied end load. This was considered acceptable for this design.

4.3.2.5 Constrictive Wrap Pressure Versus Radial Deflection. The relationship of the change of radius of the outside surface of the insulation from the "as-built" tank conditions of 0 psig and 70°F versus strand load and corresponding strand crush pressure is plotted in Figure 4-2. The change in radius for each of the three tank environmental conditions was obtained from the change in circumference due to the conditions referred to previously for calculating strain requirements. The change in radius for the nominal radius case of the three tank environmental conditions is noted in the figure.

4.3.2.6 Constrictive Wrap Design Parameters. A summary of the constrictive wrap design parameters is shown in Figure 4-3. Also shown in the figure is a history of the wrap strand crush pressure on the panel versus prelaunch and flight time. The crush pressure was obtained by calculating the insulation panel outer surface radius change from the "as-built" condition to instantaneous tank pressure, temperature, and dimensional tolerance conditions; and then obtaining the crush pressure from Figure 4-2. The minimum and maximum crush pressure represents the minimum and maximum tank and insulation panel dimensional tolerances respectively.

4.3.2.7 Detail Design of Constrictive Wrap Segments. After establishing that the constrictive wrap would be a loaded strand design employing fiberglass strands, and that the wrap would be fabricated in quarter segments 93.926 inches long, the detail design was begun. A brief description of the final design follows. For complete details, see engineering drawing 55-07227.

The method of attaching the quarter segments was by an aluminum hinge fitting end tab. An enlarged view of the hinge fitting assembly is shown pictorially in Figure 4-4. The hinge fittings were designed so that the load line of action of the fiberglass strands passed through the center of the hinge, giving a zero moment about the hinge pin. This

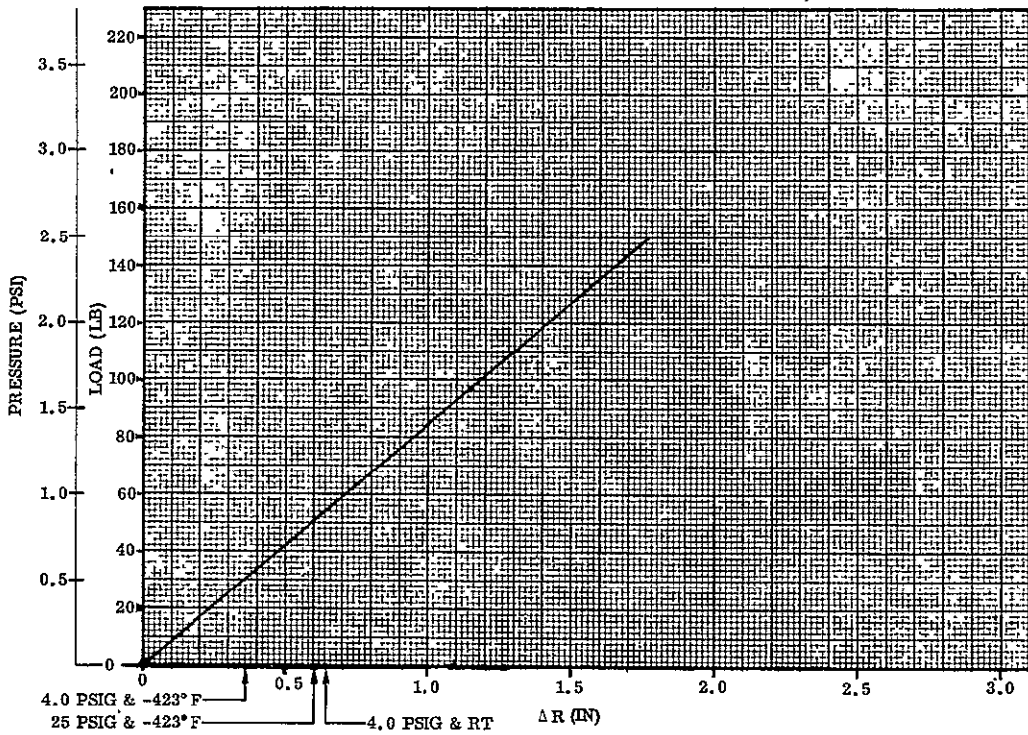


Figure 4-2. Wrap Pressure Versus Radial Deflection

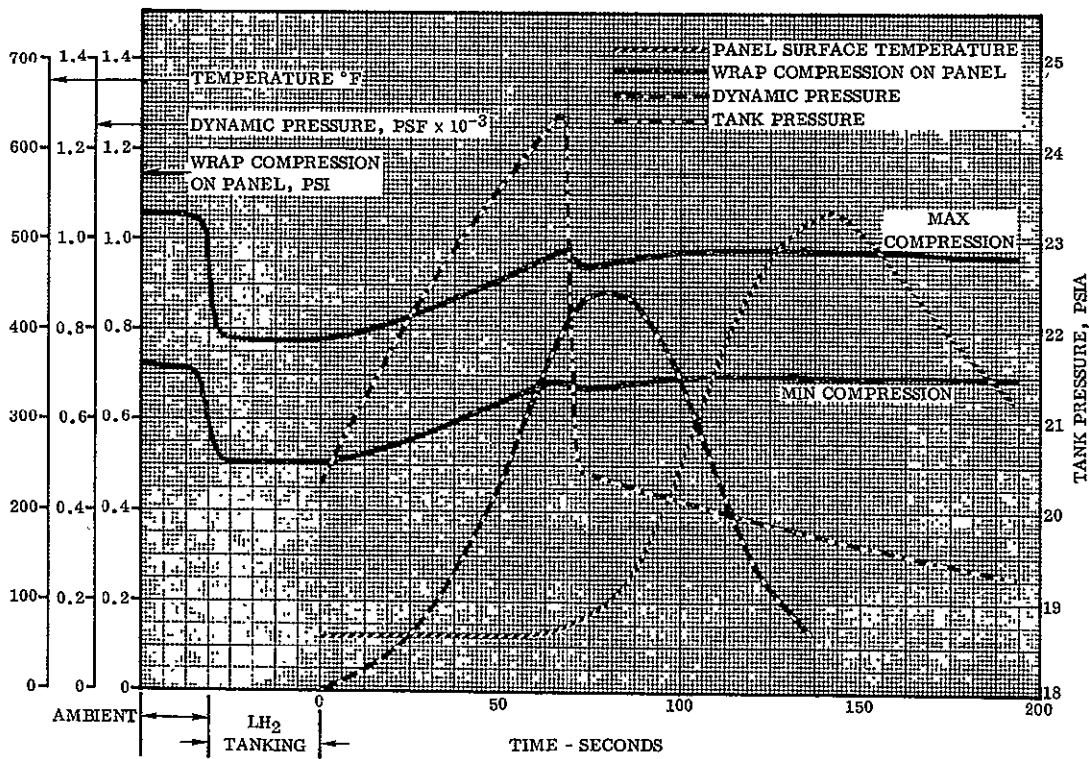


Figure 4-3. Constrictive Wrap Design Parameters

concept is shown pictorially in Figure 4-5. Since the bend radius of the hinge fitting had to be smaller than that recommended for normal practice, tests were run to determine the strength of the fitting at the bend radius. The test results are shown in Table 4-3. It should be recalled from Table 4-2 that the maximum expected strand load is 63 pounds, while the test results of Table 4-3 show load cycling capability of greater than 200 pounds with no yielding, and a yield load of greater than 300 pounds.

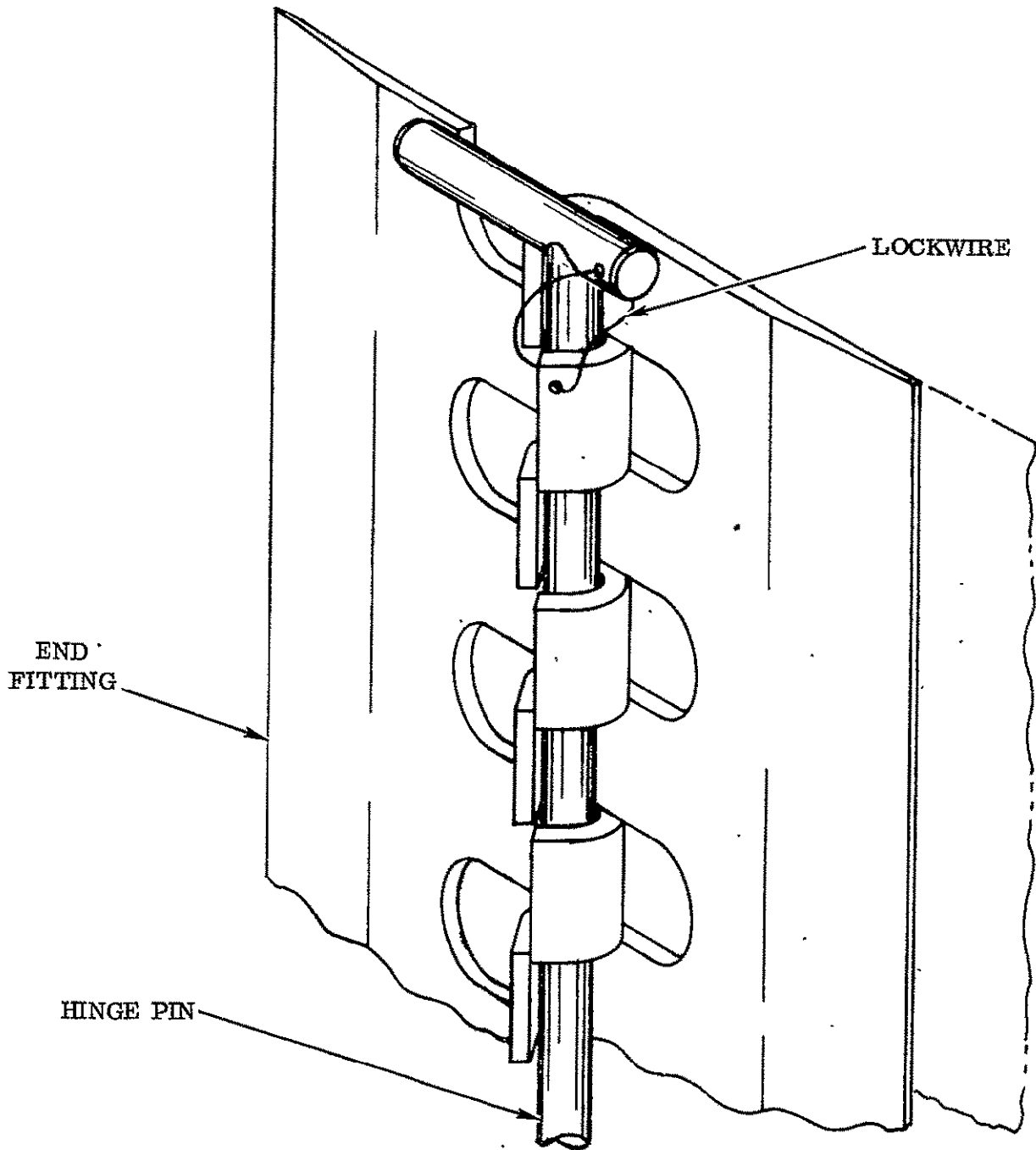


Figure 4-4. Constrictive Wrap End Fitting Configuration

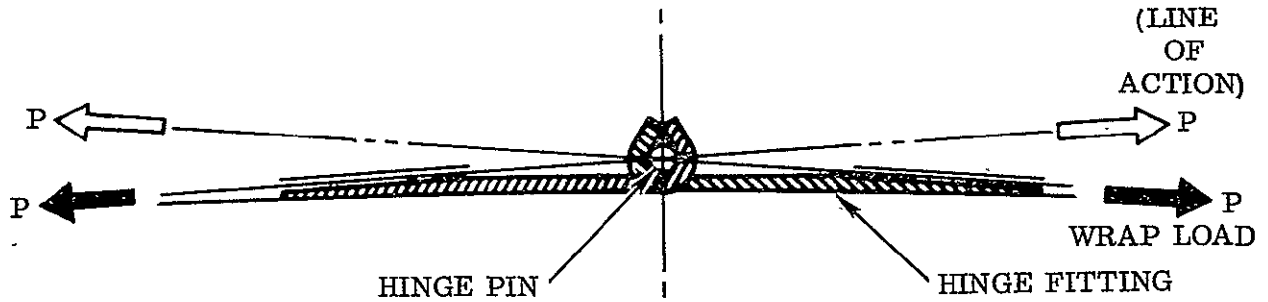


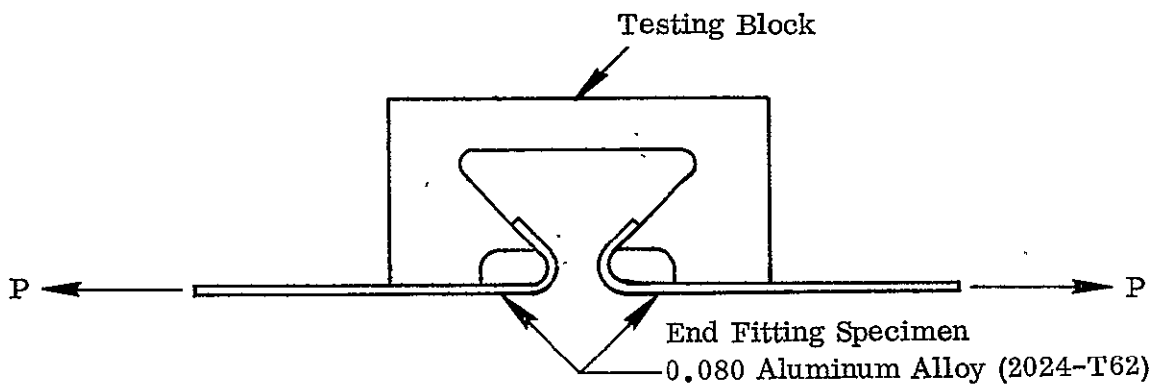
Figure 4-5. Constrictive Wrap Hinge Fitting (Zero Moment Design)

TABLE 4-3. CONSTRICTIVE WRAP ALUMINUM END FITTING TEST DATA

Specimen Number	Run Number	Applied Load (lb/in.)	Load Initiating Yielding (lb/in.)	Number Of Load Cycles	Specimen Failed	Duration Of Applied Load Min/Cycle
1	1	395	—	1	No	—
	2	545	410	1	No	—
	3	497	—	1	*Yes	—
2	1	325	—	1	No	10
	2	325	—	1	No	—
	3	482	365	1	*Yes	—
3	1	200	—	10	No	2

*Cracks occurred on the inside radius (0.07R)

SPECIMEN TEST CONFIGURATION



The fiberglass strands were attached to the aluminum hinge fittings by adhesive bonding. First, the strand interlaminar shear pullout properties of epoxy and phenolic reinforced glass fabric were investigated. The results were shown in Table 2-13. Since the average ultimate load did not develop the strength of the strand, the use of adhesives was considered to improve the pull-out properties. Test results were shown in Table 2-14. As can be seen, the phenolic materials did develop the strength of the strand. It was therefore decided to use a phenolic strand resin reinforcement and either HT-424 or 422J film adhesive. Both the HT-424 and 422J films are bought to the same specification, and the use of either is acceptable. Specifically, the HT-424 and 422J are aluminum filled epoxy-phenolic adhesives on a glass scrim cloth.

4.3.2.8 Operational Problems. During the fabrication, installation, and operational analysis of the fiberglass strand constrictive wrap, several problem areas became evident. Fabrication and installation problems are discussed in Subsections 5.3 and 5.4, respectively. These problems deal with strand brittleness and the requirement for "tender-loving-care" of the wrap segments, which would require special handling procedures. Additionally, there was a question as to the susceptibility of the strands to flutter under certain aerodynamic conditions, especially where the strands had to bridge local depressions in the foam insulation. It was felt that wind tunnel testing would be required to determine whether critical flutter modes would develop during flight.

Because of these rather extreme problem areas, it was decided by NASA/LeRC and Convair to study other constrictive wrap designs.

4.3.3 OTHER CONSTRICTIVE WRAP DESIGNS. Several other constrictive wrap design ideas were investigated in varying detail in order to identify a wrap which did not have the "tender-loving-care" and questionable flutter aspects of the fiberglass strand design. Those designs studied were:

1. Thin flat sheet in hoop tension:
 - a. Stainless steel
 - b. Aluminum
 - c. Fiberglass
 - d. Spring loaded fiberglass
2. Flat wire titanium springs
3. Pressurized compartmented sheet
4. Titanium metal grid
5. Wire screen

6. Corrugated sheet in hoop tension:
 - a. Hat section type (aluminum and fiberglass)
 - b. Sinusoidal (fiberglass)
7. Corrugated sheet retained with pre-tensioned wire:
 - a. Aluminum
 - b. Fiberglass

The above designs were studied in enough detail to determine comparative trade-off factors with the fiberglass strand constrictive wrap design. These trade-off factors are tabulated in Table 4-4. Based on the comparisons in Table 4-4, it was decided by NASA/LeRC and Convair to pursue the design of an 0.020 inch aluminum corrugation retained with wire.

4.3.4 CORRUGATED CONSTRICTIVE WRAP CONFIGURATION. The corrugated constrictive wrap design concept is shown in Figures 4-6 and 4-7. The design consists of a corrugated aluminum sheet, 0.020 inch thick, with the corrugations 0.80 inch wide by 0.30 inch deep. In order to preclude the requirement for purge under the corrugation, and to allow gasses to vent during ascent, 0.38 inch diameter holes are drilled in the corrugations on 0.80 inch centers.

The constrictive force is applied through the use of 0.045 inch diameter titanium wire which passes through the corrugations by means of holes drilled in the corrugation corner radii. A total of 20 wire strands are used, located approximately 10 inches on center along the length of the tank.

A summary of the titanium wire load conditions is shown in Table 4-5.

4.3.5 CONSTRICTIVE WRAP COMPARISONS. After the corrugated constrictive wrap design had been investigated in enough detail to be certain that no large problem areas had been overlooked, the two constrictive wrap concepts were compared to decide which concept should be used to complete the remainder of the development program. Table 4-6 is a tabulation of the pertinent parameters for comparison of the two systems.

The fiberglass strand constrictive wrap was eliminated from future consideration because of its questionable flutter aspects and requirement for tender-loving-care. One of the design objectives for Improved Centaur is to design items that do not require tender-loving-care. Additionally, it was not considered feasible to spend either the time or money required to learn to what degree the strands are susceptible to flutter.

TABLE 4-4. COMPARATIVE TRADE-OFF FACTORS FOR MANY CONSTRICTIVE WRAP DESIGNS

Wrap Concepts	Flutter Resistant	Requires Tender Loving Care	Mfg. Development Time Required	Installation and Removal	Purge Required	Venting Required	Surface Optical Degradation	Net Change in Weight From Fiberglass Strands	Design Development Time	Cost	Adaptable To External Thermal Protection
Preloaded Thin Sheet	No	Yes	None	Difficult	No	Yes	None	-25 TO +45 lb	Short	Low	Yes
Spring Loaded Fiberglass Sheet	No	Yes	Long	Medium	No	No	None	+195 lb	Long	High	Yes
Flat Wire Titanium Springs	No	No	Medium	Medium	No	No	None	+285 lb	Medium	Low	Yes
Pressurized Compartmented Sheet	No	Yes	Long	Difficult	Yes	Yes	None	+ 50 lb	Long	High	Yes
Titanium Metal Grid	No	No	Short	Difficult	No	No	None	+140 lb	Short	Low	No
Wire Screen	Yes	No	Medium	Difficult	No	No	None	+ 51 lb	Medium	Low	No
Corrugated Aluminum Sheet in Hoop Tension	Yes*	No	None	Difficult	No	Yes	30%	+275 lb	Medium	Low	Yes
Corrugated Fiberglass Sheet in Hoop Tension	Yes*	No	Long	Difficult	No	Yes	30%	+320 lb	Medium	Medium	Yes
Sinusoidal Corrugated Fiberglass Sheet in Hoop Tension	Yes*	No	Short	Difficult	No	Yes	None	+ 95 lb	Medium	Medium	Yes
0.020 Corrugated Aluminum Sheet Retained with Wire	Yes*	No	Short	Easy	No	Yes	30%	+155 lb	Short	Low	Yes
0.030 Corrugated Fiberglass Sheet Retained with Wire	Yes*	No	Medium	Easy	No	Yes	30%	+155 lb	Short	Medium	Yes
Existing Fiberglass Strands	No	Yes	None	Easy	No	No	None	—	None	Low	Yes

* Based On Extrapolated Equivalent Flat Plate Flutter Parameters Analysis.

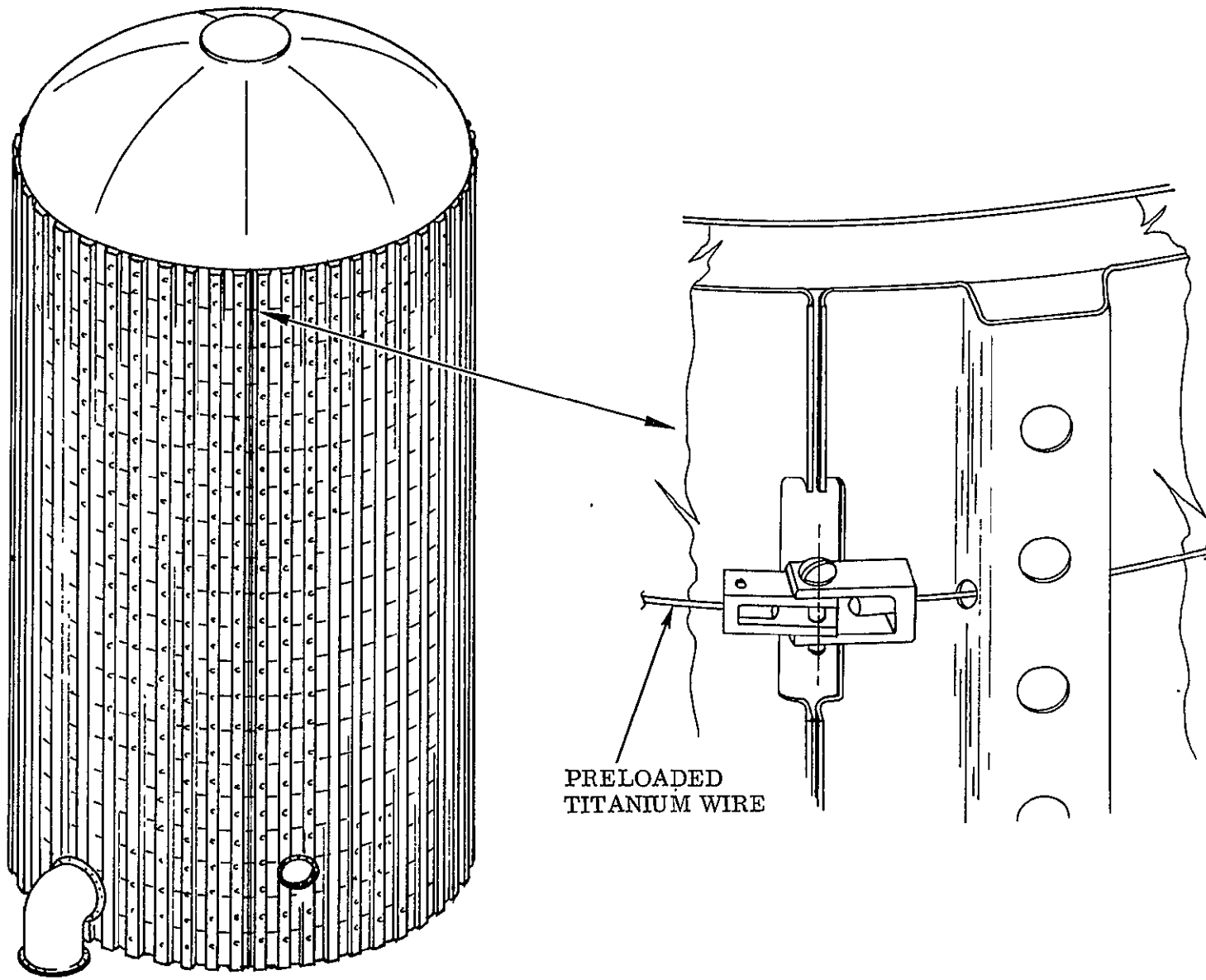


Figure 4-6. Corrugated Constrictive Wrap Concept

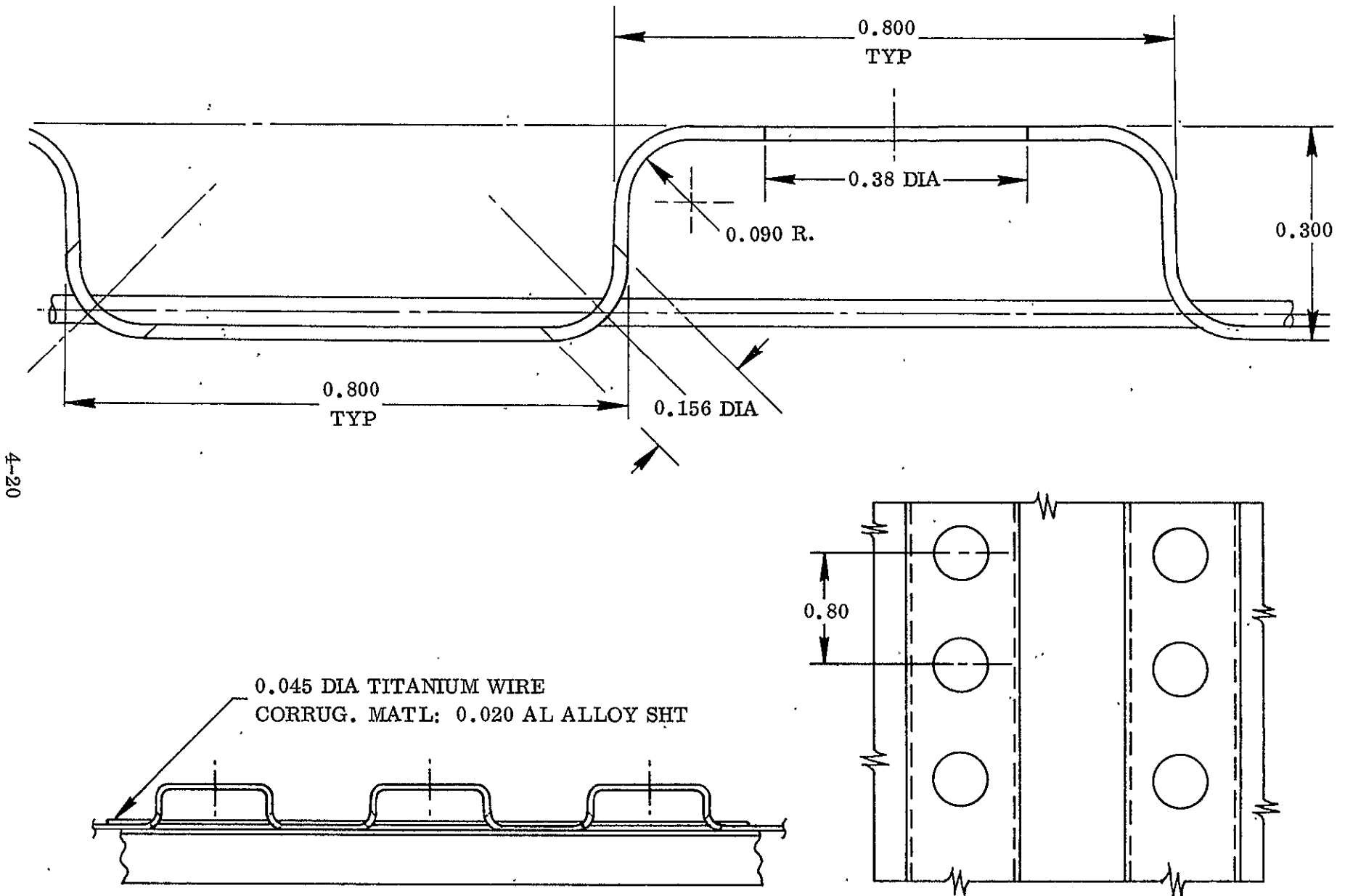


Figure 4-7. Corrugated Constrictive Wrap Details

TABLE 4-5. WIRE LOAD CONDITIONS

Condition	Wire Temperature ° F	Wire Strain in. \ in.	Wire Load lb	Wire Stress psi	Local Bearing on Tank Wall, psi
1. Installation (Tank @ 4 psig & Room Temperature)	Room Temperature	0.00715	182	114,448	2.01
2. Tanking (Tank @ 4 psig & -423° F)	Room Temperature	0.00225	57	36,021	0.63
3. Flight Max p (Tank @ 31.5 psig & -423° F)	100	0.00422	107	67,560	1.18
4. Flight Max Band Temperature (Tank @ 19.5 psig & -423° F)	500	0.00135	30	19,077	0.33

Wire Properties

Material: 6 Al-4V Titanium

Diameter: 0.045 inch

E_{Tm} : 157,000 psi

E_{Tb} : 143,000 psi

TABLE 4-6. FIBERGLASS STRAND VERSUS ALUMINUM CORRUGATION
CONSTRICTIVE WRAP COMPARISON

Aluminum Corrugation Constrictive Wrap	Fiber Glass Strand Constrictive Wrap	Flutter Resistant	Requires Loving Care	Mfg. Development Time	Venting Required	Surface Optical Degradation	Design Development Time	Weight Difference	Degradation From Jetisonable System
Yes	No	Yes	None	Short	Yes	30%	Short	+158 lb	113 lb
No	Yes	No	Yes	None	No	None	None	—	355 lb

Also, the aluminum constrictive wrap was eliminated from future consideration after examination of the payload degradation results. The payload degradation from the jettisonable system was obtained from Tables 7-1 and 7-2. The additional 242 pounds of payload loss over the fiberglass strand system was not acceptable for the Improved Centaur.

4.4 PROTECTIVE SHELL

Both the hermetically sealed foam insulation panels and the fiberglass strand constrictive wrap were susceptible to handling damage after being installed on the tank. Consequently, a ground handling protective shell was to be designed which would encompass the tank in the area of the fixed insulation, and would protect the insulation from inadvertent damage.

In the event that the aluminum corrugation constrictive wrap was used in lieu of the fiberglass strand constrictive wrap, no protective shell would be required. The aluminum corrugation would adequately protect the sealed foam panels.

4.4.1 DESIGN OBJECTIVES. The following objectives were established for design of the ground handling protective shell.

1. The shell had to be designed to remain in place from the time of installation in the factory until removal in the launch tower. It had to be compatible with normal ground handling conditions of the vehicle including:
 - a. factory transport,
 - b. highway transport,
 - c. air transport,
 - d. site erection, including tank stretch.
2. It was assumed that a wiring tunnel and 13-inch diameter LH₂ outlet fairing would be installed on the tank and had to be protected by the protective shell.
3. The constrictive wrap would be installed prior to installation of the protective shell. The shell should not be allowed to damage the constrictive wrap or cause it to shift position.
4. The shell had to provide for the existing LH₂ fill and drain line and be removable in the launch tower with the line and valve connected.
5. The shell had to be water tight when subjected to a 4 ± 1 inch per hour rain with the tank in either the horizontal or vertical position.

6. Provisions were considered for a purge or air conditioning system and for ventilation and moisture condensation drainage.
7. The shell had to be capable of sustaining the impact of a two-inch steel ball dropped from a height of six feet, and could not deflect to adversely affect the insulation system.
8. Contact pressures on the insulation could not exceed three psi nor affect the surface optical characteristics.
9. Temperature within the shell, with the vehicle inside, could not exceed 200°F steady state, assuming maximum solar heating during ground transportation with the vehicle stationary.
10. The shell had to be capable of being installed or removed in:
 - a. the factory horizontal dock within four hours,
 - b. the launch tower within two hours.

4.4.2 SHELL CONFIGURATION. The fixed insulation program was stopped, then terminated, prior to completion of design details of the protective shell. However, preliminary layouts had been completed. The design configuration envisioned was a 0.06 inch thick laminated fiberglass shell fabricated in quarter segments. The fiberglass shell had 0.50 inch thick sponge rubber pads bonded to the inside surface to provide bearing pads on the insulation panels. A series of over-center quick disconnect latches were employed at the split lines to meet the time requirement for removal. Special treatment was devised to provide for the end closeouts, the wiring tunnel, and fuel fill and drain outlet.

5

FABRICATION

5.1 T-9 TANK PANELS

The basic method for fabricating the sealed foam panels was developed by Goodyear Aerospace Corporation under a previous contract with NASA/LeRC (Reference 1-1). To take advantage of this previous experience by Goodyear, Convair subcontracted to Goodyear the fabrication of the panels required for this program.

5.1.1 MATERIAL SYSTEMS (COMBINATIONS). Several combinations of materials were fabricated and tested in the T-9 tank material evaluation tests and the repair technique evaluation tests. These material systems have been previously identified as System A through System E, and have been tabulated in Table 4-1.

5.1.2 MANUFACTURING PROCEDURES. Foam slabs 0.4 inch thick were cut from the as-received foam blocks. Slicing was done on a large bandsaw having a hydraulically controlled feed table which moved the foam block past a bandsaw blade set 0.400 inches from a backup plate. With this setup, a thickness tolerance of ± 0.008 inches was achieved over the entire area of the slab.

To seal the foam insulation slabs, each flat slab was placed on a male wooden die having a 60-inch radius of curvature, covered with one of the three types of outer laminate adhesives, and then covered with the outer MAM (Mylar-aluminum-Mylar) sealing laminate face sheet. A vacuum bag was applied, and the face sheet was bonded to the foam slab by either ironing with a hand iron set at 265°F for the PE-207 adhesive, placing in an oven for the Metlbond 225 adhesive, or allowing to cure at room temperature for the EPON 956 adhesive. After the outer MAM face sheet was bonded to the foam slab, the slab maintained its 60-inch radius contour. The contoured foam slab was then placed in a female wooden die having a 60.4-inch radius of curvature, the inner sealing laminate adhesive (PE-207) was applied, and the foam surface was covered with the inner MAM sealing laminate face sheet. A vacuum bag was applied, and the face sheet was heat sealed to the foam slab by ironing with a curved-shoe hand iron set at 265°F. The face-sealed foam slab was next placed on a trim fixture and trimmed to final size with a razor-type knife guided by metal straight-edge bars clamped to each side of the slab.

The edges of the face-sealed foam slabs were sealed by bonding premolded 0.002-inch thick Mylar channels to the perimeter of the slab. The Mylar channels were premolded by vacuum forming on steel molds and heat set at 275°F for 45 minutes. Before bonding to the edges, the Mylar channels were rough trimmed to length, and the channel

legs were finish trimmed to a width of 0.62 inches. The inside surfaces of the channels and the perimeter of the face sheets of the foam slabs were precleaned with methylethylketone, brush coated with PE-207 resin, and allowed to dry. The channels were then assembled onto the edges of the foam slab. The edge channel on any two opposing edges of the foam panel were finish trimmed to the length of the panel. The edge channel on the other two edges of the panel extended beyond the length of the panel at each end. The excess lengths were carefully folded over to form the corner seal. The assembly was vacuum bagged, and the channels were heat sealed to the face sheets by using a 265°F hand iron. The channel-to-face-sheet bond was further reinforced and sealed with 0.75-inch wide, 0.001-inch thick Mylar doubler strips centered along the edge of the channel. The doubler strips were applied in the same manner as the channels. To further ensure that the insulation panel was leak tight, the corners and all edges were double-dipped in a bath of PE-207 resin to a depth sufficient to coat all edges and doublers.

5.1.3 ACCEPTANCE CRITERIA. Two key steps in the processing of each panel were carefully controlled. The procedures for process control of the two steps were established during the earlier NASA/LeRC program, and were followed during this program.

First, rolls of the MAM laminate were visually inspected over a back-lighted glass table, and the frequency of pinhole light leaks was noted. In the previous NASA/LeRC program, samples were cut from the pinhole areas and tested for leakage in a Dow-cell gas diffusion test apparatus. Since no leakage was noted, it was concluded that the pinhole light leaks were holes in the aluminum foil only, and that the backup layers of Mylar sealed the pinholes in the aluminum foil.

Second, qualification of the completed panels included the following two tests:

1. Visual Inspection. All panels were inspected for possible leak areas along the bonded channel legs, and all such questionable areas were repaired with a patch of MAM sealing laminate and an overwipe of PE-207 resin. All questionable areas in the channel web were repaired by dipping in PE-207 resin.
2. Leak Test By Liquid-Nitrogen Submergence. A method of leak testing for vacuum tightness was developed during the previous NASA/LeRC program which attempted to duplicate the sealing requirements under actual conditions. The cryopumped vacuum normally obtained when the panels are attached to a liquid hydrogen filled tank was at least partially duplicated by immersing the panels in a bath of liquid nitrogen for five minutes. The cooling caused the contained gases to contract or condense with a resultant decrease in internal pressure. If a leak of small size existed anywhere in the seal material, some nitrogen was drawn into the panel. Upon removal from the nitrogen bath, the panel warmed up, and the entrapped liquid nitrogen vaporized rapidly. However, the nitrogen vapor could not escape through the small hole at a rapid enough rate to keep the internal pressure from increasing to the point where a blister would appear in the laminate covering on the panel. Larger holes

were not easily detected by this method since the vaporized gases were able to escape without producing significant pressure increases. However, these larger leak sources could be found by careful visual inspection of the panel after removal from the liquid nitrogen. A small trail of vapor could usually be seen emerging through the larger hole in the MAM covering.

It should be noted that this leak test obviously did not duplicate the operational sealing requirements closely enough, as indicated by the panel blistering observed during the ground hold tests discussed in Section 10. Some panels which were judged leak tight by the results of this submergence test did indeed cryopump outside gases into the panel during the first cryogenic tanking. Therefore, a new acceptance test which more nearly duplicates the operational sealing requirements should be devised for any future sealed foam panel fabrication.

5.1.3.1 Material Integrity Proof Tests. To determine the capability of the material to withstand six liquid hydrogen tanking cycles while installed on a liquid hydrogen tank, the first production panels of the Systems A, B, and C panels were each subjected to six immersion cycles in LN₂ for five minutes per cycle. See Reference (5-1) for a detail test procedure. See Subsection 5.1.5.1 for a discussion of test results.

5.1.3.2 Individual Acceptance Tests. Prior to Convair acceptance of production panels, each panel was subjected to one immersion cycle in LN₂ for five minutes. See Reference 5-2 for a detail test procedure. See Subsection 5.1.5.2 for a discussion of test results.

5.1.4 FABRICATION HISTORY.

5.1.4.1 Goodyear 222 Foam. The first foam slabs fabricated by Goodyear revealed the foam to be of unacceptable quality due to a rather uniform distribution of air bubbles 1/8 inch to 1/4 inch in diameter. The basic cell structure of the foam was good; however, the bubbles appeared to be caused by trapping the entrained air from foam mixing. The foam processing was adjusted to reduce mixing time and lower the temperature of the premix. This, in turn, provided a slowing of the reactivity of the foam and allowed release of entrained air. With these process adjustments a foam block of acceptable quality was produced and sliced for fabrication of insulation panels.

5.1.4.2 CPR 32-2C Foam. The quality of the CPR 32-2C foams was below the minimum standards set up for the Goodyear 222 foam with respect to uniformity of texture and size of voids. Due to the experimental nature of the foam and schedule requirements, it was decided to use the foam as-received for manufacture of the T-9 tank insulation panels. The presence of excessive voids presented no noticeable fabrication difficulties. However, as noted later in this report, the material integrity proof tests revealed defects which were attributed to voids in the foam.

Four 10-inch by 24-inch by 48-inch foam blocks were bonded together with Epon 956 resin applied at a controlled weight of 10 grams per square foot of bond area. Approximately one pound per square inch load was applied to the bond lines during a 36-hour room temperature cure. No difficulty was experienced in slicing the bonded blocks; however, the foam thickness in the bond line areas was slightly under the nominal thickness of the foam slab. The thickness variation was caused by breaking out or chipping of small pieces of the brittle adhesive at the bond lines during slicing, and can be seen in Figure 5-1. Figure 5-1 is a picture of the MAM covering in the area of a typical foam butt joint.

After fabrication of the CPR 32-2C foam into the T-9 tank insulation, another order was placed with specific purchasing requirements as to foam quality. Upon receipt of this shipment of foam, visual examination of the blocks showed them to be of good quality with uniform texture and free of large open cells. The foam blocks were not of uniform color due to a pattern of light-brown colored streaks running through the block. The presence of these streaks through the entire thickness was verified when one block was cut into three slabs, each approximately 3.25 inches thick by 24 inches wide by 41 inches long. These three slabs were edge glued with Epon 956 adhesive to form one slab 3.25 inches thick by 41 inches wide by 72 inches long. The resultant slab was then sliced into 0.4 inch thick slabs which verified the absence of large open cells.

5.1.4.3 System A Panels. No problems or significant events occurred during fabrication of the System A panels. This system was identical to the system used in the previous NASA/LeRC tests, and all fabrication problems had been worked out during that program.

5.1.4.4 System B Panels. The System B insulation panels presented several processing difficulties due to the Metlbond 225 adhesive. The problems are discussed in the following paragraphs.

1. Resin Penetration through Foam

The first production panel was fabricated with the outer MAM sealing laminate face sheet applied first to the foam. The Metlbond 225 resin penetrated through the voids in the foam and bonded the foam to the layup tool, causing the panel to be destroyed during removal from the tool. Figure 5-2 shows the tool after removal of the panel. Note the areas which were bonded to the tool.

To eliminate the resin penetration through the foam, a series of resin flow tests were conducted to determine a resin cure schedule which would reduce the resin flow during the high temperature portion of the cure cycle. The following cure schedule reduced the resin penetration to approximately 10 to 20 percent of the penetration experienced on the first production panel:

2.5 hours at 150°F; 3.0 hours at 175°F; 1.5 hours at 200°F

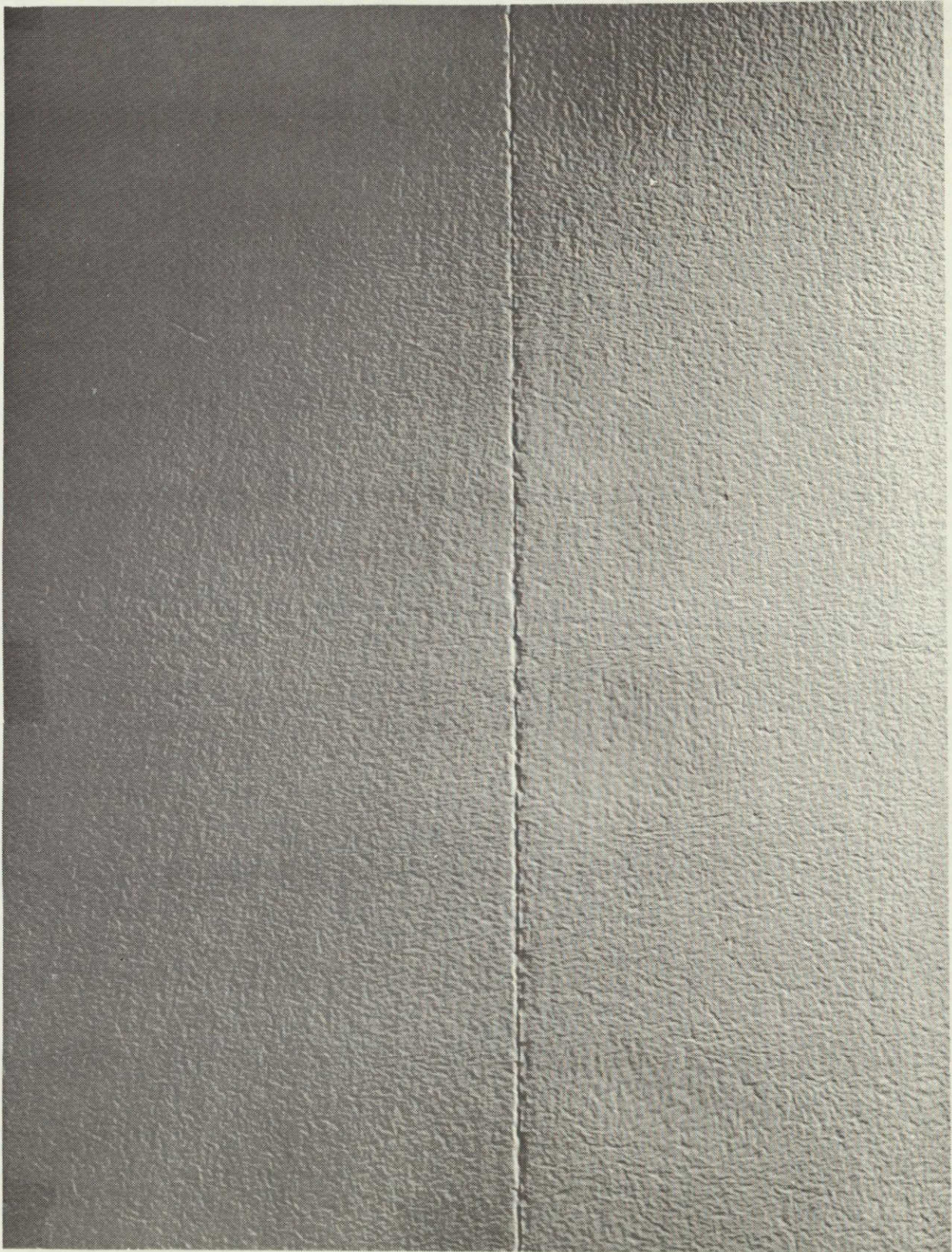


Figure 5-1. MAM Covering of Foam Butt Joint

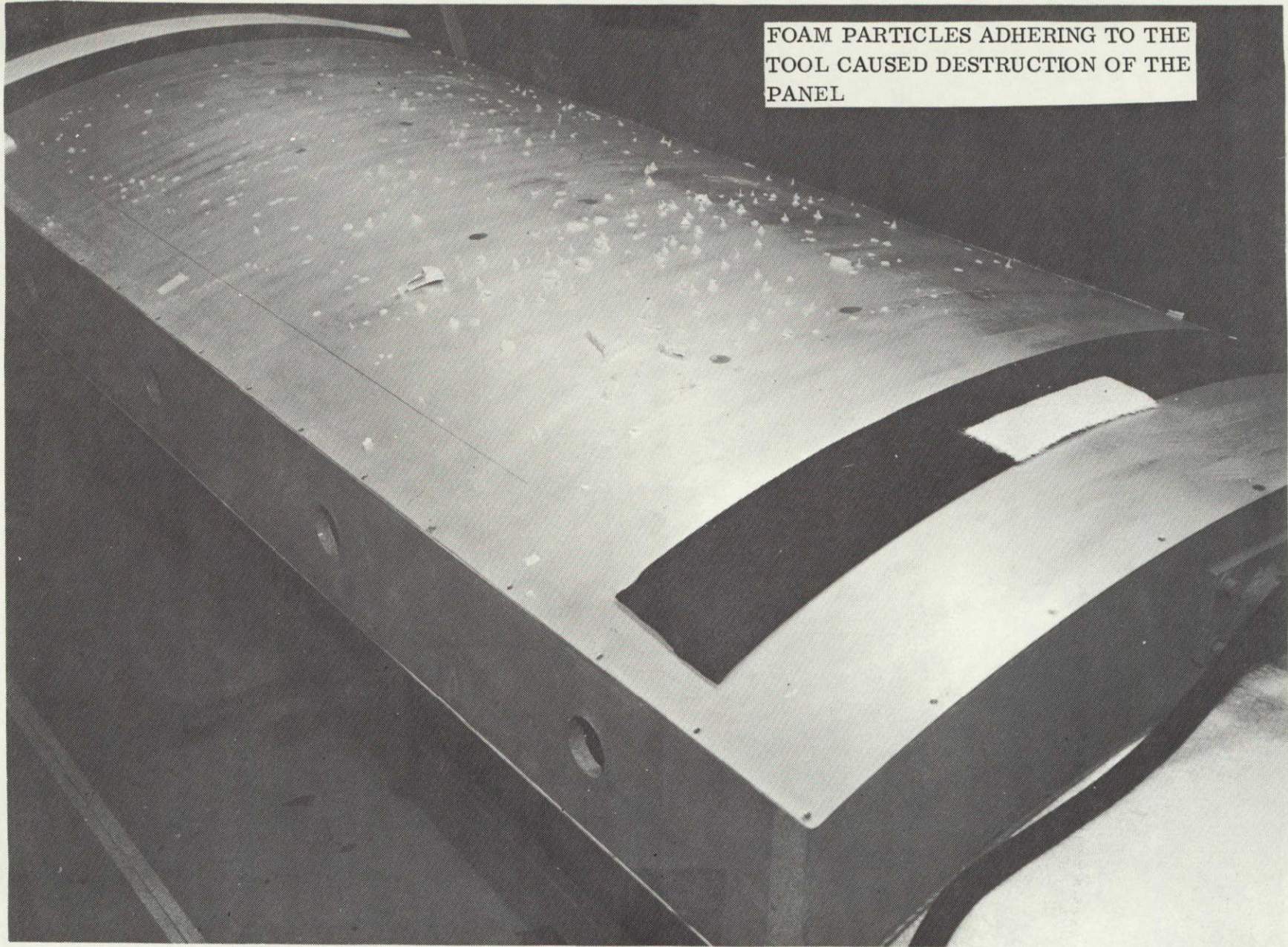


Figure 5-2. Layup Tool After Removing the First System B Panel

It is obvious that the above cure schedule, while necessary to prevent excessive resin strike-through on the T-9 tank panels, would seem to lose the advantage of rapid cure that may be achieved with the film-type adhesive. To overcome this deficiency, several recommendations were considered.

- a. Obtain foam with uniform cell structure which would not have voids of length sufficient to penetrate the 0.4 inch thickness of the foam slab.
- b. Use a thinner resin film.
- c. Adjust the resin gel and flow rates to provide faster gelation and less resin flow at 200-225° F temperature range.
- d. After applying the foam and outer skin to the layup mold, invert the mold before placing it in the oven. The concave face of the mold would then be pointed up.

On the basis of recommendations c., and d., the System B panels were successfully fabricated using the revised resin cure cycle for reduced penetration and inverting the mold before placing it in the oven.

2. Insulation Panel Warpage

When the outer MAM skins were bonded to the foam with the Metlbond 225 resin, the resin expansion during cure prestressed the foam slab to cause the foam to warp to a smaller contour radius than the nominal radius of the panel male mold. Because of this warpage the panels had to be forced to the contour of the female mold when applying the inner MAM skin. On some panels the prestress induced sufficient interlaminar shear to fail the bond between the foam and the inner MAM skin in local areas of the panel having a marginal bond. The inner MAM skin bond on one panel was post cured two hours at 200° F before removing the panel from the female mold. No delamination of the inner skin was experienced with this panel and the residual warpage of the panel was somewhat reduced. This panel failed during IAT tests, but the failure could not be traced to the post cure of the panel.

3. Panel Trimming Problems

Due to the heavy glue line of the Metlbond 225 resin, difficulty was experienced in obtaining a smooth trim line around the perimeter of the panels. The hard resin would break off and carry away pieces of foam leaving undesirable voids in the panel edges. A thinner glue line may prevent this process difficulty.

5.1.4.5 System C Panels. No fabrication problems were encountered. However, considerable fabrication time was spent allowing for the 24-hour cure requirement of the EPON 956 resin. To reduce the cure time requirement, peel tests of the MAM face sheet-to-foam bond were conducted on an Instron test machine. Test results are shown in Table 5-1.

TABLE 5-1. PEEL TEST RESULTS

Specimen Number	Hours Room Temperature Cure Time	Lbs Peel Load	Specimen Number	Hours Room Temperature Cure Time	Lbs Peel Load
1-1	16	0.23	2-1	16	0.18
1-2	16	0.27	2-2	16	0.18
1-3	16	0.29	2-3	16	0.17
		0.25 Average			0.173 Average
1-1	24	0.25	2-1	24	0.19
1-2	24	0.23	2-2	24	0.15
1-3	24	0.23	2-3	24	0.17
		0.24 Average			0.17 Average

Notes:

1. Specimens 1-1, 1-2, and 1-3 were constructed with one coat of Epon 956 resin applied to the MAM sheet only. Total glue line thickness was approximately 0.0035 inch.
2. Specimens 2-1, 2-2, and 2-3 were constructed with two coats of Epon 956 resin applied; one coat to foam and one coat to MAM face sheet. Total glue line thickness was approximately 0.007 inch.
3. Specimens were 3 inches wide by 12 inches long. Peel width was 3 inches.

From the results of the peel tests, it was concluded that no significant improvement in bond strength is noted between 16- and 24-hour room temperature cure of the Epon 956 resin. Therefore, the insulation panel may be safely removed from the bonding fixture after 16 hours of room temperature cure. Significant savings in fabrication and schedule time accrued by reducing the minimum cure time to 16 hours.

The one-coat system exhibited approximately 43 percent higher peel strength than the two-coat system.

On the basis of the above test results the three System C insulation panels were fabricated with the following resin processing variations:

- One panel with a 24-hour minimum room temperature cure of two-coat system
- One panel with a 16-hour minimum room temperature cure of two-coat system
- One panel with a 16-hour minimum room temperature cure of one-coat system

5.1.5 ACCEPTANCE TEST RESULTS.

5.1.5.1 Material Integrity Proof Test Results. As described earlier, the material integrity proof test consisted of six immersion cycles in LN₂ for five minutes per cycle. The results are listed below for each material system. See Table 4-1 for a tabulation of material system components.

System A

During the third LN₂ dip test cycle a small (1/2-inch by 3/4-inch) blister was observed in the Mylar doubler on the concave side of the panel. The blister appeared only in the Mylar doubler and did not affect the basic edge seal of the panel, therefore, it was decided to continue the test to complete the required six LN₂ dip cycles and observe the blister for change in size or character. No further change was noted in either the blister or the appearance of the whole panel.

System B

During the first LN₂ dip test cycle a small blister approximately 3/8 inch in diameter was noted in the MAM skin on the concave side of the panel. The blister appeared to be associated with a void or soft area in the foam, therefore, it was decided to continue the test and observe the blister. During the second LN₂ dip cycle three more small blisters were noted which were about the same size and character as the first blister. During the third dip test cycle three very small blisters were noted in the area of foam joints. During the fourth dip test cycle two blisters approximately 1-1/2 inches long were noted in the edges of the panel and one wrinkle blister approximately 1/8 inch wide by 4 inches long was found in the center of the concave surface of the panel. This blister was aligned parallel to the long axis of the panel and appeared to be a compressive buckle type of wrinkle that may have been caused by panel deflection during immersion in LN₂. During the fifth dip test cycle the wrinkle blister grew approximately two inches longer and one edge blister doubled in length. During the sixth dip test cycle the above noted blisters did not change; however, numerous very small blisters up to 1/8 inch in diameter were observed on the concave surface. These small blisters all appeared to be associated with void holes in the surface of the foam. All the blisters lost pressure within 30 minutes after the conclusion of the test. After the conclusion of the sixth dip test, the blistered areas were cut open. Figure 5-3 shows the long blister in the center of the concave surface of the panel; the blister first appeared on the fourth dip cycle. Figure 5-4 shows typical blisters which have been cut open, showing that the blisters were associated with voids or soft spots in the foam.

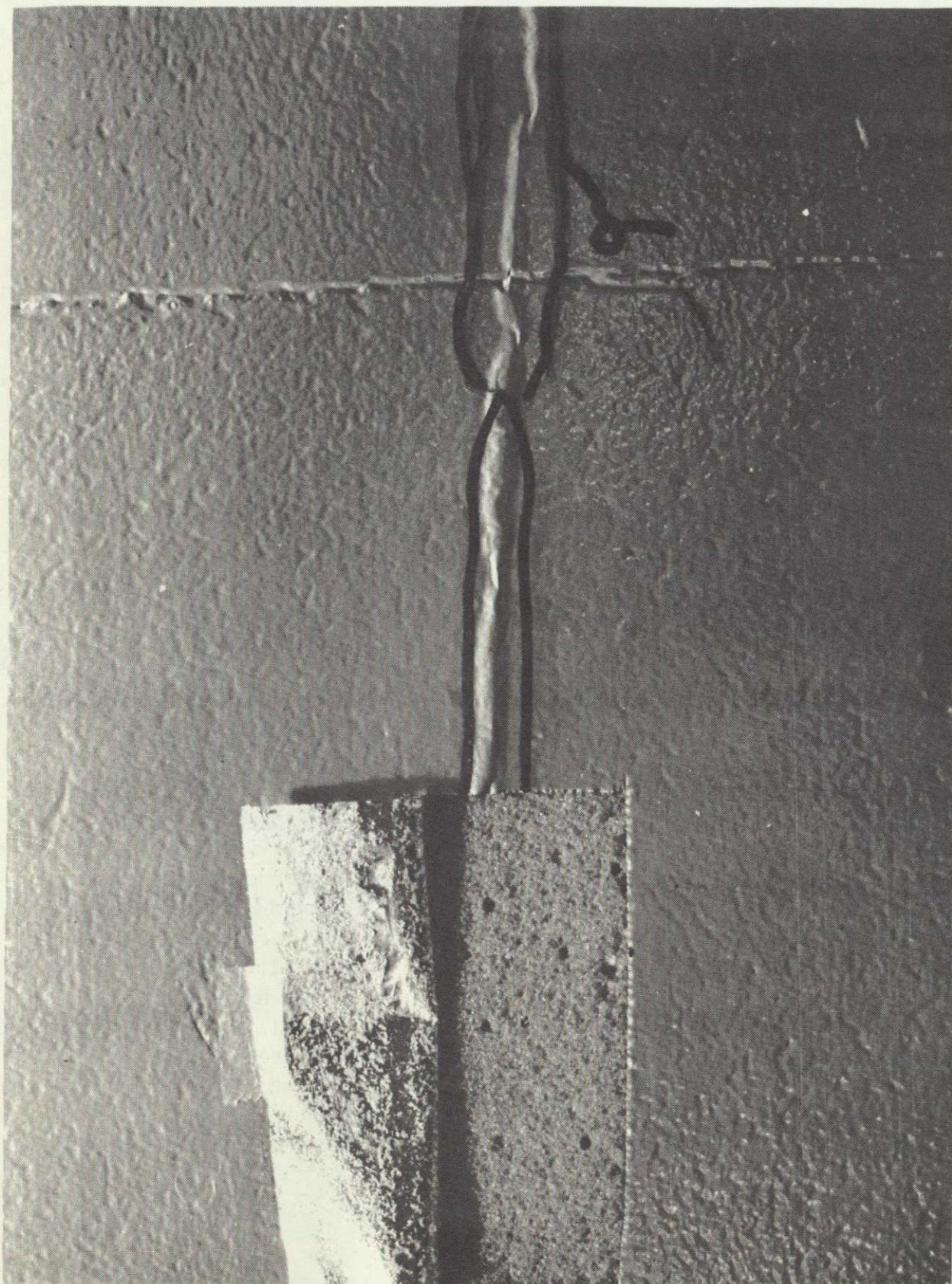


Figure 5-3. Blister in the Center of the Concave Surface of the System B DPT Test Panel

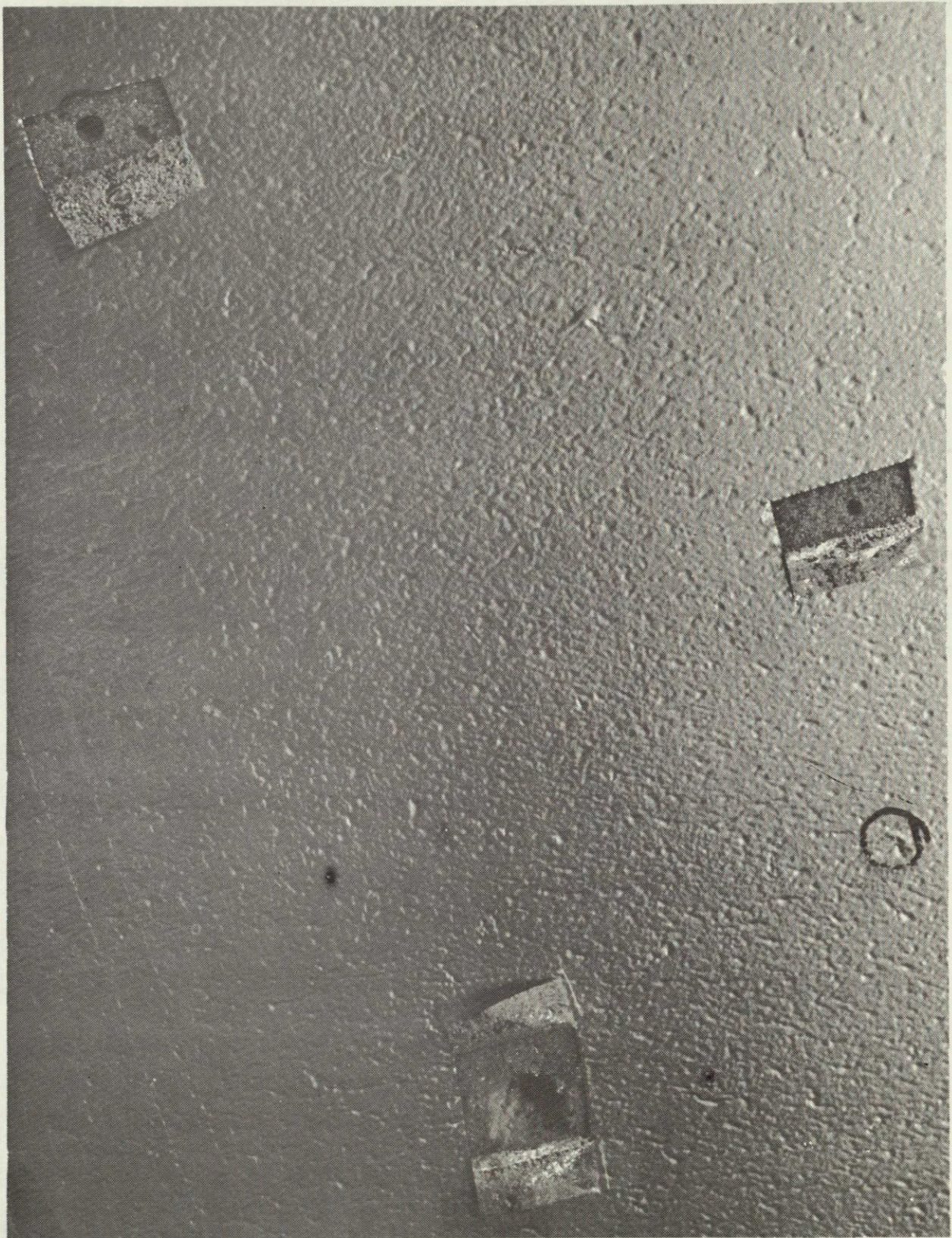


Figure 5-4. Typical Blister Showing Blister Association with Foam Voids

System C

During the first LN₂ dip cycle several blisters were noted along the edges of the panel. The blistered areas were marked and the test continued to complete six LN₂ dip cycles. The blisters progressed very slowly to approximately 3/8 to 1/2 inch longer than the length observed on the first cycle. No blisters of the MAM skins were observed on this panel.

5.1.5.2 Individual Acceptance Test Results. As described earlier, the individual panel acceptance tests consisted of immersion of each panel in LN₂ for five minutes, then observing the panel for blister formation during warmup. The results of each panel acceptance test are listed in Table 5-2 for the System A panels, Table 5-3 for System B panels, Table 5-4 for System C panels, and Table 5-5 for all spare panels.

TABLE 5-2. INDIVIDUAL ACCEPTANCE TEST RESULTS FOR SYSTEM A PANELS

Convair Panel Number	Goodyear Panel Number	Comments
55-07053-1	603A000-002-101 S/N 1	Panel met requirements of GER-13311 IAT test specification.
55-07053-1	603A000-002-101 S/N 2	Panel met requirements of GER-13311 IAT test specification after repair of one blister in Mylar channel and repair of one location where vapor plumes were escaping from edge of Mylar doubler.
55-07053-1	603A000-002-101 S/N 3	Panel met requirements of GER-13311 IAT test specification.
55-07053-1	603A000-002-101 S/N 4	Panel met requirements of GER-13311 IAT test specification after repair of one blister in Mylar channel and repair of one location where vapor plumes were escaping from edge of Mylar doubler.
55-07053-2	603A000-002-103 S/N 1	Panel met the requirements of GER-13311 IAT test specification.
55-07053-2	603A000-002-103 S/N 2	Panel met requirements of GER-13311 IAT test specification after repair of blister in Mylar channel and repair of three locations where vapor plumes were escaping from edge of Mylar doubler.

TABLE 5-3. INDIVIDUAL ACCEPTANCE TEST RESULTS FOR SYSTEM B PANELS

Convair Panel Number	Goodyear Panel Number	Comments
55-07053-7	603A000-002-105	Panel met requirements of GER-13311 IAT test specification.
55-07053-6	603A000-003-103	Panel met requirements of GER-13311 IAT test specification before and after making cutout in panel.
55-07053-12	603A000-004-103	Panel met requirements of GER-13311 IAT test specification before making cutout in panel. After making cutout in panel, some blistering of the Mylar channels was noted during the preliminary one-minute dip of the cutout area. Testing was stopped and the panel edges were reworked by re-ironing and redipping in PE-207 resin. After rework the panel was tested satisfactory and met the requirements of GER-13311 IAT test specification.

TABLE 5-4. INDIVIDUAL ACCEPTANCE TEST RESULTS FOR SYSTEM C PANELS

Convair Panel Number	Goodyear Panel Number	Comments
55-07053-4	603A000-002-107 S/N 1	Panel met requirements of GER-13311 IAT test specification.
55-07053-4	603A000-002-107 S/N 2	Panel met requirements of GER-13311 IAT test specification
55-07053-11	603A000-004-105	Panel met requirements of GER-13311 IAT test specification before and after making cutout in panel.

TABLE 5-5. INDIVIDUAL ACCEPTANCE TEST RESULTS FOR SPARE PANELS

Convair Panel Number	Goodyear Panel Number	Material System	Comments
55-07053-7	603A000-002-105	B	Panel met requirements of GER-13311 IAT test specification.
55-07053-6	603A000-003-103	B	Panel met requirements of GER-13311 IAT test specification before and after making cutout in panel.
55-07053-12	603A000-004-103	B	Panel met requirements of GER-13311 IAT test specification before and after making cutout in panel.
55-07053-4	603A000-002-107	C	Panel met requirements of GER-13311 IAT test specification.
55-07053-11	603A000-004-105	C	Panel met requirements of GER-13311 IAT test specification before and after making cutout in panel.

At the end of the T-9 tank material evaluation tests, but prior to the T-9 tank repair technique evaluation tests, three panels were removed and replaced with new panels of different material. The acceptance test results of these panels, Systems D and E, are listed in Tables 5-6 and 5-7, respectively.

TABLE 5-6. INDIVIDUAL ACCEPTANCE TEST RESULTS FOR SYSTEM D PANELS

Convair Panel Number	Goodyear Panel Number	Comments
55-07053-13	603A000-002-109 S/N 1	Panel met requirements of GER-13311 IAT test specification.
55-07053-13	603A000-002-109 S/N 2	Panel met requirements of GER-13311 IAT test specification.
55-07053-14	603A000-002-107	Panel met requirements of GER-13311 IAT test specification before and after making cutout in panel.

TABLE 5-7. INDIVIDUAL ACCEPTANCE TEST RESULTS FOR SYSTEM E PANELS

Convair Panel Number	Goodyear Panel Number	Comments
55-07053-15	603A000-002-113	Panel met requirements of GER-13311 IAT test specification.

It should be noted that the System B insulation panels warped severely during the LN₂ dip test due to the shrinkage of the relatively heavy glue line of Metlbond 225 adhesive. The warpage was severe enough to cause a reverse curve in the panel along the longitudinal axis and nearly straighten the panel single curvature radius. Undoubtedly this warpage put a strain on all channels and MAM skin bonds which may account for the higher incidence of channel blistering with the System B panels. The use of the thinner Metlbond 225 adhesive in the System D panels caused much less warpage during the LN₂ dip test, but some warpage was still observed.

5.2 INSTALLATION OF T-9 TANK PANELS

5.2.1 SUMMARY OF METHOD OF INSTALLATION. For complete details of installation of the sealed foam panels and erosion cloth on the T-9 tank, see notes 1.1 through 1.11 of Convair drawing 55-07224. Following is a brief summary of the installation procedure:

1. The tank and panels were first cleaned with trichloroethane.
2. The tank and panels were then primed with PE-207 and allowed to cure a minimum of six hours. See Figure 5-5 for a picture of a typical priming operation of an insulation panel.
3. Beads of Narmco 7343 adhesive were applied in a 6-inch grid pattern to the concave surfaces of six insulation panels (Figure 5-6).
4. The panels were then applied to the tank and vacuum bagged at a minimum of 20.5 inches of mercury for 8 hours.
5. A 100 percent coat of Narmco 7343 was applied to the remainder of the tank. See Figure 5-7 for a typical application operation.
6. The remaining six panels were then installed on the tank and vacuum bagged at a minimum of 20.5 inches of mercury for 8 hours.
7. The outer surface of the insulation panels was cleaned with trichloroethane.
8. General Electric SR-585/SC-3900 prime coat adhesive was applied to the uncoated side of the erosion cloth, and allowed to cure a minimum of one hour.



Figure 5-5. Priming An
Insulation Panel

Figure 5-6. Applying Adhesive
Beads To An
Insulation Panel

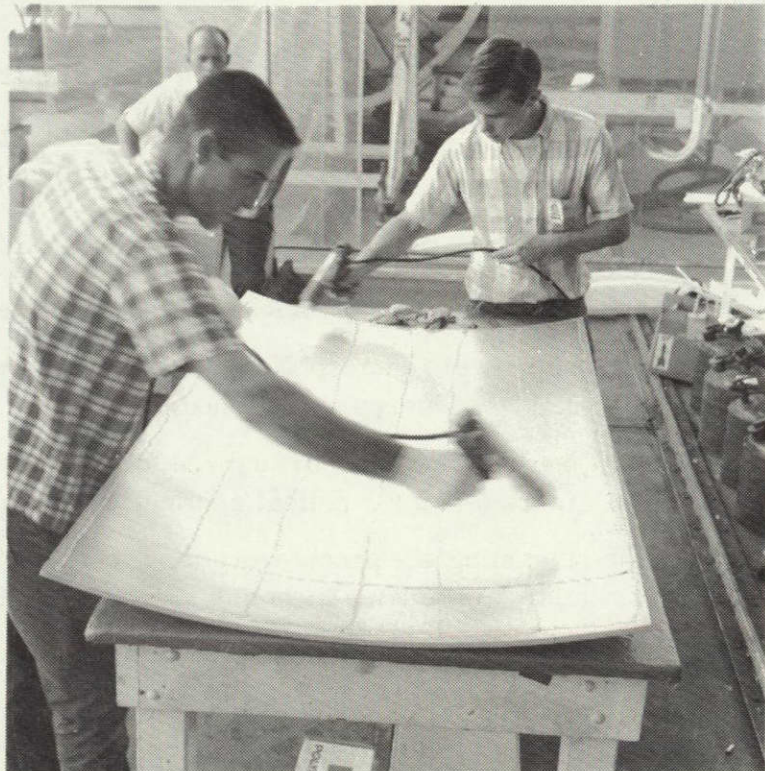




Figure 5-7. Applying Adhesive To The T-9 Tank

5.2.2 INSTALLATION OF THE PANELS ON THE T-9 TANK. In order to provide a clean environment for mixing and applying adhesives, and to comply with Convair's fire and safety requirements for handling and applying flammable materials, application of the insulation panels and erosion cloth was accomplished in a portable clean room. See Figure 5-8 for a picture of the portable clean room with the T-9 tank inside.

For the T-9 tank material evaluation tests, the panels were installed on the tank as shown in Figure 5-9. The circled number in the upper right hand corner of each panel is an arbitrary number assigned for convenience in identifying the panels.

For the T-9 tank repair technique tests, all System C panels were removed and replaced with System D and E panels, as shown in Figure 5-10. The System A and B panels were repaired in areas of damage and/or post-test evaluation sectioning.

The panel system identification refers to the various material systems tabulated in Table 4-1.

The actual installation of the panels and erosion cloth followed the steps outlined in Subsection 5.2.1 with no serious problems. However, several significant events occurred and are detailed here.

1. Upon removal from the shipping crate, one of the 55-07053-1 System "A" panels was found to have an 8-inch square MAM-to-foam unbonded area on the concave side. No reason has ever been discovered for the unbonding occurring during shipment. The area was repaired by slitting the MAM, folding it back, and re-applying PE-207 adhesive. A 10-inch square MAM patch was then bonded to the area. The standard five-minute LN₂ dip test was performed and no leaks were observed. See Figure 5-11 for a view of the patched area. The panel was ultimately installed on the T-9 tank and identified as panel number 11 in Figure 5-9.

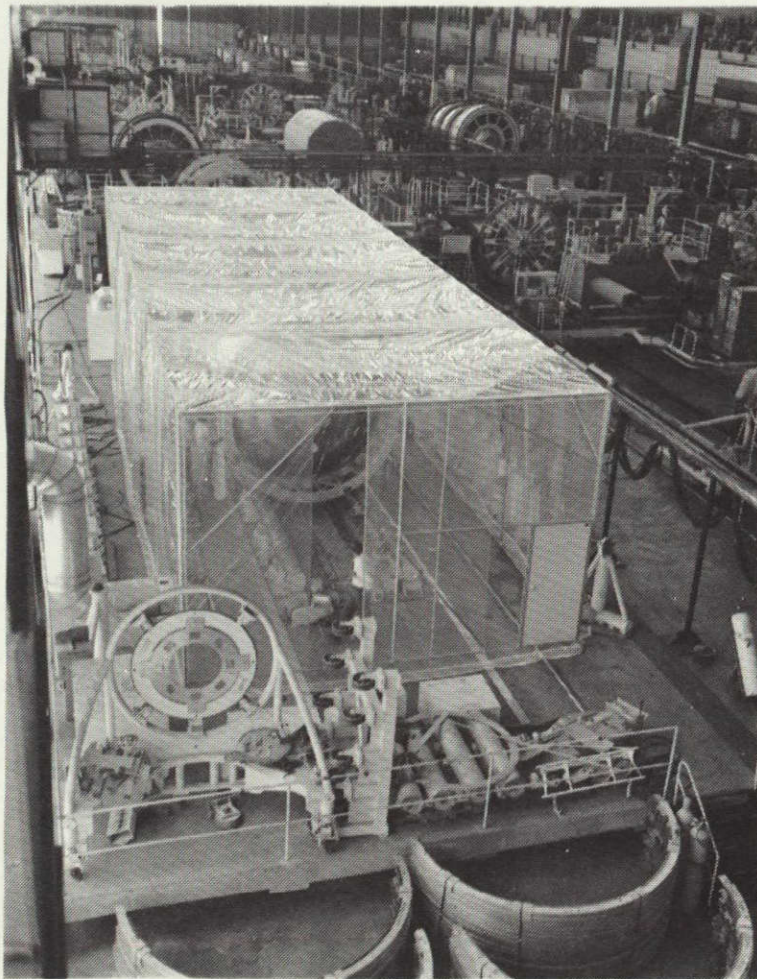


Figure 5-8. Installing Insulation Panels On The T-9 Tank In A Portable Plastic Clean Room

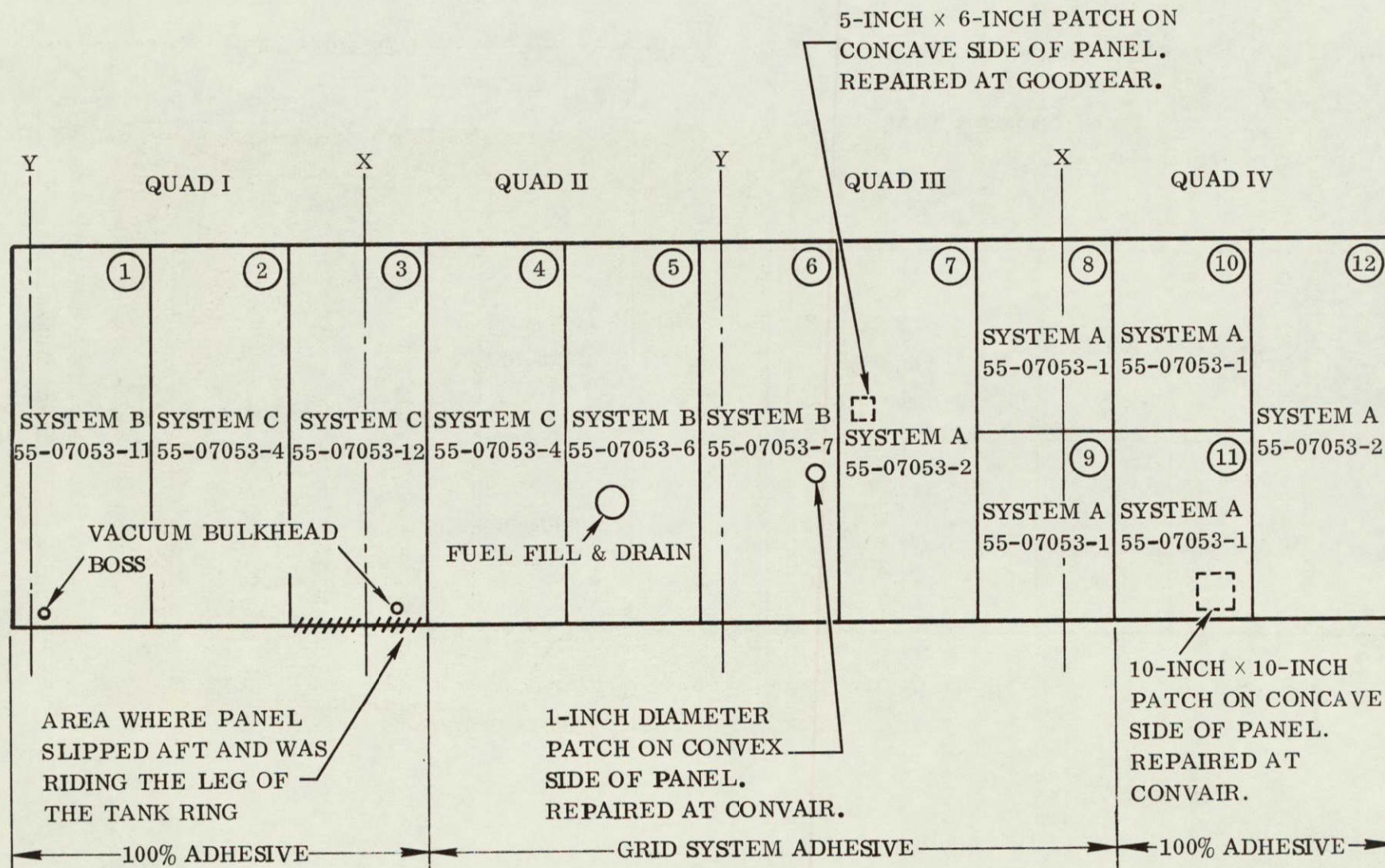


Figure 5-9. Arrangement Of Insulation Panels On The T-9 Tank Material Evaluation Tests

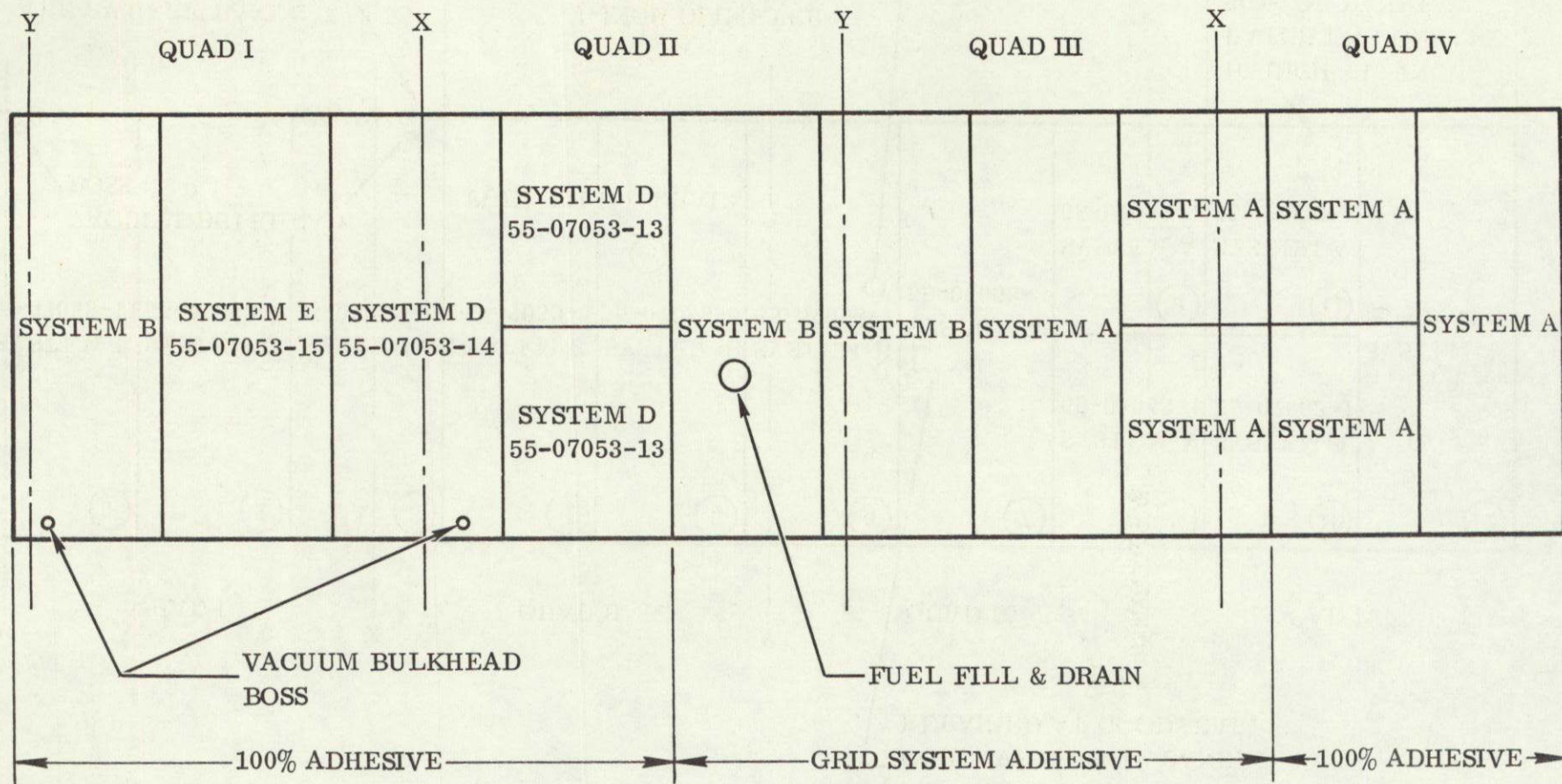


Figure 5-10. Arrangement Of Insulation Panels On The T-9 Tank Repair Technique Tests

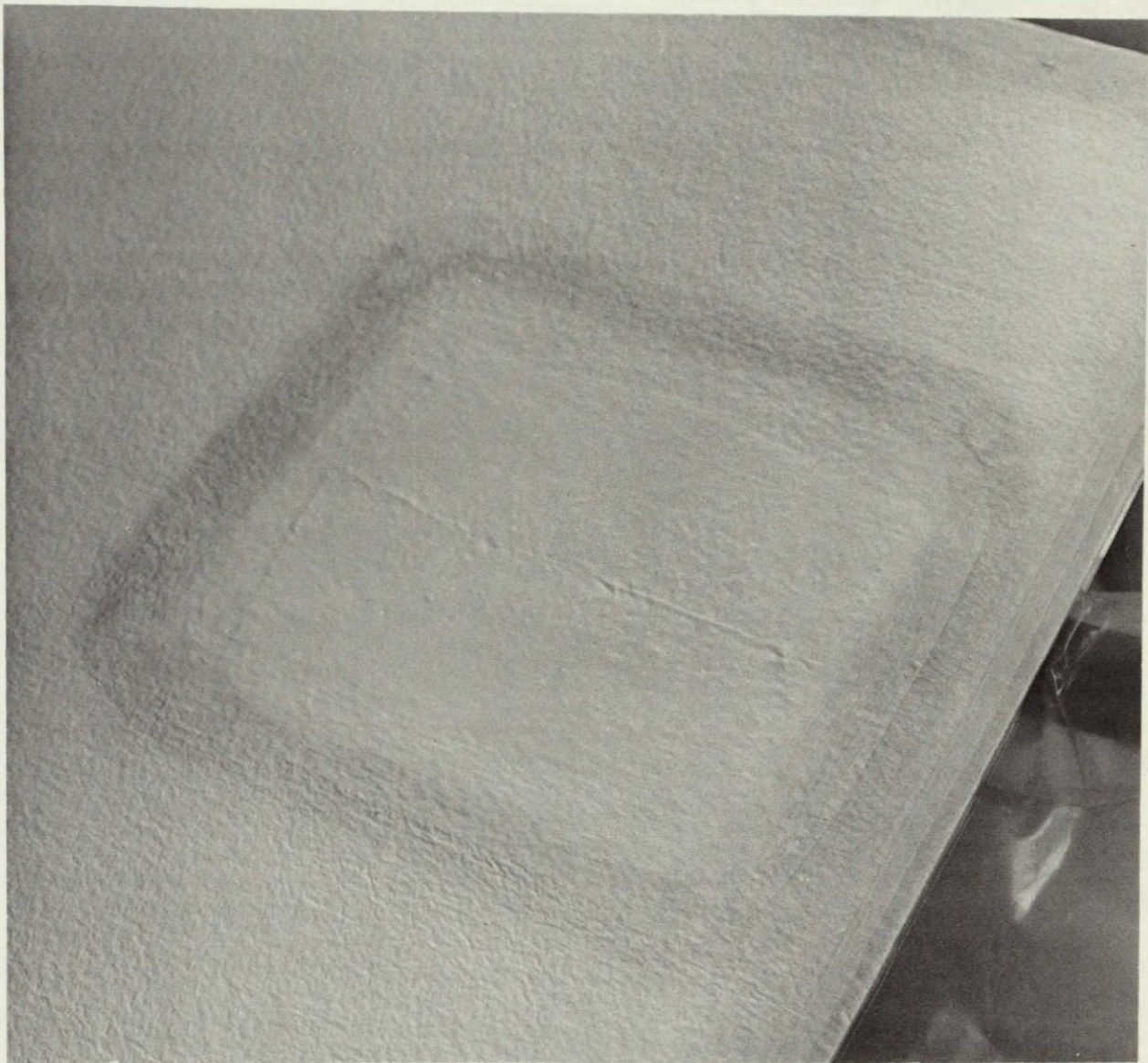


Figure 5-11. Patched Area On Concave Side Of Panel Number 11

2. It was discovered that the T-9 tank is 0.25 inch shorter between the forward and aft rings than required per blueprint. Therefore, instead of the anticipated generous tolerance between the end of the panels and the flange of the tank rings, the panels fit tightly between the rings. Consequently, during the vacuum bagging of the panels, panel number 3 slipped aft and rode up the leg of the aft ring. The area was subsequently filled with resin as much as possible. The location of the area is noted in Figure 5-9. Since the shorter tank was discovered prior to fabrication of the System D and E panels, those panels were fabricated 0.25 inches shorter than the System A, B, and C panels. Consequently, no problems were encountered in installing the System D and E panels.

3. After installation on the tank, it was discovered that the outer MAM of panel number 6 was damaged. The location of the damaged area is noted in Figure 5-9. The damaged area was approximately $\frac{3}{8}$ inch in diameter, and it appeared that the aluminum layer in the MAM laminate had been cracked. The damage appeared to have been made by a finger tip or a tool. See Figure 5-12 for a view of the damaged area. The area was repaired by application of a 1-inch diameter MAM patch located as shown on panel number 6 of Figure 5-9.

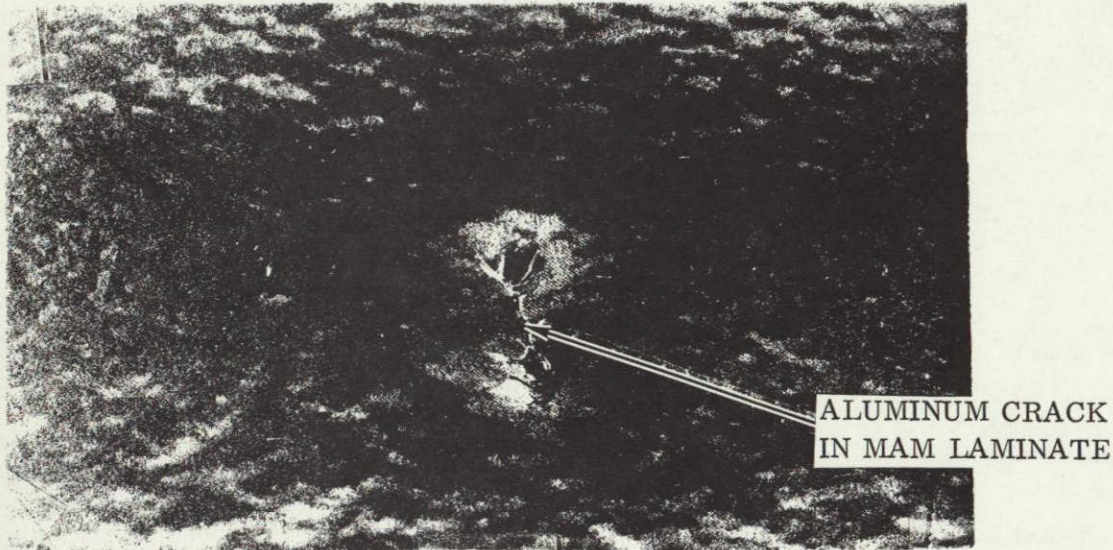


Figure 5-12. Damaged Area Of Panel Number 6

4. After installation of the insulation panels, it was observed that several of the foam filler strips, installed during the panel bonding sequence, did not fit tightly between the panels. The foam strips were removed and replaced with foam strips having a better fit between the panels. The loose fit of the filler strips was caused by movement of the panels as vacuum was being applied to the vacuum bag. Since it would be extremely difficult, if not impossible, to maintain the panels in their exact position while applying vacuum to the vacuum bag, it was recommended that the installation sequence be modified to install the foam filler strips after the panels had been bonded to the tank. In order to hold the panels in place during the vacuum bagging operation, temporary filler strips should be used. The temporary filler strips could be wood or plastic, coated with Teflon or silicone so they would be easily removable.
5. Laboratory tests on a fiberglass erosion cloth impregnated with silicone rubber on both sides showed that the General Electric SR-585 silicone adhesive could be sprayed on the surface of the erosion cloth and remain tacky for several days. Even though the erosion cloth used on the T-9 tank was to be impregnated with silicone rubber on one side only (the outer side as installed),

tests were run on fiberglass cloth impregnated with silicone rubber on both sides because it was the only type of material available for test when it became necessary to decide on an adhesive. However, when the SR-585 was sprayed on the cloth side of the fiberglass cloth impregnated with silicone rubber on one side only, the cloth did not become tacky. It was found that the cloth absorbed the adhesive immediately upon being applied. Therefore, a heavier coat of adhesive was brushed (not sprayed) on the erosion cloth and it did become tacky.

The day after the cloth was installed, several small bubbles were noted under the erosion cloth, indicating the presence of trapped gas. Even though care was taken to roll out the trapped gas, it became evident that extreme care must be used to remove the trapped gas. However, as detailed later in this report, the presence of these small bubbles between the erosion cloth and sealed panels did not cause any problems in the test program.

5.3 FABRICATION OF CONSTRICTIVE WRAP

5.3.1 ORIGINAL METHOD OF FABRICATION. The original method of fabrication devised was a two-step operation as follows:

1. The individual fiberglass strands were layed-up and cured in a slotted tool (Figure 5-13), while the strands were held in tension. The slots were to provide a means of hand rubbing the strands to a constant width, and to make certain the strands were flat and would not tend to curl.
2. After the strands had been oven cured, they were placed on an assembly tool for secondary bonding to the aluminum hinges. This tool held only the bond area under pressure during the oven cure by means of a rubber bladder pressurized to 15 psi. The strands were not under tension during this operation in order to preclude the possibility of tool elongation, during the oven cure, stretching the strands to a new, longer length. As explained earlier, the length of each wrap segment was extremely critical since the amount of constrictive load was dependent on the amount of stretching required to install four wrap segments around the tank circumference.

Test coupons were fabricated along with the wrap segments. The test coupons of the first four segments failed at the end fitting bond lines. After further analysis and laboratory testing, several production changes were made to improve the bond strength.

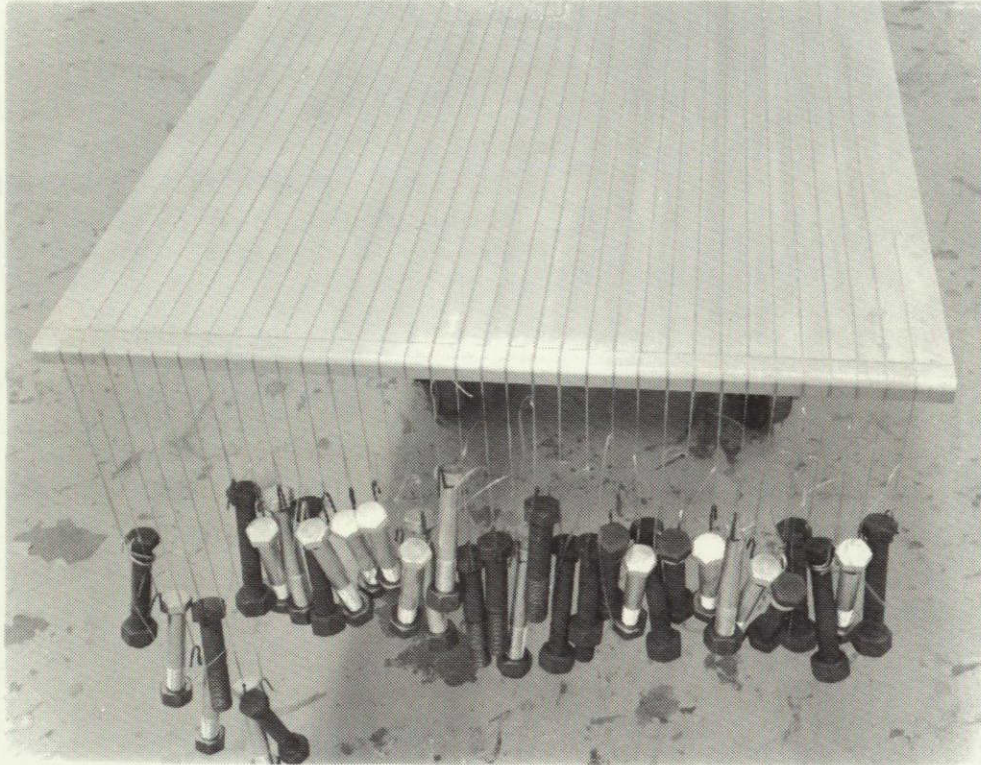


Figure 5-13. Fiberglass Strand Curing Tool

5.3.2 REVISED METHOD OF FABRICATION. The production changes made to improve the end fitting bond strength were:

1. The fiberglass strands and the strand end fitting bond were cured at the same time, as opposed to the original method of curing strands alone with a second operation for bonding the strands to the end fitting. This permitted a primary strand bond, as opposed to the original secondary bond. A picture of the tool used for this one operation cure cycle is shown in Figure 5-14.
2. The end fitting adhesive bond contact pressure was reduced from 15 to 10 psi. It was suspected that the higher pressure was pushing much of the adhesive out of the bond area.
3. Use of a parting agent on the tool was eliminated. A parting agent was originally used in some areas to preclude the strands from bonding to the tool. However, some of the parting agent could have accidentally gotten on the strands in the bond area, which would have weakened the bond.
4. The entire layup was performed in a clean room.

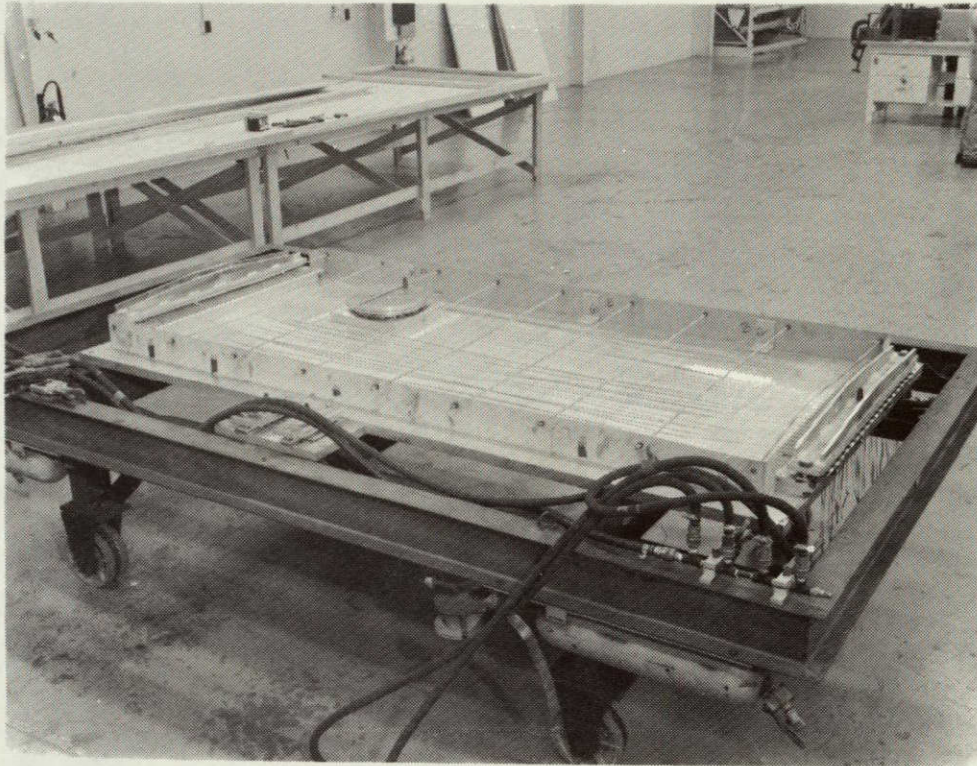


Figure 5-14. One Operation Cure Cycle Tool

Test coupons of parts fabricated to the above procedure were acceptable and the entire ship set, eight parts, were completed. However, three of the eight parts, when examined closely, had questionable areas in the strand at the strand-to-hinge joint. The strands appeared to be damaged, probably by handling. Two of the three parts did fail on installation, and three strands in the third part failed.

Further investigation showed that the strands of all eight parts were extremely brittle, and a large percentage of the glass in the strand could be fractured if the strands were flexed during handling. The strands were especially susceptible to damage at the point where the strands enter the hinge bond. The cause of the brittleness was that the excess resin in the pre-impregnated strands did not bleed-off during the cure cycle, but just laid on the surface of the strand. Upon curing, the strand was resin-rich and brittle.

Again changes were made to the production process to improve the quality of the parts.

5.3.3 FINAL METHOD OF FABRICATION. This final process entailed the use of a completely new tool. This tool allowed the strands and hinge bond to be cured at the same time as before, but both areas, plus the strands, could be cured under vacuum. The new tool is shown in Figure 5-15. The use of a vacuum bag for the entire part, in

lieu of the rubber bladder in the bond area only, allowed for the use of bleeder cloths to absorb excess resin from the strands. The strands fabricated by this method were extremely flexible, and therefore less susceptible to handling damage.

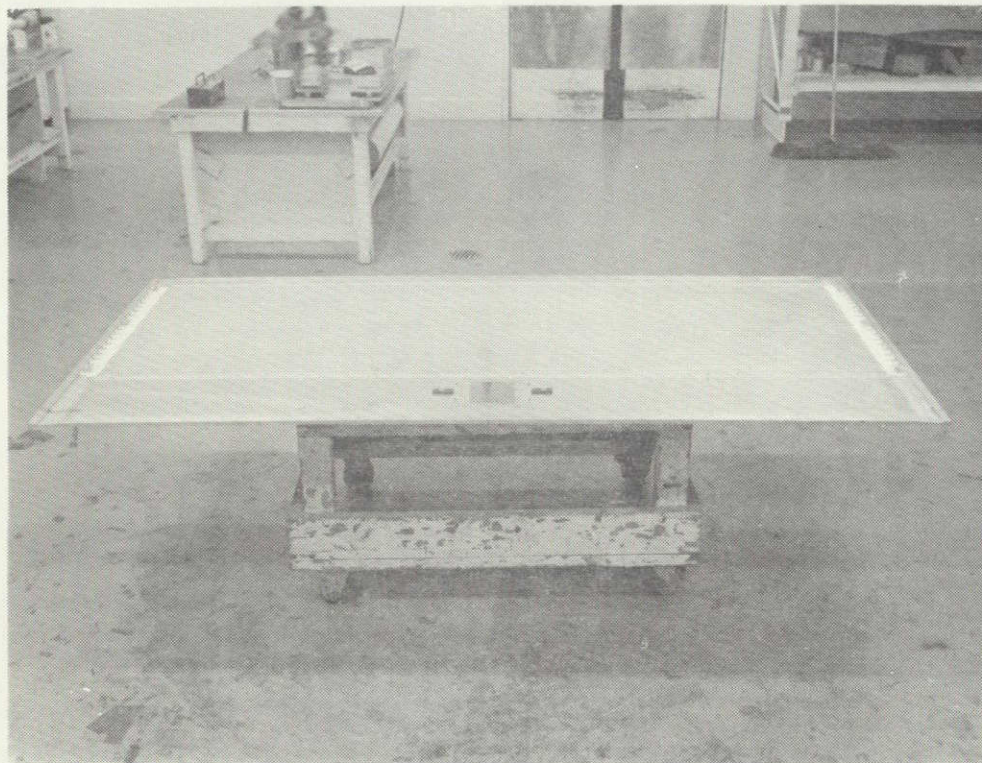


Figure 5-15. Final Configuration Of Strand And Hinge Bond Cure Cycle Tool

The major problem posed by the use of this method was to make certain that each strand in the wrap segment was the same length as all other strands after the cure cycle. If only one strand was shorter than the rest, it would carry all the load during installation until it elongated enough for the others to start sharing load. In order to determine the amount and relationship of elongation of the tool and strands during the oven cure, scribe marks were placed on the tool and several strands, under load, were cured on the tool. The procedure was repeated several times and it was determined that the change in length of the strands on that tool with a known preload and oven cure cycle was constant and predictable. Therefore, the required layup strand length was determined and the tool was machined at each end to support the hinge fitting, as seen in Figure 5-15. The strands were installed under a constant preload using a spring scale (Figure 5-16). After preloading, the strands were held in place with Mylar tape.

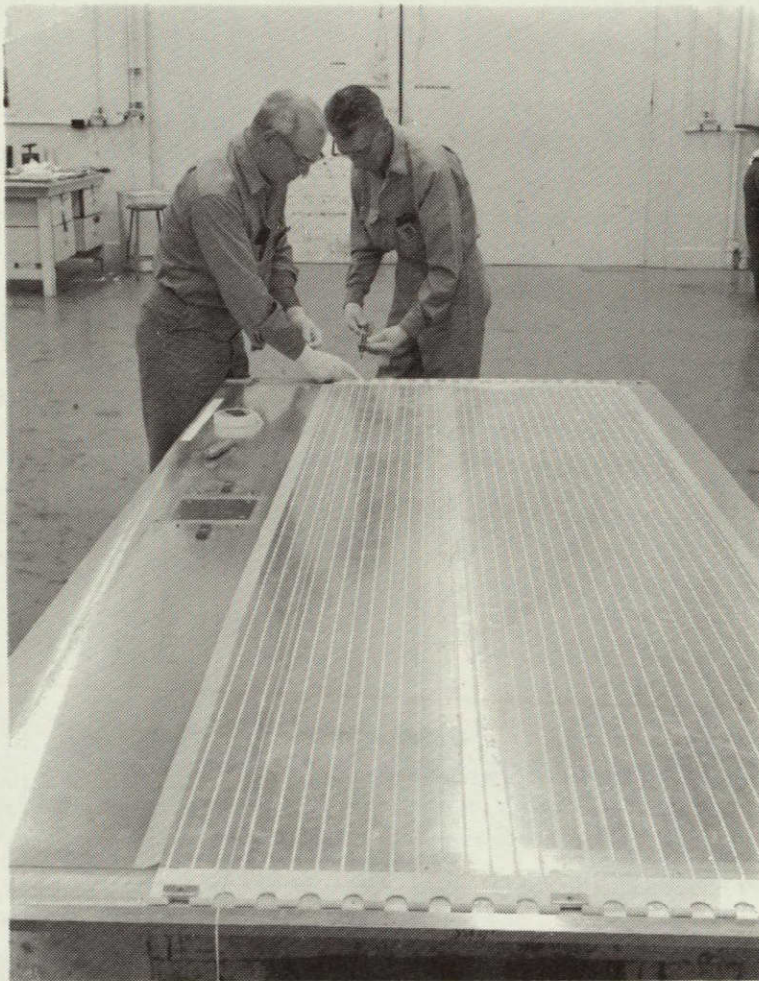
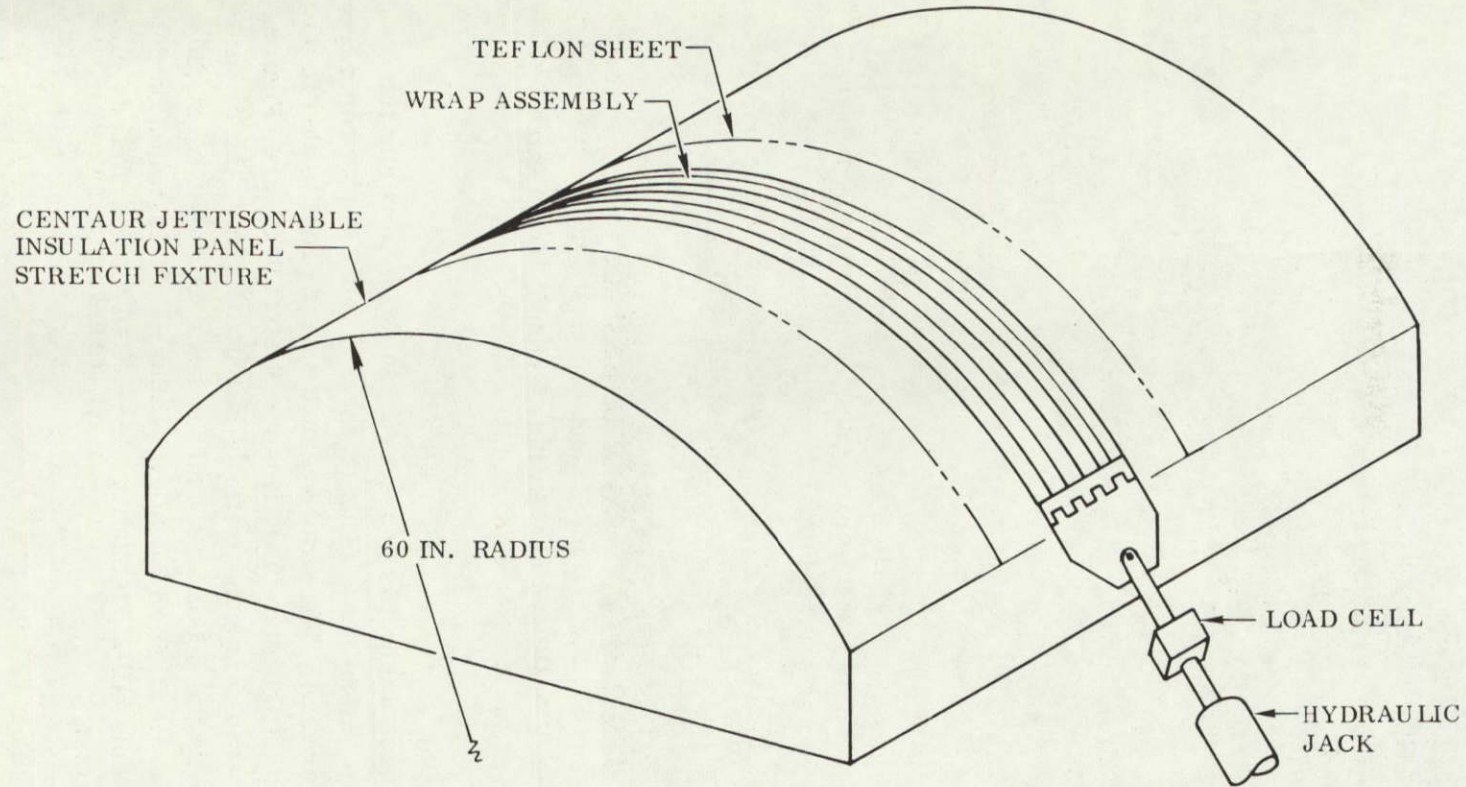


Figure 5-16. Pre-Loading The Fiberglass Strands Prior To Oven Cure

Four wrap segments were fabricated using this procedure. In order to verify the structural integrity of these parts before installation on the T-9 tank, each wrap segment was proof loaded after fabrication. The wrap segments were proof loaded to 90 pounds per strand on the Centaur jettisonable insulation panel stretch fixture (Figure 5-17). One strand of one of the wrap segments partially failed; however, the remainder of the strand continued to carry the proof load, and the segment was used on the T-9 test. The four wrap segments fabricated by this procedure were installed on the T-9 test tank and none of the strands failed, including the partially failed strand, either during installation or during the test.



LOADING CONDITION	LOAD/STRAND LB	PERCENT TANK INSTL. LOAD
ULTIMATE - VENDOR TEST MIN.	185	273 NOM 212 MAX
DWG. REQUIREMENT (TAG END)	150	227 NOM 176 MAX
PROOF TEST	90	136 NOM 106 MAX
MAX. INSTL. LOAD - OVERSIZE TANK - HIGH FRICTION (CLEAN SURF)	85	
NOMINAL INSTL. LOAD - NOM. TANK MEDIUM FRICTION (TALC SURFACE)	66	

Figure 5-17. Wrap Assembly Proof Testing

5.4 INSTALLATION OF CONSTRICTIVE WRAP

As stated previously, one complete circumferential "band" of the fiberglass constrictive wrap consisted of four wrap segments. The four-wrap segments were fabricated slightly shorter than would be necessary to fit around the circumference of the tank without "stretching" the wrap. Therefore, in order to install the constrictive wrap, the following procedure was followed (see note 1.17 of drawing 55-07227 for a detailed procedure):

1. Four wrap segments were first loosely installed around the tank. There was approximately a one-inch gap between the ends of the wrap hinge fittings.
2. The four 55-07227-BN constrictive wrap assembly tools were then installed on the hinge ends, as shown in Figure 5-18. The tools were mounted into the nodes of the hinges, and provided a threaded "C" clamp for clamping and stretching the wrap segments. Figure 5-19 shows the "C" clamps being tightened. All four tools were tightened simultaneously, thereby putting equal strain in all four wrap segments. Note that the assembly tool in Figure 5-18 has two "C" clamps, while that in Figure 5-19 has three "C" clamps. It was found that the two-clamp arrangement allowed too much beam deflection between clamps, making it impossible to properly line up the hinge nodes. The tool was subsequently modified by adding one clamp.
3. Clamping was continued until the hinge pin could be inserted into the nodes of the hinge. Figure 5-20 shows the wrap segments completely clamped, with the hinge pin partially inserted.
4. After the hinge pin had been inserted, the assembly tool was removed. The wrap segments then remained in the stretched condition, and maintained a constrictive force on the insulation. Figure 5-21 shows a view of the wrap in place on the T-9 test tank. Note that in Figure 5-21 the sixth strand from the top on the right hand wrap segment has been broken. The cause for strand failures has been previously discussed.

5.5 PANEL REPAIR PROCEDURE

A repair procedure manual (Reference 5-3) was prepared by Goodyear Aerospace Corporation describing repairs to panels which might be damaged either during manufacture or while on the tank. The repair procedures for panels damaged during manufacture were established and proven during the previous Goodyear program for NASA/LeRC and during manufacture of the T-9 test tank panels for this program. However, a test program, described in the following subsections, was performed by Goodyear to establish methods of repairing sealed foam panels which might be damaged while on the tank. It should be noted that the repair manual had not been approved by Convair at the time this fixed insulation program was terminated by NASA.

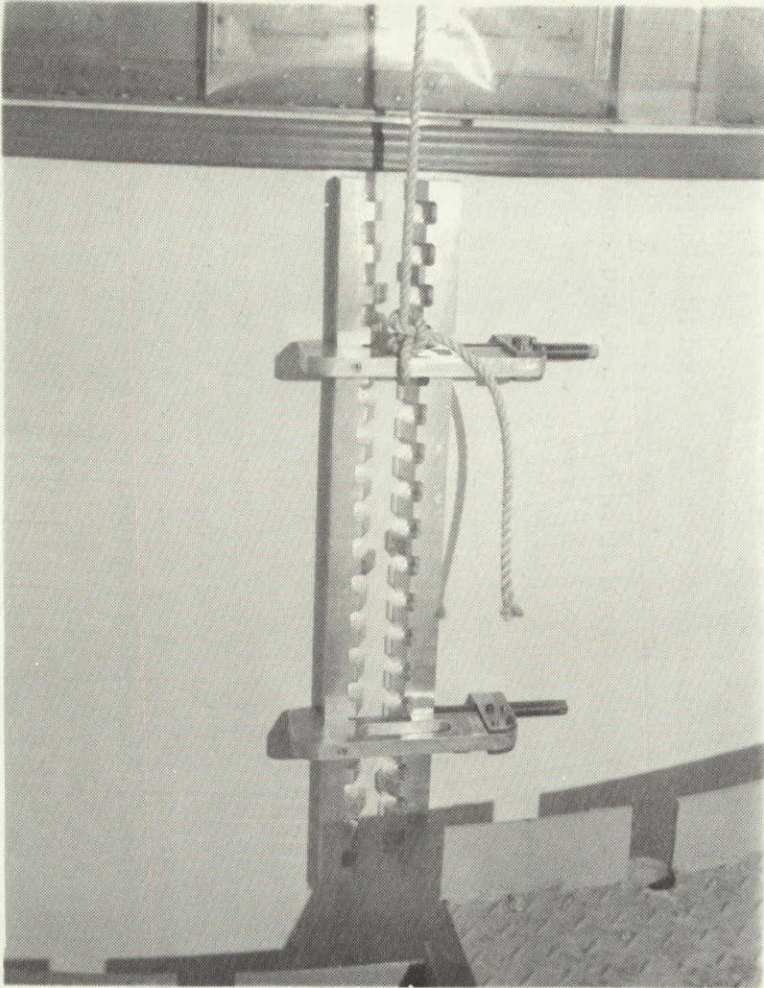


Figure 5-18. Constrictive Wrap Assembly Tool In Place Prior To Clamping The Constrictive Wrap



Figure 5-19. Clamping The Constrictive Wrap

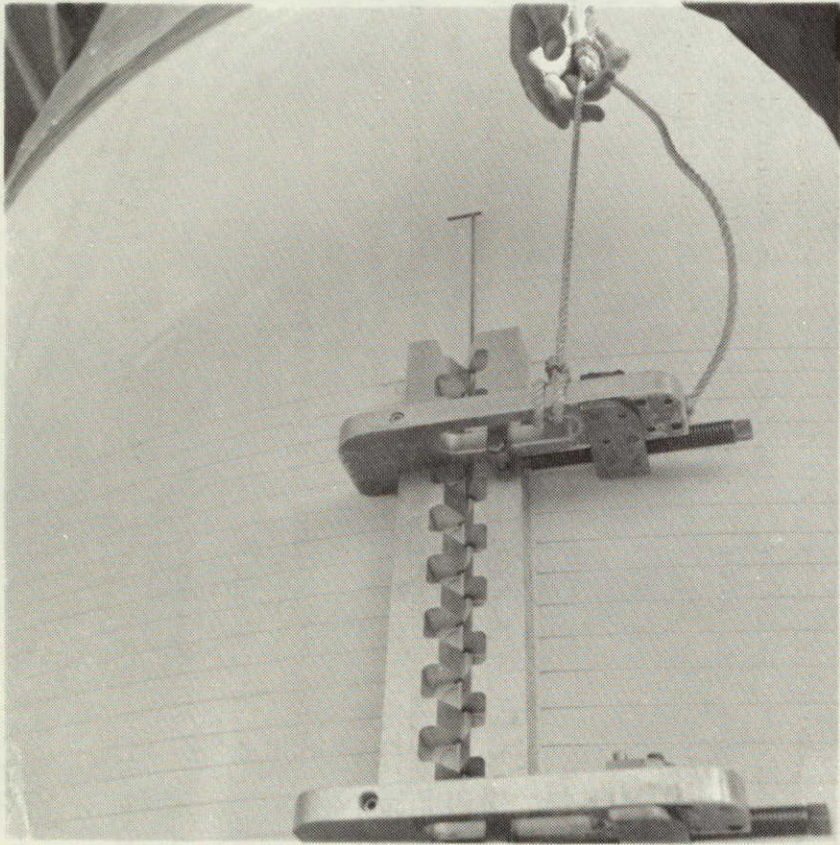


Figure 5-20. Wrap Segments Completely Clamped,
Hinge Pin Partially Inserted

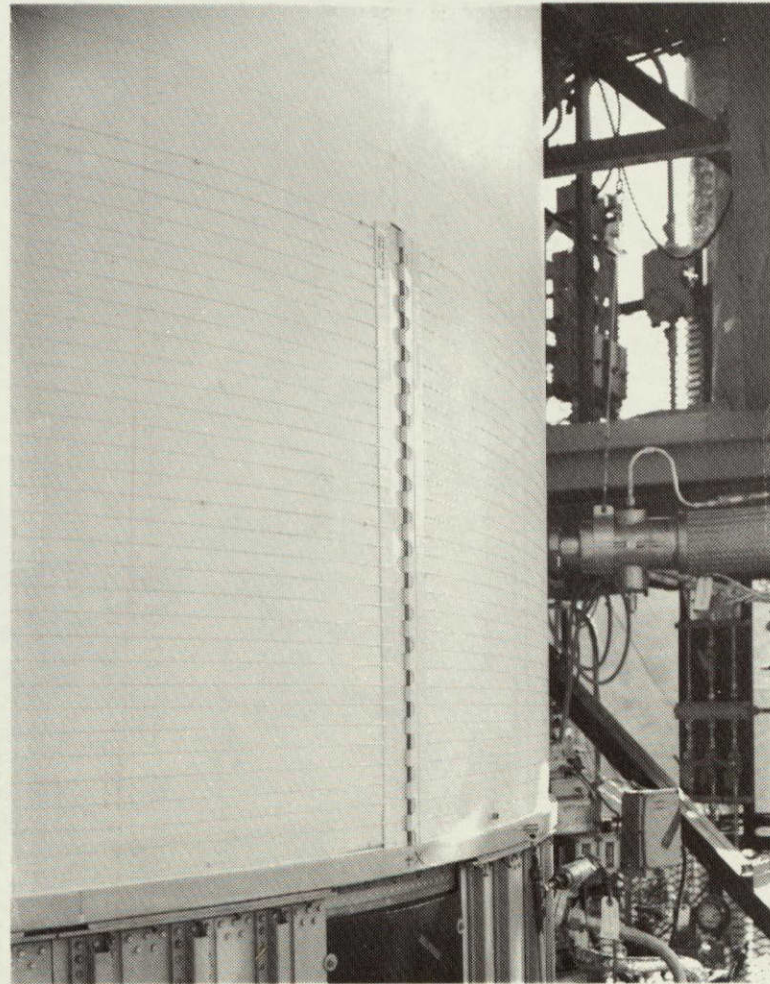


Figure 5-21. Constrictive Wrap In Place On The
T-9 Test Tank

5.5.1 TEST PANEL MATERIAL SYSTEMS. Three material systems were evaluated as follows:

	<u>System A</u>	<u>System B</u>	<u>System C</u>
• Outer Sealing Laminate	MAM	MAM	MAM
• Outer Sealing Laminate Adhesive	PE-207	Metlbond 225 0.06-lb per sq. ft	EPON 956
• Foam	GAC 222	CPR 32-2C	CPR 32-2C
• Foam Thickness	0.4 inch	0.4 inch	0.4 inch
• Inner Sealing Laminate Adhesive	PE-207	PE-207	PE-207
• Inner Sealing Laminate	MAM	MAM	MAM

5.5.2 TYPES OF DAMAGES

5.5.2.1 Panels Damaged While Installed on the Tank. For tests of panels damaged while on the tank, the test panels were bonded to stainless steel sheets after fabrication and acceptance test. The bonding was accomplished with Narmco 7343 adhesive applied in a pattern as shown in Table 5-8. Table 5-8 also shows panel code number and size, and type of damage to each panel.

Simulated joints between insulation panels were created for repair evaluation by bonding two 3c panels, a foam filler strip and a MAM doubler to a stainless steel sheet to form a test specimen 0.4 inches by 12 inches by 16.25 inches. A simulated corner joint was created in a similar manner with three 3f panels, two foam filler strips, and two MAM doublers. In the plan view of the test panel assembly, the filler strips and doublers were aligned to form a "T".

To ensure that LN₂ would not leak under the foam panels during LN₂ dip tests, the perimeter edges of the panels were sealed to the stainless steel sheets by an extra bead of NARMCO 7343 resin applied after the initial bonding of the panels to the sheets.

5.5.2.2 Panels Damaged During Manufacture. The following types of damage defects occurring to the panels during manufacture are covered in the repair manual:

1. Delamination between MAM skins and foam core
2. Blisters under doubler strips
3. Puncture entirely through panel
4. Delamination or peeling of outer Mylar layer from MAM skin.

TABLE 5-8. SUMMARY OF PANEL CONFIGURATIONS TESTED IN
PANEL REPAIR PROGRAM

Test Panel Code Number	Insulation Panel Type	Glue Line Type	Quantity	Type of Damage
3a	0.4" x 12" x 16" System "A" Material Construction	100%	3	Puncture of Outer MAM Skin and Foam Core
3b	0.4" x 12" x 16" System "A" Material Construction	Grid Pattern	3	Puncture of Outer MAM Skin, Foam Core and Inner MAM Skin
3c	0.4" x 8" x 12" System "A" Material Construction (2 Pieces)	Grid Pattern	3	Puncture of Channels and Doublers at Panel to Panel Joint
3d	0.4" x 12" x 16" System "B" Material Construction	Grid Pattern	3	Puncture of Mylar Zee Section on LH ₂ Fill and Drain Cutout
3e	0.4" x 12" x 16" System "C" Material Construction	100%	3	Puncture of Channel on Small Panel at Vaccum Bulkhead Boss Cutout
3f	0.4" x 6" x 12" System "C" Material Construction (3 Pieces)	Grid Pattern	1	Puncture of Channels and Doublers at Panel Corner

5.5.3 DAMAGE TEST PROCEDURES.

5.5.3.1 Panels Installed on Tank. The test procedure consisted of fabricating sealed foam panels approximately 12 inches by 16 inches by 0.4 inches and leak testing in LN₂ per the acceptance test procedures for full size panels. The panels were then inflicted with controlled damages, repaired, then retested per the material integrity proof test procedure established for the full size panels. The material integrity proof test procedure required six immersion cycles in LN₂.

5.5.3.2 Panels Damaged During Manufacture. As noted previously, testing of panels was not performed to establish methods of repairing panels damaged during manufacture, since the repair methods were previously established, and proven, during the Goodyear program for NASA/LeRC and during manufacture of the T-9 test tank panels for this program.

5.5.4 TEST RESULTS.

5.5.4.1 Panels Installed On Tank. All test panels successfully passed the six-cycle LN₂ immersion test, thereby qualifying the repairs for the damages listed in Subsection 5.5.2. However, during the tests some difficulty was experienced with strains on the test panel induced by excessive bending of the panel during the LN₂ immersion cycles. The bending was caused by differential contraction of the plastic panel and the metal backup plate. In some cases the strains caused delamination of the panel-to-metal plate bond line which allowed migration of LN₂ behind the insulation panel. Generally, this did not cause a serious problem because the trapped gasses vented through the delaminated portion of the bond line. However, the effect of these strains on the leak-tight integrity of the panel could not be determined on three test panels which blistered during the test program. Two of the three panels (3e1 and 3e2) blistered in a manner that was difficult to contribute to the repair, therefore, the differential contraction strains were considered the source of leaks. To validate the assumptions, these test panels were duplicated without being bonded to a steel backup plate. During LN₂ testing, the panels remained flat and tested satisfactorily to qualify the repairs.

Repairs to a damaged Mylar Zee section at the fuel line cutout (Panel code No. 3d) were made on Zee sections oriented as incorporated on the T-9 tank panels. Also, on one test panel the Zee section was inverted to the T-9 tank panel orientation. This orientation would have been incorporated on the full scale Centaur tank insulation panels. Due to improved accessibility, the latter orientation proved easier to repair.

One test panel (3a4s) was covered with the fiberglass erosion cloth bonded with SR-585 silicone resin. The damage to this panel was repaired in the vertical position to simulate the position of an insulation panel installed on a tank. The repaired panel was successfully tested and the repair qualified although the erosion cloth was delaminated from the surface of the panel after the sixth LN₂ dip cycle. In the area which had PE-207 painted over the repair, the erosion cloth still adhered to the panel.

Additional LN₂ immersion tests were conducted to evaluate the effects of silicone adhesive on repairs involving the bonding of MAM patches to the MAM outer skin of insulation panels. It is well known that silicone are used as parting agents, therefore, the primary concern in this investigation was the potential loss of bond line integrity due to silicone migration into the surface of the MAM skins of the insulation panels. Peel test specimens were cut from two-ply MAM sheets bonded together with PE-207 and Epon 956 adhesives. Before bonding the MAM plies together, one ply was coated with silicone SR-585 adhesive and air dried a minimum of one hour. The dried silicone was then washed from the MAM with toluene followed by MEK. The washing operation was performed in a local area of the MAM sheet leaving a perimeter of silicone adhesive in the same manner as a local repair on an insulation panel. The washed surface and the mating sheet of MAM were primed with a brush coat of PE-207 or Epon 956 adhesive and laminated together with vacuum bag pressure. One-inch wide test specimens were cut from the washed and unwashed area of the laminated MAM sheets.

Control specimens were cut from two-ply MAM sheets bonded together with PE-207 and Epon 956 adhesive without prior use of silicone adhesive. The following average peel loads were determined:

<u>Bond Line Adhesive</u>	<u>Specimen</u>		
	<u>Control</u>	<u>Washed Area</u>	<u>Unwashed Area</u>
PE-207	1.03 lb	0.90 lb	1.05 lb
Epon 956	0.040 lb	0.015 lb	—

The test results of the PE-207 specimens indicate that the silicone adhesive, if thoroughly washed off, reduces bond line strength approximately 10 percent. The slightly higher peel strength in the unwashed area is probably due to the elasticity of the silicone adhesive. Nevertheless, in making repairs, a leak-tight seal could likely not be made unless the silicone adhesive had been removed. When compared with the PE-207 resin bond, the Epon 956 resin exhibited relatively low peel strength which was degraded to a greater degree in the washed areas. Thus, Epon 956 was not considered for applying MAM and Mylar patches in the repair program.

5.5.4.2 Panels Damaged During Manufacture. Repair methods were established during the previous Goodyear program.

6

WEIGHT SUMMARY

A detail weight summary of the Systems A, B, and C material panels with a fiberglass strand constrictive wrap system is shown in Table 6-1. The system letter designation is the same as defined in Subsection 4.1.3. Systems D and E are not tabulated since they are merely other combinations of the materials of Systems A, B, and C. Systems D and E would be approximately 12 pounds and 2 pounds less than System B.

Table 6-2 summarizes the three material system panels with the aluminum corrugation constrictive wrap system.

TABLE 6-1. FIXED INSULATION WEIGHT SUMMARY
(Fiberglass Strand Constrictive Wrap Configuration)

	System A	System B	System C
Panel	(55.5)(1)	(86.9)(1)	(67.0)(1)
Foam	32.6 (2)	34.2 (3)	34.2 (3)
MAM	13.8	13.8	13.8
Mylar Channels	0.9	0.9	0.9
Mylar Doublers	0.9	0.9	0.9
Resin	7.3 (4)	37.1 (6)	17.2 (5)
Panel Gap Joint	(1.6)	(1.6)	(1.6)
Foam Filler Strips	0.8	0.8	0.8
Cover Strips	0.8	0.8	0.8
Panel Bonding System	(15.7)	(15.7)	(15.7)
Vitel PE 207 Resin Primer	(5.7)	(5.7)	(5.7)
Polyurethane Resin	10.0 (7)	10.0 (7)	10.0 (7)
Glass Cloth Overlay	(39.5)	(39.5)	(39.5)
Impregnated Fiberglass	28.1 (8)	28.1 (8)	28.1 (8)
Silicone Adhesive	11.4 (1)	11.4 (1)	11.4 (1)
Constrictive Wrap System	(32.9)(9)	(32.9)(9)	(32.9)(9)
Fiberglass Strands	3.2	3.2	3.2
Hinges	20.4	20.4	20.4
Rods	3.0	3.0	3.0
Fiberglass	0.3	0.3	0.3
LH ₂ Outlets	2.9	2.9	2.9
Adhesive	3.1	3.1	3.1
Ring Insulation	(17.0)	(17.0)	(17.0)
Foam Station 219	9.0	9.0	9.0
Foam Station 413	8.0	8.0	8.0
Contingency	(16.0)	(19.0)	(17.0)
Wiring Tunnel	(50.0)	(50.0)	(50.0)
Total System Weight	(228.2)	(262.6)	(240.7)
Notes:	(5) Epon 956 Adhesive (Shell Oil Co.-Shell Chemical Division)		
(1) Ratioed by length from T-9 Tank Actual Weights	(6) Metlbond 225 adhesive (Whittaker Corp-Narmco Material Division)		
(2) 2 lb/cu. ft density foam	(7) Adhesive applied over 100% of the Bond Area		
(3) 2.1 lb/cu. ft density foam	(8) 8-oz./sq. yd. glass cloth		
(4) Vitel PE207 adhesive (Goodyear Tire and Rubber Co.)	(9) Actual weight		

TABLE 6-2. FIXED INSULATION WEIGHT SUMMARY
 (Aluminum Corrugation Constrictive Wrap Configuration)

	System A	System B	System C
Panel	(55.5)*	(86.9)*	(67.0)*
Panel Gap Joint	(1.6)*	(1.6)*	(1.6)*
Panel Bonding System	(15.7)*	(15.7)*	(15.7)*
Glass Cloth Overlay	N/A	N/A	N/A
Constrictive Wrap System	(191.0)	(191.0)	(191.0)
.020 in. Painted Al Aly Skin	175.0	175.0	175.0
.045 in. Dia. Titanium Wire	2.0	2.0	2.0
Wire Fittings	3.0	3.0	3.0
Collars	1.0	1.0	1.0
Station 412 Support Ring	10.0	10.0	10.0
Ring Insulation	(17.0)*	(17.0)*	(17.0)*
Contingency	(28.1)	(31.2)	(29.2)
Wiring Tunnel	(50.0)*	(50.0)*	(50.0)*
Total System Weight	(358.9)	(393.4)	(371.5)
Note:			
* Weights taken from Table 6-1.			

7

COMPARISON OF PAYLOAD LOSSES

Payload losses attributable to each of the three foam systems are tabulated for the fiberglass strand constrictive wrap and the corrugated aluminum constrictive wrap configurations in Tables 7-1 and 7-2, respectively. The current jettisonable insulation system payload losses are also shown in Tables 7-1 and 7-2. Although the hardware weight for the jettisonable panels is greater than that of the fixed panels, total payload loss for the jettisonable panels is small because the panels are jettisoned when the payload trade-off factor is high.

7.1 SPECIFIC LOSSES

Since each pound of hardware represents a pound of payload loss for the fixed insulation systems, the payload loss attributable to hardware is the total hardware weight obtained from the "maximum" columns of Tables 6-1 and 6-2 for the fiberglass wrap and corrugated wrap systems, respectively. The large payload loss attributable to ice shown for the corrugated wrap system (Table 7-2) is caused by freezing water inside the corrugations, as explained in Subsection 3.2.3. The payload loss attributable to hydrogen venting, gaseous residuals, ullage pressure decay between 0-250 seconds of flight, and propellant density effects are obtained from the results of the thermodynamic study of Reference 3-1. This study is discussed in detail in Section 3, with payload loss for some typical configurations tabulated in Table 3-6. Model 4 of Table 3-6 shows payload loss due to hydrogen losses for System A. Hydrogen losses are higher for Systems B and C since the foam of those systems had a higher thermal conductivity than the foam of System A. Propellant density losses were calculated using the jettison system as a basis for comparison. Therefore, losses attributable to propellant density effects for the jettison system are zero.

7.2 TOTAL LOSSES

The total payload loss comparison shows that a fiberglass constrictive wrap system will reduce current payload capability by between 68 pounds (System A) and 112.4 pounds (System B); and that a corrugated constrictive wrap system will reduce current payload capability by between 323.2 pounds (System C) and 345.1 pounds (System B).

A comparison between the fiberglass and corrugated aluminum constrictive wrap systems shows the corrugated system payload loss to be about 241 pounds greater than the fiberglass system (comparing Systems B and C only).

TABLE 7-1. COMPARISON OF PAYLOAD LOSSES
(FIBERGLASS CONSTRICTIVE WRAP CONFIGURATION)

	Payload Loss (lb)			
	Jettison System	System A	System B	System C
Total Due to Hardware	(141.3)	(228.2)	(262.6)	(240.7)
Due to Weight Jettisoned with Insulation Panels	93.3	—	—	—
Due to Weight Jettisoned with Nose Fairing	1.9	—	—	—
Due to Weight Jettisoned with Interstage Adapter	10.1	—	—	—
Due to Weight Carried on Cen- taur Stage	36.0	228.2*	262.6*	240.7*
Ice	—	(-8.0)	(-8.0)	(-8.0)
Total Due to Hydrogen Losses	(122.0)	(103.1)	(113.1)	(113.1)
Hydrogen Venting				
(0-155 Sec)	9.7	6.9	7.1	7.1
(155-250 Sec)	4.3	8.0	9.1	9.1
(250-2100 Sec)	41.5**	36.5**	45.5**	45.5**
Gaseous Residuals	59.5	61.0	61.0	61.0
Pressure Decay (0-250 Sec)	7.0	2.6	2.6	2.6
Propellant Density	0.0	-11.9	-12.2	-12.2
Total Payload Loss	(263.3)	(323.3)	(367.7)	(345.8)

* Total hardware weights taken from the "maximum" column of Table 6-1 for the three fixed insulation systems.

** Based on 25-minute coast.

Assumptions:

1. Zero insulation weight represents zero payload loss.
2. Zero boiloff and venting represents zero payload loss.
3. Propellant density effects are based on the weight of liquid hydrogen in the LH₂ tank for the jettison insulation system (5315 pounds).

TABLE 7-2. COMPARISON OF PAYLOAD LOSSES
(ALUMINUM CORRUGATION CONSTRICTIVE WRAP CONFIGURATION)

	Payload Loss (lb)			
	Jettison System	System A	System B	System C
Total Due to Hardware	(141.3)	†	(485.4)	(463.5)
Due to Weight Jettisoned with Insulation Panels	93.3		—	—
Due to Weight Jettisoned with Nose Fairing	1.9		—	—
Due to Weight Jettisoned with Interstage Adapter	10.1		—	—
Due to Weight Carried on Centaur Stage	36.0		393.4*	371.5*
Ice	—		(92.0)	(92.0)
Total Due to Hydrogen Losses	(122.0)		(123.0)	(123.0)
Hydrogen Venting				
(0-155 Sec)	9.7		6.5	6.5
(155-250 Sec)	4.3		9.7	9.7
(250-2100 Sec)	41.5**		56.2**	56.2**
Gaseous Residuals	59.5		61.0	61.0
Pressure Decay (0-250 Sec)	7.0		2.6	2.6
Propellant Density	0.0		-13.0	-13.0
Total Payload Loss	(263.3)		(608.4)	(586.5)

* Total hardware weights taken from the "maximum" column of Table 6-2 for the three fixed insulation systems.

** Based on 25-minute coast.

† The corrugated wrap configuration was not analyzed with System A.

Assumptions:

1. Zero insulation weight represents zero payload loss.
2. Zero boiloff and venting represents zero payload loss.
3. Propellant density effects are based on the weight of liquid hydrogen in the LH₂ tank for the jettison insulation system (5315 pounds).

8

SIMULATED ASCENT TRAJECTORY TESTS

As described in Section 4, the fixed insulation design provided a hermetically sealed panel so as to produce a cryopumped vacuum cavity when the panels were on a cryogenic filled tank. However, the insulation panel materials will outgas due to the temperature rise during the aerodynamic heating portion of the ascent trajectory, and also due to the vacuum environment. Since the panels were hermetically sealed, these gases, which would normally be vented off to the local environment, would accumulate in the panels, causing a positive internal pressure. If the internal pressure became high enough, it was possible that the seal material-to-foam adhesive would fail and the seal material would blister or burst.

In order to test the sealed panels for pressure buildup, two types of tests were run: (1) small panels were mounted on a curved steel plate and subjected to the ascent heating and vacuum environment, and (2) small panels were mounted on a curved cryogenic tank and subjected to the ascent heating and vacuum environment. The first test was run in an effort to perform a quick, inexpensive, conservative test to determine if further testing with cryogenics was necessary. The panels did fail during this test, therefore the second, more realistic test was performed with cryogenics. These two tests are described in Subsections 8.1 and 8.2, respectively.

8.1 SIMULATED HEATING/VACUUM TESTS

8.1.1 TEST OBJECTIVE. The objective of these tests was to determine if failure of the sealed foam panels would be caused by the combined action of a vacuum environment plus simulated aerodynamic heating, without the benefit of cryopumping of internal gases.

If failure was noted, a further objective was to determine, if possible, which materials contributed to the outgassing effects, and to discover other suitable materials or configurations which would reduce, or eliminate, panel failure.

8.1.2 TEST SPECIMEN CONFIGURATION. Six-inch square panels were fabricated using both the GAC 222 and CPR 32-2C foam, and various adhesives. The panels were mounted in a test fixture so that they were pulled around a 60-inch radius by six fiberglass constrictive wrap strands.

8.1.3 TEST FIXTURE CONFIGURATION. The test fixture (Figure 8-1) consisted of a base plate which provided a 60-inch radius and a bank of eight quartz lamps, all placed in a bell-jar vacuum chamber.

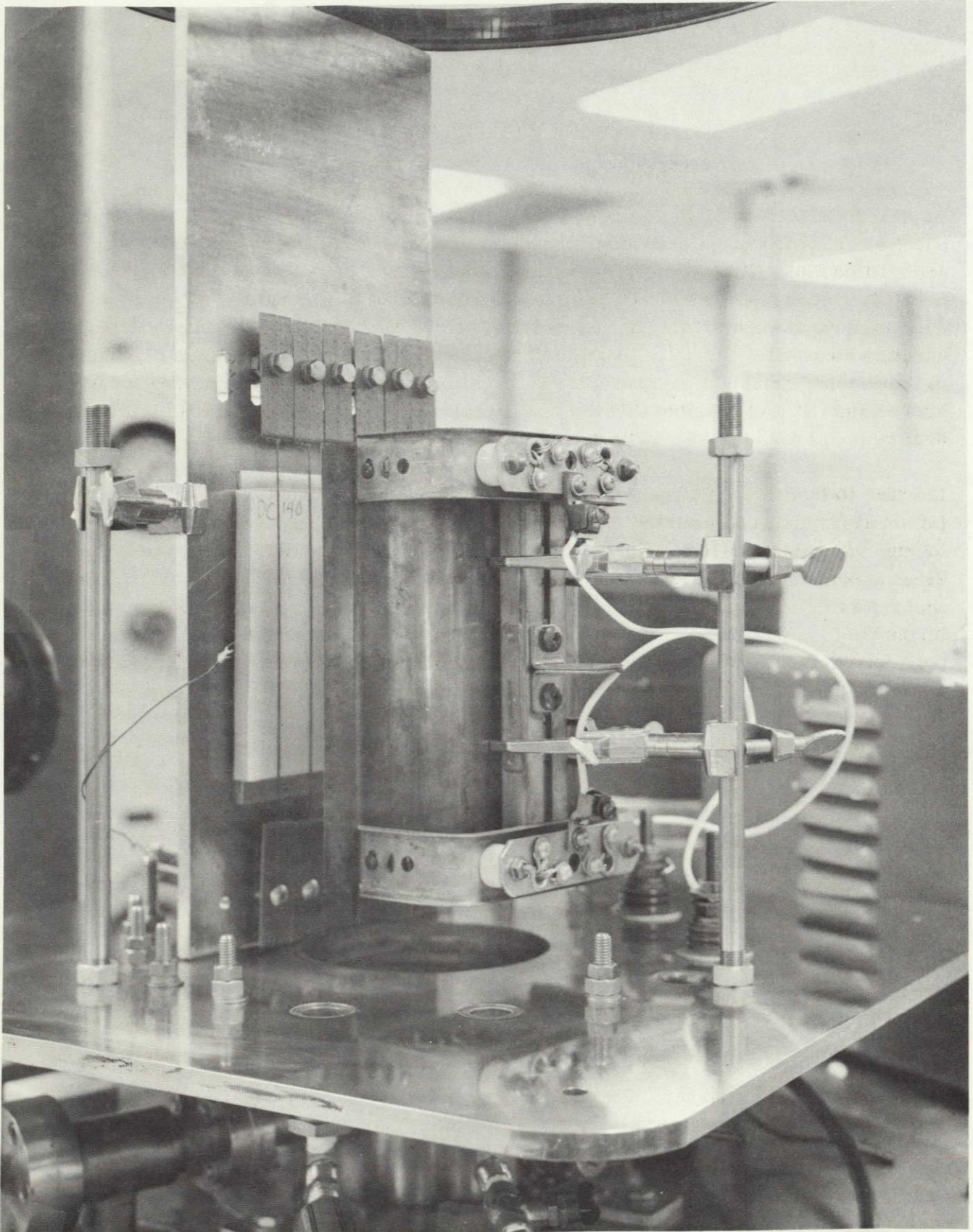


Figure 8-1. Test Fixture Configuration for Simulated Vacuum/Heating Tests

8.1.4 TEST RESULTS. Results of the tests are presented in Tables 8-1 and 8-2. About 75 percent of the failures were in the foam. When the failure did not occur in the foam, it was always in the MAM-to-foam bond line. When there was either a complete bond or foam failure, the pressure inside the panel was sufficient to raise the strands approximately 0.25 inches.

The first eight panel configurations of Table 8-1 were used on the T-9 full scale tests (see Section 9). As noted, all panels failed. In an effort to determine if the major pressure buildup was due to outgassing of adhesives or gas in the foam cells, the foam variable was eliminated by bonding the various outer films and adhesives to an aluminum sheet, as shown in tests 9 through 12. As noted, the PE-207 outgassed to a small degree while the SR 585 did not outgas enough to cause a blister. In tests 13 through 18, the vacuum level was varied to determine if the failure was sensitive to that variable. As noted, the blister temperature for 1, 15, and 21 mm of mercury was approximately the same as for the previous tests run at 10 microns. Tests 19 through 22 were repeats of previous tests, except that pressure and temperature were applied simultaneously. As noted, these tests verified that the previous method of applying first the vacuum, then the temperature, did not influence the results. Tests 23 and 27 measured the internal pressure in the panel when it blistered. Tests 24 through 26 contained small holes, approximately 0.030-inch diameter, spaced every one-half inch. These small holes appeared to be sufficient to release any pressure buildup in the panels, since no major blistering occurred.

Table 8-2 shows the test results of a dual panel configuration. This configuration consisted of the basic sealed panel, with an unsealed panel bonded to it, and the outer rubberized glass cloth bonded to the unsealed panel. Small holes were placed in the outer glass cloth to allow it to outgas. This configuration attempted to limit the outer surface of the sealed panel to a low enough temperature to preclude blistering. There were no failures with this configuration.

8.1.5 SUMMARY OF TEST RESULTS. A summary of the Heat/Vacuum test results is presented in Table 8-3. The results are grouped into the six basic material configurations tested.

Figure 8-2 presents curves of dynamic pressure and panel outer surface temperature versus flight time superimposed on curves of the test temperatures versus test time. It should be noted that the blister range indicated (from the above test results) occurs when the dynamic pressure is between 350 to 700 PSF. This indicates a possibility that aerodynamic buffet or flutter of the insulation system could occur.

8.1.6 CONCLUSIONS. All panels blistered except those with holes and those of the dual configuration. Outgassing of the panel materials appeared to be the cause for blistering. The material outgassing the most appeared to be the foam, but the adhesives also outgassed to a lesser extent. The conclusion that the adhesives outgassed to a lesser extent was also substantiated by the thermogravimetric analyses of foams and adhesives shown previously in Figures 2-17 and 2-21, respectively.

TABLE 8-1. RESULTS OF TESTING SEALED FOAM PANELS WITH HEAT/VACUUM

Number	Foam	MAM to Foam Adhesive	Silicone Rubber to MAM Adhesive	Vacuum	Blister Temp. °F	Remarks
1	CPR 32-2C	Epon 956	SR 585	10 μ Hg	492	Foam Failure
2	CPR 32-2C	Epon 956	SR 585	↑ ↓	417	Adhesive Failure
3	CPR 32-2C	Metlbond 225	SR 529		385	Foam Failure
4	CPR 32-2C	Metlbond 225	Dow Corning 140		332	Foam Failure
5	CPR 32-2C	Metlbond 225	A-4000		530	Foam Failure
6	GAC 222	Vitel PE-207	SR 585		485	Foam Failure
7	GAC 222	Vitel PE-207	SR 585		278	Foam Failure
8	GAC 222	Vitel PE-207	SR 585		255	Foam Failure
9	Aluminum Sheet	Vitel PE-207	No Silicone Rubber		330	Small Blister
10	Aluminum Sheet	No MAM	SR 585		No Blister	
11	Aluminum Sheet	SR 585	No Silicone Rubber		400	Small Blister
12	Aluminum Sheet	Vitel PE-207	SR 585	10 μ Hg	370	MAM to Aluminum Adhesive Failure
13	CPR 32-2C	Epon 956	SR 585	15 mm Hg	510	Slight Blister
14	CPR 32-2C post cured at 500° F for 12 hours	Epon 956	SR 585	21 mm Hg	457	Adhesive Failure
15	CPR 32-2C	Epon 956	SR 585	21 mm Hg	310	Foam Failure
16	CPR 32-2C	SR 585	SR 585	1 mm Hg	300 Minor 450 Major	Adhesive Failure
17	CPR 32-2C	Epon 956	SR 585	↑	370	Adhesive Failure
18	GAC 222	Epon 956	SR 585		360	Adhesive Failure
19	CPR 32-2C post cured at 100° F for 12 hours	Epon 956	SR 585		270 Minor 410 Major	Foam Failure
20	CPR 32-2C	Epon 956	SR 585	↓	350	Foam Failure
21	CPR 32-2C	Metlbond 225	A-4000		370	Foam Failure
22	GAC 222	Vitel PE-207	SR 585		1 mm Hg	270

TABLE 8-1. RESULTS OF TESTING SEALED FOAM PANELS WITH HEAT/VACUUM (Continued)

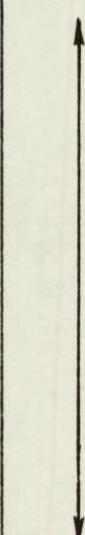
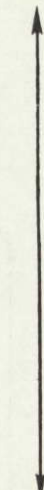
Number	Foam	MAM to Foam Adhesive	Silicone Rubber to MAM Adhesive	Vacuum	Blister Temp. °F	Remarks	
23	GAC 222	Vitel PE-207	SR 585	1 mm Hg	330	Measured a Pressure of 3 psia in panel	
24	GAC 222	Vitel PE-207	SR 585		400 Minor No Major Failure	Small surface blisters, small holes in MAM and rubberized glass cloth	
25	GAC 222	Vitel PE-207	SR 585		400 Minor No Major Failure	Small surface blisters, small holes in MAM and rubberized glass cloth	
26	GAC 222	Vitel PE-207	SR 585		No Failure	Small holes in MAM and rubberized glass cloth	
27	GAC 222	Vitel PE-207	SR 585		1 mm Hg	310	Measured a pressure of 4.5 psia in panel

TABLE 8-2. RESULTS OF TESTING DUAL SEALED/UNSEALED FOAM PANELS WITH HEAT AND VACUUM

Number	Sealed Panel	Unsealed Panel	Unsealed to Sealed Panel Adhesive	Silicone Rubber to Unsealed Panel Adhesive	Vacuum	Blister Temp. °F	Remarks
1	(1)	CPR 32-2C Foam 0.2 inch thick	Epon 956	SR 585	1 mm Hg  1 mm Hg	No Failure ⁽⁴⁾	Small holes in silicone rubberized glass cloth
2	Rerun of panel No. 1 after 28 hours at 98% relative humidity ⁽²⁾					No Failure ⁽⁴⁾	
3	(1)	CPR 32-2C Foam 0.2 inch thick	Epon 956	SR 585		No Failure ⁽⁴⁾	Small blisters in silicone rubberized glass cloth
4	(1)	GAC 222 Foam 0.2 inch thick	Epon 956	SR 585		No Failure ⁽⁵⁾	Small holes in silicone rubberized glass cloth
5	(1)	GAC 222 Foam 0.2 inch thick	Epon 956	SR 585		No Failure ⁽⁵⁾	Small blisters in silicone rubberized glass cloth
6	Rerun of panel No. 5 after 68 hours in water ⁽³⁾					No Failure ⁽⁵⁾	

(1) Configuration of sealed panel:

- Foam, GAC 222, 0.4-inch thick
- MAM to foam adhesive, Vitel PE-207

(2) Picked up 1.1% in weight.

(3) Picked up 35% in weight.

(4) Maximum temperature at outside surface of sealed panel was 360° F.

(5) Maximum temperature at outside surface of sealed panel was 310° F.

Both the dual configuration and the configuration with holes have disadvantages from the standpoint of the objectives of this program. Punching holes in the panel destroys its hermetic seal and permits the panels to cryopump outside gases when they are on a cryogenic tank. The dual configuration adds weight and complicates panel repair.

TABLE 8-3. SUMMARY OF HEAT/VACUUM TESTING

System	Failure Temperatures	Types of Failure
GAC	278° F, 255° F, 270° F, 330° F, 485° F*	50% Foam Failures, 50% Adhesive Failures
Modified GAC (Epon 956 Adhesive)	360° F	Adhesive Failure
High Temperature (Epon 956)	492° F, 417° F, 510° F, 457° F, 410° F, 350° F	50% Foam Failures, 50% Adhesive Failures
High Temperature (Metlbond 225)	385° F, 332° F, 530° F, 370° F	100% Foam Failures
GAC with Small Vent Holes	400° F (Small Blisters), 400° F (Small Blisters), >550° F (N.F.), >550° F (N.F.)	
Dual Foam	>550° F (N.F.), >550° F (N.F.), >550° F (N.F.)	

* Old thermal conductivity test panel.

8.2 SIMULATED CRYOGENIC/HEAT/VACUUM TESTS

As detailed above, gas blisters did form when 6-inch by 6-inch panels were subjected to the combination of low pressure and radiant heating. Additionally, as detailed in Subsection 9.5.3, two 6-inch by 6-inch areas of the sealed insulation panel on the T-9 test tank were heated during a cryogenic test cycle at the same rate and same maximum temperature as the 6-inch by 6-inch panels in the laboratory. Blistering of the outer skin of the panel did not occur. This introduced the possibility that blistering in the laboratory tests may not have occurred if one side of the panels had been at liquid hydrogen temperatures.

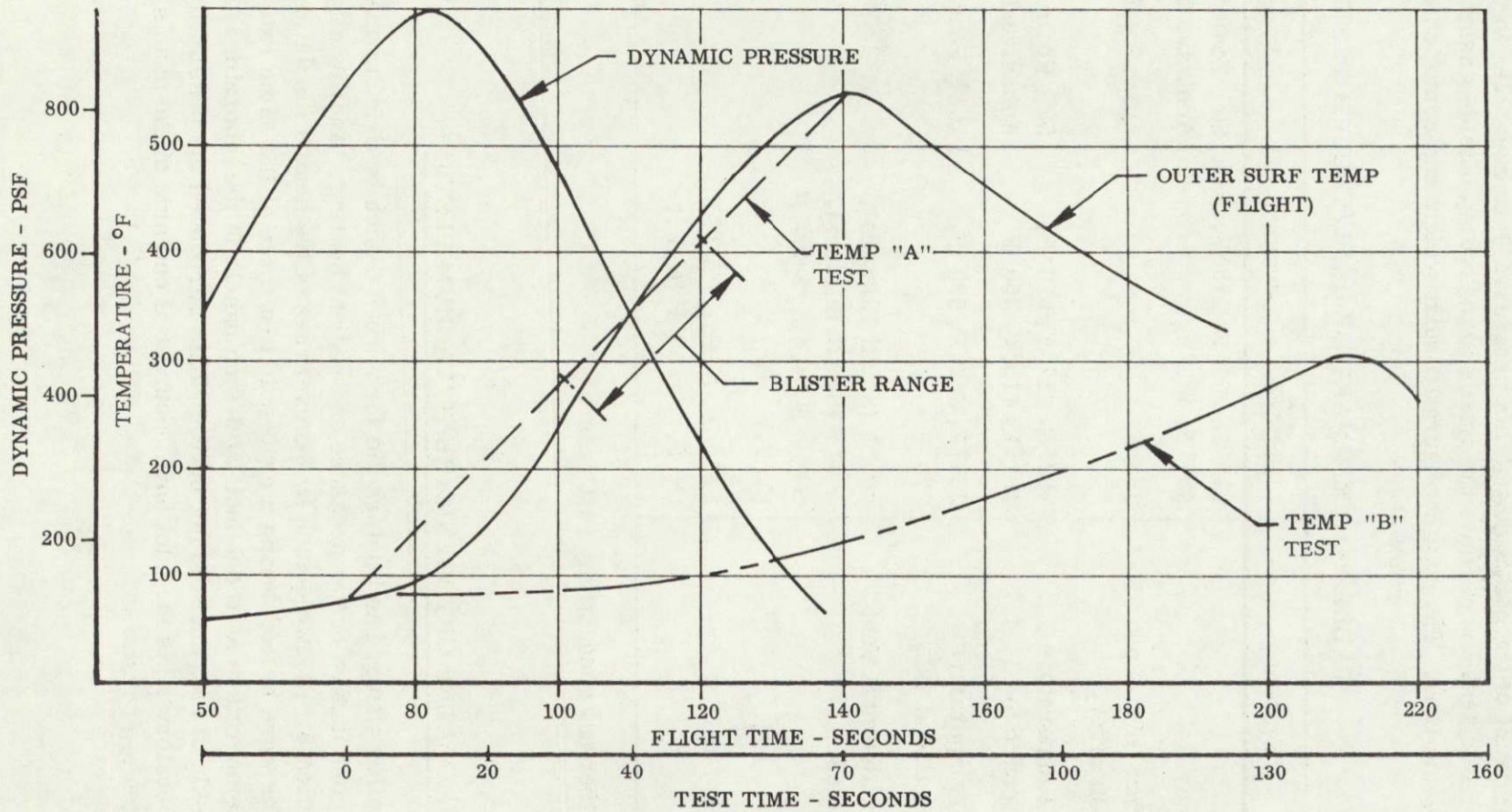
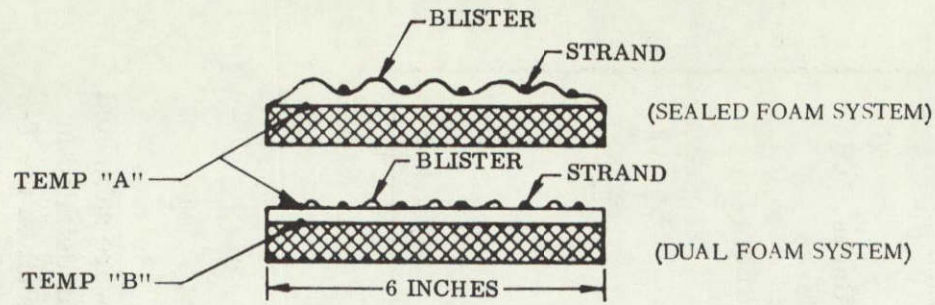


Figure 8-2. Heat/Vacuum Tests

Blistering of the sealed foam insulation panels is caused by (1) the increase in gas temperature in the foam at constant volume caused by aerodynamic heating, (2) out-gassing of adhesive, Mylar, and foam materials at high temperature, and (3) the decrease of atmospheric pressure during ascent. The situation is aggravated as the tensile strength of the foam decreases with an increase in temperature due to ascent heating. The differential pressure eventually forces the foam to separate at the MAM/foam interface where the foam cell pressure is the greatest.

The tests described in Subsection 8.1 simulated only reduced atmospheric pressure and maximum surface temperature conditions. The tests were begun with the insulation panels at room temperature. No effort was made to produce liquid hydrogen temperature on the "cold" side of the insulation panel test specimen. As mentioned earlier, it was recognized in advance that this test was very conservative, but if no problems had occurred it would not have been required to perform the more expensive test with a hydrogen cold wall.

8.2.1 EFFECTS OF TESTING ON A COLD WALL. The foam insulation system design was evaluated to determine the effects of a cold wall on the gas pressure within the foam cells. This was accomplished by plotting the temperature and pressure gradients through the foam as shown on Figure 8-3. The steady-state prelaunch temperature gradient is plotted for a cold-wall temperature of -420°F . The pressure gradients that correspond to these temperatures are plotted for both CO_2 -blown and Freon-blown foams.

The pressure gradient in CO_2 -blown foam between points (1) and (2) on Figure 8-3 is established by Charles Law effects wherein pressure varies directly with temperature (constant volume). The pressure gradient between points (2) and (3) for CO_2 -blown foam is a function of the vapor pressure of solid CO_2 . Note that the pressure gradient between points (1), (2), and (3) is very steep. If the foam is sufficiently porous, CO_2 gas will diffuse from the warm surface to a point 0.2 inch from the cold surface (for 0.4-inch thick foam). This will cause the foam pressure to decrease to some lower value, say points (1') and (2'). If a sufficient quantity of gas diffuses away from the warm panel surface, foam pressure may be reduced sufficiently at the MAM/foam interface to prevent panel failure.

The pressure gradient in the Freon-blown foam (Figure 8-3) between points (4) and (5) is a function of the vapor pressure of liquid Freon-11. The pressure gradient is very steep and close to the surface of the panel. Gas will transfer away from the surface of the panel if the foam is sufficiently porous.

The conditions described in the foam demonstrate that it is necessary to provide a cold wall for the insulation tests. Tests of 6-inch by 6-inch foam panels similar to those described in Subsection 8.1 were accomplished with one surface exposed to liquid hydrogen temperatures.

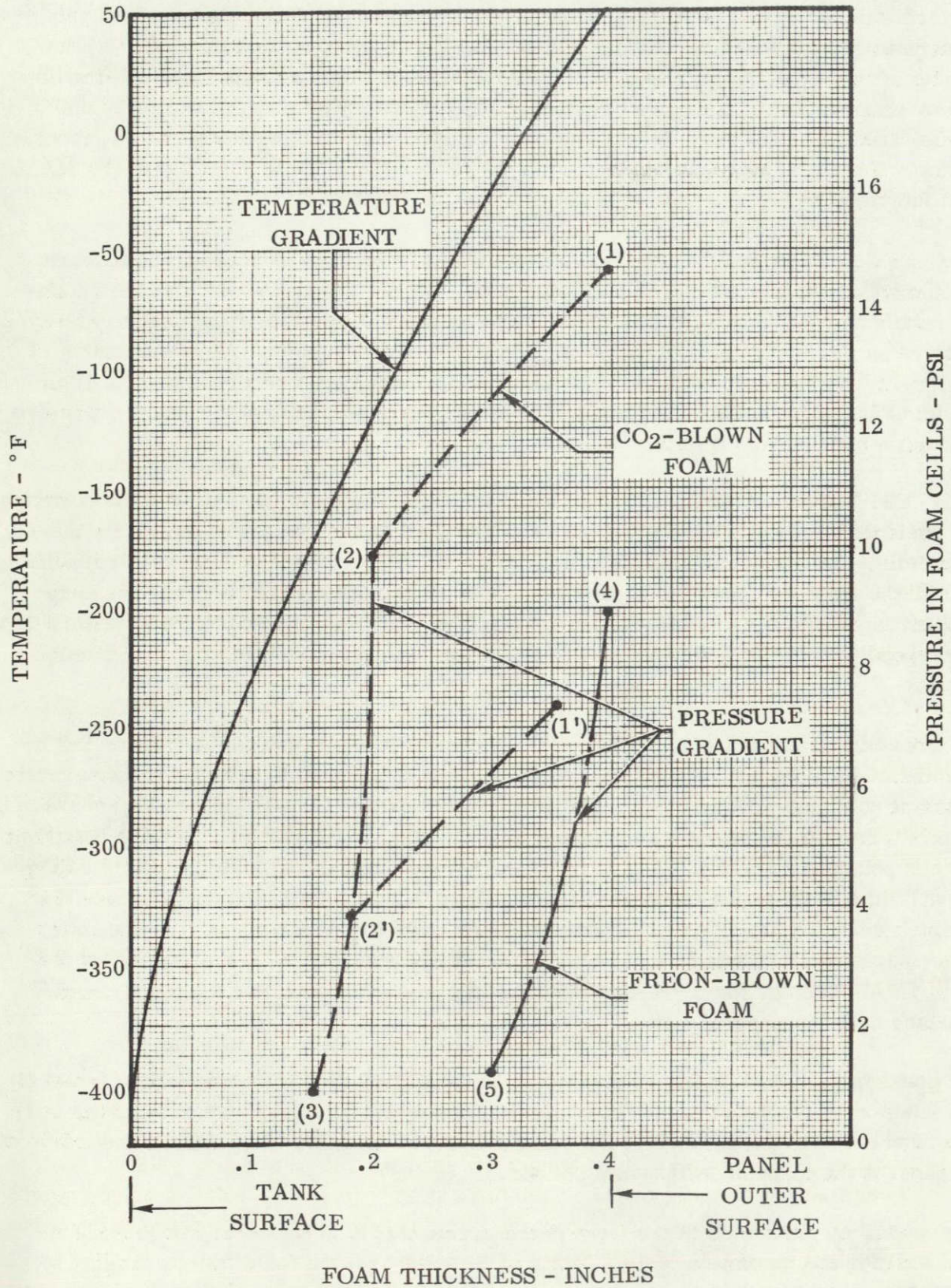


Figure 8-3. Prelaunch Steady-State Temperature and Pressure Gradients through Sealed Fixed Foam Insulation Panel

8.2.2 TEST OBJECTIVE. Since neither of the previous tests simulated all the flight conditions, a series of tests were run in which all three flight conditions of (1) aerodynamic heating, (2) flight profile pressures, and (3) liquid hydrogen temperatures on the back side of the insulation were imposed simultaneously on the specimen panels. The objective of these tests was to determine if blistering of the hermetically sealed fixed insulation panels could be prevented by cryopumping of gases generated on the heated side of the panel to the cold side of the panel during simulated flight conditions of atmospheric pressure and aerodynamic heating.

Convair had obtained nine "spray-on" type foam insulation specimens from North American Rockwell Corporation. These spray-on type foam insulation specimens were indicative of the Saturn S-II insulation. Therefore, an additional objective of these tests was to subject the North American insulation panels to the simulated Centaur launch profile conditions of temperature and pressure, and observe the results.

8.2.3 TEST SPECIMEN CONFIGURATION. Five test specimen configurations were tested. All test specimens were bonded to an 0.016-inch thick by 6.4-inch by 7.0-inch aluminum panel. The test specimen configurations are tabulated in Table 8-4. Seven panel specimens of each configuration A through D were tested. Three of the seven specimen panels of each configuration A through D were fabricated with a small leak (0.008 to 0.010-inch diameter hole) centered in the face of each panel, and the remaining four specimen panels of each configuration A through D were fabricated leak tight.

8.2.4 TEST FIXTURE CONFIGURATION. The test specimen panels were installed on the face of the test fixture shown in Figure 8-4. Figure 8-5 shows the face of the test fixture with a test specimen panel installed. The test fixture was then installed in an eight cubic-foot vacuum chamber. Heat was supplied by six 1000-watt quartz lamps in the vacuum chamber. In order to maintain sea-level pressure during the cryogenic hold period, and to control the temperature on the face of the panel, a gaseous nitrogen purge was directed across the face of the panel.

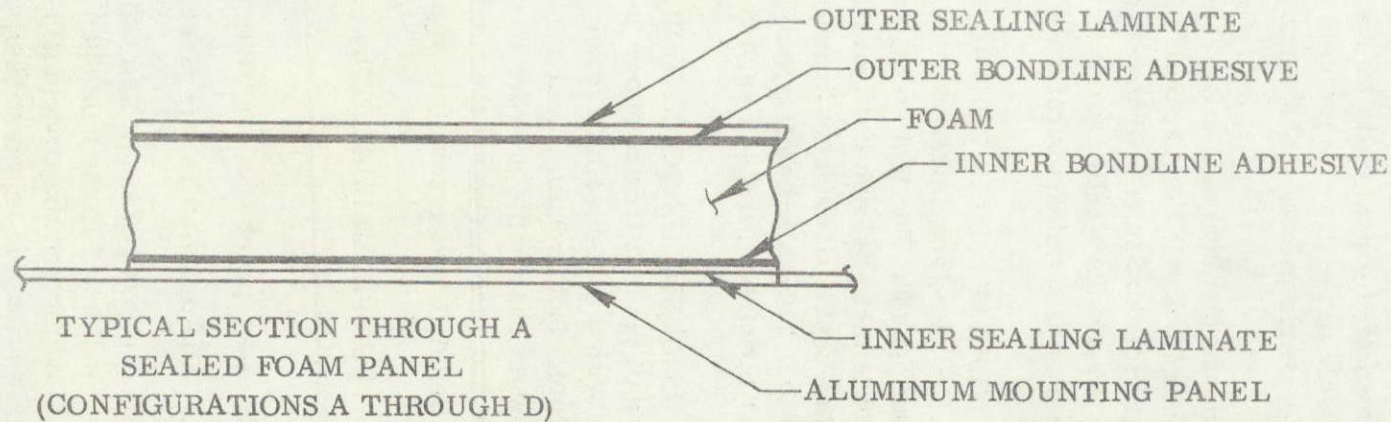
8.2.5 TEST PROCEDURE. The panel specimens were tested according to the following procedure:

1. Each panel specimen was installed on the face of the test fixture.
2. The test fixture was placed in the vacuum chamber.
3. One each of the sealed panels of configurations A through D, was immediately subjected to the combined vacuum and heating rate simulating ascent. This duplicated the environment of the tests of Subsection 8.1, and provided verification that this test setup gives the same results as the test setup and environment of the tests of Subsection 8.1.

TABLE 8-4. SIMULATED CRYOGENIC/VACUUM/HEATING TEST SPECIMEN CONFIGURATIONS

Config-uration	Outer Sealing Laminate	Outer Bondline Adhesive	Foam	Foam Thickness	Inner Bondline Adhesive	Inner Sealing Laminate	Remarks
A	MAM	PE-207	GAC 222	0.4 in.	PE-207	MAM	Same as System "A" in Table 4-1.
B	MAM	Metlbond 225 0.06 lb per sq. ft.	CPR 32-2C	0.4 in.	PE-207	MAM	Same as System "B" in Table 4-1.
C	MAM	Metlbond 225 0.045 lb per sq. ft.	CPR 32-2C	0.4 in.	PE-207	MAM	
D	MAM	PE-207	GAC 222	0.8 in.	PE-207	MAM	Same as System "A" in Table 4-1 except for foam thickness.
E	0.80 by 6.0 by 6.0-inch polyurethane spray-on foam samples obtained from North American Rockwell Corporation.						

8-12



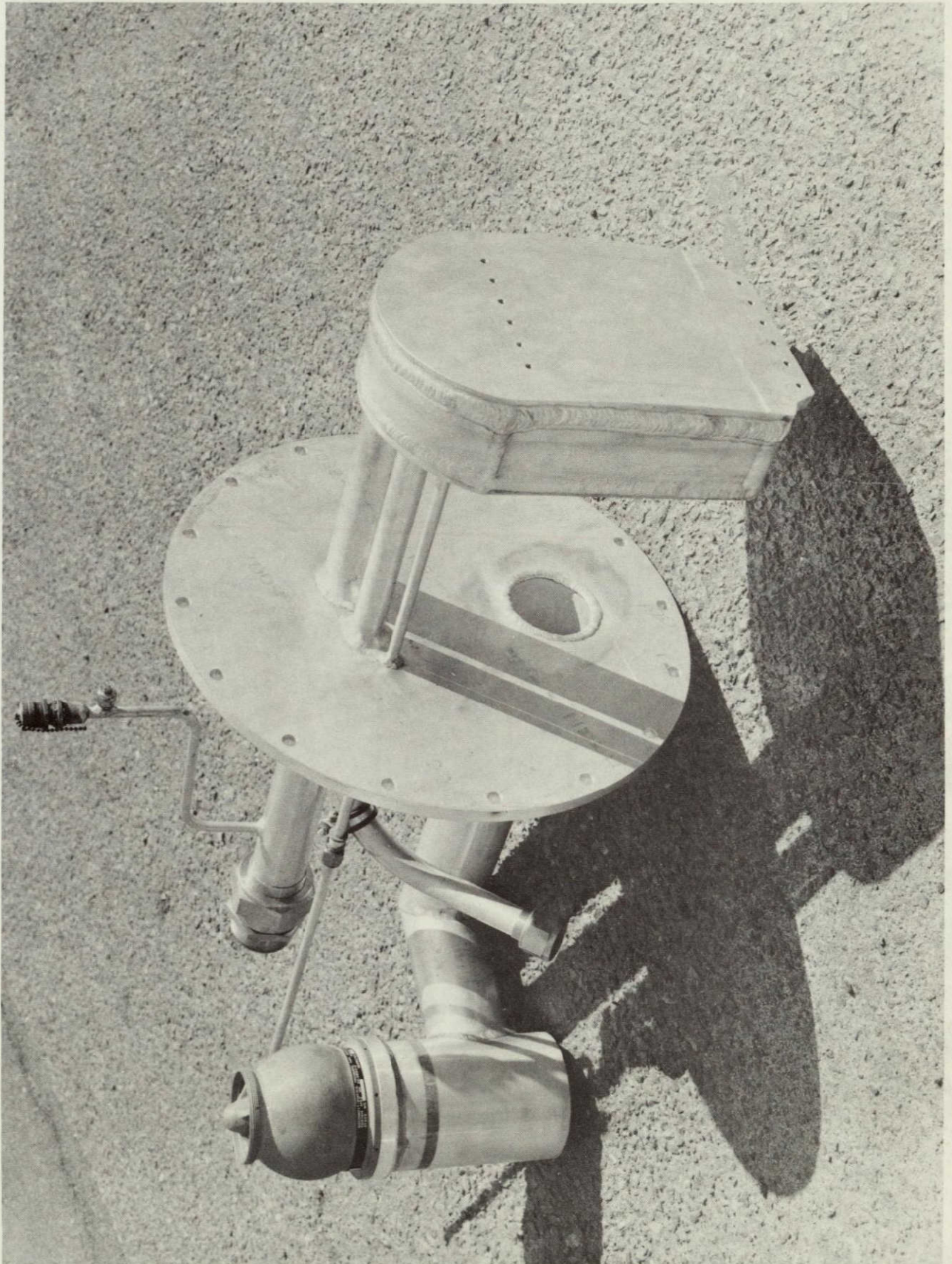


Figure 8-4. Insulation Panel Test Fixture Before Installation of Panel Specimen

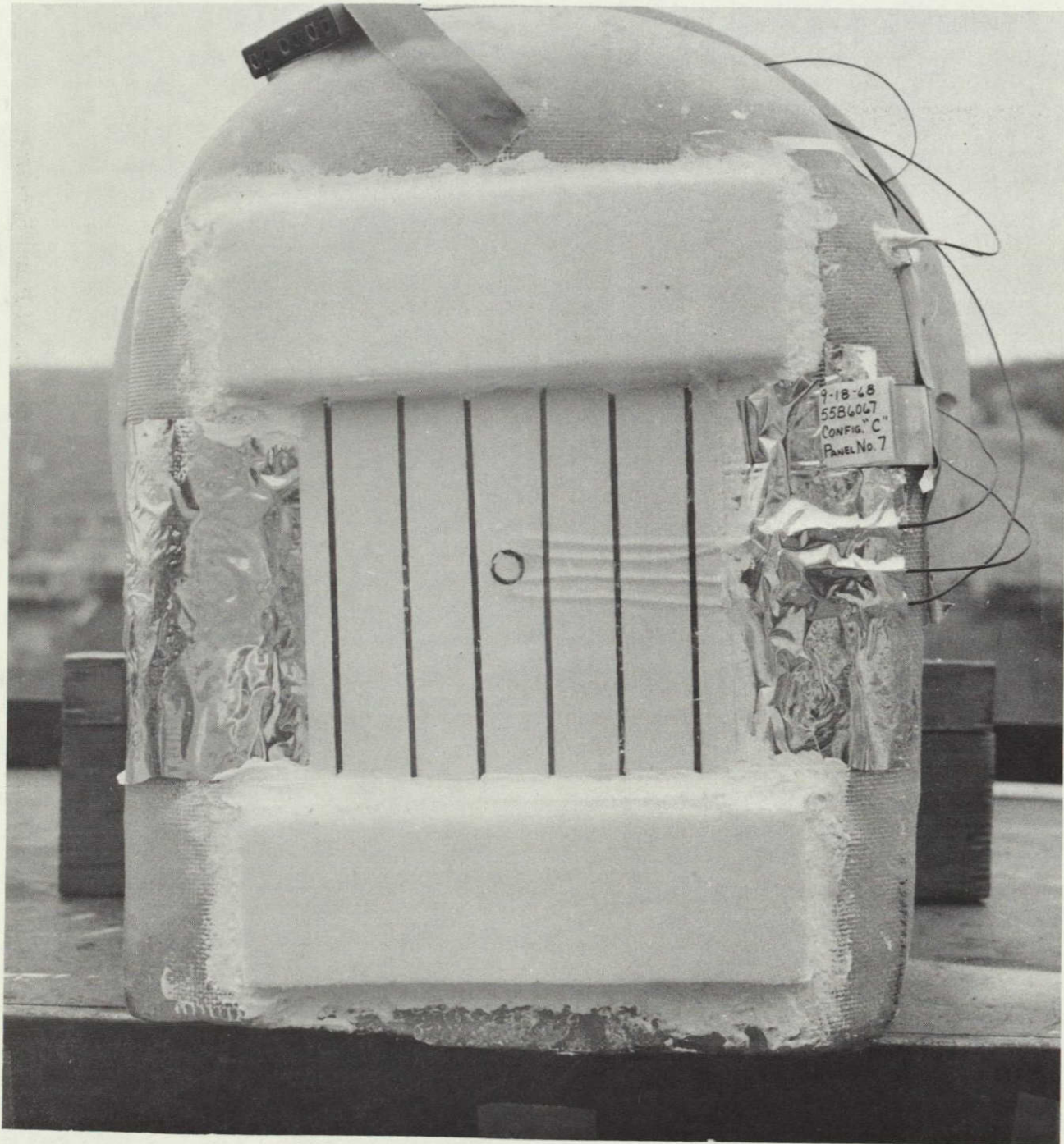


Figure 8-5. Typical Installation of Specimen Panel for Configurations 1 through 4

For the remaining six panels of each configuration A through D, the LH₂ chamber was filled and the GN₂ purge across the face of the panel was activated. This state was held for 20 minutes for the three remaining sealed panels of each configuration A through D, and for two hours for the three panels of each configuration A through D with the small leak.

4. At the end of the hold the GN₂ purge was stopped and the panels were subjected to the combined vacuum and heating rate to simulate ascent.

8.2.6 TEST RESULTS. For a complete description of the test configuration and test results, see References 8-2 and 8-3. A summary of test results follows.

Some blistering occurred in all panels of configurations A through D. Photographs of typical blisters are shown in Figures 8-6 through 8-14. Figures 8-6 through 8-8 show blisters in panels tested without LH₂ in the test fixture (back face of panel at ambient temperature.) Figures 8-9 through 8-11 show blisters in sealed panels which have been held with the back face at LH₂ temperature for 20 minutes. Figures 8-12 through 8-14 show blisters in those panels fabricated with small leaks, and held with the back face at LH₂ temperature for two hours.

The accrued time at blistering and the temperature of the panel when a blister occurred are listed in Table 8-5. Measurements were not obtained on panels B1 and C1 because of instrumentation difficulties. After testing, all panels were cut in half perpendicular to the front face and visually examined. The results of the examination are listed in Table 8-6.

Several things are readily apparent upon review of Tables 8-5 and 8-6. Panels A1 and D1 failed at the lowest temperature of all panels in their respective configuration. This becomes very significant when coupled with the fact that they were the only panels with the back face at ambient temperature when the heating cycle started. It is postulated that chilling the back face to approximately -415°F prior to the heating cycle reduced the gas pressure in the cells throughout the foam, and caused some migration of the gases toward the back face. This would result in a longer heating cycle before the internal pressure could overcome the strength of the foam, and would then explain why the chilled panels failed at higher temperatures. Unfortunately, panels B1 and C1 had instrumentation problems, and there was no way of checking this hypothesis with the CPR 32-2C foam.

There appeared to be no significant differences in blistering temperature whether the panel was leak tight or contained a small leak, although there was a slight trend for the panels with leaks to blister at higher temperatures. The blister temperature of the D set of panels (0.8-inch thick foam) averaged about 30°F higher than the blister temperature of the A set of panels (0.4-inch thick foam). There is no explanation for this phenomenon, although it may just be the overall scatter in the data, considering the small number of test panels. In general, the panels made with the Goodyear 222

foam failed in the foam immediately below the outer bondline. (See Table 8-4 for a definition and location of the bondlines.) Panels A1, D4, and D6 appeared to have failed and then resealed themselves after pressure was raised to ambient pressure. This phenomena was also noted in the tests described in Subsection 8.1.

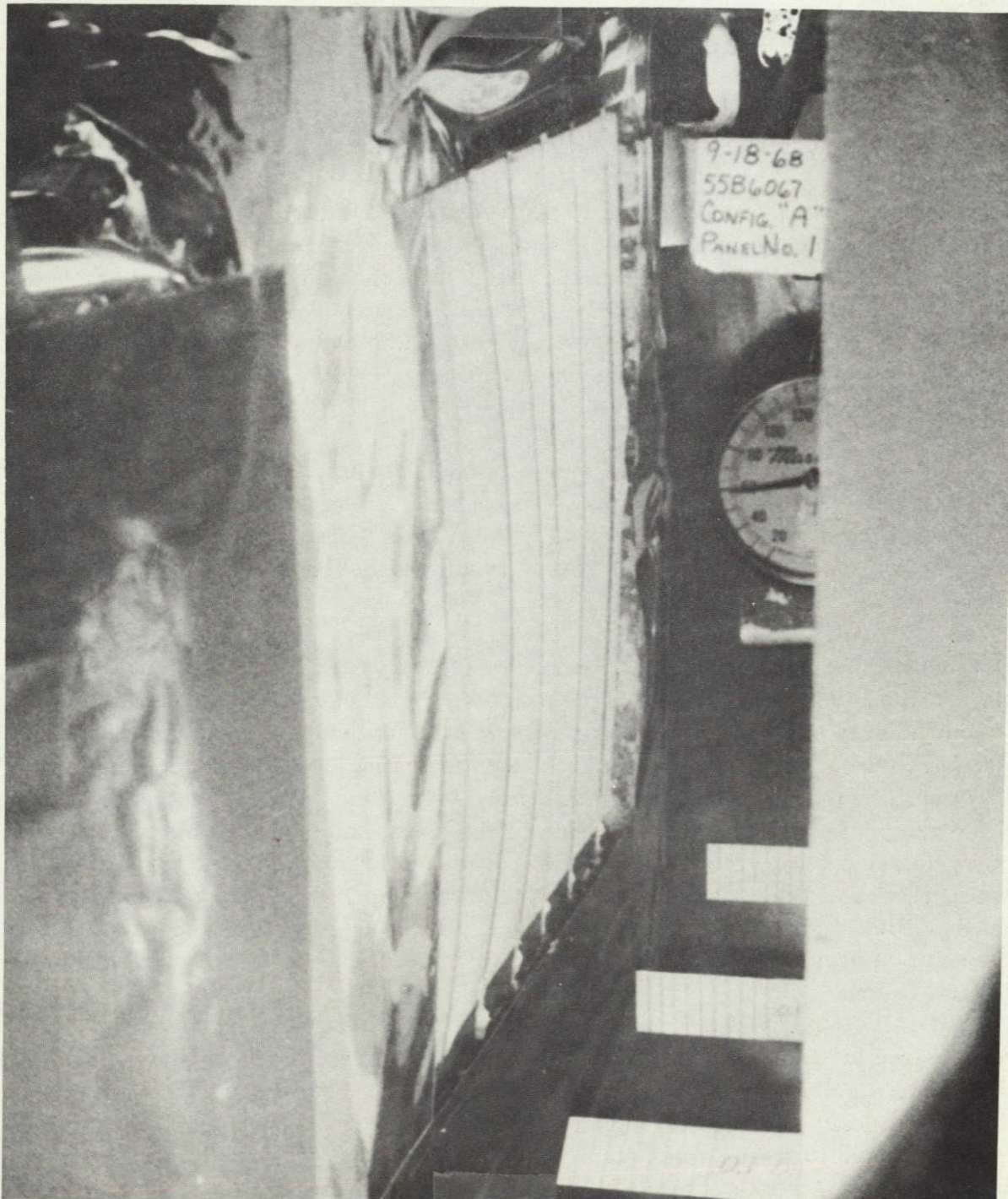


Figure 8-6. Specimen Panel A1 Showing First Blister Formation — Back Face of Panel at Ambient Temperature Before Test

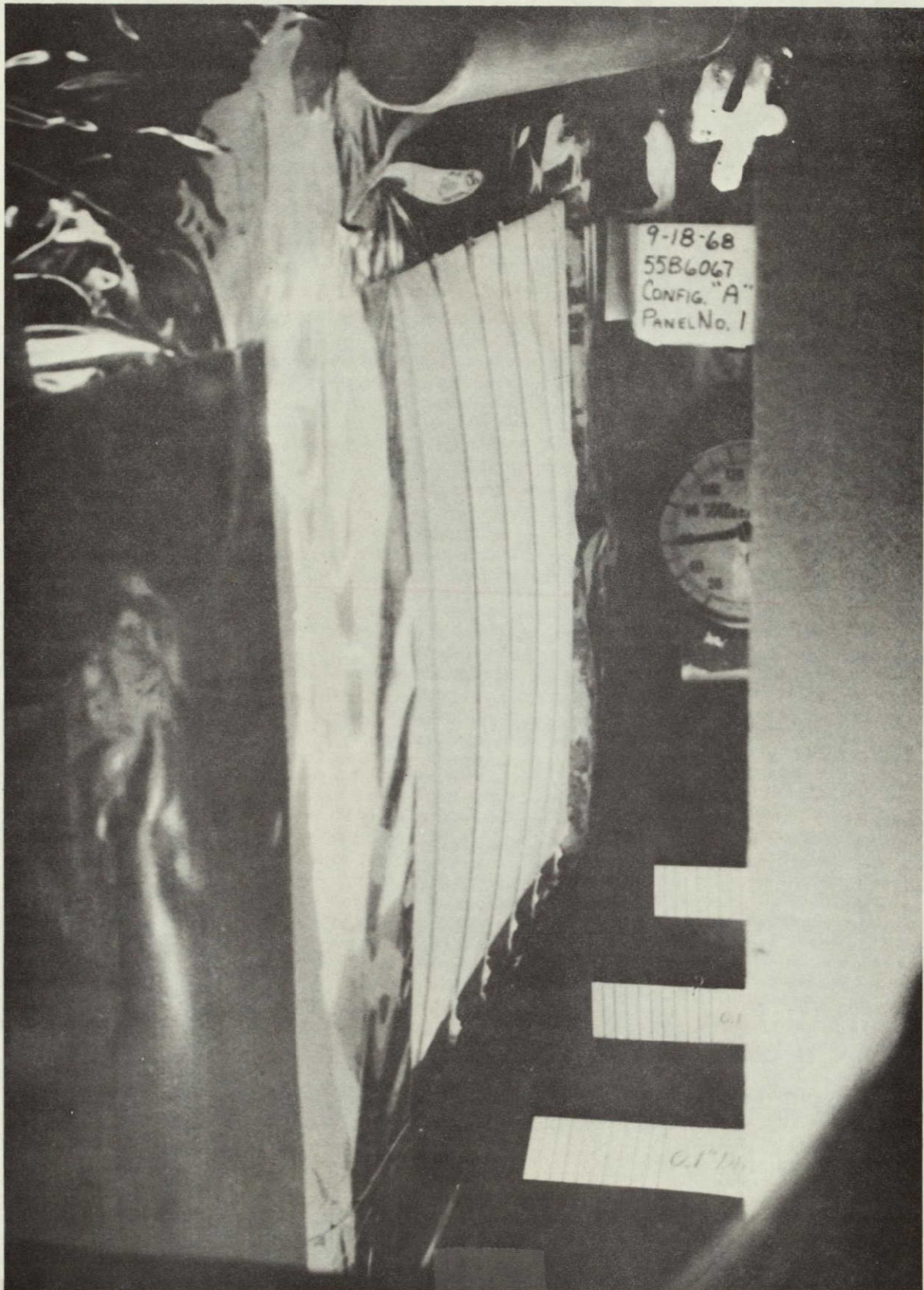


Figure 8-7. Specimen Panel A1 Showing Maximum Blister Formation — Back Face of Panel at Ambient Temperature Before Test

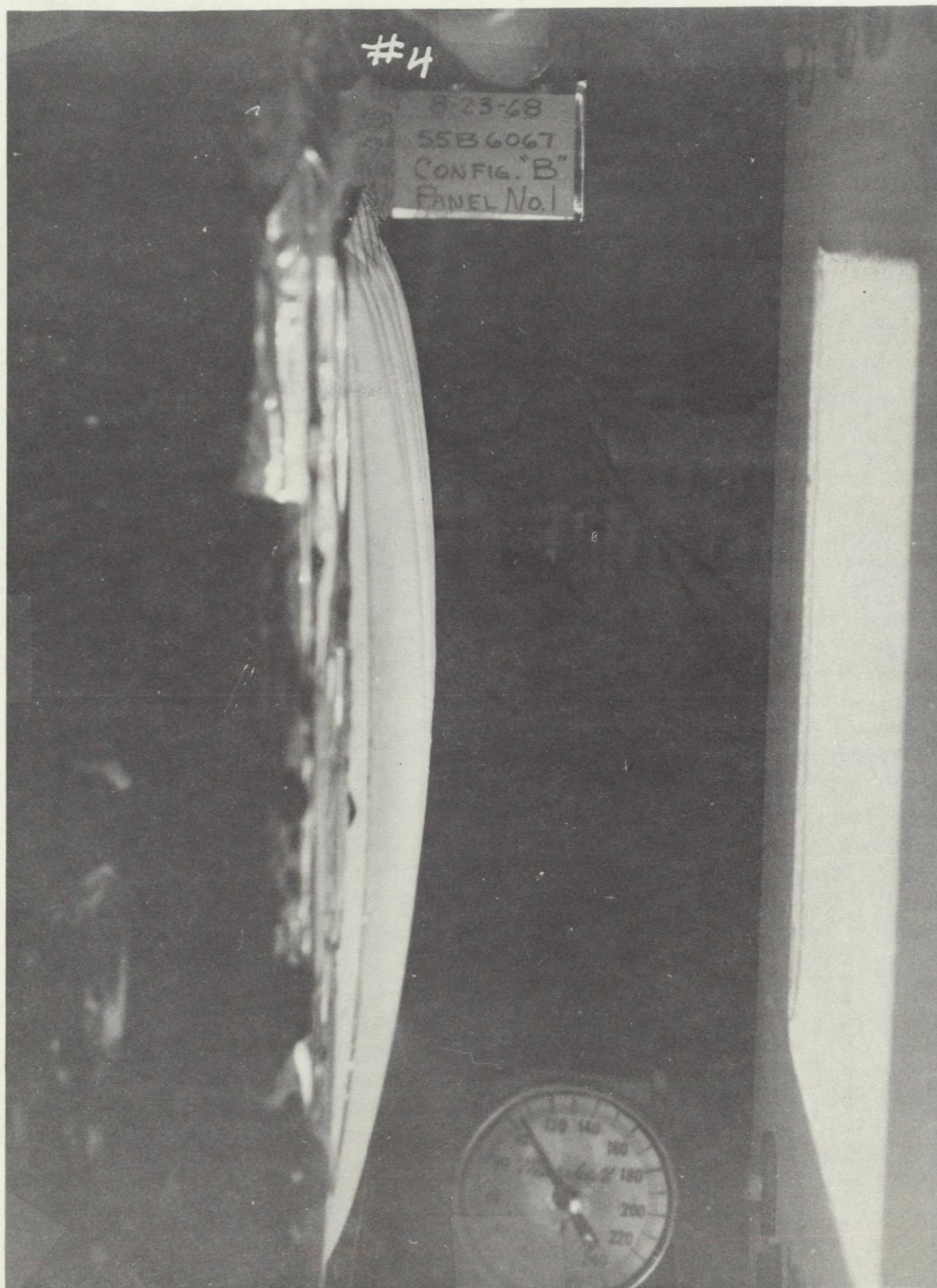


Figure 8-8. Specimen Panel B1 Showing Maximum Blister Formation — Back Face of Panel at Ambient Temperature Before Test

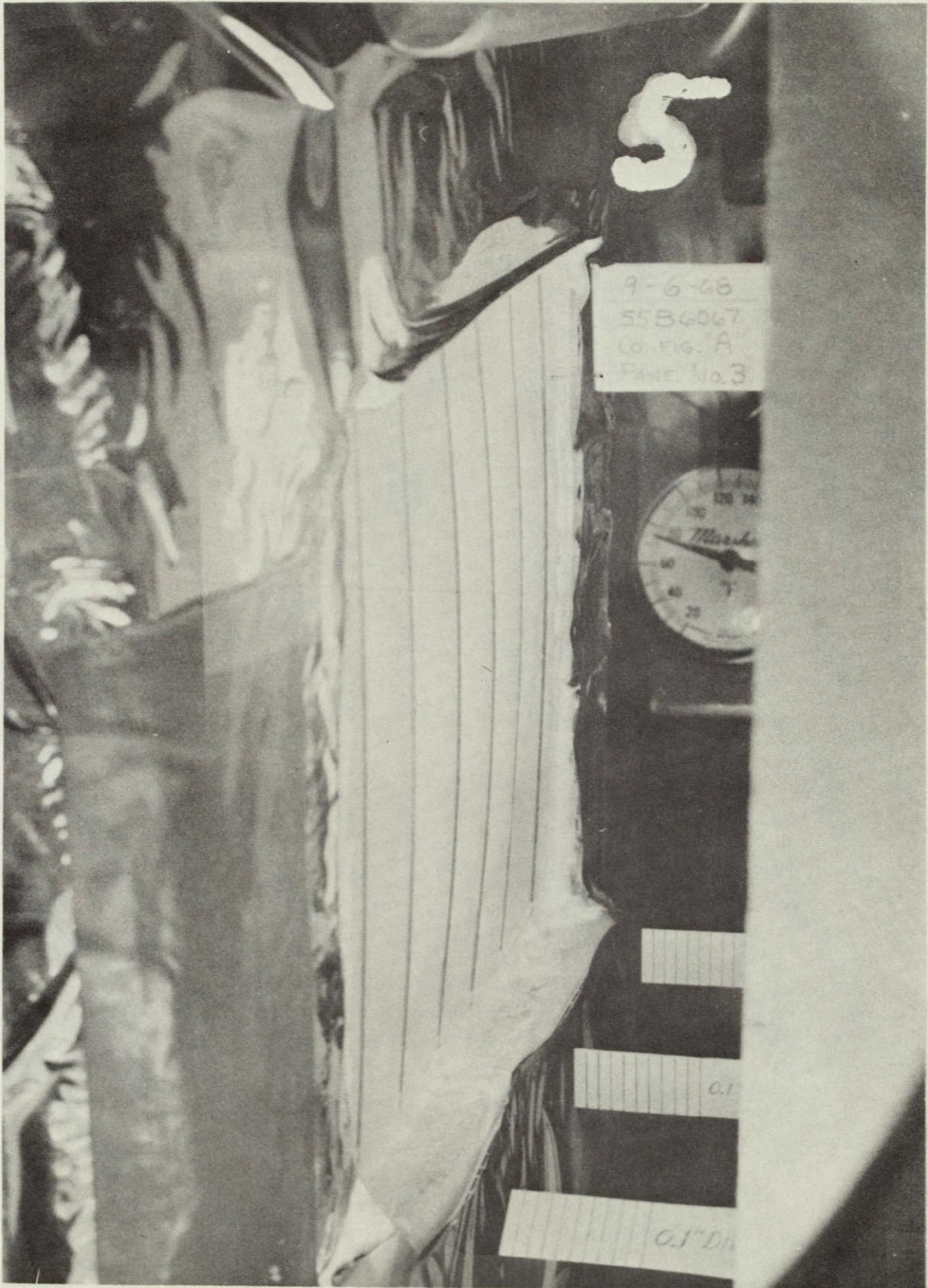


Figure 8-9. Specimen Panel A3 Showing Maximum Blister Formation — Back Face of Panel at LH_2 Temperature for 20 Minutes Before Test



Figure 8-10. Specimen Panel B3 Showing Maximum Blister Formation — Back Face of Panel at LH_2 Temperature for 20 Minutes Before Test

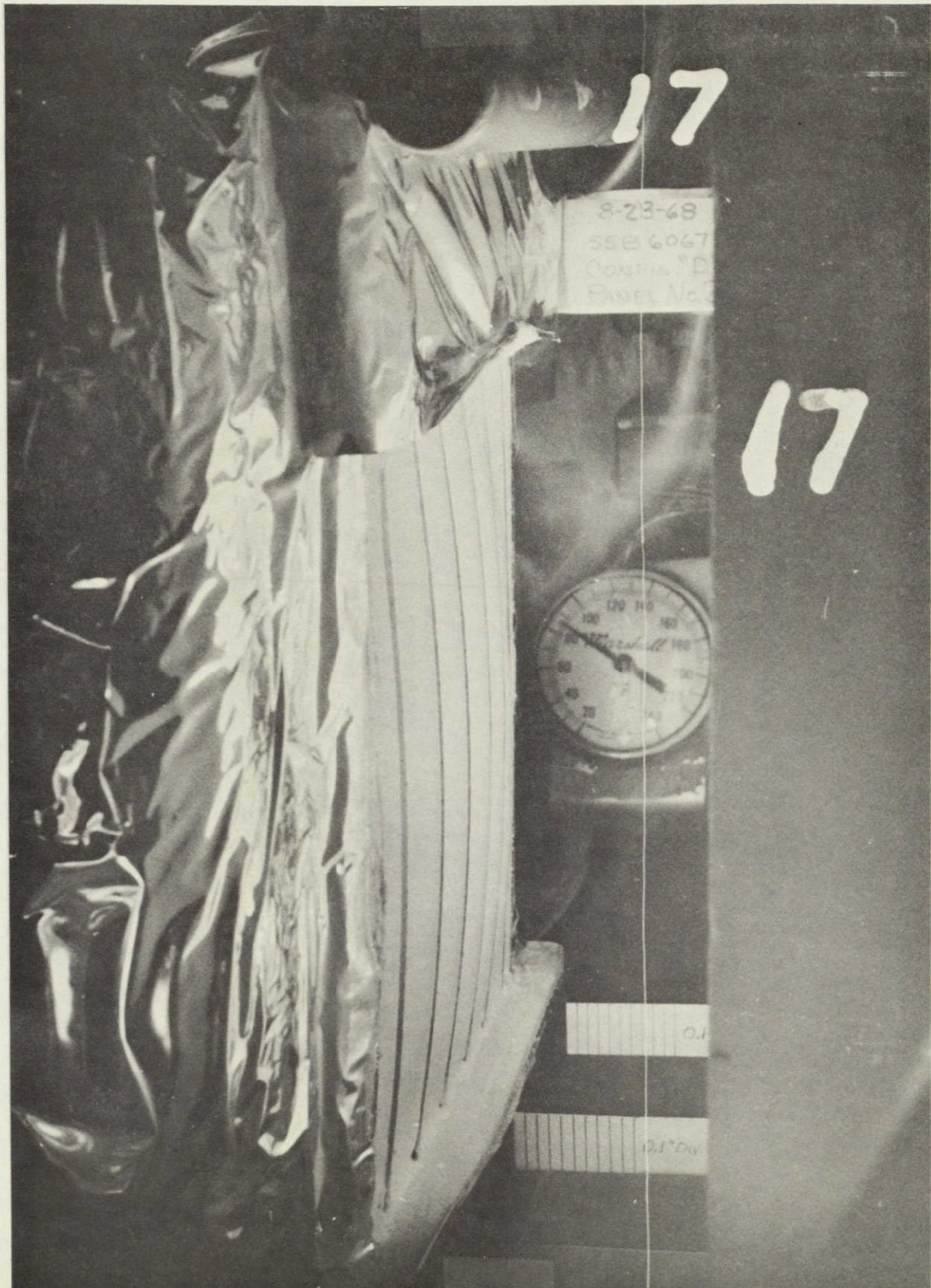


Figure 8-11. Specimen Panel D2 Showing Maximum Blister Formation — Back Face of Panel at LH₂ Temperature for 20 Minutes Before Test



Figure 8-12. Specimen Panel A6 Showing Maximum Blister Formation -- Back Face of Panel at LH₂ Temperature for 2 Hours Before Test

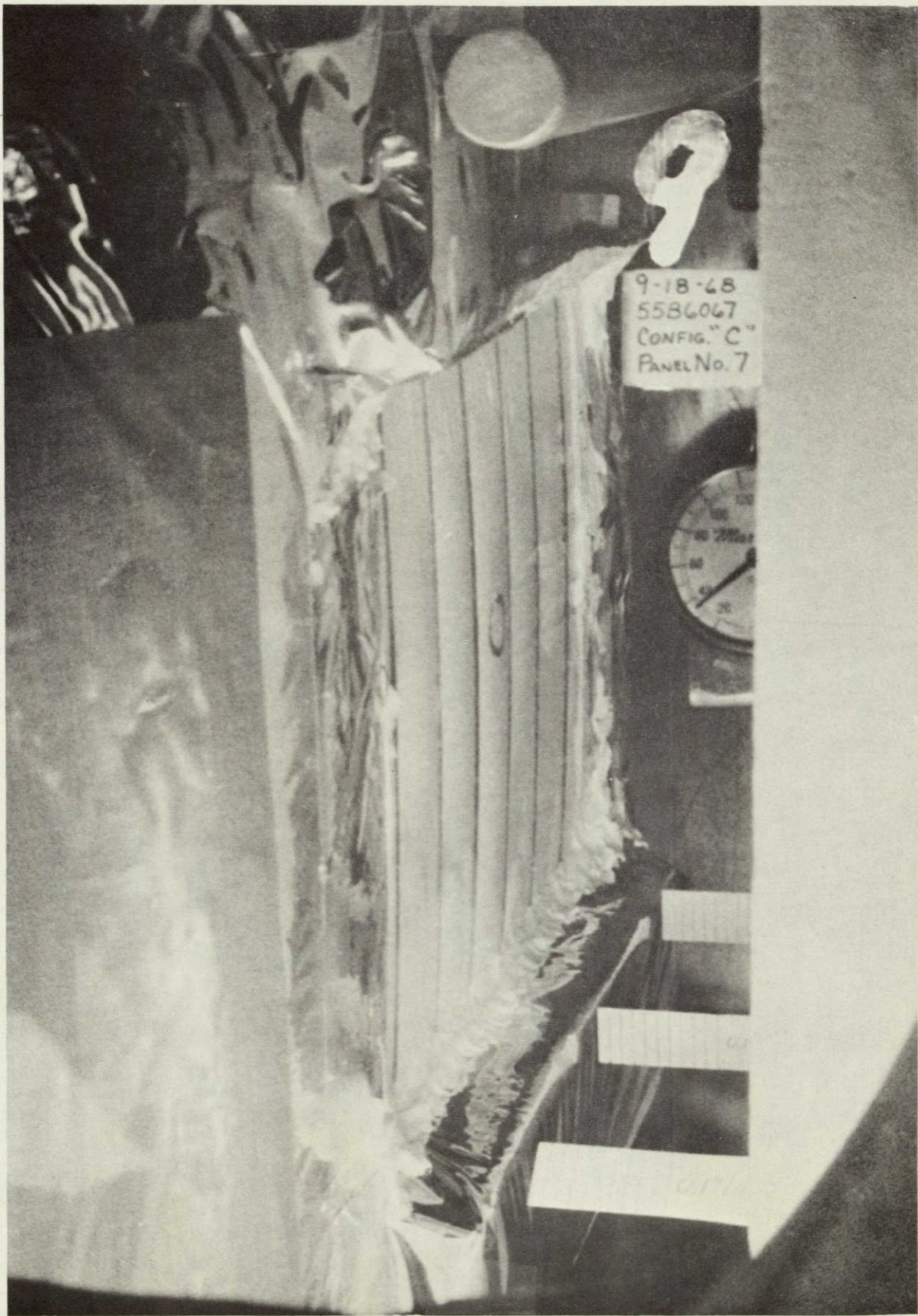


Figure 8-13. Specimen Panel C7 Showing Maximum Blister Formation — Back Face of Panel at LH₂ Temperature for 2 Hours Before Test

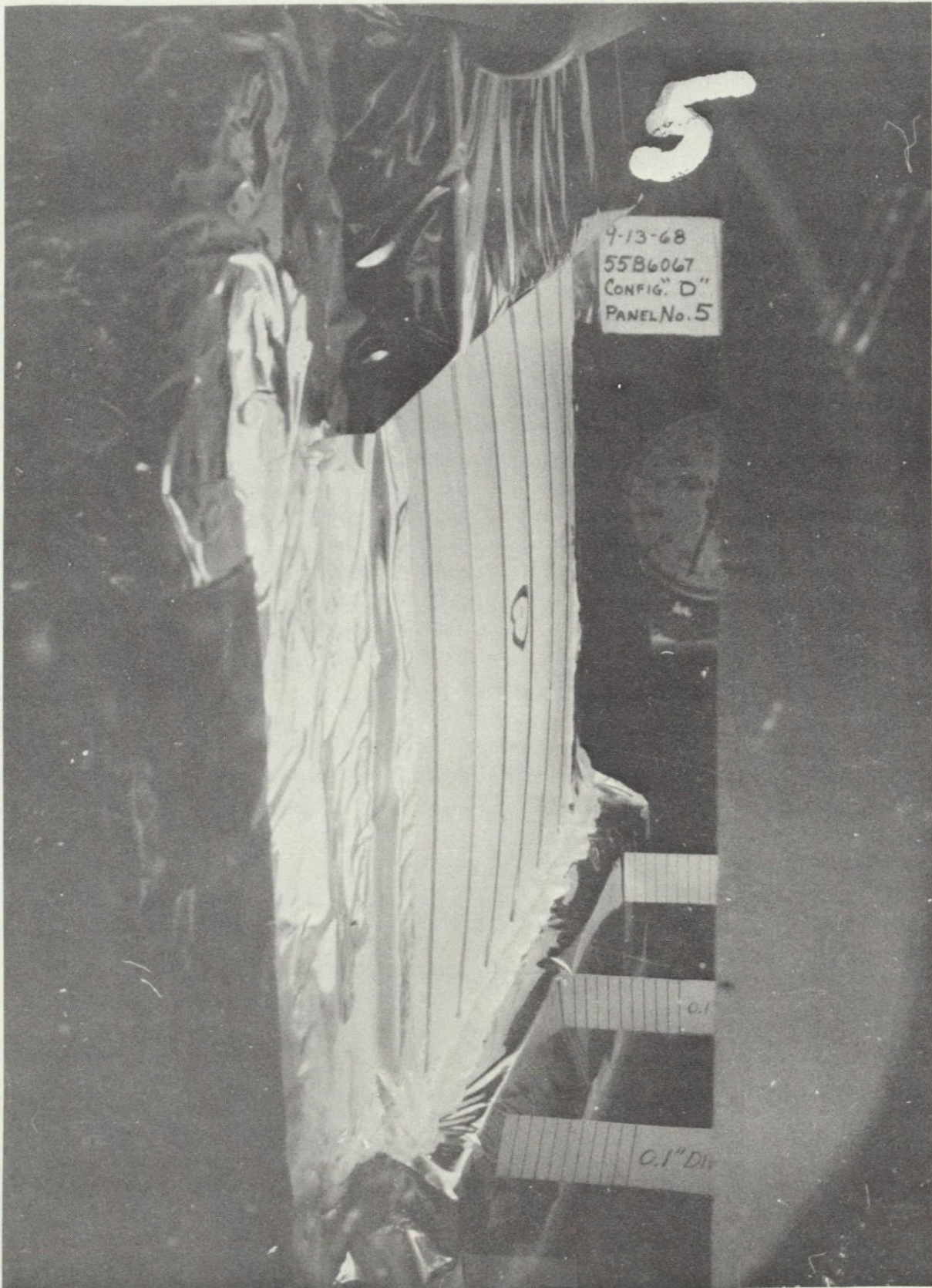


Figure 8-14. Specimen Panel D5 Showing Maximum Blister Formation — Back Face of Panel at LH_2 Temperature for 2 Hours Before Test

TABLE 8-5. TIME/TEMPERATURE HISTORY OF BLISTERING ON TEST PANELS

Panel	Time (sec) To Start of Blistering	Temp. (° F) of Panel When Blister Occurred
A1	101	225°
A2	118	385°
A3	124	363°
A4	128	455°
A5	144	385°
A6	140	420°
A7	133	450°
Average of A2 through A7: 410°		
B1	—	not recorded
B2	124.5 to 130.5	495° to 515°
B3	121 to 125	440° to 470°
B4	144	520°
B5	120	460°
B6	127	355°
B7	128	449°
Average of B2 through B7: 474°		
C1	—	not recorded
C2	119	385°
C3	141	488°
C4	135	475°
C5	224	475°
C6	138	510°
C7	113	307°
Average of C2 through C7: 440°		
D1	111.7 to 115.2	280° to 300°
D2	115.6 to 119.8	370° to 385°
D3	148	380°
D4	140	440°
D5	100	448°
D6	158	510°
D7	154	490°
Average of D2 through D7: 440°		

TABLE 8-6. ANALYSIS OF FIXED INSULATION TEST PANELS

Panel Number	Observations
A1	Partial foam and partial outer bond failures.
A2	Complete foam failure immediately below outer bondline.
A3	Complete foam failure immediately below outer bondline.
A4	Extensive foam failure immediately below outer bondline.
A5	Complete foam failure immediately below outer bondline.
A6	Partial foam failure immediately below outer bondline, overall wrinkling.
A7	Complete foam failure immediately below outer bondline.
B1	Complete foam failure immediately below outer bondline.
B2	Adhesive failure on outer bondline at MAM-adhesive interface, local Mylar to aluminum bond failure.
B3	Partial adhesive failure in outer bondline, general wrinkling.
B4	Complete adhesive failure in outer bondline at MAM-adhesive interface, local blister.
B5	Partial adhesive failure in outer bondline at MAM-adhesive interface, foam failed below outer bondline.
B6	Complete adhesive failure in outer bondline at MAM-adhesive interface, local Mylar-aluminum bond failure.
B7	Complete adhesive failure in outer bondline at MAM-adhesive interface.
C1	Complete foam failure immediately below outer bondline.
C2	Failure between Mylar and aluminum at outer face, some foam failure immediately below and foam failure above inner bondline.
C3	Same as C2.
C4	Same as C2 with more extensive Mylar-aluminum bond failure.
C5	Same as C2 with some small blisters in outer bondline.
C6	Foam failure immediately below outer bondline.
C7	Same as C2 with small blisters in outer bondline.
D1	Foam failure immediately below outer bondline, about 2 inch diameter.
D2	Foam failure immediately below outer bondline covering full area of panel.
D3	Same as D2.
D4	Approximately 1-inch diameter failure in foam below outer bondline, general wrinkling and blisters.
D5	Same as D2.
D6	No apparent failure, outer surface wrinkling and small amounts of blistering.
D7	Bond failure at MAM-adhesive interface on outer surface over full panel.

The primary mode of failure with the chilled CPR 32-2C foam panels (sets B and C) occurred at the outer bondline. With the heavier adhesive layer (set B), the mode was mostly adhesive failure at the MAM-adhesive interface and partially adhesive between the Mylar and aluminum in the composite MAM film. The latter may have been a secondary effect resulting from peeling as the blister grew. The tendency to peel would be greater with the thinner and lighter adhesive film used in the set B panels. In general, the blistering temperature for the CPR 32-2C foam panels was higher than that for the Goodyear 222 foam panels. The fact that the mode of failure for the CPR 32-2C panels was in the outer bond and in the face material suggests that the CPR foam could possibly withstand some slightly higher temperature exposures than those at which blistering occurred. Foam failure occurred with the panels in the C set immediately above the inner bondline. There was no explanation for this except that the faces of the C panels were not as stiff as the faces of the B panels. This difference in stiffness may have appreciably changed the stress at the inside bond interface.

Based on this test program, the B panel configuration appeared to be significantly better than the others evaluated. As will be seen in the results of the full scale tests described in Section 9, the B panel material configuration also was better than others evaluated for full scale ground hold conditions. However, all panels did blister, and blistering occurred at approximately the same temperature as the non-cryopumped panels previously tested. The blisters on the panel appeared to be less severe than those which occurred on non-cryopumped test panels and occurred at a different location. The non-cryopumped test panels failed in the foam along the MAM/adhesive interface. The latter failure was probably caused by excessive outgassing of either the adhesive, foam, or Mylar.

It can be concluded that the foam is not sufficiently porous to permit the gas in the foam cells to diffuse or flow away from the panel surface toward the colder, lower pressure region fast enough to prevent panel failure. Since all panels did blister, it must be assumed that the combined action of the positive internal pressure due to the panel being in a vacuum environment, and an internal pressure increase due to heating of the gases within the panel, was greater than the cryopumping action within the panel. Therefore, an internal pressure was allowed to build up which exceeded the strength of the foam and/or adhesive, and caused the panel to blister.

The configuration E panels (the spray-on foam panels obtained from North American Rockwell Corporation) were tested to the same procedure as the configuration A through D panels. It was of interest to observe their behavior during a simulated Atlas/Centaur ascent environment. Photographs of the foam after the completion of testing for three of the specimens are shown in Figures 8-15 through 8-17.

Two interesting characteristics of this foam insulation are evidenced in the photographs. First, the surface coating is badly charred, which would give extremely adverse outer surface thermodynamic properties for space coast. And second, even though the surface coating is charred and broken, the foam structure appears to be relatively unaffected.



Figure 8-15. Specimen Panel E1 after Test

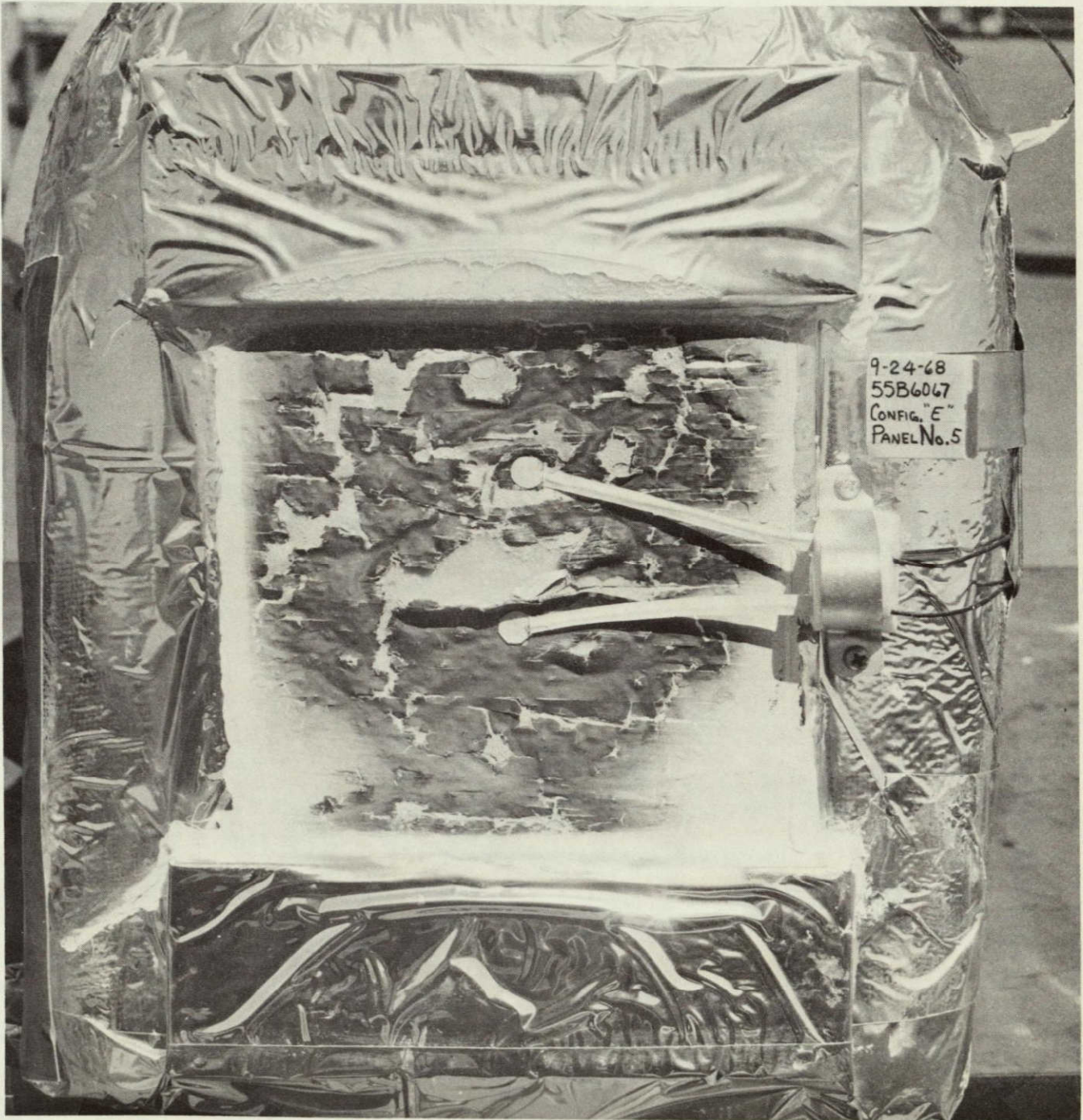


Figure 8-16. Specimen Panel E5 after Test

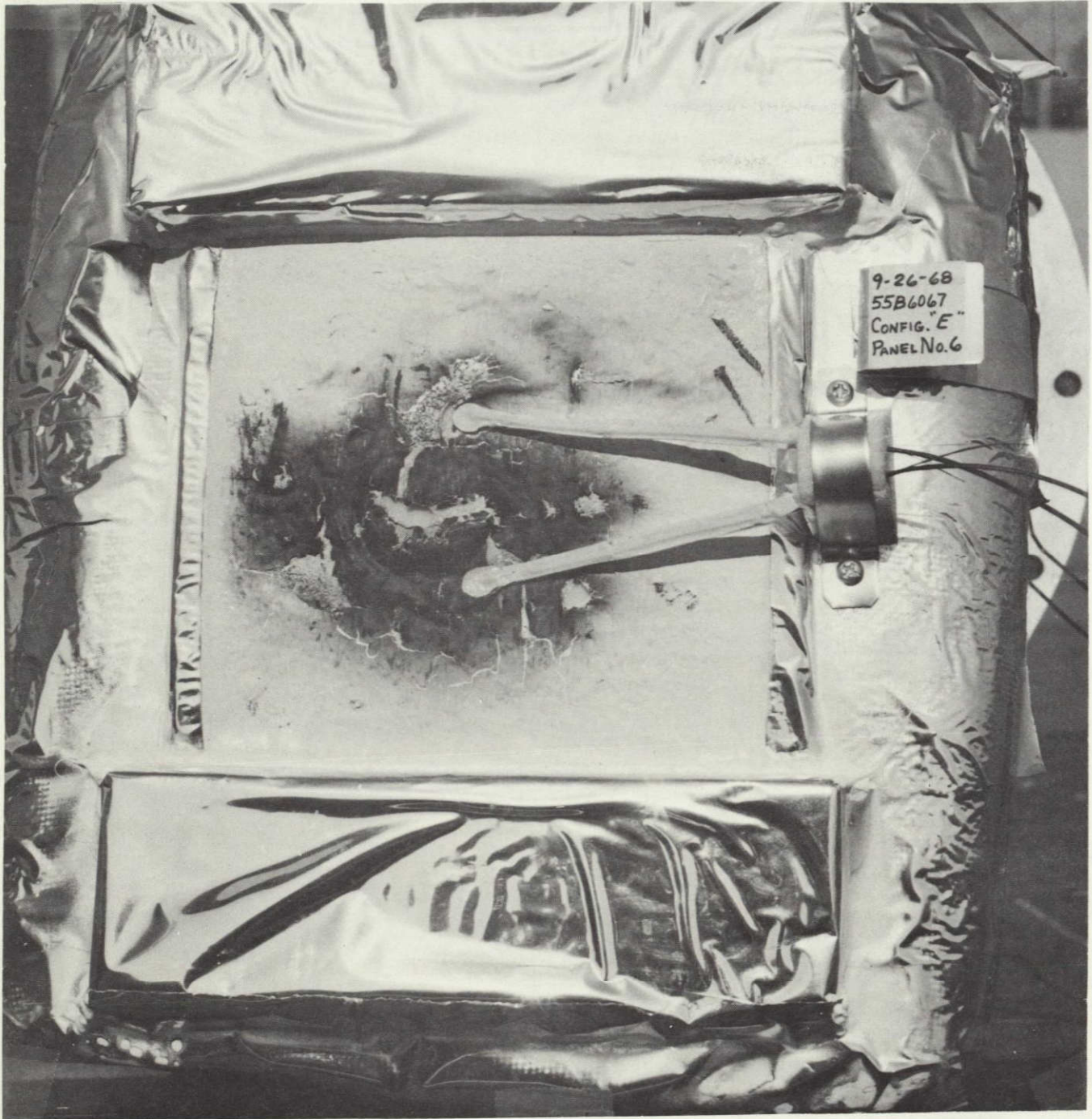


Figure 8-17. Specimen Panel E6 after Test

9

CRYOGENIC GROUND HOLD TEST

9.1 TEST OBJECTIVES

The cryogenic ground hold test was conducted in two phases. The first phase, referred to as the material evaluation test, was conducted with material systems A, B, and C on the T-9 test tank. The system designations refer to the material systems tabulated in Table 4-1. The objectives of the material evaluation test were:

1. Investigate the thermal degradation of Systems A, B, and C materials under repeated cryogenic tankings.
2. Investigate the seal and joint performance of Systems A, B, and C materials under repeated cryogenic tankings.
3. Evaluate the adequacy of the tank-to-panel adhesive bonds in both the grid and 100 percent patterns.

The second phase, referred to as the repair technique test, was conducted with repaired Systems A and B materials and new Systems D and E materials on the T-9 test tank. The objectives of the repair technique test were to:

1. Investigate the thermal degradation of the Systems D and E materials under repeated cryogenic tankings.
2. Investigate the seal and joint performance of Systems D and E materials under repeated cryogenic tankings.
3. Investigate the adequacy of repair techniques on Systems A and B materials.

9.2 TEST SPECIMEN CONFIGURATION

The test article was the T-9 stub tank, EID 55-7501, equipped with sealed foam insulation panels and a fiberglass strand constrictive wrap on the cylindrical section of the tank. The forward bulkhead of the tank was insulated with existing production type Centaur foam insulation. The insulated tank was tested in the S-4 test tower at the Sycamore Canyon test site. Figure 9-1 shows the S-4 test tower with the T-9 test tank installed.

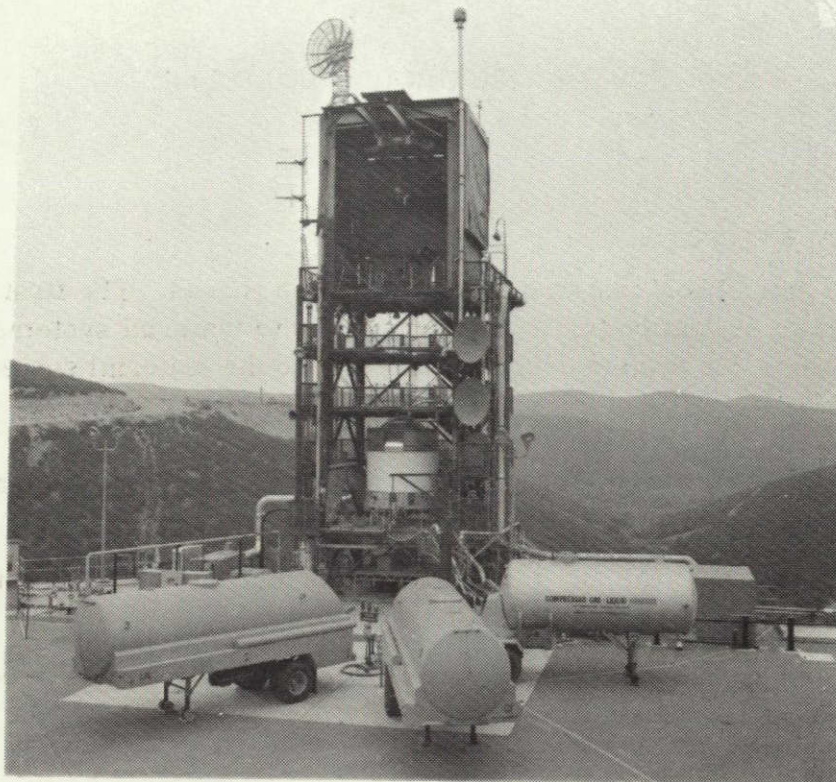


Figure 9-1. Sycamore Canyon S-4 Test Tower With The T-9 Test Tank Installed

9.2.1 SEALED FOAM PANEL CONFIGURATION.

9.2.1.1 Panel Configuration for Material Evaluation Test. As stated previously, three types of material systems were tested during this phase of the cryogenic ground hold test. The three material systems are defined as Systems A, B, and C and are tabulated in Table 4-1. The location of the panels on the T-9 tank is shown in Figure 9-2, and is shown in flat pattern in Figure 9-3. Figure 9-3 also shows the tank bonding system for the panels, the Convair drawing part number, and three areas where panels had been damaged and repaired prior to the start of testing. In addition, each panel has been arbitrarily assigned a number for convenience in identifying the panels. The panel closeouts at the forward and aft tank rings are shown in Figure 9-4.

9.2.1.2 Panel Configuration for Report Technique Test. After completion of the material evaluation tests, the System C panels were removed and replaced with Systems D and E panels as shown in Figure 9-5 and in flat pattern in Figure 9-6. Also, repairs were made on those areas in the Systems A and B panels that had degraded during the material evaluation test, or had been cut open during the post test material evaluation. These areas are defined in detail later in this report.

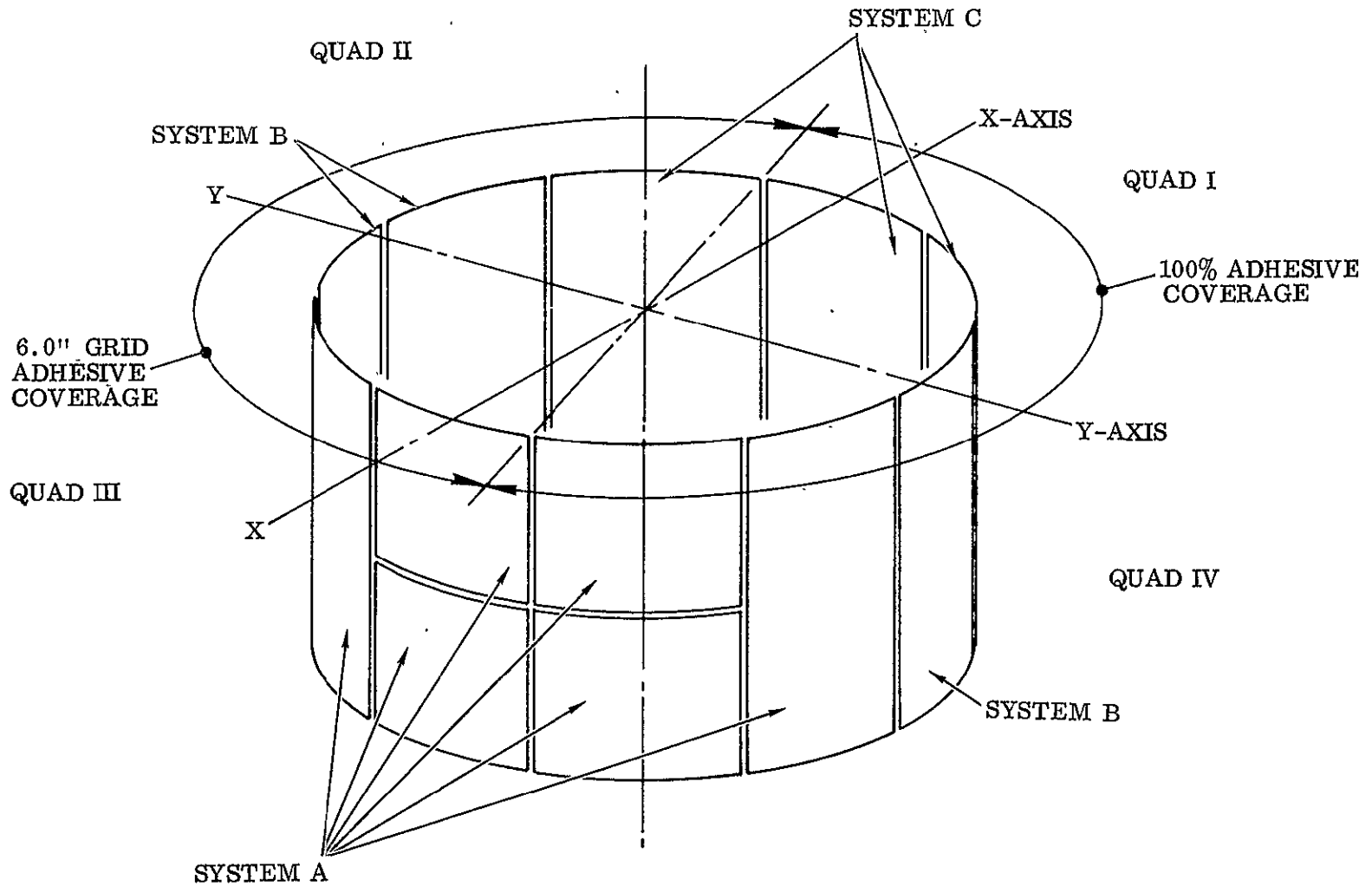


Figure 9-2. T-9 Test Tank Insulation Panel Configuration for the Material Evaluation Test

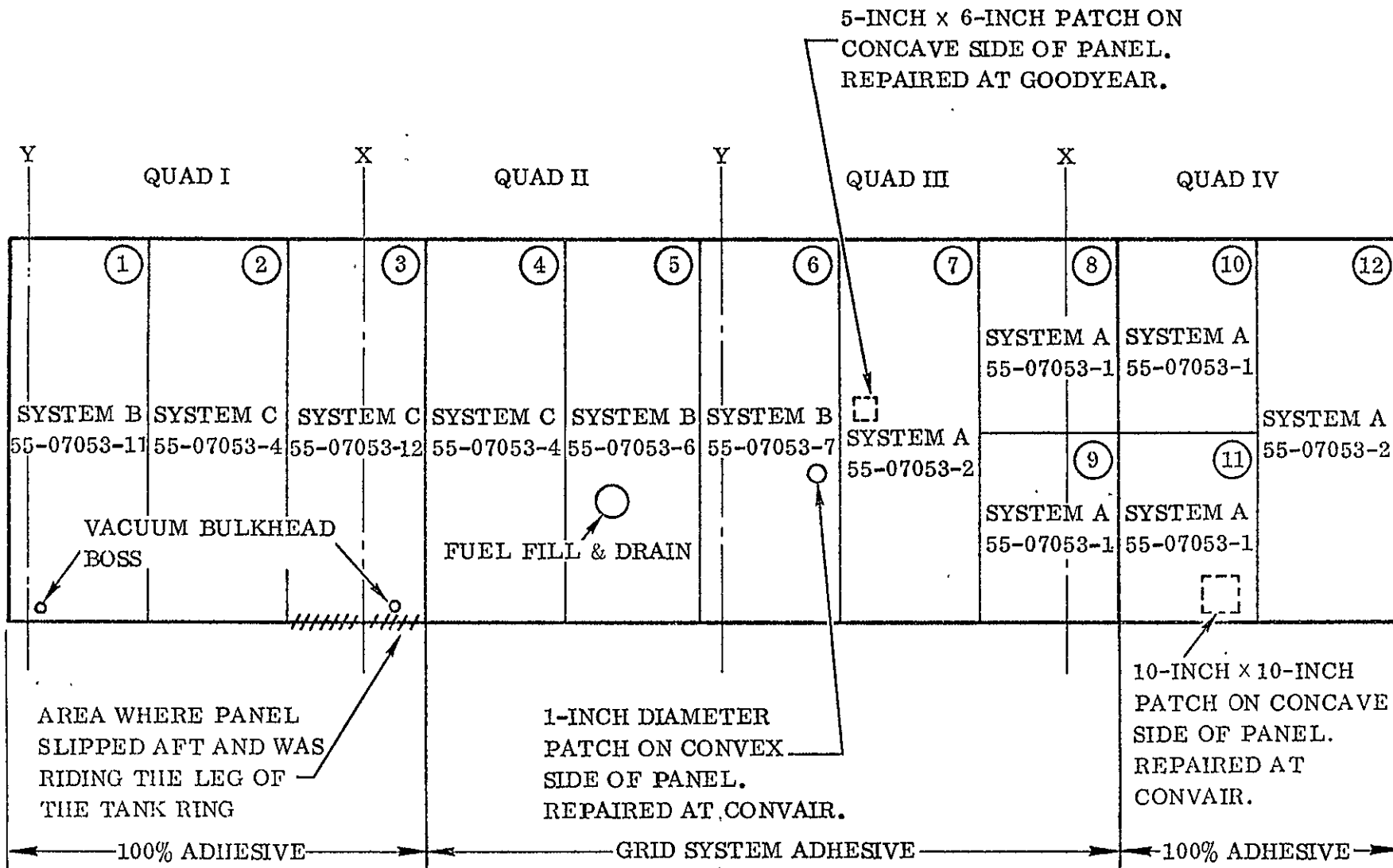


Figure 9-3. Arrangement of Insulation Panels on the T-9 Tank for the Material Evaluation Tests

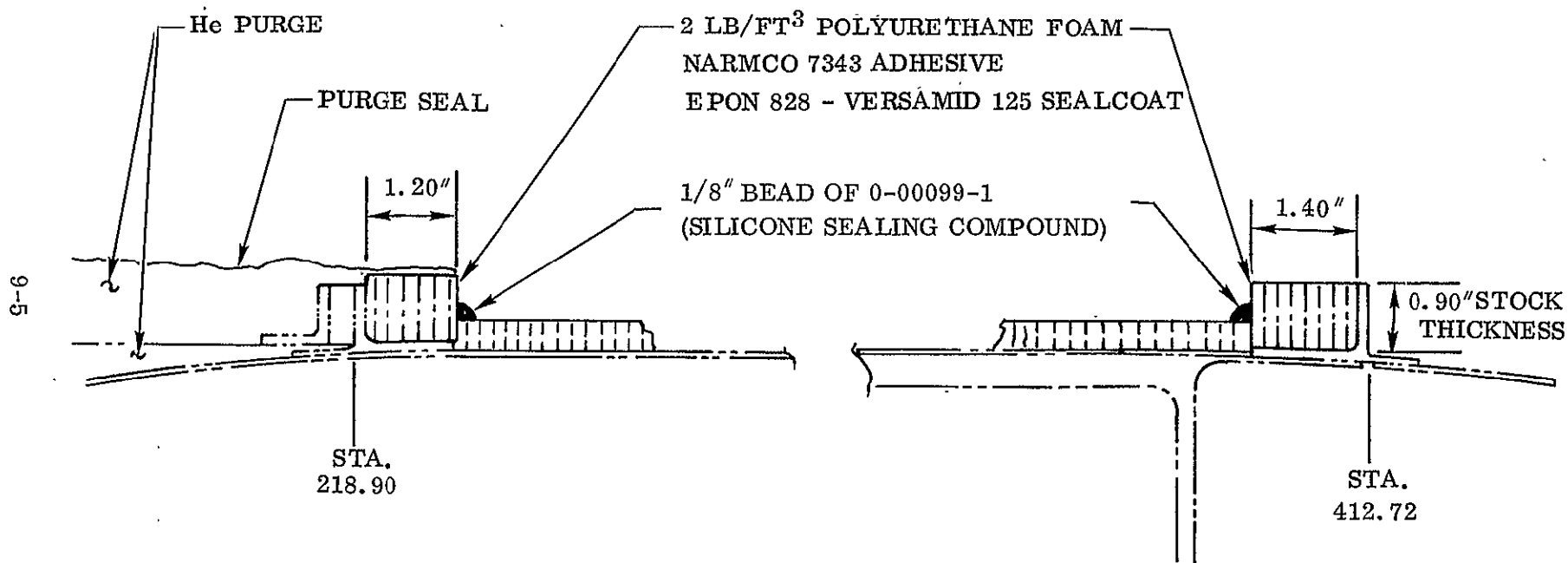
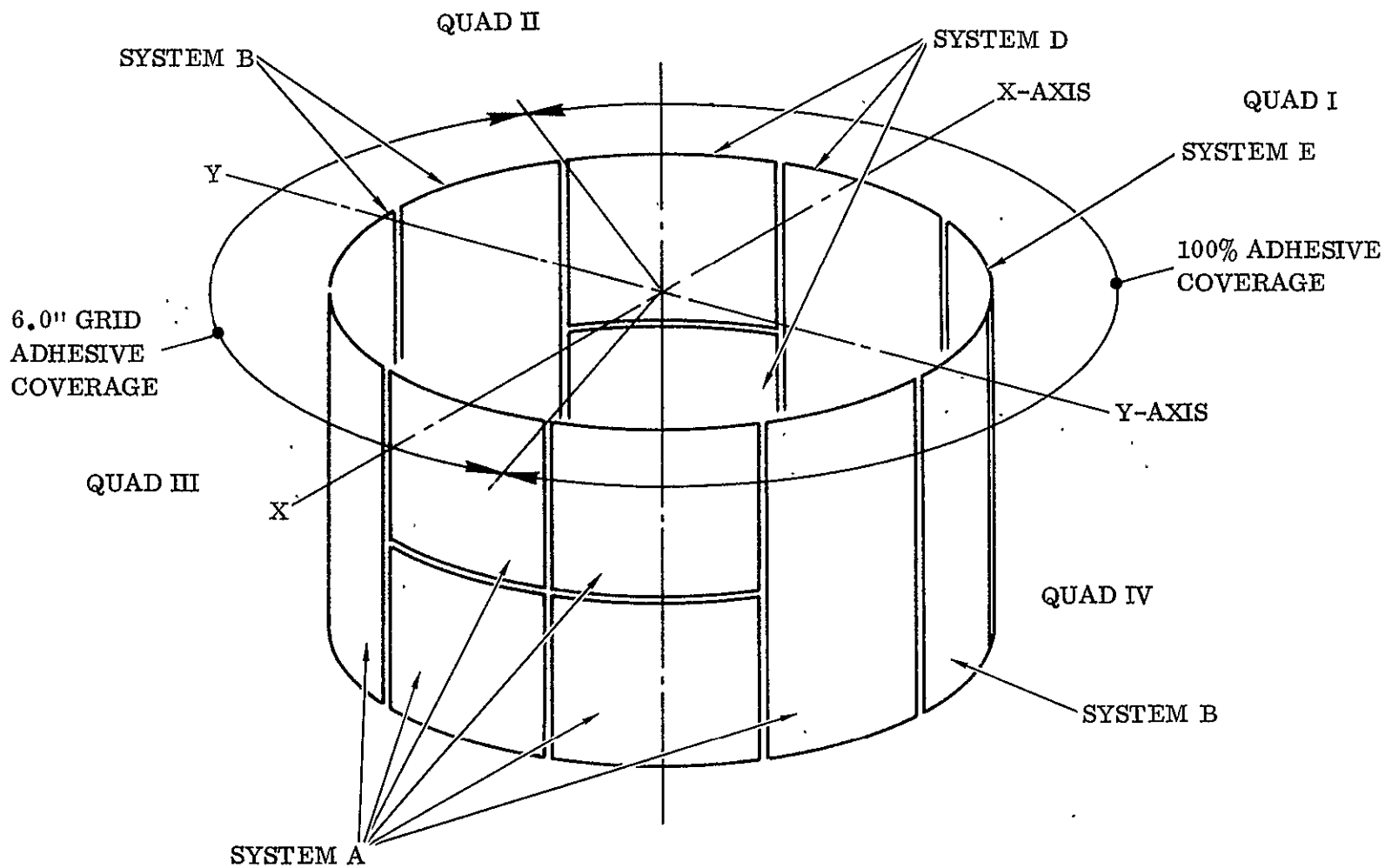


Figure 9-4. T-9 Test Tank Station 218.9 and Station 412.7 Tank Rings Insulation



9-6

Figure 9-5. T-9 Test Tank Insulation Panel Configuration for the Repair Technique Test

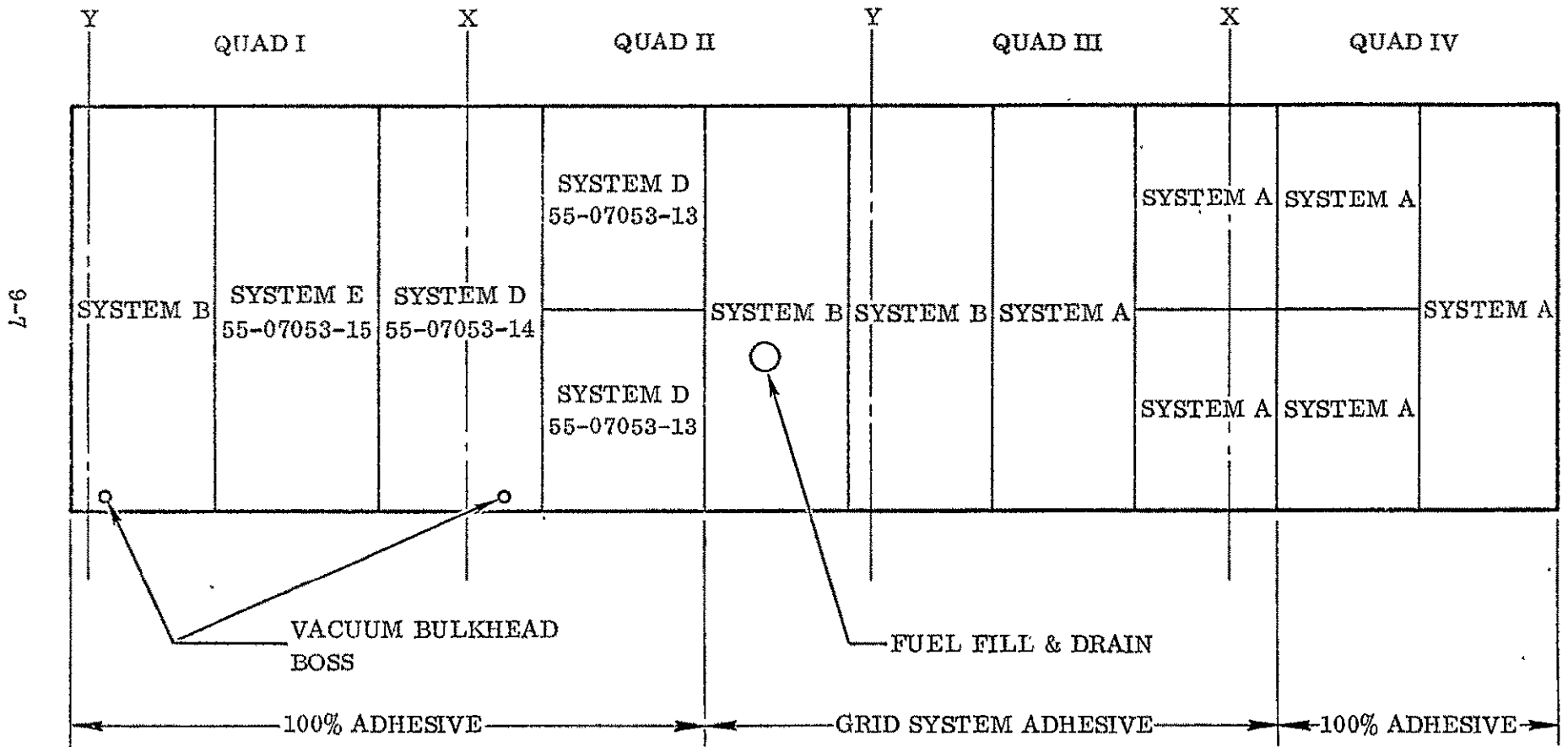


Figure 9-6. Arrangement of Insulation Panels on the T-9 Tank for the Repair Technique Tests

9.2.2 SEALED FOAM PROTECTIVE COVERING CONFIGURATION. As explained previously, a rubber impregnated fiberglass erosion cloth was bonded to the sealed foam insulation to protect the panels from erosion during periods of aerodynamic heating and loading. The erosion cloth configuration is shown in Figure 9-7.

9.2.3 CONSTRICTIVE WRAP CONFIGURATION. As explained previously, a fiberglass constrictive wrap was installed on the T-9 tank to maintain a constrictive force on the sealed foam insulation panels. The installed configuration of the wrap is shown in Figure 9-8.

9.2.4 INSTRUMENTATION CONFIGURATION. Instrumentation consisted of (1) four closed circuit television cameras (one for each quadrant) with commutated tape recorder, (2) dowels of various thicknesses dispersed on the tank to monitor frost thickness (via video), and (3) thermocouples mounted on the external surface of the insulation. Figure 9-9 shows the frost thickness dowel configuration, and Figure 9-10 shows the location of thermocouple measurements.

9.3 TEST PROCEDURE

9.3.1 MATERIAL EVALUATION TEST. The material evaluation test phase consisted of six tankings and de-tankings of LH₂ and LN₂. A step-by-step procedure follows:

1. First, Second, Third, and Fourth Tests
 - a. The oxidizer tank was filled with LN₂.
 - b. The fuel tank was filled with LH₂.
 - c. The oxidizer tank pressure was raised to 20.0 ± 0.5 psig.
 - d. The fuel tank pressure was adjusted to 5.8 ± 0.5 psig.
 - e. The tank was held in this condition for two hours.
 - f. The fuel tank pressure was raised to 12.0 ± 0.5 psig and stabilized for one minute.
 - g. The fuel tank pressure was decreased to 5.8 ± 1.5 psig.
 - h. Propellants were detanked and both tanks were allowed to return to ambient temperature.
 - i. The test specimens were inspected and photographed.
2. Fifth Test
 - a. Steps a. thru g. of paragraph 1. were performed.
 - b. The oxidizer tank pressure was increased to 38.0 ± 0.5 psig.
 - c. The fuel tank pressure was increased to 25.0 ± 0.5 psig, and stabilized for one minute.

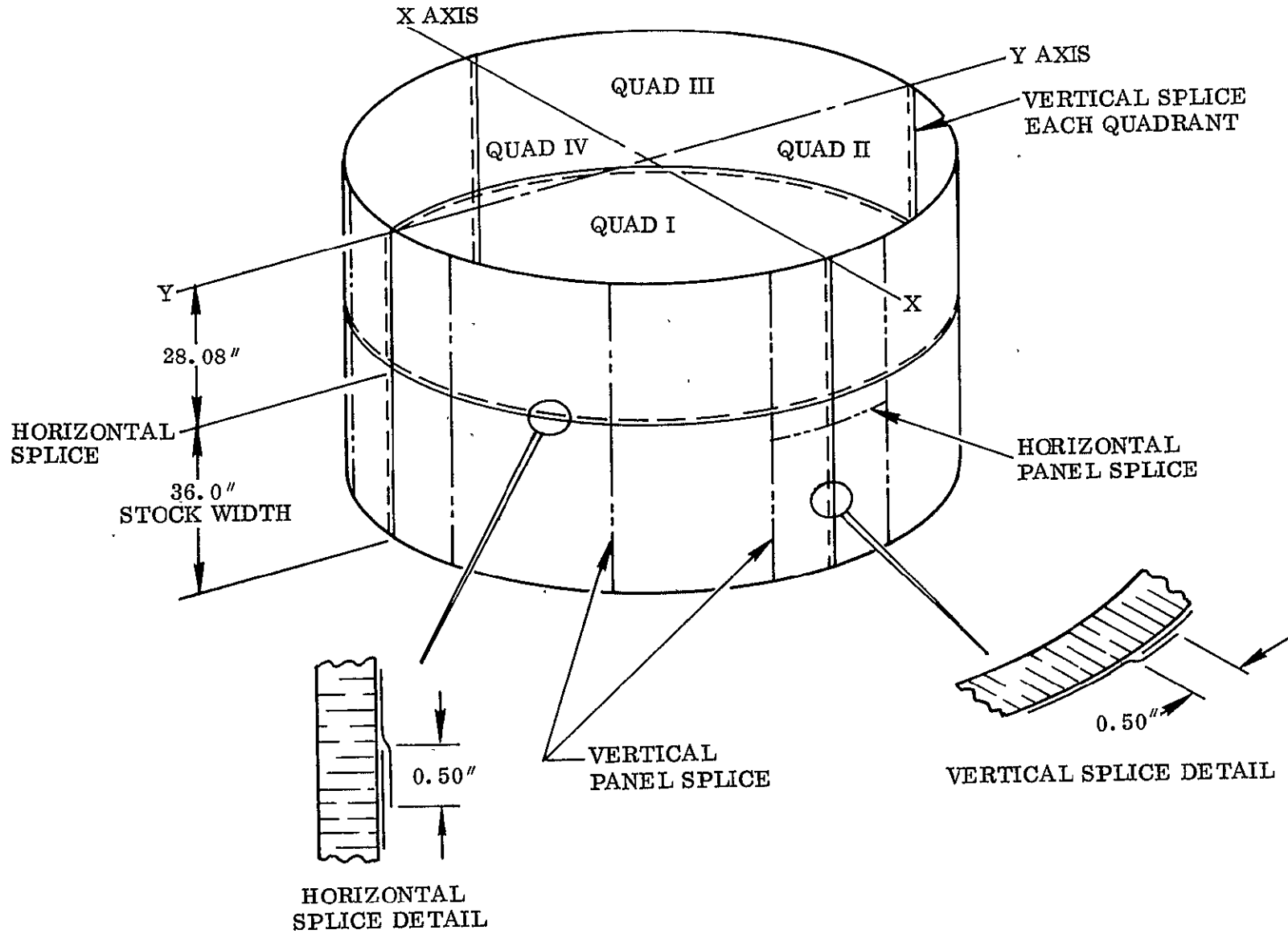


Figure 9-7. T-9 Test Tank Erosion Cloth Cover Installation

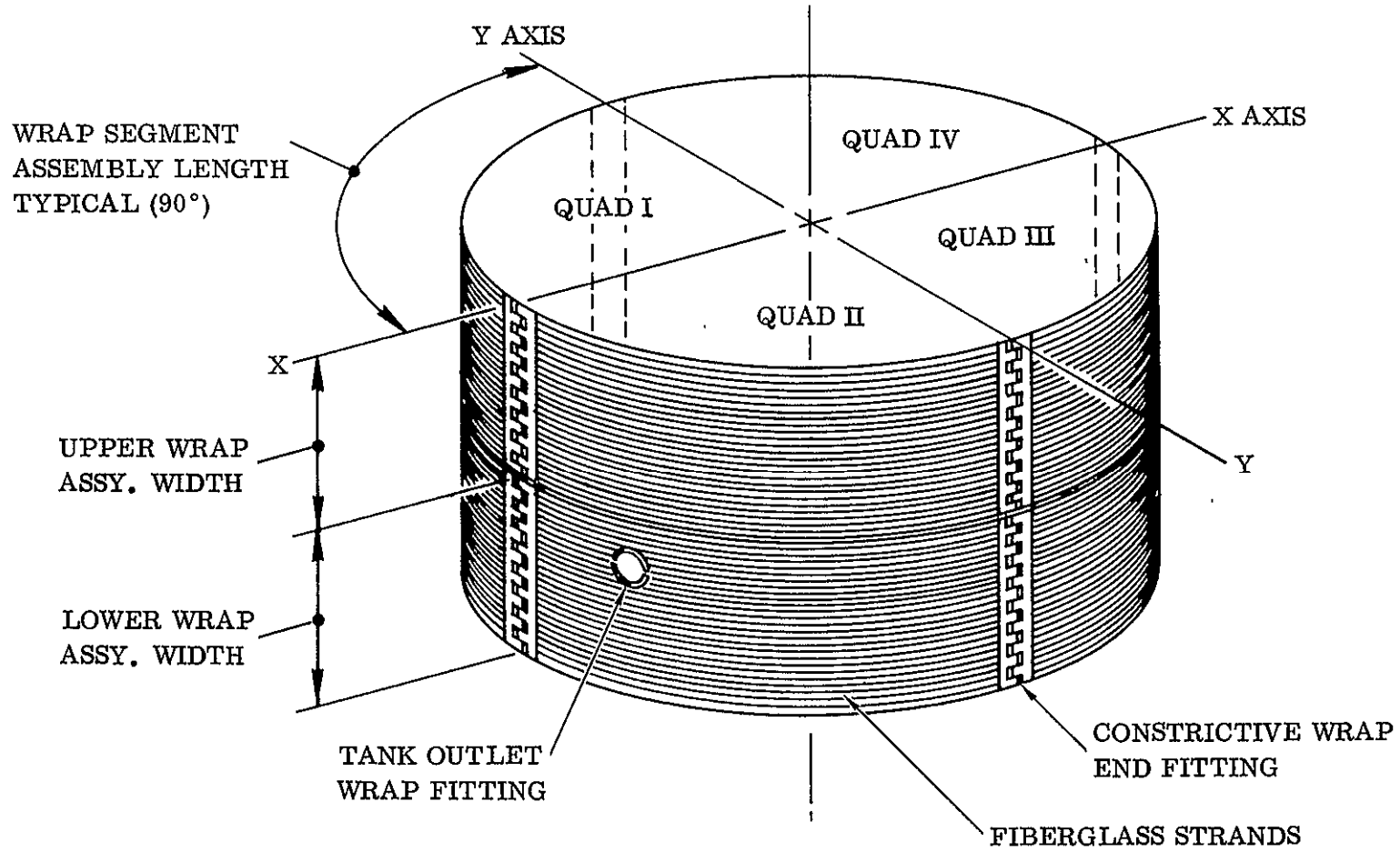


Figure 9-8. T-9 Test Tank Constrictive Wrap Configuration

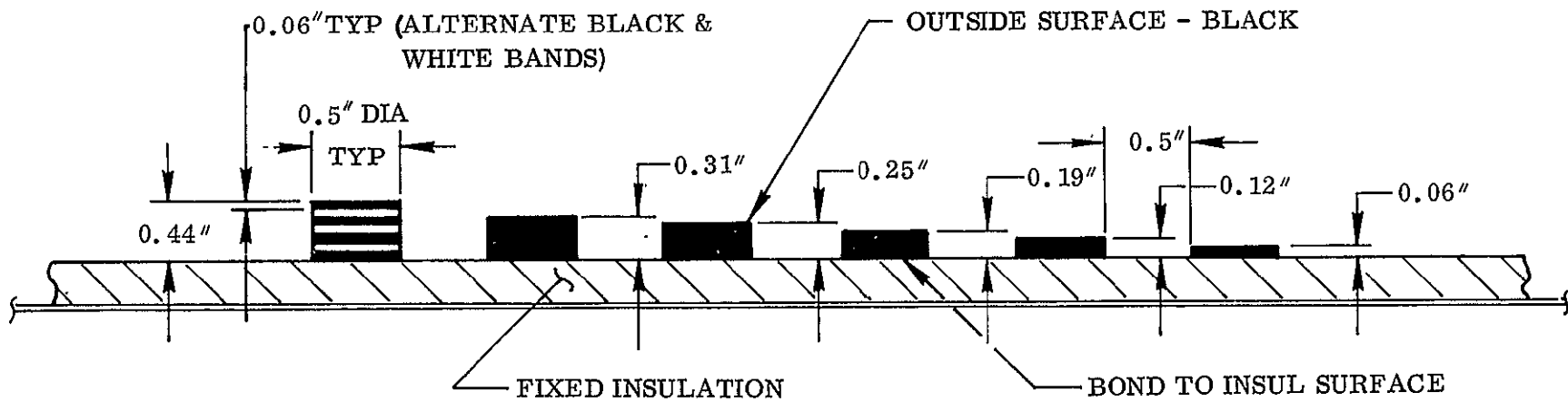
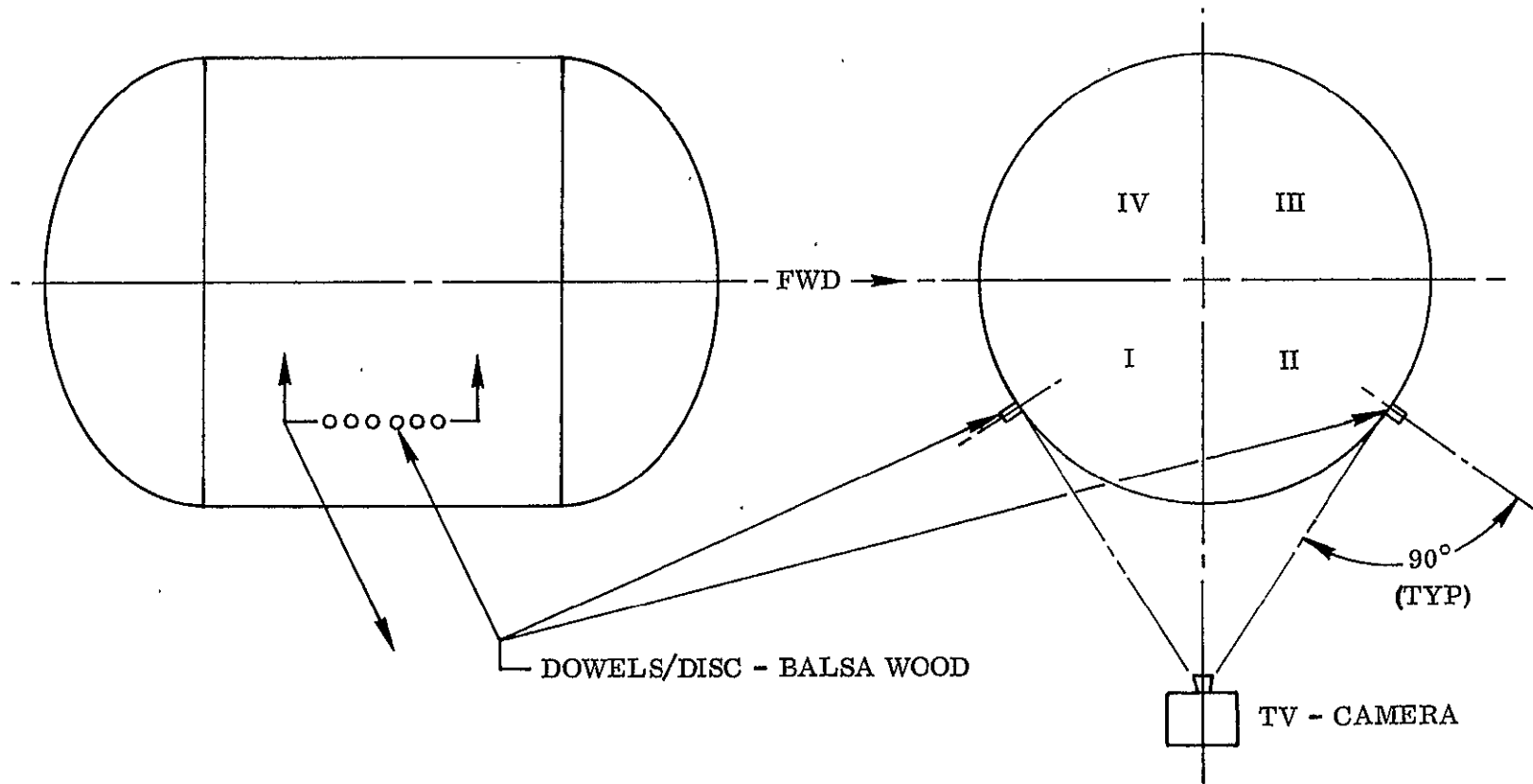


Figure 9-9. T-9 Test Frost Determination Instrumentation

- d. The fuel tank pressure was reduced to 5.8 ± 1.5 psig.
 - e. The oxidizer tank pressure was reduced to 20.0 ± 0.5 psig.
 - f. Propellants were detanked and both tanks were allowed to return to ambient temperature.
 - g. The test specimens were inspected and photographed.
3. Sixth Test
- a. Steps a. thru e. of paragraph 1. were performed.
 - b. The oxidizer tank pressure was increased to 38.0 ± 0.5 psig.
 - c. The fuel tank pressure was increased to 25.0 ± 0.5 psig, and stabilized for one minute.
 - d. The fuel tank pressure was reduced to 5.8 ± 1.5 psig.
 - e. The oxidizer tank pressure was reduced to 20.0 ± 0.5 psig.
 - f. Steps b. thru e. were repeated two additional times.
 - g. Propellants were detanked and both tanks were allowed to return to ambient temperature.
 - h. The test specimens were inspected and photographed.

These procedures are shown schematically in Figure 9-11.

9.3.2 REPAIR TECHNIQUE TESTS. The repair technique test phase consisted of four additional tankings and de-tankings of LH₂ and LN₂, performed in conjunction with the structural test of the OAO nose fairing barrel section. A step-by-step procedure follows:

1. Seventh Test
- a. The oxidizer tank was filled with LN₂.
 - b. The fuel tank was filled with LH₂.
 - c. The oxidizer tank pressure was increased to 30.0 ± 1.0 psig.
 - d. The fuel tank pressure was increased to 18.1 ± 0.5 psig.
 - e. An axial compressive load of 70,000 pounds was applied.
 - f. A shear load of 15,300 pounds was applied along the minus X axis.
 - g. The axial load was reduced to 19,400 pounds.
 - h. The shear load was reduced to 15,000 pounds.
 - i. The shear load was reduced to zero.

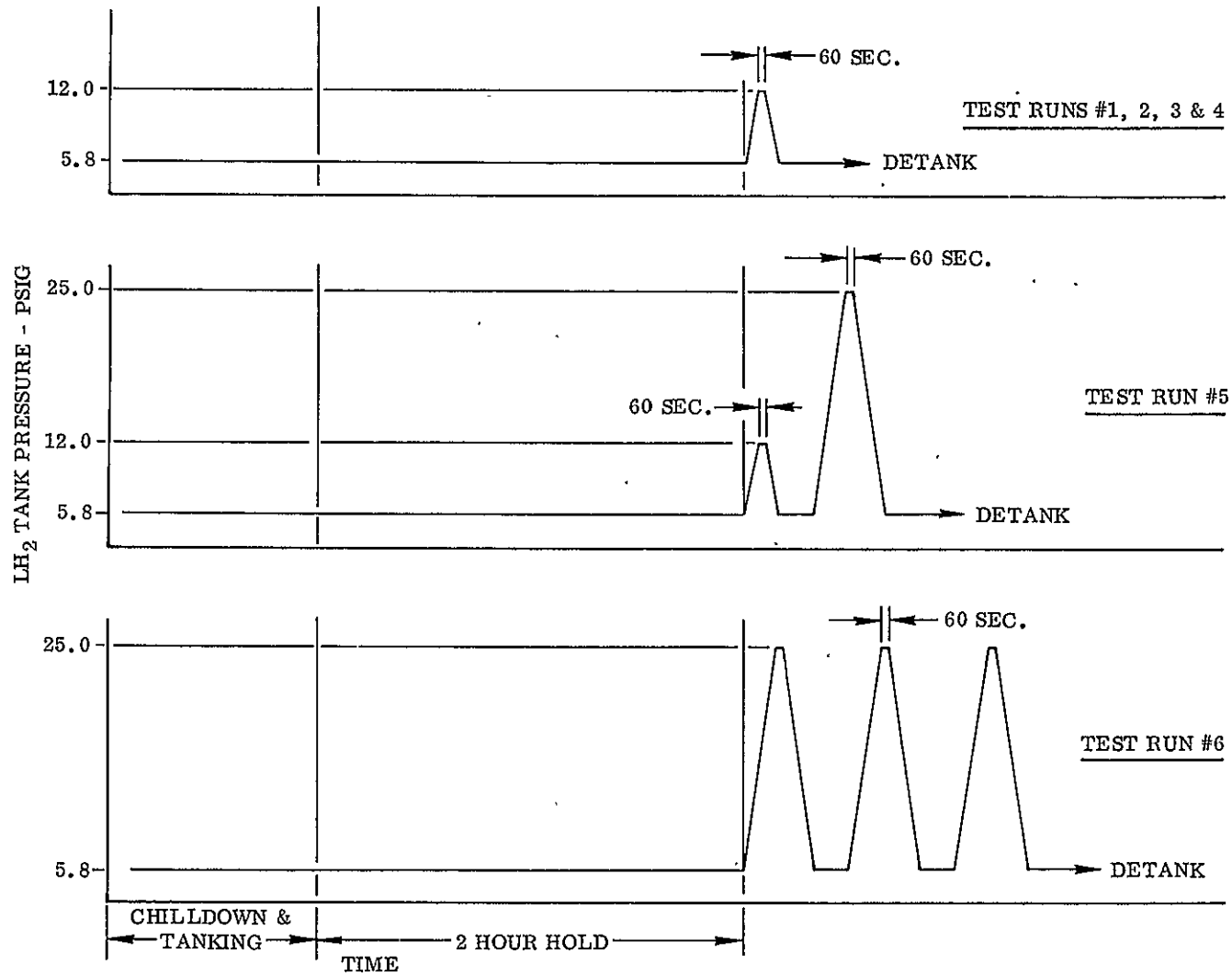


Figure 9-11. T-9 LH₂ Tank Pressure Cycles

- j. The axial load was reduced to zero.
- k. The fuel tank pressure was decreased to 5.0 ± 1.0 psig.
- l. The oxidizer tank pressure was decreased to 10.0 ± 1.0 psig.
- m. Propellants were detanked and both tanks were allowed to return to ambient temperature.
- n. The test specimens were inspected and photographed.

During this test the tank contained cryogenics for approximately four hours.

2. Eighth Test

- a. Steps a. thru d. of Paragraph 1. (Seventh Test) were performed.
- b. An axial compressive load of 70,000 pounds was applied.
- c. A shear load of 15,000 pounds was applied along the plus X axis.
- d. The axial load was reduced to 19,400 pounds.
- e. The shear load was reduced to 16,000 pounds.
- f. The shear load was reduced to zero.
- g. The axial load was reduced to zero.
- h. Steps k. thru n. of Paragraph 1. (Seventh Test) were performed.

During this test the tank contained cryogenics for approximately four hours.

3. Ninth Test

- a. Steps a. thru d. of Paragraph 1. (Seventh Test) were performed.
- b. An axial compressive load of 70,000 pounds was applied.
- c. A shear load of 20,800 pounds was applied along the plus X axis.
- d. The axial load was reduced to 19,400 pounds.
- e. The shear load was increased to 24,300 pounds.
- f. The shear load was reduced to zero.
- g. The axial load was reduced to zero.
- h. An axial compressive load of 70,000 pounds was applied.
- i. A shear load of 20,800 pounds was applied along the plus X axis.
- j. The shear load was reduced to zero.
- k. The axial load was reduced to zero.
- l. Steps k. thru n. of Paragraph 1. (Seventh Test) were performed.

During this test the tank contained cryogenics for approximately 4-1/2 hours.

4. Tenth Test

- a. Steps a. thru d. of Paragraph 1. (Seventh Test) were performed.
- b. An axial compressive load of 70,000 pounds was applied.
- c. A shear load of 19,100 pounds was applied along the minus X axis.
- d. The shear load was reduced to zero.
- e. The axial load was reduced to zero.
- f. An axial load of 19,400 pounds was applied.
- g. A shear load of 25,200 pounds was applied along the minus X axis.
- h. The shear load was reduced to zero.
- i. The axial load was reduced to zero.
- j. An axial compressive load of 70,000 pounds was applied.
- k. A shear load of 20,800 pounds was applied along the minus X axis.
- l. The shear load was reduced to zero.
- m. The axial load was reduced to zero.
- n. Steps k. thru n. of Paragraph 1. (Seventh Test) were performed.

During this test the tank contained cryogenics for approximately 3-1/2 hours.

9.4 SUMMARY OF TEST RESULTS

9.4.1 MATERIAL EVALUATION TESTS. The complete results of the material evaluation tests (tests 1 through 6) are documented in Reference 9-1. A summary evaluation of the three systems tested is shown in Figure 9-12. It is apparent from Figure 9-12 that all the material failures can be classified into four general modes of failure, namely:

1. Erosion cloth to outer MAM failure
2. Outer MAM/adhesive/foam interface failure
3. Panel-to-tank bond failure
4. Panel joint-doubler failure.

Seventeen areas on the foam panels, representative of all four material failure classes, were sectioned after the sixth tanking test. The location of the section cut areas are shown on Figure 9-12, and the results of the sectioning are tabulated in Table 9-1.

TABLE 9-1. EVALUATION OF MATERIAL FAILURES DURING THE T-9 MATERIAL EVALUATION TEST

Type of Failure	System	Location No. (Ref. Fig. 9-12)	Remarks
Erosion Cloth to Outer MAM	A	12	Small blister, non-propagating possibly there before test.
	A	13	Heated Area, 1 in. x 3 in. between strands.
	A	14	Heated Area, 1 in. x 1 in. between strands.
Outer MAM-Adhesive-Foam Interface	B	1	Non-cryopumping.
	C	2	Longitudinal external wrinkles.
	C	4	
	C	5	Non-pressure holding, failure above splice in foam.
	B	6	Outside inactive, failure below splice in foam.
	A	9	Long pressure holding.
	C	10	Hard spot prior to testing.
	A	11	Small hard spot in large blister.
	A	13	Heated blistered area.
Panel-to-Tank Bond	C	2	Not opened, may be extension of #10.
	C	3 & 10	Hard spot prior to test, no bond to begin with.
	A	11	Small hard spot in large blister, 1-1/2 in. wide grid unbonded in one area.
	A	15	Grid area, grid broken.
Panel Joint-Doubler	C	3	No bond to MAM doubler, foam broken out.
	A	8	No bond to MAM doubler.
	C	16	No bond to MAM doubler, foam broken out.

As seen in Figure 9-12, several outer MAM/adhesive/foam interface failures occurred during the warm-up period following the first tanking. The failures were caused by small leaks in the MAM hermetic seal which allowed air to be cryopumped into the panels over the two-hour hold period. During the relatively short warmup period, the cryopumped air vaporized rapidly and was not able to vent quickly enough to prevent a pressure buildup. Consequently, a pressure was built up between the outer MAM and the foam, causing the outer MAM to bulge, or blister. On succeeding tankings, the blisters cryopumped down tight during the tanking and hold periods, but again reappeared, and in most cases grew larger, during de-tanking. As seen in Figure 9-12, the outer MAM covering of all System C panels was almost entirely delaminated by the end of the third test. All System A panels showed external blistering except panel numbers 8 and 9. The System B panels showed the best results. It was assumed the oven-cure film-type adhesive of System B provided, in effect, an additional barrier to leaks during cryopumping, and that the type of foam did not significantly affect the performance of the systems. Based on this reasoning, the foam of System A and the adhesive of System B were used in Systems D and E.

It can also be seen from Figure 9-12 that some panels bonded to the tank with the grid adhesive system did blister between the panel and tank during the tests, while no blisters between the panel and tank occurred during the tests on panels which had a 100 percent adhesive bond area. Prior to the start of testing, several small "bumps" were noted in two of the panels (panel numbers 2 and 3 in Figure 9-12) which had been bonded to the tank using the 100 percent adhesive system. These "bumps" were actually air gaps between the panel and tank, and they occurred during the bonding of the panels to the tank. However, the bumps neither grew in size or number nor caused the panels to bulge during the tests, as occurred on panel numbers 7 and 9 of Figure 9-12. This indicated that the air gaps in panels 2 and 3 were sealed and no outside gases were being cryopumped into the air gaps during the tests.

The two areas subjected to simulated aero-heating, shown on panel Numbers 7 and 8, were part of a special test which is explained more fully in Subsection 9.5. The results of the thermocouple and frost instrumentation are also explained in Subsection 9.5.

Photographs of the final condition of the insulation surface in all four quadrants are shown in Figures 9-13 through 9-17. The outline of all failed areas has been marked on the insulation, and corresponds to the areas defined in Figure 9-12.

9.4.2 REPAIR TECHNIQUE TESTS. The complete results of the repair technique tests (test Numbers 7 through 10) are documented in Reference 9-2. A summary evaluation of the systems tested is shown in Figure 9-18. As seen in the figure, the number and degree of failed areas were significantly less than in the material evaluation tests, even though the Systems A and B panels had been failed and repaired in the previous material evaluation tests.

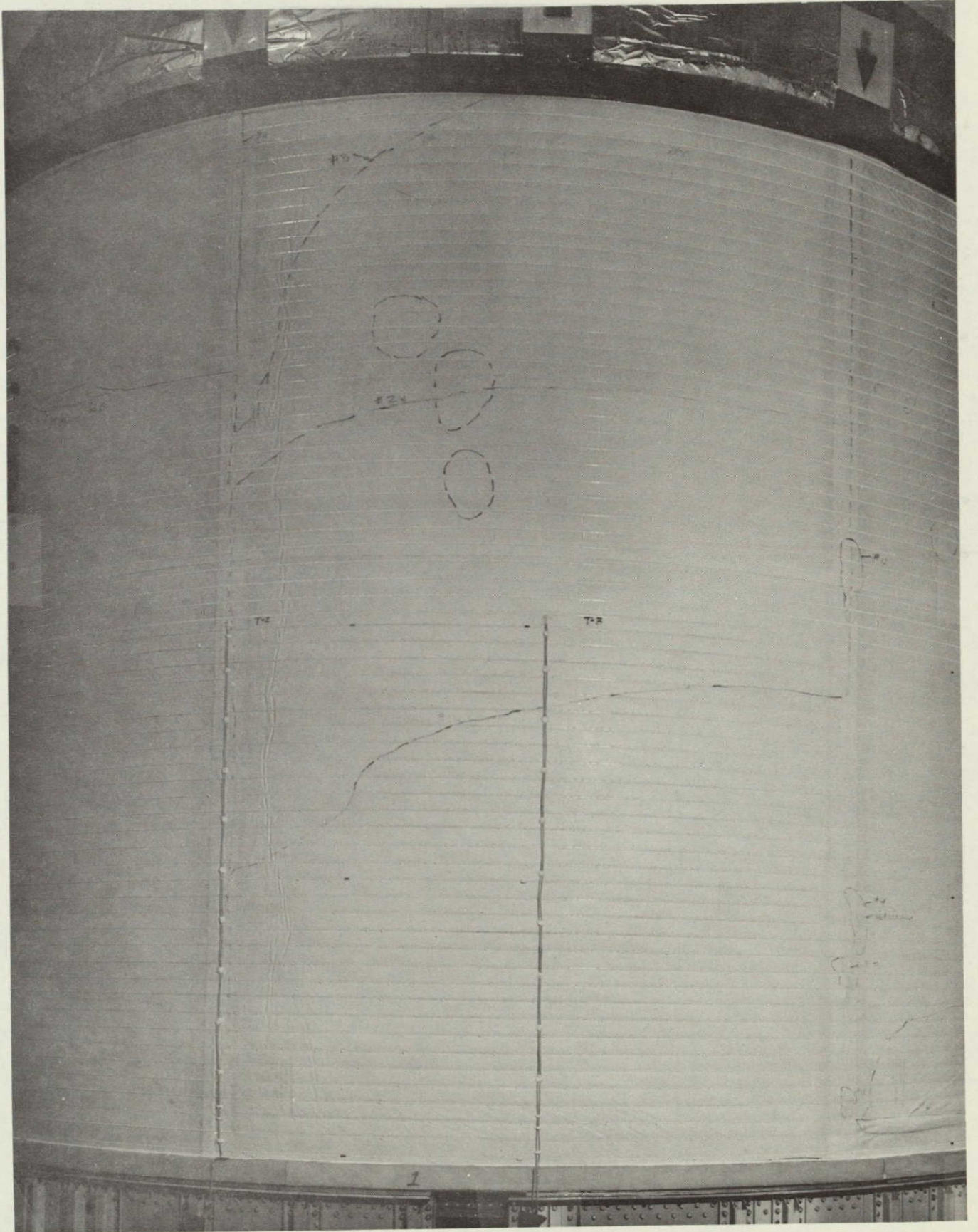


Figure 9-13. T-9 Test Tank after Sixth Tanking — Quad I

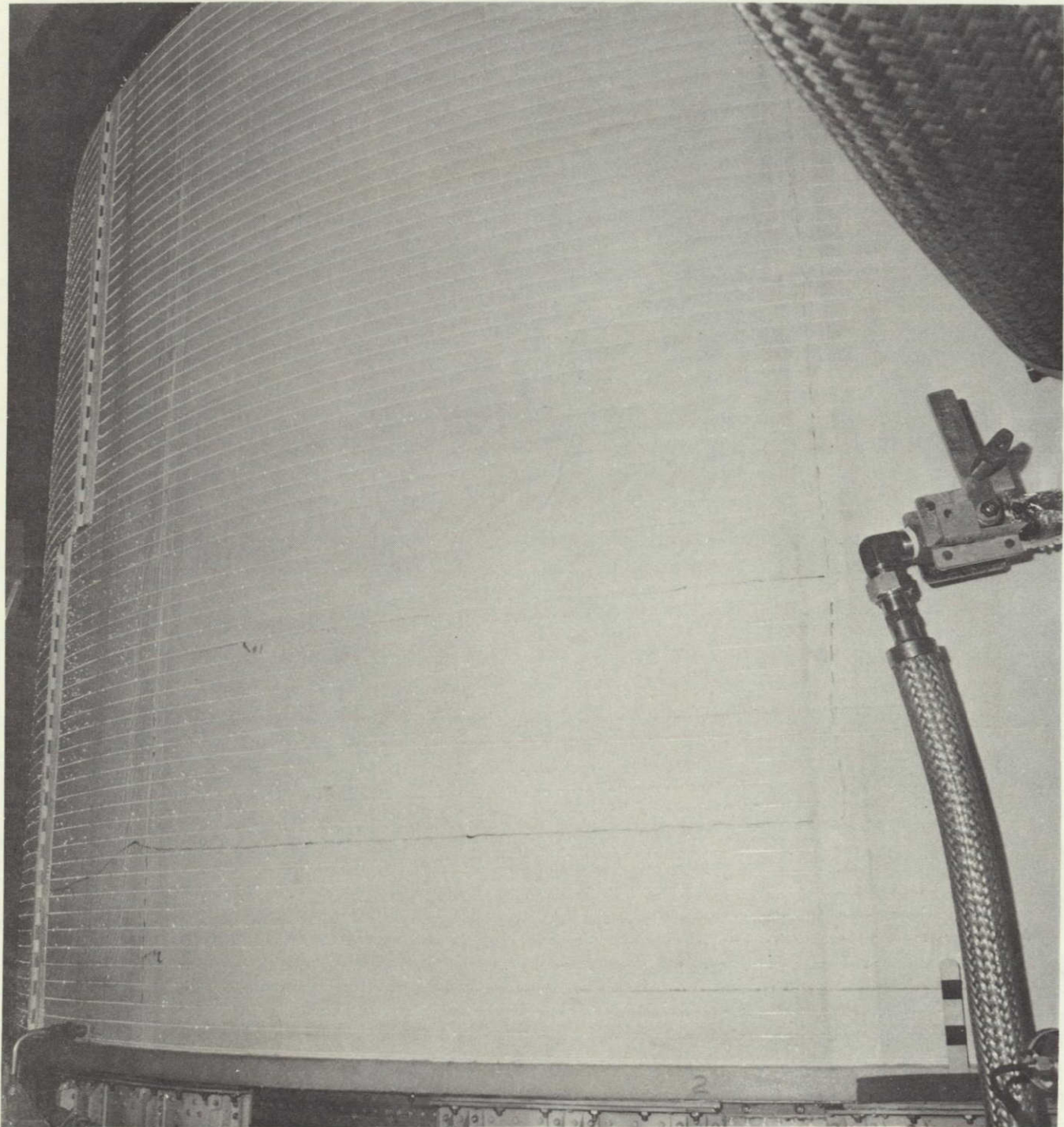


Figure 9-14. T-9 Test Tank after Sixth Tanking — Quad II

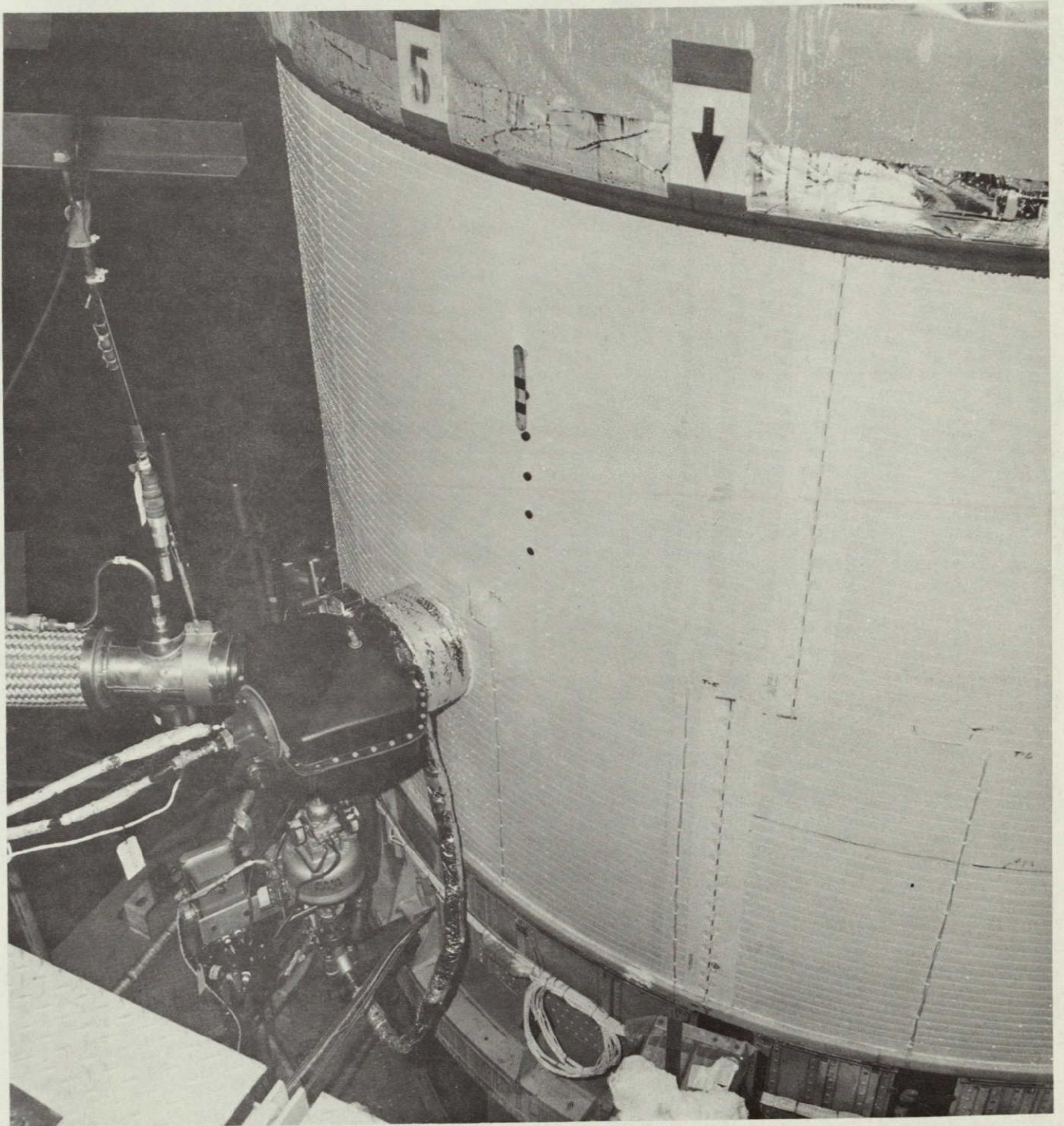


Figure 9-15. T-9 Test Tank after Sixth Tanking — Quad II and III

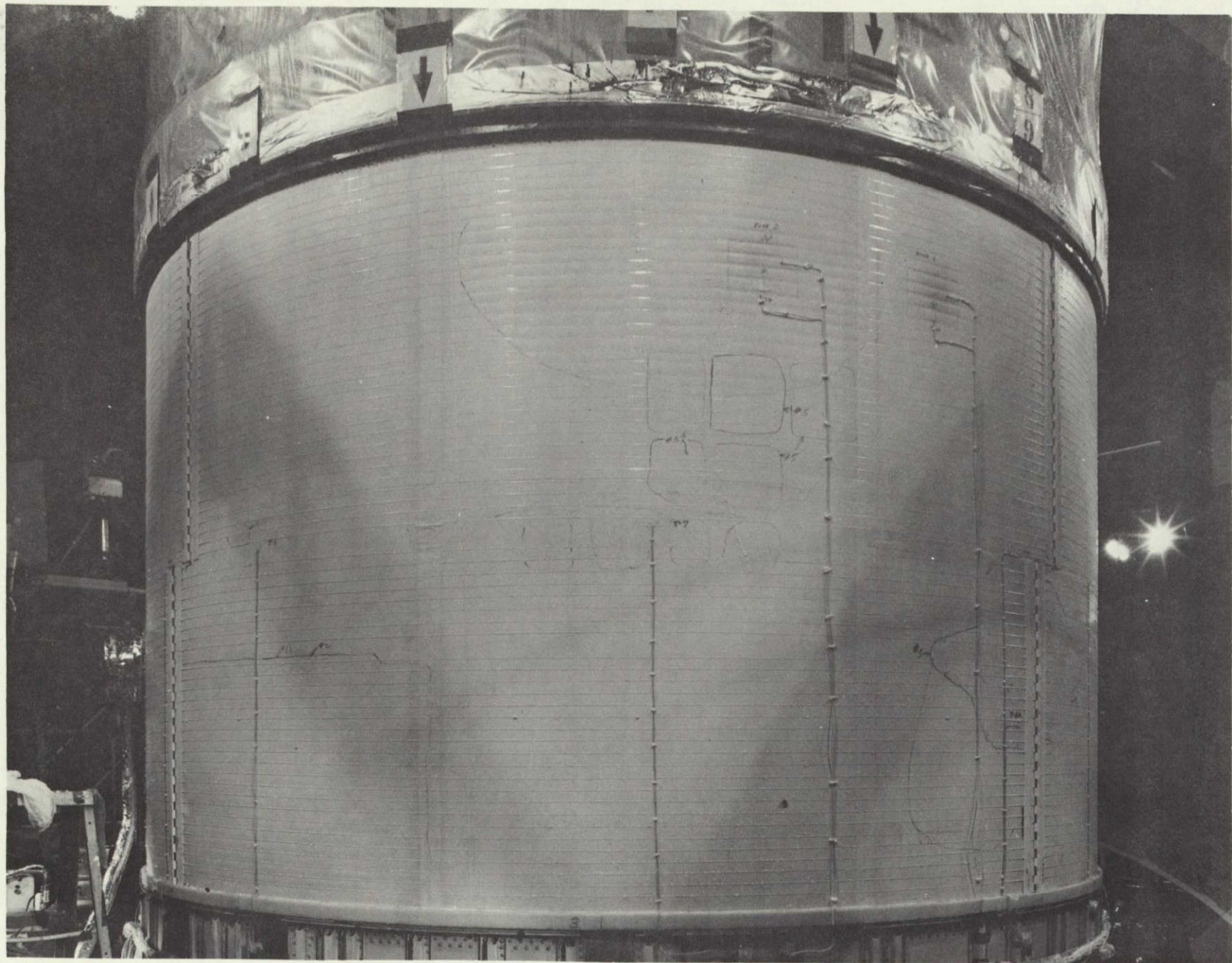


Figure 9-16. T-9 Test Tank after Sixth Tanking — Quad III

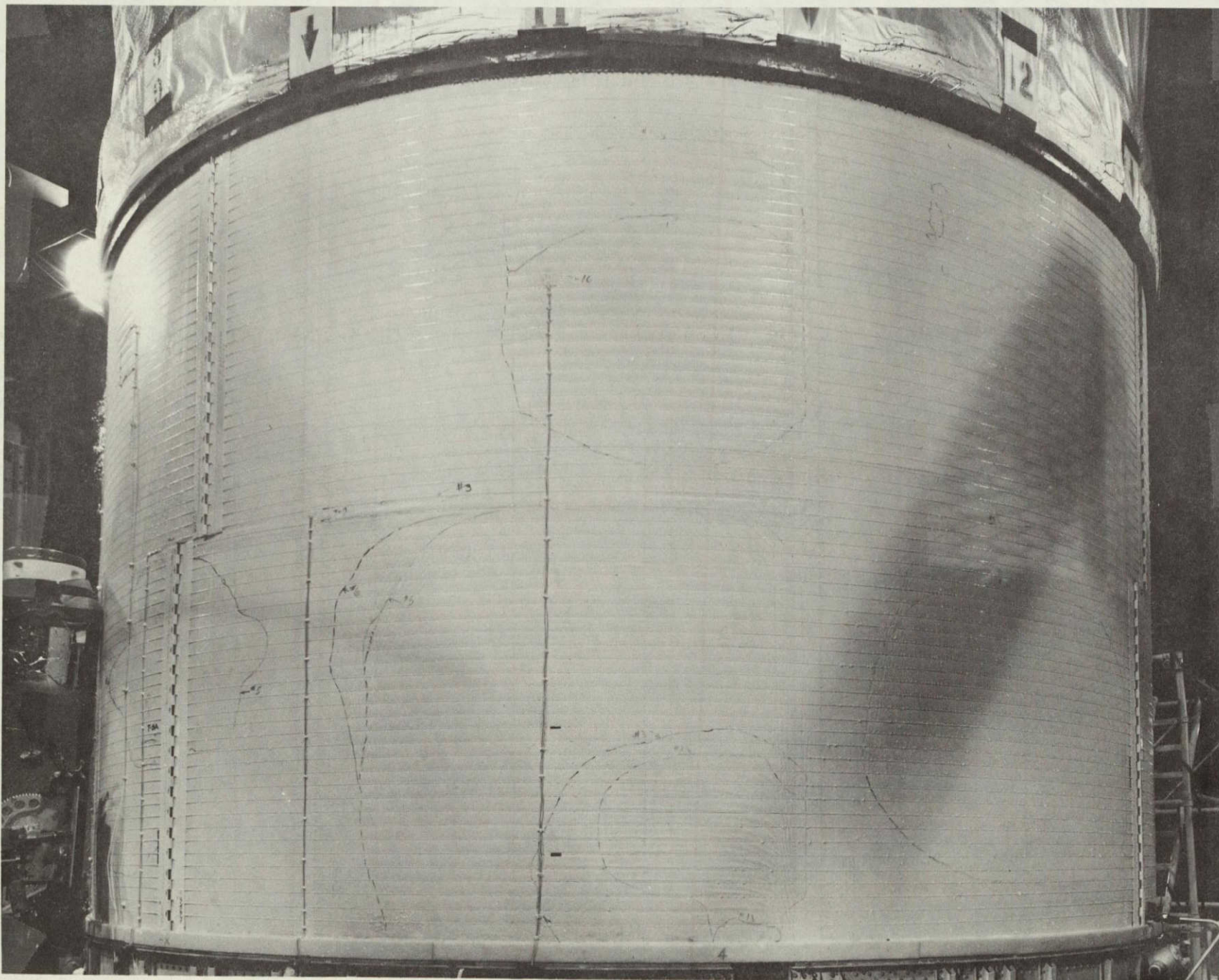
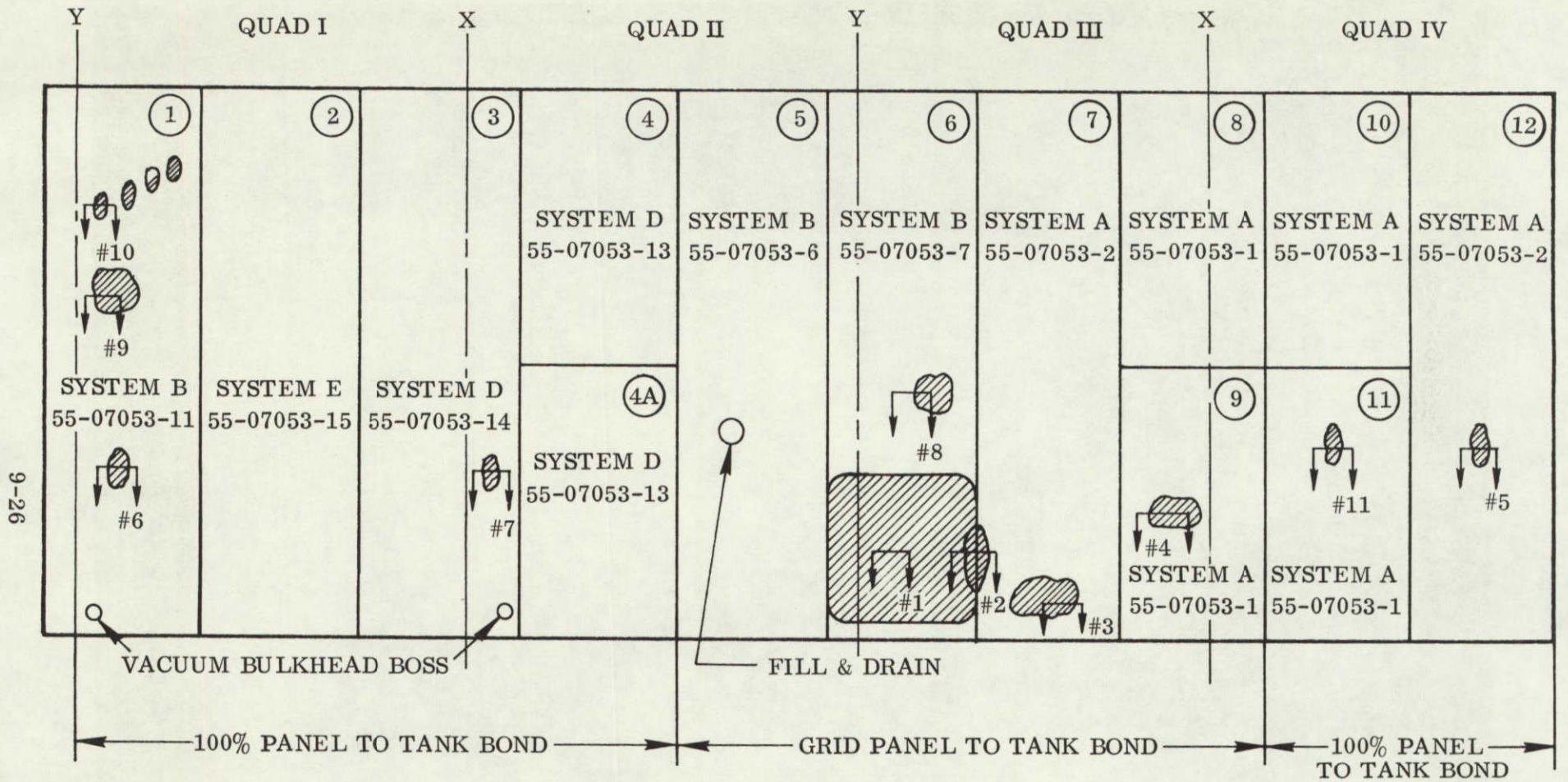

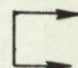


Figure 9-17. T-9 Test Tank after Sixth Tanking — Quad IV



 DENOTES FAILED AREA

 DENOTES EXAMINATION AREA AFTER TEST #10

FAILED AREA

TYPE OF FAILURE

#1, 3, 8 & 9

FOAM AT OUTER MAM

#1, 4, 5, 6, 7, 10 & 11

PANEL TO TANK BOND

#2

PANEL JOINT-DOUBLER

Figure 9-18. T-9 Test Tank-Fixed Insulation Test Results After Tanking Test Numbers 7 Through 10
(100% Repaired After Tanking Test Number 6)

During these tests, there were no blister areas which continued to hold gas pressure after the tank had been de-tanked, as was observed in the material evaluation tests (test Numbers 1 through 6). Eleven failure areas on the panels were sectioned after completion of testing. The locations of the section cut areas are shown in Figure 9-18, and the results of the sectioning are tabulated in Table 9-2. Only one failure was detected in the four new panels, and that failure was a panel-to-tank bond which probably occurred during installation of the panels. Only four outer MAM/adhesive/foam interface failures were detected, two in previously repaired areas, one at a foam splice (similar to a previous failure in the material evaluation tests), and one which could be attributable to a buckle in the foam caused by the intentional post-buckling of the tank during the tests. A picture of the buckle is shown in Figure 9-19.

TABLE 9-2. EVALUATION OF MATERIAL FAILURES DURING THE T-9 REPAIR TECHNIQUE TEST

Type of Failure	System	Location No. (Ref. Fig. 9-18)	Remarks
Outer MAM-Adhesive-Foam Interface	B	1	Previously repaired area, adhesive failure.
	A	3	1.5 inch wide failed band, foam cracked, inner MAM torn but bonded to tank.
	B B	8 9	Previously repaired area. Foam failure at foam splice.
Panel-to-Tank Bond	A	4	Located in grid panel-to-tank bond area.
	A	5	Located in previous outer MAM-to-foam repair area, not noted after first series of 6 tests.
	B	6	Adhesive smooth, indicates no initial bond.
	D	7	New panel after first series of 6 tests, adhesive smooth, indicates no initial bond.
	B	10	Located in previous outer MAM-to-foam repair area.
	A B	11 1	Located in previous outer MAM-to-foam repair area. Located in previous outer MAM-to-foam repair area.
Panel Joint-Doubler	A-B	2	Located in previously repaired area.

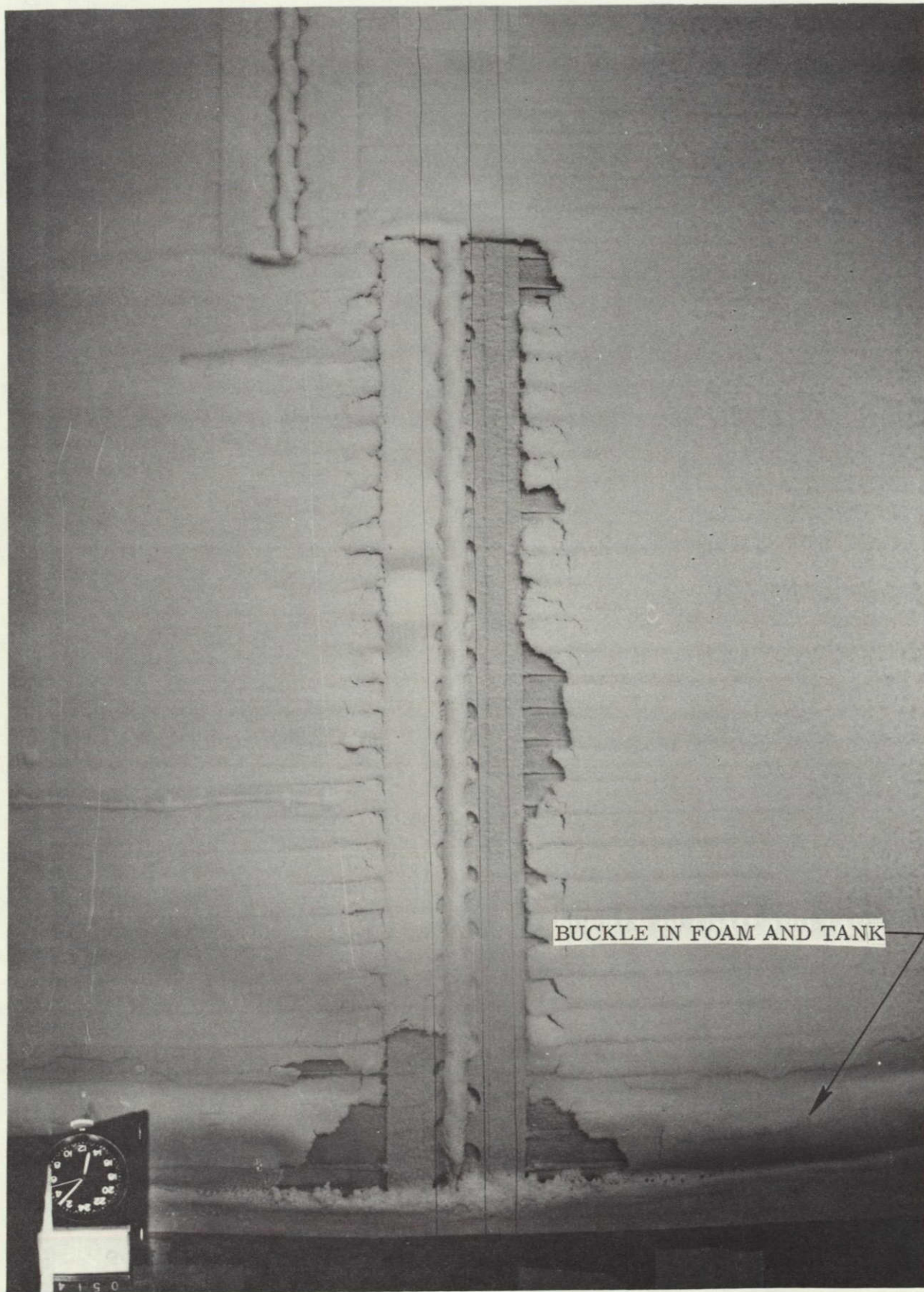


Figure 9-19. Station 412 Area of T-9 Test Tank Under Post-Buckling Load

Of the panel-to-tank bond failures, most were in previous repair areas. However, during these tests, none of the failed areas caused the panels to bulge as occurred during the material evaluation tests.

The results of the thermocouple and frost instrumentation are explained in Subsection 9.5.

9.5 THERMODYNAMIC EVALUATION OF TEST RESULTS

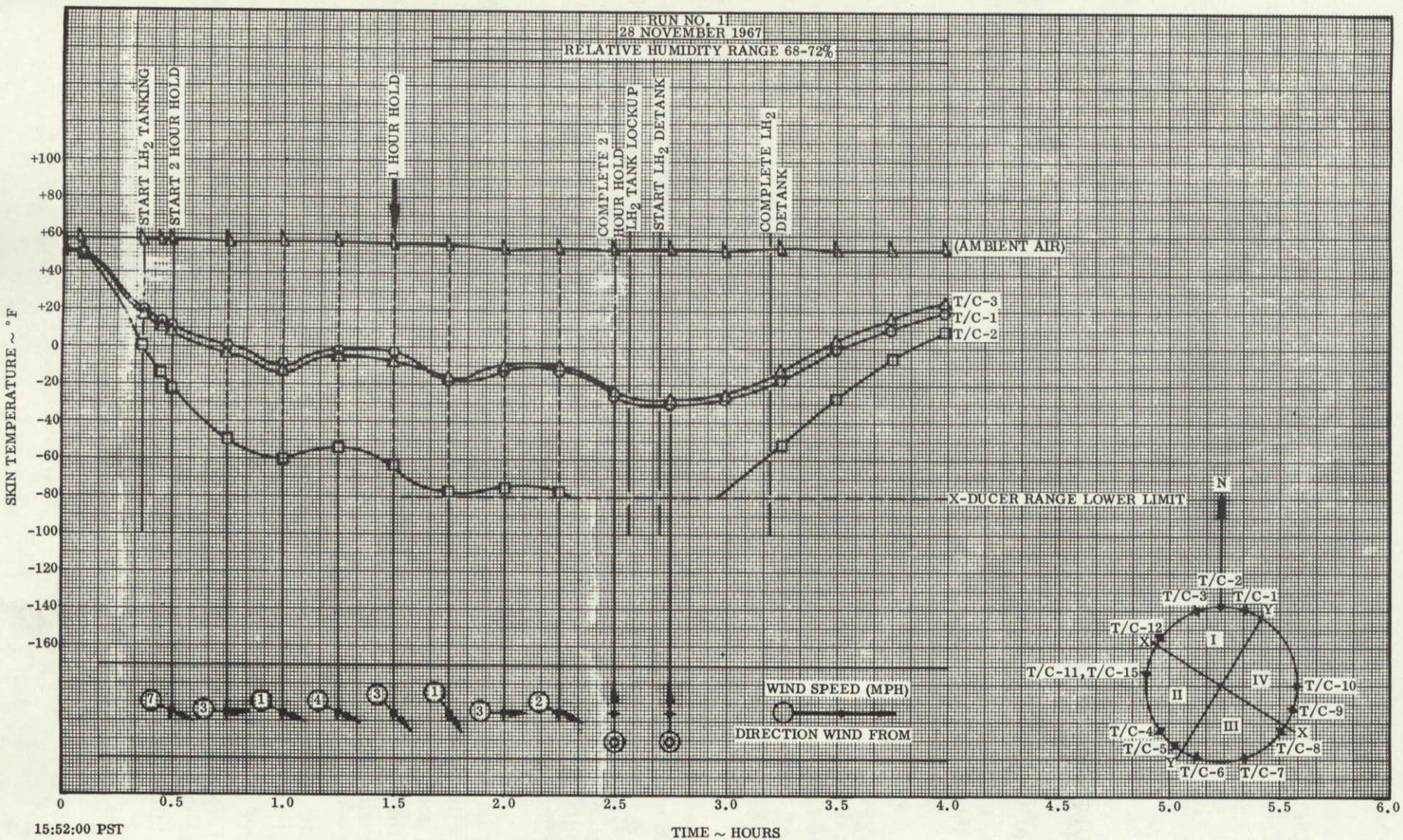
Thermal evaluation of insulation panel quality was limited to: (1) an analysis of surface temperature data, (2) observation of the frost and ice buildup, and (3) determination of the effects of simulated aerodynamic heating.

9.5.1 ANALYSIS OF SURFACE TEMPERATURE DATA. Insulation surface temperatures recorded during each of the tests are shown in detail in References 9-1 and 9-2. A typical plot of insulation temperature as a function of time is shown in Figure 9-20. Wind velocity and direction are also plotted as a function of time. Note the strong relationship between wind velocity and surface temperature of the insulation panels. Surface temperature increases as wind velocity increases and decreases as wind velocity decreases. This condition is typical for all the tanking tests and verifies analytical results summarized in Figure 3-16, which shows surface temperature as a function of wind velocity for various ambient temperatures. Skin temperature measurements on Figure 9-20 vary by about 20° F as the wind velocity changes from 4 mph to 1 mph. This change in temperature is predictable from Figure 3-16. The effect of wind velocity on panel temperatures is uniform around the tank circumference. Wind turbulence within the test tower is apparently evenly distributed by the tower structure.

Insulation temperature at the panel joint (thermocouple T/C-2, Figure 9-20) is lower than the temperature at the center of the panels as expected and is attributable to: (1) the heat short through the Mylar at the edge of each panel, and (2) possible leakage of air through the MAM splice at the panel edge, which permits air to cryopump into the unsealed foam filler strip, thereby increasing thermal conductivity.

Insulation temperatures approach steady-state about 60 minutes after tanking LH₂. Several representative insulation temperatures (measured 60 minutes from start of hold) are plotted in Figure 9-21 for each tanking test. Note that the panel joint temperature (T/C-2) is consistently lower than the insulation temperatures at the center of the panels. The departure of T/C-2 from other temperature measurements is attributable to the failure of the insulation panels in adjacent areas.

Figure 9-20. Insulation Skin Temperature (T/C-1, T/C-2, T/C-3)



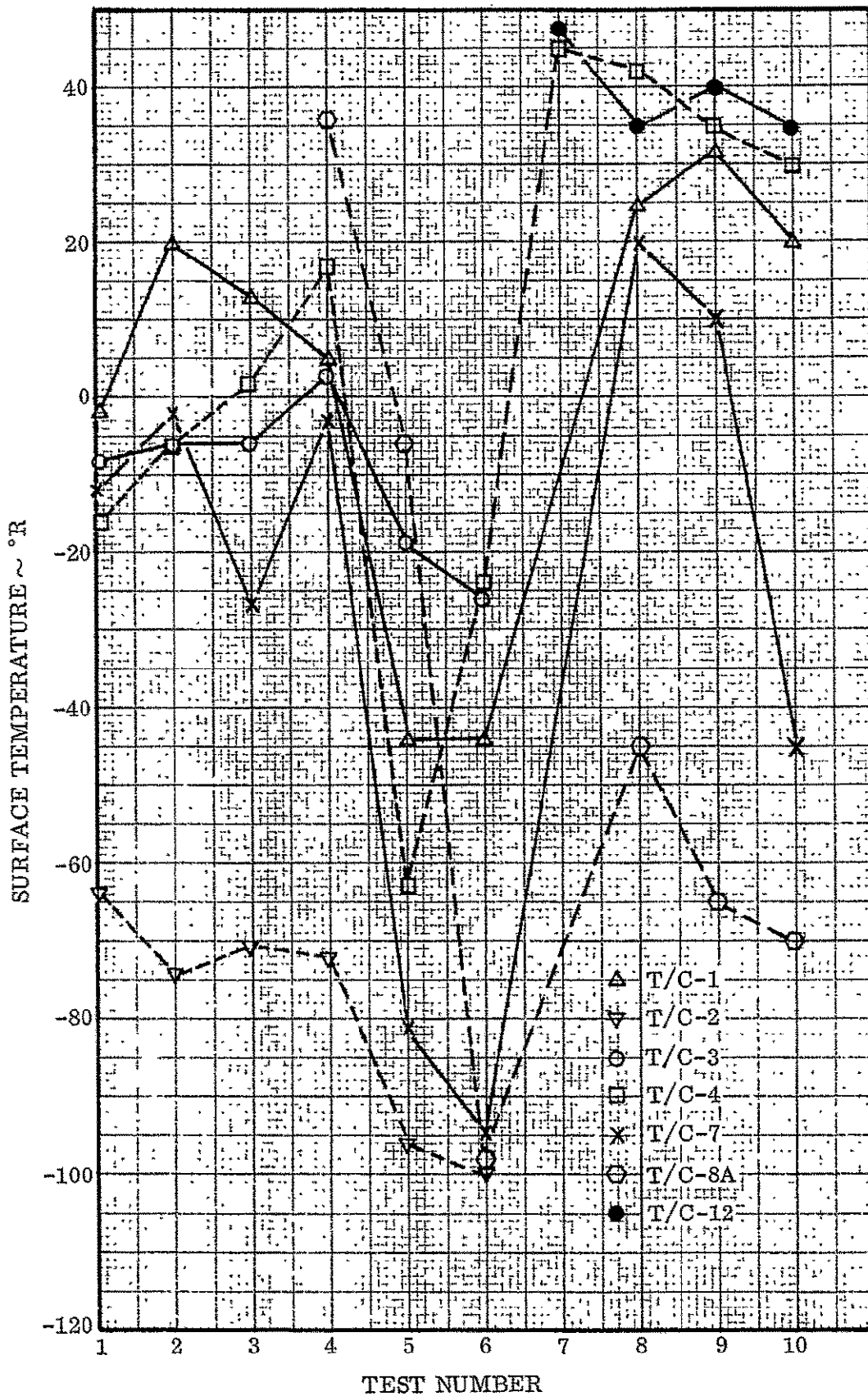
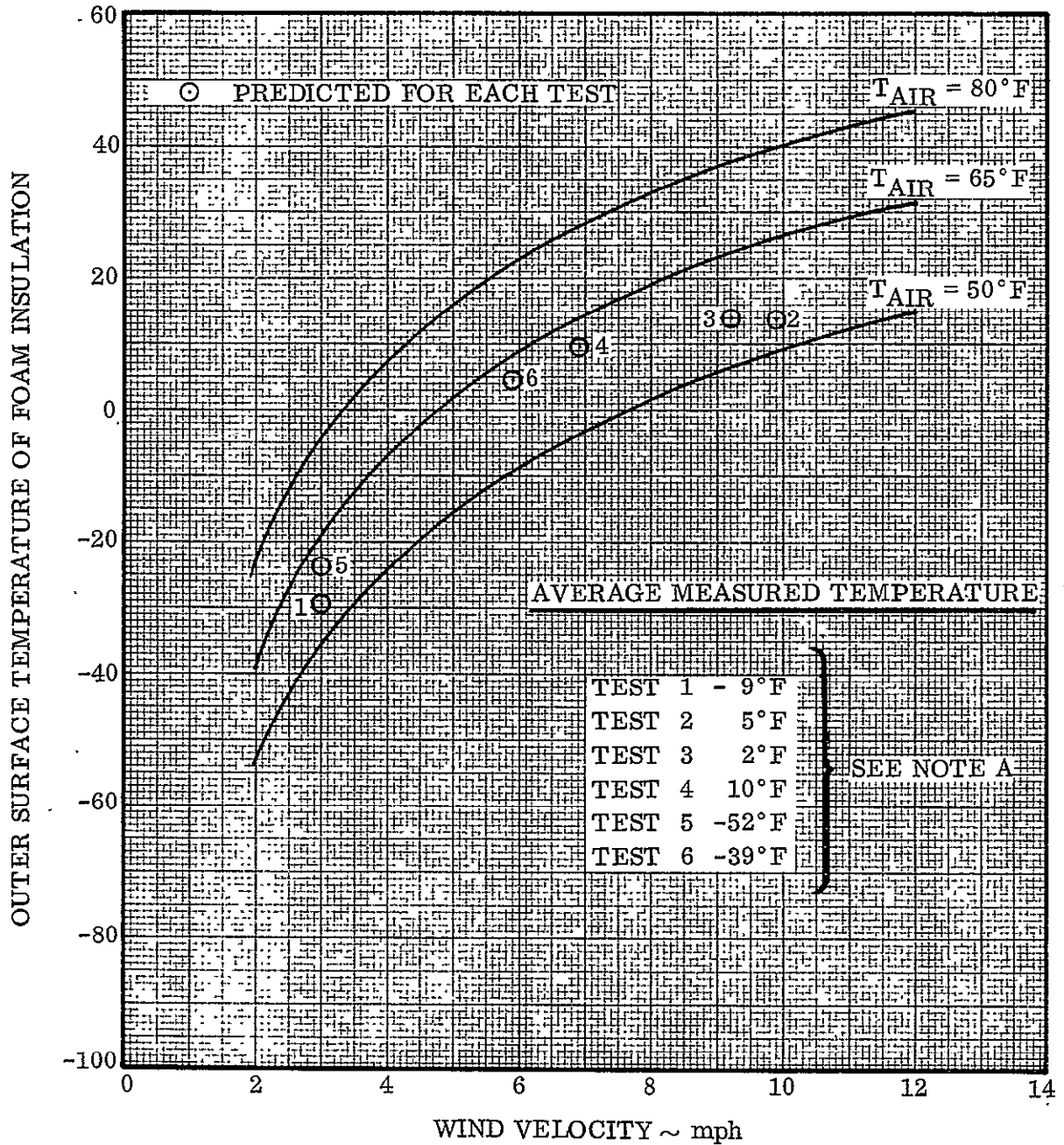


Figure 9-21. T-9 Test Tank Erosion Cloth Temperature after 60-Minute Hold

Insulation panel number 9 was the only panel without ice on the exterior surface for the first three tests. Thermocouple T/C-8A was added to panel 9 for tests 4 through 10, and recorded a temperature above freezing for test 4, but decreased to very low temperatures in succeeding tests. Subsequent failure analysis showed that panel 9 was not in contact with the tank, which probably accounted for the fact that its surface temperature was above freezing and higher than the other panels during the first three tests. Further deterioration of the panel insulation, and cryopumping of air into the void behind the panel probably caused the surface temperature (T/C-8A) to decrease in later tests. The region of the panels adjacent to T/C-7 and T/C-8A was repaired prior to tests 7 through 10. Temperature measurements indicate that repairs were only partly successful from an insulating standpoint. Note that T/C-7 and T/C-8A record much lower surface temperatures than other thermocouples during tests 8, 9, and 10.

Surface temperatures were predicted for each test based upon the prevailing wind velocity and ambient temperature, and are plotted in Figure 9-22. The average of the measured temperatures for each test was obtained by averaging the temperatures where there was no apparent deterioration of the foam panels. These averages are plotted in Figure 9-22. Thermocouples T/C-1, T/C-3, T/C-4, T/C-6, T/C-7, and T/C-10 (Figure 9-10) were averaged during tests one and two. Thermocouples T/C-7 and T/C-10 were not included in the average temperature calculation for tests three through six. Wind velocity was not recorded for tests 7 through 10. Only results of tests one through six are shown in Figure 9-22. There is general agreement between measured and predicted values. Predicted and measured (average) temperatures shown in Figure 9-22 are cross-plotted in Figure 9-23. A "corrected" temperature prediction was made to account for the accuracy of the wind temperature measurement of ± 1 mph. A 1 mph "correction" in wind velocity was made for tests 1, 5, and 6 that brought predicted and measured temperatures into closer agreement. Figure 9-23 shows that temperature predictions for tests 1 through 5 are within 12°F of measured values. Even with the "corrected" temperature prediction, the measured surface temperature for test 6 is 30°F below the predicted value. General deterioration of the insulation quality is evident in test 6. Subsequent panel repairs were only partly successful in restoring the original insulation capability of the foam panels.

9.5.2 OBSERVATION OF ICE AND FROST BUILD-UP. Frost build-up on the surface of all panels was observed and monitored visually (via video) for all 10 tests. The maximum thickness observed on any test was approximately 5/16-inch. The average thickness for all tests was approximately 0.2-inch. The frost had a light, powdery appearance, which indicated it was of a low density. An analysis of the effects of frost build-up was discussed in Subsection 3.1.3.



NOTE A T/C-1, T/C-3, T/C-4, T/C-6, T/C-7, AND T/C-10 WERE USED TO DETERMINE AVERAGE TEMPERATURE FOR TESTS 1 AND 2. T/C-1, T/C-3, T/C-4, T/C-6 WERE USED TO DETERMINE AVERAGE TEMPERATURE FOR TESTS 3, 4, 5, AND 6.

Figure 9-22. T-9 Test Tank Erosion Cloth Temperature Versus Wind Velocity

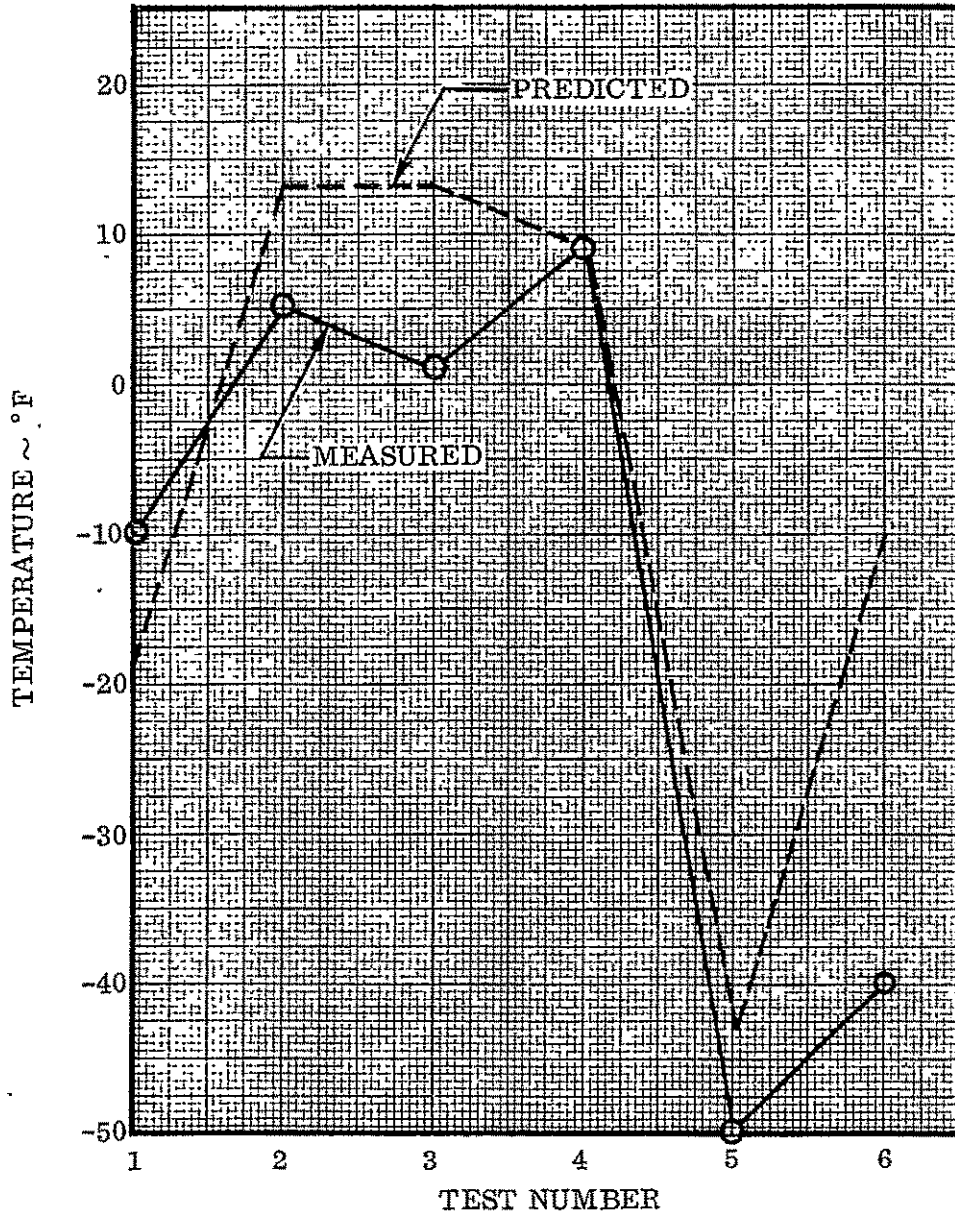


Figure 9-23. T-9 Test Tank Erosion Cloth Temperatures (Predicted and Measured) (From Figure 9-22)

9.5.3 EFFECTS OF SIMULATED AERODYNAMIC HEATING. Prior to the completion of the tests, a number of 6- by 6-inch sealed foam specimens were tested in a vacuum chamber and radiant heat was applied to simulate aerodynamic heating (see Subsection 8.1). These test specimens were not in contact with a cryogenically-cooled wall. Two 6- by 6-inch areas of the T-9 tank insulation (see Figure 9-12, panel Numbers 7 and 8) were subjected to the temperature effects of aerodynamic heating in an attempt to evaluate the effects of a cold wall on the formation of blisters described in Subsection 8.1. Blisters did not appear and it was concluded that additional tests were required to evaluate cold-wall conditions in a vacuum. These tests are described in Subsection 8.2.

10

CONCLUSIONS AND RECOMMENDATIONS

Although the sealed foam insulation system has been eliminated from further consideration for Improved Centaur, the system could be used in other applications where the requirements are less severe. However, before beginning a development program for these other uses, some conclusions and recommendations can be drawn from this program. This section will identify those conclusions and recommendations concerning first the sealed foam panels, then the constrictive wraps.

10.1 PANEL CONFIGURATION

As a result of the tests performed, the best panel configuration of those investigated was System B. The System B configuration consisted basically of the CPR 32-2C foam with the Metlbond 225 film-type adhesive for the outer MAM-to-foam bond. However, all material systems tested had some material failures in the outer MAM-to-foam bond, and none of the material systems were considered acceptable for an Improved Centaur mission. These bond failures, or blisters, were shown to occur both during warm-up after a cryogenic tanking, and while the panel was being subjected to the ascent trajectory environment. These blister occurrences are discussed in detail in the following two subsections.

The 100 percent panel-to-tank adhesive bond proved unquestionably to be superior to the grid system bond.

10.1.1 PANEL BLISTERING DURING WARM-UP AFTER CRYOGENIC TANKING.

Even though all panels ultimately passed the prescribed acceptance test, some panels of all material systems blistered during the warm-up period after cryogenic tanking, and some did not. Obviously, either the LN₂ submergence acceptance test was inadequate, or the panels' sealed integrity was destroyed in some way after the acceptance test. Before pursuing this insulation concept, it is recommended that the answer to this question be determined, and appropriate action taken to rectify the problem.

10.1.2 PANEL BLISTERING WHILE BEING SUBJECTED TO THE ASCENT TRAJECTORY ENVIRONMENT.

Small panels, when subjected to the ascent trajectory environment, blistered in every case. It was found that the cryopumping action within the panel was not sufficient to prohibit the panel internal pressure from increasing beyond the limits of the panel material capability. The cause for internal pressure increase was aerodynamic heating and the reduced external pressure environment. It could be argued that panel blistering during that portion of the flight is not harmful to the system

efficiency, and could be tolerated. However, before that can be stated, it is recommended that the effect blistering has on panel flutter and on components mounted on the insulation (such as the wiring tunnel) be investigated.

Two panel configurations were identified which apparently did restrict panel blistering. These configurations were a dual panel system of sealed and unsealed panels, and a system with holes punched through the sealing laminate. However, neither configuration was suitable for the Improved Centaur vehicle, as explained in Subsection 8.1.6. It is possible, though, that these configurations would be suitable for other applications. Even though an unsealed panel no longer provides an entire panel capable of cryopumping, it is possible that the individual cells of the closed cell foam could cryopump to a degree which would provide almost as good an insulator as the sealed panels.

10.2 CONSTRUCTIVE WRAP CONFIGURATION

As explained in Section 4, two constrictive wrap designs were considered in detail. The fiberglass strand wrap was designed, fabricated, and tested, and the aluminum corrugation wrap was studied. As was further explained in Subsection 4.3.5, neither of the wrap designs was acceptable, and no other designs were conceived that would satisfy all the requirements. Therefore, the entire fixed insulation development program was terminated. However, it should be remembered that the only problem with the aluminum corrugation constrictive wrap was its weight, which caused excessive payload degradation for the Improved Centaur. Therefore, if in other applications a constrictive wrap is required, it is recommended that the aluminum corrugation constrictive wrap be used. The fiberglass strand constrictive wrap is not recommended because of its "tender-loving-care" fabrication and handling requirement, and its suspected susceptibility to flutter.

11

REFERENCES

- 1-1 "Sealed-Foam. Constrictive-Wrapped, External Insulation System for Liquid — Hydrogen Tanks of Boost Vehicle," NASA TND-2685, NASA Lewis Research Center Staff, March 1965.
- 2-1 "Permanent Insulation Development Program," Hertz, J., Convair Memo M-53, March 1967. (Literature Survey of Foam)
- 2-2 "Permanent Insulation Development Program (Preliminary Test Phase, Part I)," Pettyjohn, R.R., Convair Memo M-103, May 1967.
- 2-3 "Chemical Engineering Progress Symposium," Series, No. 30, Volume 56, Underwood, W.M., and McTaggart, R.B.
- 2-4 "Permanent Insulation Development Program," May, L.C., Convair Memo M-63, No date. (Literature Survey of Adhesives)
- 2-5 "Flexible Vacuum Jacket Development Program," Goodyear Aerospace Corporation, Progress Report No. 11, 15 June 1965.
- 2-6 "Physical-Thermal Properties of Mylar," Technical Bulletin M-2C (#A-48424) E.I. DuPont de Nemours and Company.
- 2-7 "Permanent Insulation Centaur External Finish Thermal Radiation Properties," Jennings, R.W., Convair Report GDC-BTD68-007, March 1968.
- 2-8 "Preliminary Evaluation of Using Strain Gages to Measure Tension Load of Fixed Insulation Constrictive Wrap — Test Results and Discussion," Neff, D.K., Convair Memo 578-4-M-67-30, July 1967.
- 2-9 "Lightweight Constrictive Wrap for External Insulation of Product Improved Centaur Vehicle — Materials Evaluations," Varlas, M., Convair Report ZZL-67-016, July 1967.
- 2-10 "Strand-Load/Strain Values for S-994 (HTS) 20 End Roving, Phenolic Resin Impregnated," Varlas, M., Convair Memo M-270, November 1967.
- 2-11 "Thermophysical Properties of Plastic Materials and Composites to Liquid Hydrogen Temperature (-423°F)," Haskins, J.F., et al., Convair Division of General Dynamics, Air Force Materials Laboratory Report ML-TDR-64-33, Part I, June 1964.

- 3-1 "Thermal Analysis of a Proposed Fixed -- Insulation System for Centaur," Worscheck, G.A., et al., Convair Memo 966-3-CR-042, 27 June 1967.
- 3-2 "Predicted Temperatures on the Constrictive Wrap Installation for the Fixed Insulation System," Worscheck, G.A., Convair Memo 966-3CHM-67-63, 19 October 1967.
- 3-3 "Thermal Analysis of Corrugated Constrictive Wrap for LH₂ Tank Sidewall Fixed Insulation," Worscheck, G.A., Convair Memo 966-3-CR-076, 19 June 1968.
- 3-4 "Space Vehicle Radiant Energy Program," Armfield, L.E., Convair Report GDC-ERR-AN-929, November 1966.
- 3-5 "Variable Boundry II Heat Conduction Program," O'Neill, R.F., Convair Report GDC-BTD67-004A, 5 September 1968.
- 3-6 "Preliminary Thermal Analysis of PI Centaur Insulation Systems," Barkdoll, R.O., Convair Memo 966-3-CR-033, 21 February 1967.
- 3-7 "Thermal Analysis of the 219 Ring Area of the Nose Fairing for AC-4 and On," Worscheck, G.A., Convair Memo CTM-200, 13 August 1964.
- 3-8 "Vacuum Bulkhead Thermal Test -- Stub Tank Heat Transfer Study," Barkdoll, R.O., Convair Memo EM 2182, 17 August 1962.
- 3-9 "Bubble Rise in Liquid Hydrogen," Boyer, R.S., Convair Report CA-E-41, 31 March 1960.
- 3-10 "Frost Formation on a Cylinder in Crossflow of Humid Air," Han, L.S., ASME Publication 64-WA/HT-9, 28 August 1964.
- 3-11 "Hypersonic Investigations on the Local and Average Heat Transfer in Cavities and After Steps of Bodies of Revolution," Wybormy, W., et al., AGARD Fluid Physics of Hypersonic Wakes, Volume I, May 1967.
- 3-12 "Thermal Radiation Absorption in Rectangular -- Groove Cavities," Johnson, V.K., and Sparrow, E.M., Journal of Applied Mechanics, June 1963.
- 4-1 "Permanent Insulation Development Program (Compression Tests on Sealed Foam)," Hertz, J., Convair Memo M-186, 17 July 1967.
- 5-1 "Test Procedure for Design Evaluation Test of T-9 Tank Insulation Panel," Shriver, C.B., GER 13285 Revision A, Goodyear Aerospace Corporation, 12 July 1967.

- 5-2 "Test Procedure for Individual Acceptance Test (IAT) of Centaur Insulation Panel," GER 13311 Revision A, Shriver, C.B., Goodyear Aerospace Corporation, 12 July 1967.
- 5-3 "Procedures for Repairing Centaur Sealed Insulation Panels," GER 13540, Goodyear Aerospace Corporation, 10 November 1967.
- 8-1 "Evaluation of Fixed-Insulation Tests Conducted in a Vacuum," Worscheck, G.A., Convair Memo 966-3-CHM67-65, 26 October 1967.
- 8-2 "Fixed Insulation Design Evaluation Test, 6 x 6 inch panels," Wegener, H.W., Convair Report 55B6067-1, 31 October 1968.
- 8-3 "Analysis of Sealed Foam Insulation Panels," Hertz, J., Convair Memo M-110, 8 October 1968.
- 9-1 "Centaur Program — Fixed Insulation Development Test, T-9 Test Tank," Takvam, N.A., Convair Report 55B5750-1, 5 February 1968.
- 9-2 "Centaur Program Fixed Insulation Development Test, T-9 Test Tank," Maxson, J.G., Convair Report 55B5935-2, 19 September 1968.

APPENDIX I

BIBLIOGRAPHY

This bibliography contains a listing of all documents published during the Fixed Insulation Development Program. Many of the documents listed herein are also included in the Reference section, however, they are included in this appendix so as to present one complete list of all published documents according to subject matter.

I.1 MATERIAL RESEARCH DOCUMENTS

Hertz, J., Permanent Insulation Development Program, Convair Memo M-53, 27 March 1967. (Literature Survey of Foams)

May, L.C., Permanent Insulation Development Program, Convair Memo M-63, no date. (Literature Survey of Adhesives)

Hertz, J., Permanent Insulation Development Program, Convair Memo M-71, 7 April 1967. (Material Recommendations for the T-9 Tank Insulation Panels)

May, L.C., Permanent Insulation Development Program, Convair Memo M-118, 2 June 1967. (Adhesive Recommendations for the T-9 Tank Insulation Panels)

Hertz, J., Evaluation of Wrap Manufacturing Processes, Convair Memo M-276, 9 November 1967.

Hertz, J., Saturn S-II Foam Insulation, Convair Memo M-64, 10 May 1968.

Hertz, J., Data from Presentation by G.T. Schjeldahl Corp. on Thermal Control, Environmental Control and Solar Shielding Films, MGR-TR-205, 24 May 1968.

Convair letter 572-1-1475, Hertz, J. to CPR Division — The Upjohn Co., Proposed Cell Size Control on CPR 32-2C Foam, 24 July 1967.

CPR Division — The Upjohn Co. letter to Hertz, J., Proposed Cell Size Control on CPR 32-2C Foam, 4 October 1967.

I.2 THERMODYNAMIC ANALYSES DOCUMENTS

Jennings, R.W., Heat Transfer Rate Through Ellipsoidal Forward Bulkhead Utilizing Permanent Foam Insulation, Convair Memo 966-3-CHM67-24, 29 May 1967.

Anderson, K.E., Jennings, R.W., Worscheck, G.A., Thermal Analysis of a Proposed Fixed-Insulation System for Centaur, Convair Memo 966-3-CR-042, 27 June 1967.

Worscheck, G.A., Predicted Temperature on the Constrictive Wrap Installation for the Fixed Insulation System, Convair Memo 966-3-CHM-67-63, 19 October 1967.

Yurczyk, R.F., Fixed Insulation Propellant Feed Duct Fairing Purge Requirement, Convair Memo 966-3-CPM67-54, 20 October 1967.

Worscheck, G.A., Thermal Analysis of Corrugated Constructive Wrap for LH₂ Tank Sidewall Fixed Insulation, Convair Memo 966-3-CR-076, 19 June 1968.

Burton, K.R., Thermal Improvements on the Station 219 Joint for the PI Centaur, Convair Memo 966-3-CR-063, 10 January 1968.

Burton, K.R., Continuation of Thermal Improvements Study on the Centaur 219 Joint, Convair Memo 966-3-CR-087, 25 September 1968.

I.3 TEST DOCUMENTS

I.3.1 THERMAL CONDUCTIVITY TESTS.

Worscheck, G.A., Thermal Conductivity Test of Hermetically - Sealed GAC Foamed Panel, Convair Memo 966-3-CHM67-29, 12 June 1967.

Campbell, M.D., Thermal Conductance of Centaur Permanent Insulation Sealed Foam Panels - Goodyear System, Convair Memo M-258, 20 October 1967.

Campbell, M.D., Thermal Conductance of Centaur Permanent Insulation Sealed Foam Panels - Experimental System, Convair Memo M-272, 6 November 1967.

I.3.2 COLDWALL VACUUM/HEAT TESTS.

May, L.C., Permanent Insulation Program, Convair Memo M-268, 22 November 1967.

Worscheck, G.A., Evaluation of Fixed-Insulation Tests Conducted in a Vacuum, Convair Memo 966-3-CHM67-65, 26 October 1967.

Hughes, J.E., Test Requirements For Fixed Insulation Panel Cold Wall Testing, Convair Report GDC-BTD68-025, 5 June 1968.

Wagener, H.W., Fixed Insulation Design Evaluation Test, 6 x 6 Inch Panels, Convair Report 55B6067-1, 31 October 1968.

Hertz, J., Analysis of Sealed Foam Insulation Panels, Convair Memo M-110, 8 October 1968.

Worscheck, G.A., Evaluation of Fixed Insulation Tests Conducted in a Vacuum, Convair Memo 966-3-CHM67-65, 26 October 1967.

I.3.3 SURFACE COAT TESTS.

Cornahan, K.R., Thermal Control Coatings for use in the Centaur Permanent Insulation Development Program, Convair Memo M-62, 28 March 1967.

Jennings, R.W., Request for the Determination of the Effects of Heating on Solar Absorptance and Emittance of Prospective Centaur Constrictive Wrap Surface Finishes, Convair Memo 966-3-CHM67-10, 22 March 1967.

Jennings, R.W., Request for the Determination of the Effects of Heating on Solar Absorptance and Emittance of Prospective Centaur Constrictive Wrap Surface Finishes, Convair Memo 966-3-CHM67-15, 13 April 1967.

Jennings, R.W., Permanent Insulation, Centaur-External Finish Thermal Radiation Properties, Convair Report GDC-BTD68-007, 12 March 1968.

I.3.4 CONSTRICTIVE WRAP STRAND FRICTION TESTING.

Campbell, M.D. and O'Barr, G.L., Evaluation of Friction Between Centaur Fixed Insulation Panel Surfaces and Constrictive Wrap Strands, Convair Memo ZZL-67-022 and MP 572-1-646, October 1967.

Campbell, M.D., Friction Between Corrugated Titanium and MAM Covered Fixed Insulation Panel, Convair Memo M-62, 7 May 1968.

I.3.5 JET ENGINE TEST.

Worscheck, G.A., Jet Engine Test Requirements for the Fixed Insulation System, Convair Memo 966-3-CR-053, 11 October 1967.

I.3.6 T-9 GROUND HOLD AND REPAIR TECHNIQUE TESTS.

Rathbun, C.L., Requirements for Fixed Insulation Development, T-9 Test Tank, Convair Report GDC-BTD67-092 Revision A, 19 July 1968.

Takvam, N.A., Centaur Program-Fixed Insulation Development Test, T-9 Test Tank, Convair Report 55B5750-1, 5 February 1968.

May, L.C., Investigation of T-9 Tank Fixed Insulation Failures, Convair Memo M-1, 4 January 1968.

May, L.C., Further Investigation of T-9 Tank Fixed Insulation Failures, Convair Memo M-66, 22 May 1968.

May, L.C., Investigation of Repaired T-9 Tank Insulation after a Second Series of Tests, Convair Memo M-22, 25 February 1969.

Maxson, J.G., Centaur Program Fixed Insulation Development Test, T-9 Test Tank, Convair Report 55B5935-2, 19 September 1968.

Worscheck, G.A., Results of 0.4 Inch Fixed Foam -- Insulation Tests on the T-9 Tank, Convair Memo 966-3-CR-075, 26 June 1968.

I.3.7 MISCELLANEOUS TESTS.

May, L.C., Permanent Insulation Development Program, Convair Memo M-83, 25 April 1967. (Composite Foam - Film Tests)

May, L.C., Testing of Styles 143 and 1543 Glass Cloth for Fixed Insulation Wrap, Convair Memo M-105, 15 May 1967.

Pettyjohn, R.R., Permanent Insulation Development Program (Preliminary Test Phase - Part 1), Convair Memo M-103, 17 May 1967.

May, L.C., Permanent Insulation Development Program, Convair Memo M-108, 17 May 1967. (Composite Foam - Film Tests)

May, L.C., Permanent Insulation Development Program, Convair Memo M-113, 24 May 1967. (Adhesive Tests)

Hertz, J., Permanent Insulation Development Program, Convair Memo M-186, 17 July 1967. (Sealed Foam Panel Compression Tests)

Campbell, M.D., Thermal Expansion of U.S. Polymeric FF-5255 (Proposed Centaur Permanent Insulation Outer Wrap Component), Convair Memo M-164, 3 July 1967.

May, L.C., Testing of Goodyear Vitel P.E. 207 in Support of Preparation of GDC Specification 0-00844, Convair Memo M-184, 12 July 1967.

Varlas, M., Lightweight Constrictive Wrap for External Insulation of Product Improved Centaur Vehicle -- Materials Evaluations, Convair Memo ZZL-67-016 and MP-572-1-642, July 1967.

Varlas, M., Strand Tensile and Bond Pull-out Creep Tests for Fixed Insulation Program, Convair Memo M-241, 29 September 1967.

Hertz, J., TGA Testing of Films and Adhesives, Convair Memo M-269, 2 November 1967.

Hertz, J., Vinylcel Foam, Convair Memo M-25, 20 February 1968.

I.3.8 T-9 TANK INSULATION PANEL ACCEPTANCE TESTS.

Shriver, C.B., Test Procedure for Design Evaluation Test of T-9 Tank Insulation Panel, GER 13285 Revision A, Goodyear Aerospace Corporation, 12 July 1967.

Shriver, C.B., Test Procedure for Individual Acceptance Test (IAT) of Centaur Insulation Panel, GER 13311 Revision A, Goodyear Aerospace Corporation, 12 July 1967.

I.4 MISCELLANEOUS DOCUMENTS

Erickson, J.W., Aerodynamic Loads for Centaur Fixed Insulation Panels, Convair Memo ABM-67-026, 20 June 1967.

Reynolds, R.J., Flutter Analysis of the Wiring Tunnel Port of the Constrictive Wrap Insulation Concept, Convair Memo SD-67-189-CEN, 30 August 1967.

Jones, R.A. and Norris, G.W., Fixed Insulation Protective Shell Design Requirements 13 October 1967.

Procedures for Repairing Centaur Sealed Insulation Panels, GER 13540, Goodyear Aerospace Corporation, 10 November 1967.

I.5 DRAWINGS

I.5.1 CONVAIR DRAWINGS.

55-07053	Insulation Panels, Sealed - T-9 Test Tank
55-07223	Hinge Fitting - Constrictive Wrap, Fixed Insulation
55-07224	Insulation Instl., Seal - T-9 Test Tank
55-07227	Constrictive Wrap - Fixed Insulation, T-9 Tank
55-07223-1 IPFM	Hinge Impact Form
55-07227-500 BNTO	Constrictive Wrap Bonding Tool
55-07227-BN ASTO	Constrictive Wrap Assembly Tool

I.5.2 GOODYEAR AEROSPACE DRAWINGS.

603A000-001	Panel Installation - Test Vehicle, Centaur T-9 Test Tank
603A000-002	Panel - Test Vehicle, Centaur, Assembly of
603A000-003	Panel - Test Vehicle, Centaur, Assembly of
603A000-004	Panel - Test Vehicle, Centaur, Assembly of

GENERAL DYNAMICS
Convair Division